USING MOTION ANALYSIS TECHNIQUES AND MUSCULOSKELETAL MODELING OF THE SPINE TO BETTER UNDERSTAND SPINAL DISORDERS AND EVALUATE TREATMENT EFFECTS

EDITED BY: Stefan Schmid, Dennis E. Anderson, Babak Bazrgari and Lennart Scheys

PUBLISHED IN: Frontiers in Bioengineering and Biotechnology

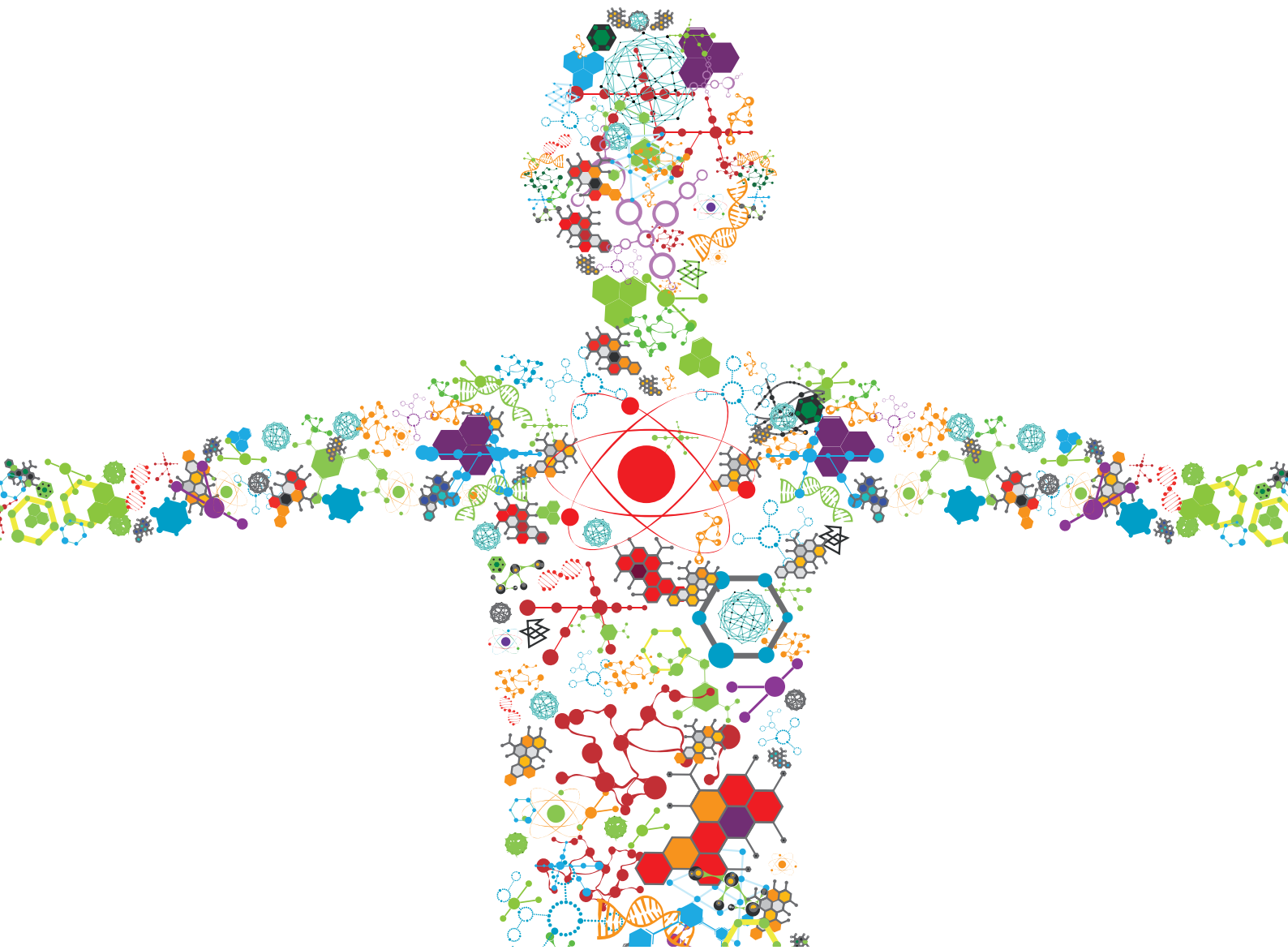

frontiers Research Topics

ISSN 1664-8714
ISBN 978-2-88976-038-1
DOI 10.3389/978-2-88976-038-1

About Frontiers

Frontiers is more than just an open-access publisher of scholarly articles: it is a pioneering approach to the world of academia, radically improving the way scholarly research is managed. The grand vision of Frontiers is a world where all people have an equal opportunity to seek, share and generate knowledge. Frontiers provides immediate and permanent online open access to all its publications, but this alone is not enough to realize our grand goals.

Frontiers Journal Series

The Frontiers Journal Series is a multi-tier and interdisciplinary set of open-access, online journals, promising a paradigm shift from the current review, selection and dissemination processes in academic publishing. All Frontiers journals are driven by researchers for researchers; therefore, they constitute a service to the scholarly community. At the same time, the Frontiers Journal Series operates on a revolutionary invention, the tiered publishing system, initially addressing specific communities of scholars, and gradually climbing up to broader public understanding, thus serving the interests of the lay society, too.

Dedication to Quality

Each Frontiers article is a landmark of the highest quality, thanks to genuinely collaborative interactions between authors and review editors, who include some of the world's best academicians. Research must be certified by peers before entering a stream of knowledge that may eventually reach the public - and shape society; therefore, Frontiers only applies the most rigorous and unbiased reviews.
Frontiers revolutionizes research publishing by freely delivering the most outstanding research, evaluated with no bias from both the academic and social point of view. By applying the most advanced information technologies, Frontiers is catapulting scholarly publishing into a new generation.

What are Frontiers Research Topics?

Frontiers Research Topics are very popular trademarks of the Frontiers Journals Series: they are collections of at least ten articles, all centered on a particular subject. With their unique mix of varied contributions from Original Research to Review Articles, Frontiers Research Topics unify the most influential researchers, the latest key findings and historical advances in a hot research area! Find out more on how to host your own Frontiers Research Topic or contribute to one as an author by contacting the Frontiers Editorial Office: frontiersin.org/about/contact

USING MOTION ANALYSIS TECHNIQUES AND MUSCULOSKELETAL MODELING OF THE SPINE TO BETTER UNDERSTAND SPINAL DISORDERS AND EVALUATE TREATMENT EFFECTS

Topic Editors:
Stefan Schmid, Bern University of Applied Sciences, Switzerland
Dennis E. Anderson, Harvard Medical School, United States
Babak Bazrgari, University of Kentucky, United States
Lennart Scheys, KU Leuven, Belgium

Citation: Schmid, S., Anderson, D. E., Bazrgari, B., Scheys, L., eds. (2022). Using Motion Analysis Techniques and Musculoskeletal Modeling of the Spine to Better Understand Spinal Disorders and Evaluate Treatment Effects.
Lausanne: Frontiers Media SA. doi: 10.3389/978-2-88976-038-1

Table of Contents

frontiers | Frontiers in Bioengineering and Biotechnology

EDITORIAL
published: 06 April 2022
doi: 10.3389/fbioe.2022.884123

Editorial: Using Motion Analysis Techniques and Musculoskeletal Modeling of the Spine to Better Understand Spinal Disorders and Evaluate Treatment Effects

Dennis E. Anderson[1,2]*, *Stefan Schmid*[3,4], *Lennart Scheys*[5] *and Babak Bazrgari*[6]

[1]Beth Israel Deaconess Medical Center, Boston, MA, United States, [2]Harvard Medical School, Boston, MA, United States, [3]School of Health Professions, Spinal Movement Biomechanics Group, Bern University of Applied Sciences, Bern, Switzerland, [4]Faculty of Medicine, University of Basel, Basel, Switzerland, [5]Department of Development and Regeneration, Faculty of Medicine, Institute for Orthopaedic Research and Training (IORT), KU Leuven, Leuven, Belgium, [6]F. Joseph Halcomb III, M.D. Department of Biomedical Engineering, University of Kentucky, Lexington, KY, United States

Keywords: motion capture, multi-body modeling, electromyography, spinal pathology, back pain, treatment intervention, prevention

Editorial on the Research Topic

Using Motion Analysis Techniques and Musculoskeletal Modeling of the Spine to Better Understand Spinal Disorders and Evaluate Treatment Effects

OPEN ACCESS

Edited and reviewed by:
Markus O. Heller,
University of Southampton,
United Kingdom

***Correspondence:**
Dennis E. Anderson
danders7@bidmc.harvard.edu

Specialty section:
This article was submitted to Biomechanics, a section of the journal Frontiers in Bioengineering and Biotechnology

Received: *25 February 2022*
Accepted: *16 March 2022*
Published: *06 April 2022*

Citation:
Anderson DE, Schmid S, Scheys L and Bazrgari B (2022) Editorial: Using Motion Analysis Techniques and Musculoskeletal Modeling of the Spine to Better Understand Spinal Disorders and Evaluate Treatment Effects. Front. Bioeng. Biotechnol. 10:884123. doi: 10.3389/fbioe.2022.884123

BACKGROUND OF THE RESEARCH TOPIC

The pathomechanics of many musculoskeletal spinal disorders are still poorly understood, which makes it challenging to develop and apply effective preventive strategies, treatment modalities and rehabilitation plans (Joshi et al., 2019; Taşkıran, 2020). Moreover, the outcomes of currently practiced care pathways are usually evaluated through clinical tests, medical imaging, or questionnaires, whereas the effects on the functional dynamics of the spine remain largely unknown (Matthew et al., 2018; Severijns et al., 2020). For these reasons, this Research Topic aimed at reporting recent efforts to apply key biomechanical analysis techniques, specifically motion analysis and musculoskeletal modeling, to study spinal disorders and their treatments. With advances over the past decade in the fields of motion capture and detailed musculoskeletal modeling of the spine, these approaches have clear potential to provide new insights into onset and progression of spinal disorders, as well as the effects of current treatments, on the biomechanical function of the spine.

To provide a complementary forum for discussion among interested researchers, we organized a virtual symposium and invited interested authors to participate. The symposium was held on 12 May 2021, with a total of 13 presentations on studies in this area from authors of nine different countries and a total of 130 participants from over 20 different countries. The abstracts and videos from this symposium may be found online here: *Motion Analysis and Musculoskeletal Modeling in Treatment of Spinal Disorders.*

OVERVIEW OF THE RESEARCH TOPIC COLLECTION

The Research Topic has a total of 13 papers, including methodological developments in spine motion analysis and modeling, studies of how spinal disorders affect spine biomechanics, and

studies of treatments and interventions. Measurement of spinal motion was a component of eight studies presented here, including six using optoelectronic motion capture, one using inertial measurement units (IMUs), and one using quantitative video fluoroscopy. Three studies used biplanar radiography (the EOS imaging system) to evaluate 3D spinal posture or curvature. Four studies used musculoskeletal models to evaluate spinal loading, and one study used finite element models to evaluate spinal strain. Seven studies examined specific spinal disorders with measurements in patients, including chronic low back pain, lumbar spinal stenosis, adolescent idiopathic scoliosis, and adult spinal deformity. Four studies focused on the effects of treatments, and two on the use of biomechanical loading outcomes to inform prediction or prevention of spine conditions.

DEVELOPMENTS IN MOTION ANALYSIS AND MODELING

Advances in the state of the art for motion capture and musculoskeletal modeling have enabled new studies focused on spinal disorders in recent years, as evidenced by many of the studies in this Research Topic. However, efforts continue to develop and improve these methods. Severijns et al. quantified palpation error on the positioning of spinal markers, and how it would affect estimates of spinal postures. Mediolateral palpation error was larger in adult spinal deformity (ASD) patients than healthy controls, but other errors were similar, and correcting palpation errors improved marker-based estimates of spine curvature. Overbergh et al. examined the test-retest reliability of spinal kinematics evaluated during seated forward bends in ASD patients based on subject-specific kinematic models. Excellent reliability was reported for some range of motion (ROM) outcomes (e.g., lumbar lordosis), but poor for others (e.g., thoracic kyphosis and pelvic tilt), and test-retest variability was greater than operator-induced uncertainty. Fasser et al. presented a procedure for generating subject-specific musculoskeletal models based on bi-planar radiography data (EOS imaging system), using these to set skeletal geometry as well as mass distributions. Breen et al. reported on lumbar intervertebral motions in healthy subjects during flexion and return motions, using quantitative video fluoroscopy. This provides an important reference standard for spinal motion, which is needed for validating other approaches for spinal motion analysis and for future comparison in patients with spinal disorders.

SPINAL DISORDERS AFFECT SPINE MOTION AND LOADING

Several studies reported significant effects of spine disorders on spinal motion or loading. Saad et al. showed that patients with ASD, particularly those with sagittal or hyperkyphotic deformities, adopt different movement strategies than healthy controls during sit-to-stand motions, including maintaining a flexed trunk and more sagittal trunk ROM. Similarly, Christe et al. examined various functional spinal movements in patients with chronic low back pain and found that sagittal movement patterns can distinguish patients from healthy controls, particularly angular velocities which are lower in patients. Finally, Mousavi et al. examined walking in patients with lumbar spinal stenosis. The presence of neurogenic claudication symptoms minimally affected spine motion and posture, but increased estimated lumbar spine loading by 7%.

EVALUATIONS OF POTENTIAL CLINICAL OR PREVENTIVE APPLICATIONS

Two studies examined spine biomechanics in patients with adolescent idiopathic scoliosis, but with different goals. Kinel et al. assessed the ability of patients to perceive and self-correct their posture and 3D spine shape. Most patients were unable to improve their spine shape instinctively, pointing to the need for careful training in appropriate exercises to develop this capacity. Bassani et al. examined the use of biomechanical parameters, including muscle and intervertebral forces, to predict scoliotic curve progression of adolescent idiopathic scoliosis. However, accounting for these measures did not improve the prediction. Huang et al. used motion analysis to quantify the motion during two different cervical manipulations (in healthy people). Two studies included simulations of spinal fusions: Loenen et al. examined the effect of a titanium interbody cage for spinal fusions on strain patterns in patient-specific finite element models, while Rasmussen et al. performed a simulation study of how lumbar fusions affected spinal loading using musculoskeletal models. The latter suggests that lateral or asymmetric lifts are a particular concern, with post-operative increases in loading regardless of surgical approach. Finally, and relevant to prevention of spinal disorders, von Arx et al. used motion capture-driven musculoskeletal full-body models to investigate spinal loads under three types of lifting techniques. Stoop lifting thereby resulted in lower compressive loading compared to squat and freestyle lifting. And even though stoop lifting resulted in higher anterior-posterior shear forces in the mid to upper parts of the lumbar spine, they were the lowest in the L5/S1 segment, which is most frequently affected by degenerative spinal disorders.

CONCLUSION

Collectively, the studies presented in this Research Topic used motion analysis and musculoskeletal modeling to gain new insights into spinal disorders and highlight the potential of these methods for clinical applications. The methodological development studies provide important information on the current state-of-the-art in motion analysis and modeling of the spine and help address limitations that must be overcome for widespread clinical translation of these techniques. The studies of spinal conditions demonstrate that the biomechanical

effects of various spinal conditions are detectable using current biomechanical analysis methods, supporting future efforts to elucidate these effects and translate these methods to clinical applications. Finally, several studies here provide important examples of how biomechanical analyses may be helpful in planning, developing, or optimizing treatments, as well as preventive strategies. As editors of, and contributors to, this topic, we sincerely hope this collection of studies can serve as a roadmap to accelerate translation of motion analysis and modeling to clinical management of spinal disorders and can ultimately lead to design and development of new and more effective interventions for spinal disorders. We look forward to continued efforts over the next few years to leverage the methodological developments and examples found here toward clinical applications in this exciting and emerging field.

REFERENCES

Joshi, R. S., Haddad, A. F., Lau, D., and Ames, C. P. (2019). Artificial Intelligence for Adult Spinal Deformity. *Neurospine* 16, 686–694. doi:10.14245/ns.1938414.207

Matthew, R. P., Seko, S., Bailey, J., Bajcsy, R., and Lotz, J. (2018). "Tracking Kinematic and Kinetic Measures of Sit to Stand Using an Instrumented Spine Orthosis," in Proceedings of IEEE EMBS (IEEE), Honolulu, HI, July 18-21, 2018 1–5. doi:10.1109/embc.2018.8512526

Severijns, P., Overbergh, T., Thauvoye, A., Baudewijns, J., Monari, D., Moke, L., et al. (2020). A Subject-Specific Method to Measure Dynamic Spinal Alignment in Adult Spinal Deformity. *Spine J.* 20, 934–946. doi:10.1016/j.spinee.2020.02.004

Taşkıran, Ö. Ö. (2020). Rehabilitation in Adult Spinal Deformity. *Turk J. Phys. Med. Rehab* 66, 231–243. doi:10.5606/tftrd.2020.6225

AUTHOR CONTRIBUTIONS

DA wrote the initial draft; DA, SS, LS, and BB all contributed equally to editing and revising, and approved the final version to be published.

ACKNOWLEDGMENTS

We express our gratitude for the following sponsors who supported this Research Topic, specifically through funding awards to help cover publication fees for top presenters in the associated virtual symposium: Frontiers in Bioengineering and Biotechnology, Vicon Motion Systems Ltd. (United Kingdom), Medtronic Belgium N.V./S.A., and the NIH-funded National Center for Simulation in Rehabilitation Research (United States).

Conflict of Interest: The authors declare that the research was conducted in the absence of any commercial or financial relationships that could be construed as a potential conflict of interest.

frontiers in Bioengineering and Biotechnology

ORIGINAL RESEARCH
published: 01 June 2021
doi: 10.3389/fbioe.2021.663394

3D Quantitative Evaluation of Posture and Spine Proprioceptive Perception Through Instinctive Self-Correction Maneuver in Adolescent Idiopathic Scoliosis

Edyta Kinel[1]†, Moreno D'Amico[2,3]† and Piero Roncoletta[2]†*

[1] Chair of Rehabilitation and Physiotherapy, Department of Rehabilitation, University of Medical Sciences, Poznań, Poland, [2] SMART LAB (Skeleton Movement Analysis and Advanced Rehabilitation Technologies), Bioengineering & Biomedicine Company Srl, San Giovanni Teatino, Italy, [3] Department of Neuroscience, Imaging and Clinical Sciences, "G. D'Annunzio" University of Chieti-Pescara, Chieti, Italy

OPEN ACCESS

Edited by:
Stefan Schmid,
Bern University of Applied Sciences, Switzerland

Reviewed by:
Sasa Cukovic,
ETH Zürich, Switzerland
Chi-Wen Lung,
Asia University, Taiwan

***Correspondence:**
Edyta Kinel
ekinel@umed.poznan.pl

† These authors have contributed equally to this work and share first authorship

Specialty section:
This article was submitted to Biomechanics, a section of the journal Frontiers in Bioengineering and Biotechnology

Received: 02 February 2021
Accepted: 14 April 2021
Published: 01 June 2021

Citation:
Kinel E, D'Amico M and Roncoletta P (2021) 3D Quantitative Evaluation of Posture and Spine Proprioceptive Perception Through Instinctive Self-Correction Maneuver in Adolescent Idiopathic Scoliosis. Front. Bioeng. Biotechnol. 9:663394. doi: 10.3389/fbioe.2021.663394

Background: Conservative treatment in the adolescent idiopathic scoliosis (AIS) population is based on individual proprioceptive and motor control training. Such training includes physiotherapeutic scoliosis-specific exercises (PSSEs) stimulating the individual capacity to perceive and control his/her posture, particularly the shape of the spine. However, limited knowledge about basic proprioception capability in AIS patients is reported in the literature.

Questions: (1) How do AIS patients, who did not receive any previous specific postural education treatment, perceive their posture and 3D spine shape? Are they able to modify their posture and 3D spine shape correctly through an instinctive self-correction (ISCO) maneuver? (2) Are posture and ISCO maneuver ability gender dependent in AIS patients? (3) Do AIS patients present different posture and spine shape characteristics as well as different ISCO ability compared with the healthy young adult population?

Methods: Cross-sectional observational study. 132 (75 females, 57 males) AIS patients' posture and 3D spine shape have been measured comparing indifferent orthostasis (IO) (neutral erect posture) to ISCO using a non-ionizing 3D optoelectronic stereophotogrammetric approach. Thirteen quantitative biomechanical parameters described the AIS patients body posture. The statistical analysis was performed using a multivariate approach to compare genders in IO, ISCO, and AIS patients vs. healthy young adults–previously published data (57 females, 64 males).

Results: Males (87.7%) and females (93.3%) of AIS patients were unable to modify posture and 3D spine shape globally. AIS patients gender differences were found in IO, ISCO, and the comparison vs. healthy young adults. When changes occurred, subjects could not focus and control their posture globally, but only in a few aspects at a time.

Conclusion: Self-correction maneuver producing an improvement in body posture and spine shape is not instinctive and must be trained. In such characteristics, AIS patients

are not so dissimilar to healthy young adults. Sagittal plane control is the highest, but ISCO in AIS patients led to worsening in this plane. Control at the lumbar level is neglected in both genders. Such outcomes support the necessity of customized PSSEs to treat AIS patients. The 3D stereo-photogrammetric approach is effective in quantitatively describing the subject's posture, motor control, and proprioception.

Keywords: scoliosis, proprioception, posture, spine, self-correction, stereophotogrammetry

INTRODUCTION

The latest literature on conservative treatment in adolescent idiopathic scoliosis (AIS) patients is predominantly based on proper individual proprioceptive (patient's awareness) and motor control training. Such training includes physiotherapeutic scoliosis-specific exercises (PSSEs) stimulating the individual capacity to perceive and control his/her posture, and particularly the shape of the spine. The aim is to reduce spine deformities, limitation of the functional spinal units, and prevent inappropriate posture, improving the stability of the spine through voluntary intervention (Monticone et al., 2014, 2016; Berdishevsky et al., 2016; Kuru et al., 2016; Negrini et al., 2018, 2019; Schreiber et al., 2019). The literature reports that relaxed postures, which are typically adopted, frequently exacerbate low back pain or deformities (O'Sullivan, 2000; O'Sullivan et al., 2002, 2006; Waongenngarm et al., 2015; Bańkosz and Barczyk-Pawelec, 2020; Jung et al., 2020). Usually, young people may be referred to rehabilitation services to enhance body posture consistency and raise awareness about proper posture value (Monticone et al., 2014; Negrini et al., 2018). Teaching the appropriate active self-correction is considered essential in the conservative treatment for idiopathic scoliosis (Czaprowski et al., 2014; Monticone et al., 2014, 2016; Negrini et al., 2018). It has been claimed that one of the factors evaluating the efficacy of corrective interventions for enhancing body posture is the ability to adopt and sustain a correctly balanced body posture when carrying out activities of daily living (Weiss et al., 2006; Monticone et al., 2014, 2016; Negrini et al., 2018). PSSEs are claimed to be more effective than "usual physiotherapy" (Monticone et al., 2014; Negrini et al., 2019) or standard-of-care (observation and bracing) (Kuru et al., 2016; Schreiber et al., 2019) in AIS care. For example, Monticone et al. (2014) used an individualized therapeutic plan involving active self-correction tailored to the type of curve scoliosis for AIS patients. The inclusion criteria for the selection of AIS patients were: Cobb angle of 10°–25°, a Risser sign of <2, and an age of >10 years. The intervention lasted until skeletal maturity had been reached (Risser sign 5). A control group with the same characteristics was provided with general exercises aimed at spinal mobilization, spinal deep muscles strengthening, and lower limb and back muscles stretching, as well as balancing (through proprioceptive training when standing) and walking exercises (mainly devoted to resistance and velocity training). Monticone et al., 2014 found that the individualized therapeutic plan of active self-correction and task-oriented exercises was superior to traditional exercises, leading to a significant improvement in reducing spinal deformities (decrease in Cobb angle of >5°) and enhancing the health-related quality of life (evaluated through the SRS-22 questionnaire) in patients with mild AIS. In contrast, control group subjects stayed stable or had worsening spinal deformities.

No significant changes in the health-related quality of life were documented in the control group. During follow-up, 1 year after the intervention ended, the PSSEs group remained stable, while there was a slight Cobb angle worsening in the control group. The same research group carried on a similar study analyzing adults with idiopathic scoliosis (main Cobb angle <35°) (Monticone et al., 2016). Even in this study, the individualized therapeutic plan involving active self-correction tailored to the type of curve scoliosis resulted superior to general physiotherapy in reducing the disability of adults with idiopathic scoliosis. Additionally, motor and cognitive rehabilitation led to improvement in dysfunctional thoughts, pain, and quality of life. As for the adolescents, changes were maintained for at least 1 year following the intervention. Though the evidence in such randomized controlled studies supports superior effectiveness of the PSSEs approach vs. traditional physiotherapy in AIS treatment, it is still a matter of open debate, which kind of approach should be preferred. Indeed, a recent review (Day et al., 2019) concluded that: there is insufficient evidence to suggest that PSSEs methods can effectively improve Cobb angles in patients with AIS compared with no intervention. On the other hand, a recent study in the healthy young adult population (D'Amico et al., 2018a) showed that: (1) instinctive posture proprioception and motor control do not produce significant global improvement of body posture and spine shape using an instinctive self-correction (ISCO) maneuver; (2) proper and effective self-correction maneuver has to be learned with specific postural training; (3) asymptomatic healthy young adults do not have an optimal posture (D'Amico et al., 2017b, 2018a). However, there is limited knowledge reported in the literature about basic proprioception capability in AIS patients. Therefore, it is essential to analyze whether the problematic management of upright posture in subjects with idiopathic scoliosis can be linked to a further reduction of proprioceptive abilities. From all the above, the following research questions are raised:

(1) How do AIS patients, who did not receive any previous specific postural education treatment, perceive their posture and 3D spine shape? Are they able to correct their posture and 3D spine shape through an ISCO maneuver?

Abbreviations: AIS, adolescent idiopathic scoliosis; PSSEs, physiotherapeutic scoliosis-specific exercises; IO, indifferent orthostasis; ISCO, instinctive self-correction.

(ISCO maneuver was stimulated by asking the subject to assume the best correct self-perceived standing posture without adding any specific indication or feedback).

(2) Are posture and ISCO maneuver ability gender-related in AIS patients?

(3) Do AIS patients present with a different posture and spine shape characteristics and different ISCO ability compared with healthy young adults (D'Amico et al., 2018a)?

MATERIALS AND METHODS

Design

The research presented here is a cross-sectional observational study. We have used a validated, innovative stereophotogrammetric method of 3D quantitative evaluation of the entire skeleton posture and spine shape utilizing an evidence-based medicine approach (D'Amico et al., 2017b, 2018a; Kinel et al., 2018).

The Ethics Committee of the University of Medical Sciences in Poznan, Poland, approved this study. Resolution number: 75/17. All parents of participants had signed a written informed consent before the data collection began.

Data collection took place between February 2017 and 2019.

The Participants

Participants diagnosed with AIS were sent to undergo quantitative 3D posture evaluation by external qualified medical specialists in orthopedics and/or rehabilitation medicine. Before the measurement session, all the interviews and physical examinations were conducted by a single qualified physiotherapist with 16 years of experience (the first-named author) to ensure consistency.

The inclusion/exclusion criteria were as follows: diagnosis of AIS, Cobb angle $\geq 10°$ (Negrini et al., 2018); males and females 11–18 years old; no ongoing brace treatment; no neurologic problems; no history of any previous specific postural education treatment; no history of musculoskeletal system injury or surgery; body weight within the normal range [as classified by Centers for Disease Control and Prevention growth charts for children 2–20 years old (Growth Charts - Clinical Growth Charts, 2019)].

A cohort of 132 AIS patients (75 females and 57 males) was recruited at the Clinic of Rehabilitation, University of Medical Sciences, Poznan, Poland.

The performances of such AIS patients in ISCO are compared with those of 121 healthy young adults, 57 females and 64 males, selected in a previously published research (D'Amico et al., 2018a). AIS patients' and healthy young adults' characteristics are summarized in **Table 1**.

Instrumentation

Our experimental recordings were based on six TV cameras (resolution 1.3 Mpix, 120 fps, error range 0.3 mm, calibrated volume 3 × 3 × 2 meters GOALS[1] (Global Opto-electronic Approach for Locomotion and Spine) stereophotogrammetric opto-electronic system derived from OptiTrack System[2] (D'Amico et al., 2017a). We used one synchronous baropodometric platform[3] to measure bilateral foot pressure maps and underfoot vertical forces exerted on each foot in a standing position. Data processing was performed using a software package named ASAP 3D Skeleton Model[1]. Such processing software implements a complete 3D parametric biomechanical human skeleton model (3D spine included). The bone anthropometric sizes of such a skeleton model fit the 3D opto-electronic measurements of a series of suitable body landmarks to assess the patient's skeleton and posture. A 27 body landmarks protocol, labeled by passive retroreflective markers (**Figure 1**), has been set and tested extensively to analyze human posture in the clinical environment (D'Amico et al., 2017b, 2018a,b; Kinel et al., 2018).

Acquisition Protocol

The standard trial session was aimed to define the participant's indifferent orthostasis (IO) (i.e., maintaining the most natural erect posture). Afterward, the patient was asked to perform his/her instinctive self-corrected orthostasis (ISCO). The ISCO was stimulated by giving a generic command, i.e., requesting the patient to assume his/her best correct self-perceived standing posture without adding any specific indication or feedback. The same generic command was given in D'Amico et al. (2018a) for healthy young adults. As with healthy adults, AIS patients performed the ISCO maneuver effortlessly without reporting any kind of discomfort. Different positions of the feet can influence IO and ISCO postures. The subject was asked to align heels on a line parallel to the frontal plane and keep feet apart (without restricting feet directions) at about pelvis width (i.e., with feet under the hip joints projection) to avoid feet position influence. At least five subsequent 2-second lasting acquisitions at a 120 Hz sampling rate were recorded per each IO and ISCO condition. This way, a minimum of 1,200 3D measurements was averaged per each static postural stance. Averages were computed after defining a subject's local coordinate system and the rotation needed in each acquired frame to align the subject's skeleton 3D reconstruction within the absolute coordinate systems (D'Amico et al., 2017a,b, 2018a; Kinel et al., 2018).

Figures 2, **3** show an example of a graphical report and the data elaboration outcomes of the IO vs. ISCO measurements comparison in the frontal and sagittal planes, respectively. A video showing the acquisition/elaboration processes can be found in the **Supplementary Material** (**Supplementary Video 1**).

Outcome Measures

Based on the 3D biomechanical human skeleton model reconstruction, a set of 13 main significant parameters describing the three-dimensional nature of body posture was computed (D'Amico et al., 2017b, 2018a; Kinel et al., 2018). Such variables were subdivided into three groups, as reported in **Table 2**, where definitions and corresponding acronyms are given. It is worth noting that the signal processing procedure implemented to

[1] Bioengineering & Biomedicine Company S.r.l., Pescara, Italy.

[2] NaturalPoint Inc., Corvallis, OR, United States.

[3] Zebris Gmbh, Isny, Germany.

TABLE 1 | Sample population characteristics: Total of 132 adolescent idiopathic scoliosis (AIS) patients and 121 healthy young adults.

Population Characteristics	AIS patients				Healthy young adults			
	Females (*n* = 75)		Males (*n* = 57)		Females (*n* = 57)		Males (*n* = 64)	
	Range	Mean (SD)	Range	Mean (SD)	Range	Mean (SD)	Range	Mean (SD)
Age (year)	11–18	14.1 (2.1)	11–18	14.2 (2.3)	19–34	23.5 ± 3.2	20–35	24.9 ± 3.9
Height (cm)	140–174	160.9 (6.9)	140–187	166.7 (11.5)	155–175	163.9 ± 5.3	164–190	178.3 ± 6.7
Weight (kg)	32–83	51.1 (9.2)	31–95	58.5 (13.5)	40–71	56.1 ± 7.0	50–90	71.8 ± 8.6
BMI (kg/m^2)	14.8–28.7	19.7 (3.2)	14.5–32.8	20.8 (3.3)	15.6–24.8	20.8 ± 2.0	18.6–24.9	22.5 ± 1.6

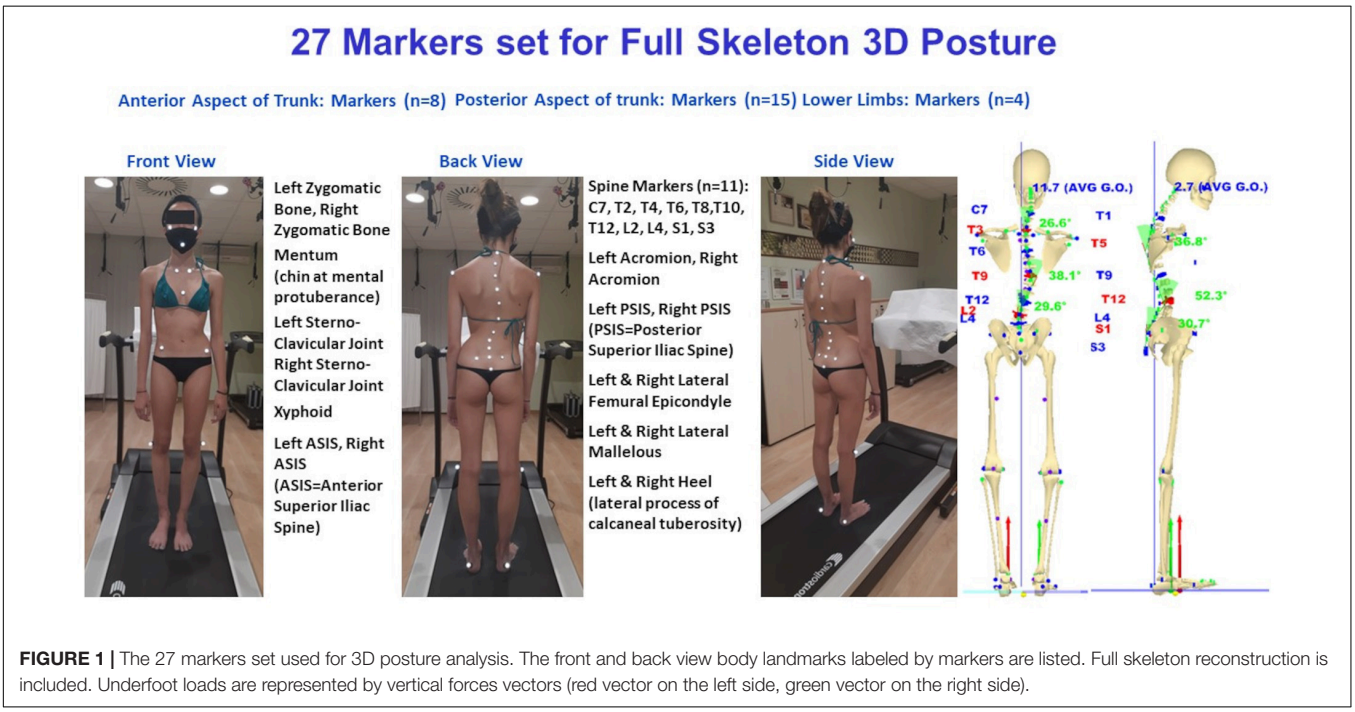

FIGURE 1 | The 27 markers set used for 3D posture analysis. The front and back view body landmarks labeled by markers are listed. Full skeleton reconstruction is included. Underfoot loads are represented by vertical forces vectors (red vector on the left side, green vector on the right side).

analyze the 3D spine shape automatically identifies all the curves present in the frontal and sagittal planes. In particular, based on measurements of the 11 labeled 3D spinous processes (from C7 down to S3 every second vertebra, **Figure 1**), data are interpolated using cubic splines in order to assess the position of each unlabeled spinous process and intervertebral disks. Smoothing is then performed on such noisy interpolated data. Next, the frontal and sagittal spine projections are derived from the filtered 3D analytical representation of the spine. Subsequently, frontal and sagittal spine shape curves are processed separately. The first and second derivative functions are assessed and used to identify the limit-vertebrae (i.e., vertebrae marking the beginning and the end of each identified curve) defined at curve inflection points (where the second derivative is equal to zero). From the values of the first derivative functions (i.e., the tangents' value to the curve) at these inflection points, the Cobb and Kypho–Lordotic angle computations are straightforward per each determined curve. As it happens for the curve identified in the frontal plane, also the kyphosis and lordosis in the sagittal plane are appropriately identified according to the actual spine curvature spatial changes at the limit-vertebrae, i.e., they are no longer restricted to specific thoracic or lumbar anatomical regions (D'Amico et al., 1995, 2017b, 2018a; Kinel et al., 2018).

We decided to consider the Cobb angle value of the two major curves (CA1, CA2, **Table 2**) for statistical analysis regarding the spinal deformities in the frontal plane.

Group Statistical Analysis

Given the verified correlation (through correlation matrices computation) among the considered 13 quantitative postural parameters, the statistical analysis to compare females vs. males, IO vs. ISCO, and AIS patients vs. healthy young adults was performed using a multivariate approach. The paired samples Hotelling's T^2 test was applied in the IO vs. ISCO comparison. Conversely, for the females vs. males and AIS patients vs. healthy young adults, the independent samples Hotelling's T^2 test was used. After Hotelling's tests were performed, the 95% confidence intervals were derived to assess the statistical significance of the difference of the means per each of the 13 quantitative parameters (Rencher, 2003). Such method is preferred over setting a battery of separate *t*-tests for each variable with Bonferroni correction on the type I error ($\alpha' = \alpha/k$) because the latter

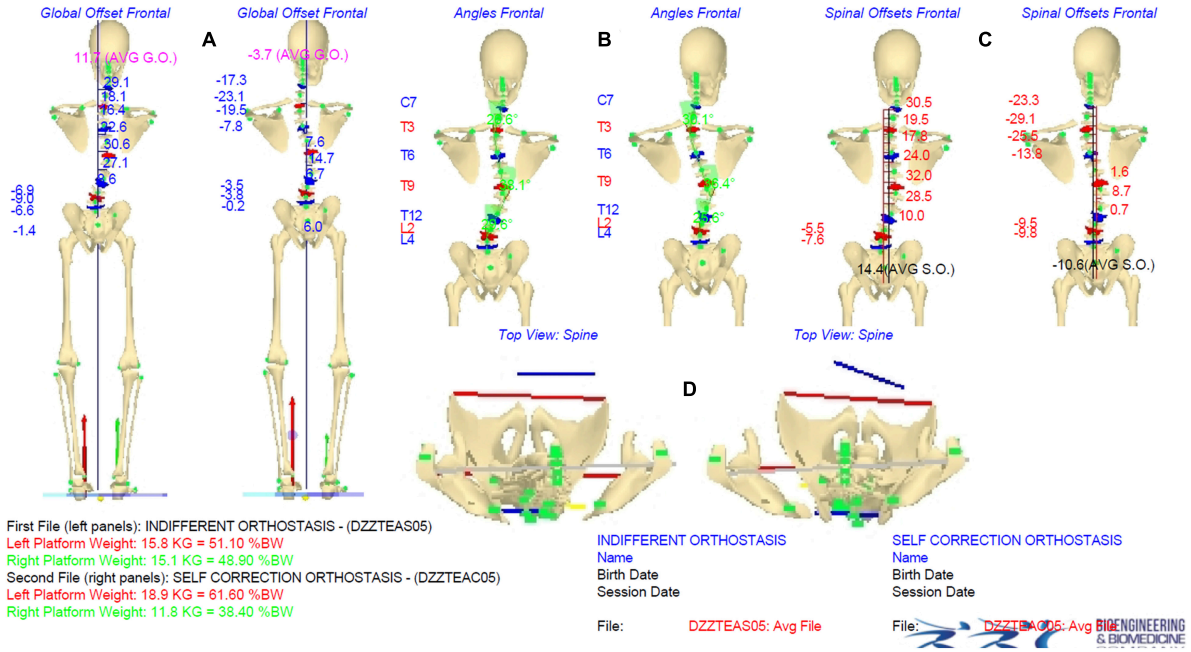

FIGURE 2 | Indifferent orthostasis (IO) vs. instinctive self-correction (ISCO) maneuver comparison graphical report. Panels **(A–C)** show the comparison IO (left side) vs. ISCO (right side) in the frontal plane of averaged global offsets (AGO), spinal deformities, and Cobb angle values, and averaged spinal offsets (ASO), respectively. Panel **(D)** shows comparison IO (left side) vs. ISCO (right side) of rotations in the horizontal plane (shoulder girdle/pelvis). Underfoot loads are represented by vertical forces vectors (red vector on the left side, green vector on the right side) graphically showing the |ΔUL| parameter.

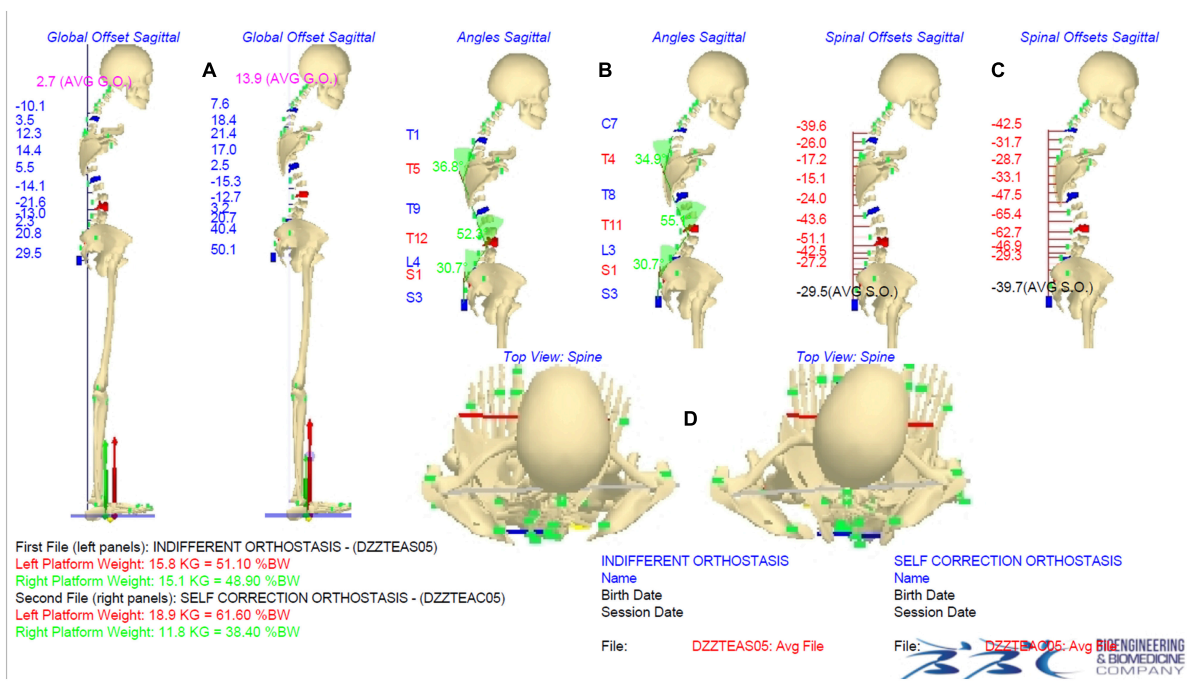

FIGURE 3 | Indifferent orthostasis (IO) vs. instinctive self-correction (ISCO) maneuver comparison graphical report. Panels **(A–C)** show the comparison IO (left side) vs. ISCO (right side) in the sagittal plane of averaged global offsets (AGO-SG), thoracic kyphosis and lumbar lordosis angle values, and averaged spinal offsets (ASO-SG), respectively. Panel **(D)** shows comparison IO (left side) vs. ISCO (right side) of rotations in the horizontal plane (head, shoulder girdle/pelvis, feet positions). Underfoot loads are represented by vertical forces vectors (red vector on the left side, green vector on the right side) graphically showing the |ΔUL| parameter.

TABLE 2 | List of considered parameters (definitions and corresponding acronyms) for indifferent orthostasis (IO) vs. instinctive self-correction (ISCO) comparison and summarizing indexes.

Global summarizing index	Parameters			Specific summarizing indexes
	Acronyms	Descriptions	Definitions	
GPI Global postural index	|ASO| (mm)	|Average frontal spinal offsets|	The ASO is the mean of the horizontal distances in the frontal plane of each labeled spine landmark respect to the vertical axis passing by S3; Absolute value of the average to disregard the side	FPI Frontal postural index
	|AGO| (mm)	|Average frontal global offsets|	The AGO is the mean of the horizontal distances in the frontal plane of each labeled spine landmark respect to the vertical axis passing through the middle point between heels; Absolute value of the average to disregard the side	
	|ΔASIS| (mm)	|ΔAnterior superior iliac spine|	Absolute ASIS height difference in frontal plane	
	|ΔPSIS| (mm)	|ΔPosterior superior iliac spine|	Absolute PSIS height difference in frontal plane	
	CA1; CA2 (degrees)	1°Cobb angle; 2°Cobb angle	Cobb angles of the two main "spinal deformities" found in the frontal plane	
	|PT (mm)|	|Pelvis torsion| = |(ΔASIS-ΔPSIS)|	Rotation of the right with respect to the left innominate bone. Rotations are intended around a horizontal axis running through the symphysis pubis. Absolute value to disregard the side	SPI Sagittal postural index
	ASO SG (mm)	Average sagittal spinal offsets	The ASO SG is the mean of horizontal distances in the sagittal plane of each labeled spine landmark respect to the vertical axis passing by S3; Negative value represent forward leaning	
	AGO SG (mm)	Average sagittal global offsets	The AGO SG is the mean of horizontal distances in the sagittal plane of each labeled spine landmark respect to the vertical axis passing through the middle point between heels; Negative value represent forward leaning	
	SA (degrees)	Sacral angle	The inclination of S1-S3 line with respect to the vertical line	
	TKA (degrees)	"Thoracic" Kyphosis angle	Kyphosis and lordosis are correctly identified following spine curvature spatial changes at inflection points, and so limit vertebrae are not strictly bounded to the specific anatomical region	
	LLA (degrees)	"Lumbar" Lordosis angle		
	|ΔUL| (%BW)	|ΔUnderfoot load|	Left vs. right sides body weight (BW) percentage difference. Absolute value to disregard the side	

approach does not take into account the correlation between the variables, and therefore, it results in an over-correction of the significance value α (Rencher, 2003). Female vs. male comparison was performed in IO to analyze eventual postural gender differences and subsequently in ISCO to investigate a possible different self-correction ability by gender. Comparisons were made between AIS patients and healthy young adults, both in IO and ISCO, to highlight any postural, proprioceptive, and motor control differences.

Intra-Subject Statistical Analysis

At the intra-subject level, we investigated how the ISCO modified the subject's posture by improving, worsening, or unchanging the original attitude. The comparison was performed through a *t*-test between the mean values of 13 considered quantitative parameters obtained per participant in the IO and the ISCO postures.

The actual postural parameter was classified "*Unchanged*" if there was no statistically significant difference.

Conversely, we defined the following as "*Improvement*":

- *Frontal Plane parameters*: when the parameter values approached the optimal theoretical zero value during the ISCO (D'Amico et al., 2018a).
- *Sagittal Plane parameters*: in this case [except for pelvis torsion (|PT|) that should be zero], there are no theoretical optimal reference values, so we decided to consider the normative data determined in previous studies in healthy young adults, for IO and ISCO, as reference values to be approached (D'Amico et al., 2017b, 2018a; Kinel et al., 2018).
- |ΔUL| (*i.e., the difference of underfoot load between the feet*): the optimal theoretical condition is achieved when there is a perfect balance of underfoot load distribution between the left and right sides; therefore, there was "*Improvement*" when changes approached this condition.

"*Worsening*": each time, during the self-correction (ISCO), a statistically significant change differed from the definitions of "*Improvement*," it was concluded that a "*Worsening*" had occurred.

Summarizing Indexes

A summarizing index was defined for each participant, assigning a +1, −1, or 0 scores when an "*Improvement*," a "*Worsening*," or "*Unchanged*" was respectively determined. Henceforth a "Global Postural Index" (GPI_i) given by the sum of scores obtained for all variables for the ith participant was defined. The frontal plane

index (FPI_i) and the sagittal plane index (SPI_i) were defined by the sum of the scores for the variables of the related group (D'Amico et al., 2017b, 2018a; **Table 2**).

Each of the summarizing indexes was regarded as "*Improvement*" if the summed parameters got a positive score ≥50% of the maximum obtainable positive score; conversely, "*Worsening*" if such sum got a negative score ≥50% of the maximum obtainable negative score; "*Unchanged*" in the other cases (D'Amico et al., 2017b, 2018a).

By counting the number of "*Improvement*," "*Worsening*," and "*Unchanged*" obtained for each participant in each parameter, it is possible to determine the percentages of "*Improvement*," "*Worsening*," and "*Unchanged*" achieved in the male and female subgroups.

Power Analysis and Sample Size

Among all the tests, the most critical condition for power analysis is given by the independent Hotelling's T^2 test when applied to AIS patients vs. healthy young adults male groups comparison. In such a case, using GPower software (Faul et al., 2007), given the AIS patients (57 males and 75 females) and healthy young adults (64 males and 57 females) sample sizes, an effect size (Mahalanobis distance) $d = 0.80$ is granted (power = 80%, $\alpha = 5\%$, and $k = 13$ number of variates). Conversely, for the Hotelling's T^2 paired version (IO vs. ISCO in AIS patients), the effect sizes $d = 0.62$ for the male group and $d = 0.53$ for the female group are granted.

RESULTS

Group Statistical Analysis

In the group statistical analysis, we investigated AIS patients gender differences both in IO and ISCO. **Table 3** shows the results of the independent samples Hotelling T^2 test between genders. By considering each variable's confidence intervals, a statistically significant postural difference between genders both in IO and ISCO is determined. It is worth noting that the gender differences in the IO are in seven out of 13 (53.8%) of the considered postural parameters, while they are reduced to four (30.76%) in the ISCO since in such condition, the difference vanishes for the 2nd Cobb angle (CA2), the thoracic kyphosis angle (TKA), and the pelvic torsion (|PT|).

Subsequently, we investigated the postural differences by gender in the IO vs. ISCO comparison through the Hotelling T^2 test for paired samples (**Table 4**). The test demonstrated a statistically significant postural difference between indifferent vs. self-corrected orthostasis.

As a final evaluation, AIS patients vs. healthy young adults were compared by gender (**Table 5**). In such a case, the Hotelling

TABLE 3 | AIS patients female vs. male comparisons in both IO and ISCO: Hotelling T^2 tests results, 95% confidence intervals, and difference of means.

		Hotelling T^2 test for independent samples: female vs. male in IO and ISCO comparison							
		IO ($n1 = 57$, $n2 = 75$, $k = 13$, $T^2 = 51.8$, $p = 8.2e\text{-}5$, $d = 1.26$, power = 0.99)				**ISCO ($n1 = 57$, $n2 = 75$, $k = 13$, $T^2 = 46.5$, $p = 3.1e\text{–}4$, $d = 1.19$, power = 0.99)**			
Parameter	**Descriptions**	**Males Mean**	**Females Mean**	**Difference of Means**	**CI 95% lower ÷ upper**	**Males Mean**	**Females Mean**	**Difference of Means**	**CI 95% lower ÷ upper**
|ASO| (mm)	|Average frontal spinal offsets|	8.1 ± 6.7	7.0 ± 4.9	1.07	−0.93 ÷ 3.07	7.3 ± 5.2	6.7 ± 4.7	0.60	−1.12 ÷ 2.31
|AGO| (mm)	|Average frontal global offsets|	12.4 ± 11.5	11.3 ± 7.4	1.14	−2.13 ÷ 4.41	10.8 ± 9.8	11.0 ± 7.8	−0.20	−3.23 ÷ 2.83
CA1 (degrees)	1°Cobb angle;	15.1 ± 6.9	16.4 ± 8.1	−1.28	−3.92 ÷ 1.35	14.3 ± 7.0	15.4 ± 7.6	−1.11	−3.66 ÷ 1.44
CA2 (degrees)	2°Cobb angle	10.0 ± 5.9	12.4 ± 7.1	**−2.49***	−4.79 ÷ −0.19	10.2 ± 5.8	11.6 ± 7.2	−1.38	−3.69 ÷ 0.94
TKA (degrees)	"Thoracic" Kyphosis angle	47.3 ± 8.5	43.3 ± 10.9	**3.99***	0.54 ÷ 7.45	38.5 ± 10.4	35.2 ± 10.9	3.26	−0.47 ÷ 6.98
LLA (degrees)	"Lumbar" Lordosis angle	39.7 ± 8.3	43.1 ± 9.5	**−3.36***	−6.49 ÷ −0.23	40.1 ± 10.0	43.3 ± 10.2	**−3.15***	−6.66 ÷ −0.36
|ΔASIS| (mm)	|ΔAnterior superior iliac spine|	10.1 ± 8.2	7.8 ± 5.6	2.29	−0.10 ÷ 4.68	9.1 ± 7.1	7.7 ± 6.3	1.39	−0.92 ÷ 3.71
|ΔPSIS| (mm)	|ΔPosterior superior iliac spine|	6.5 ± 4.2	5.6 ± 4.5	0.91	−0.60 ÷ 2.43	6.1 ± 3.9	5.3 ± 3.8	0.76	−0.58 ÷ 2.11
|PT| (mm)	|Pelvis torsion| = | (ΔASIS-ΔPSIS)|	6.7 ± 5.6	5.0 ± 3.6	**1.71***	0.13 ÷ 3.28	6.6 ± 5.1	5.5 ± 5.3	1.11	−0.69 ÷ 2.92
SA (degrees)	Sacral angle	16.8 ± 5.6	18.9 ± 6.3	**−2.12***	−4.22 ÷ −0.03	18.6 ± 5.0	21.1 ± 5.9	**−2.49***	−4.41 ÷ −0.56
ASO SG (mm)	Average sagittal spinal offsets	−14.1 ± 12.8	−24.2 ± 12.6	**10.15***	5.75 ÷ 14.56	−21.7 ± 12.6	−30.7 ± 13.4	**9.02***	4.48 ÷ 13.56
AGO SG (mm)	Average sagittal global offsets	−10.4 ± 23.3	−2.9 ± 19.0	**−7.53***	−14.81 ÷ −0.24	−14.9 ± 24.5	−6.7 ± 19.1	**−8.10***	−15.61 ÷ −0.59
|ΔUL| (%BW)	|ΔUnderfoot load|	6.3 ± 5.2	6.2 ± 3.8	0.09	−1.46 ÷ 1.64	6.9 ± 4.7	7.2 ± 4.2	−0.26	−1.81 ÷ 1.29

*The * associated with bold numbers indicates the statistically significant differences of means.*

TABLE 4 | Per-gender IO vs. ISCO comparisons in AIS patients: Hotelling T^2 tests results, 95% confidence intervals, and difference of means.

		Hotelling T^2 test for paired samples: per-gender IO vs. ISCO comparison							
		Males (n = 57, k = 13, T^2 = 248.6, p = 4e-12, d = 2.08, power = 0.99)				**Females (n = 75, k = 13, T^2 = 123.0, p = 5.2e-9, d = 1.21, power = 0.99)**			
Parameter	**Descriptions**	**IO Mean**	**ISCO Mean**	**Difference of Means**	**CI 95% lower÷upper**	**IO Mean**	**ISCO Mean**	**Difference of Means**	**CI 95% lower ÷ upper**
|ASO| (mm)	|Average frontal spinal offsets|	8.1 ± 6.7	7.3 ± 5.2	0.81	−0.41 ÷ 2.03	7.0 ± 4.9	6.7 ± 4.7	0.34	−0.56 ÷ 1.24
|AGO| (mm)	|Average frontal global offsets|	12.4 ± 11.5	10.8 ± 9.8	1.59	−1.09 ÷ 4.27	11.3 ± 7.4	11.0 ± 7.8	0.26	−1.10 ÷ 1.61
CA1 (degrees)	1°Cobb angle	15.1 ± 6.9	14.3 ± 7.0	0.84	−0.40 ÷ 2.08	16.4 ± 8.1	15.4 ± 7.6	**1.01***	0.09 ÷ 1.94
CA2 (degrees)	2°Cobb angle	10.0 ± 5.9	10.2 ± 5.8	−0.27	−1.15 ÷ 0.60	12.4 ± 7.1	11.6 ± 7.2	0.84	−0.02 ÷ 1.70
TKA (degrees)	"Thoracic" Kyphosis angle	47.3 ± 8.5	38.5 ± 10.4	**8.84***	6.42 ÷ 11.25	43.3 ± 10.9	35.2 ± 10.9	**8.10***	5.20 ÷ 11.01
LLA (degrees)	"Lumbar" Lordosis angles	39.7 ± 8.3	40.1 ± 10.0	−0.41	−3.11 ÷ 2.29	43.1 ± 9.5	43.3 ± 10.2	−0.20	−2.07 ÷ 1.67
|ΔASIS| (mm)	|ΔAnterior superior iliac spine|	10.1 ± 8.2	9.1 ± 7.1	0.96	−0.28 ÷ 2.20	7.8 ± 5.6	7.7 ± 6.3	0.06	−1.06 ÷ 1.19
|ΔPSIS| (mm)	|ΔPosterior superior iliac spine|	6.5 ± 4.2	6.1 ± 3.9	0.38	−0.10 ÷ 0.87	5.6 ± 4.5	5.3 ± 3.8	0.23	−0.26 ÷ 0.73
|PT| (mm)	|Pelvis torsion| = |(ΔASIS-ΔPSIS)|	6.7 ± 5.6	6.6 ± 5.1	0.04	−0.87 ÷ 0.94	5.0 ± 3.6	5.5 ± 5.3	−0.56	−1.81 ÷ 0.69
SA (degrees)	Sacral angle	16.8 ± 5.6	18.6 ± 5.0	**−1.82***	−3.13 ÷ −0.52	18.9 ± 6.3	21.1 ± 5.9	**−2.18***	−3.50 ÷ −0.86
ASO SG (mm)	Average sagittal spinal offsets	−14.1 ± 12.8	−21.7 ± 12.6	**7.60***	4.21 ÷ 10.99	−24.2 ± 12.6	−30.7 ± 13.4	**6.47***	3.55 ÷ 9.38
AGO SG (mm)	Average sagittal global offsets	−10.4 ± 23.3	−14.9 ± 24.5	4.46	−0.36 ÷ 9.28	−2.9 ± 19.0	−6.7 ± 19.1	**3.88***	0.67 ÷ 7.08
|ΔUL| (%BW)	|ΔUnderfoot load|	6.3 ± 5.2	6.9 ± 4.7	−0.64	−2.15 ÷ 0.87	6.2 ± 3.8	7.2 ± 4.2	−1.00	−2.42 ÷ 0.43

*The * associated with bold numbers indicates the statistically significant differences of means.*

T^2 test for independent samples demonstrated a statistically significant postural difference in all four comparisons.

It is worth noting that only for a subset of parameters, the differences are present in both IO and ISCO.

Intra-Subject Statistical Analysis

Table 6 shows results at the intra-subject level. The number of obtained *Improvement*, *Worsening*, and *Unchanged* for each considered parameter is reported, separately by genders, as percentages of the total AIS patients. Each parameter is also referenced to already published healthy young adults values (D'Amico et al., 2018a). Only four for males and five for females, out of 13 parameters, reach up to about 30% or just above in *Improvement*, either in the frontal or sagittal plane, i.e., absolute ASIS height difference in the frontal plane (|ΔASIS|), pelvis torsion (|PT|), sacral angle (SA), and TKA for males; averaged spinal offset (|ASO|), the primary and secondary Cobb angles (CA1, CA2), TKA, and lumbar lordosis angle (LLA) for females. However, *Worsening* shows parameters with a relevant percentage (over 30%), such as |PT| and TKA for males, |PT|, TKA, and the underfoot load difference (|ΔUL|) for females.

From **Table 6**, by simply computing the signed differences concerning the corresponding values determined in healthy young adults, it is possible to compare AIS patients' behavior with that of healthy young adults. For example, looking at the SPI row shows that: *Improvement* percentage is 8% lower; the *Worsening* percentage is 3.3% higher, and the *Unchanged* percentage is 4.7% higher if we compare AIS males with healthy young adults' values.

DISCUSSION

The paper's overall goal was to study ISCO maneuver in AIS patients who did not receive any previous specific postural education treatment. In ISCO, a generic command (i.e., the request to assume the best correct self-perceived standing posture without adding any specific indication or feedback) was given to AIS patients, the same way it was given for healthy young adults (D'Amico et al., 2018a). The reason for this generic command was to evaluate if such patients can perceive and modify their posture and spine shape, in a spontaneous way, without previous conditioning training. Further questions were related to establishing differences by gender, if any, for AIS patients, in IO and ISCO. Finally, AIS patients' posture was compared with healthy young adults' posture to establish if AIS patients presented a compromised ability to perform a self-correction maneuver.

To answer the above questions, we used the advanced non-ionizing real-time optoelectronic stereophotogrammetric measuring method (D'Amico et al., 2017a) that proved to be a very accurate detailed solution in 3D posture analysis and self-correction measurement on a healthy young adult

TABLE 5 | Per-gender AIS patients vs. healthy young adults comparisons in both IO and ISCO: Hotelling T^2 tests results, 95% confidence intervals, and difference of means.

		Hotelling T^2 test for independent samples: AIS patients vs. healthy young adults in IO and ISCO comparison							
		Females							
		IO ($n1$ = 75, $n2$ = 57, k = 13, T^2 = 43.9, p = 6.0e-4, d = 1.16, power = 0.99)				**ISCO ($n1$ = 75, $n2$ = 57, k = 13, T^2 = 66.3, p = 2.1e-6, d = 1.43, power = 0.99)**			
Parameter	**Descriptions**	**AIS patients mean**	**Healthy young adults mean**	**Difference of Means**	**CI 95% lower÷upper**	**AIS patients mean**	**Healthy young adults mean**	**Difference of Means**	**CI 95% lower÷upper**
|ASO| (mm)	|Average frontal spinal offsets|	7.0 ± 4.9	6.5 ± 4.6	0.46	−1.20 ÷ 2.12	6.7 ± 4.7	6.3 ± 4.1	0.35	−1.20 ÷ 1.89
|AGO| (mm)	|Average frontal global offsets|	11.3 ± 7.4	12.1 ± 8.1	−0.78	−3.46 ÷ 1.90	11.0 ± 7.8	11.0 ± 8.1	−0.01	−2.76 ÷ 2.75
CA1 (degrees)	1°Cobb angle;	16.4 ± 8.1	10.3 ± 5.0	**6.09***	3.69 ÷ 8.49	15.4 ± 7.6	9.5 ± 4.8	**5.92***	3.65 ÷ 8.19
CA2 (degrees)	2°Cobb angle	12.4 ± 7.1	7.5 ± 4.1	**4.98***	2.89 ÷ 7.07	11.6 ± 7.2	7.2 ± 3.9	**4.45***	2.36 ÷ 6.54
TKA (degrees)	"Thoracic" Kyphosis angle	43.3 ± 10.9	47.2 ± 8.6	**−3.89***	−7.36 ÷ −0.42	35.2 ± 10.9	40.8 ± 8.7	**−5.63***	−9.12 ÷ −2.15
LLA (degrees)	"Lumbar" Lordosis angle	43.1 ± 9.5	44.2 ± 9.7	−1.12	−4.45 ÷ 2.20	43.3 ± 10.2	43.7 ± 10.4	−0.44	−4.01 ÷ 3.13
|ΔASIS| (mm)	|ΔAnterior superior iliac spine|	7.8 ± 5.6	8.2 ± 5.5	−0.42	−2.37 ÷ 1.52	7.7 ± 6.3	8.0 ± 5.6	−0.32	−2.41 ÷ 1.77
|ΔPSIS| (mm)	|ΔPosterior superior iliac spine|	5.6 ± 4.5	4.8 ± 2.6	0.82	−0.50 ÷ 2.13	5.3 ± 3.8	4.7 ± 2.6	0.63	−0.54 ÷ 1.79
|PT| (mm)	|Pelvis torsion| = |(ΔASIS-ΔPSIS)|	5.0 ± 3.6	5.45 ± 3.9	−0.49	−1.78 ÷ 0.80	5.5 ± 5.3	5.6 ± 4.4	−0.04	−1.69 ÷ 1.61
SA (degrees)	Sacral angle	18.9 ± 6.3	17.3 ± 5.9	1.66	−0.48 ÷ 3.80	21.1 ± 5.9	18.2 ± 5.0	**2.88***	0.95 ÷ 4.80
ASO SG (mm)	Average sagittal spinal offsets	−24.2 ± 12.6	−20.6 ± 11.9	−3.59	−7.87 ÷ 0.68	−30.7 ± 13.4	−23.5 ± 11.6	**−7.18***	−11.58 ÷ −2.78
AGO SG (mm)	Average sagittal global offsets	−2.9 ± 19.0	−1.8 ± 26.7	−1.09	−8.96 ÷ 6.79	−6.7 ± 19.1	−0.4 ± 26.9	−6.36	−14.29 ÷ 1.58
|ΔUL| (%BW)	|ΔUnderfoot load|	6.2 ± 3.8	5.1 ± 4.3	1.10	−0.29 ÷ 2.49	7.2 ± 4.2	5.4 ± 3.7	**1.81***	0.41 ÷ 3.22
		Males							
		IO ($n1$ = 57, $n2$ = 64, k = 13, T^2 = 56.2, p = 3.7e-5, d = 1.36, power = 0.99)				**ISCO ($n1$ = 57, $n2$ = 64, k = 13, T^2 = 54.5, p = 5.7e-5, d = 1.34, power = 0.99)**			
Parameter	**Descriptions**	**AIS patients mean**	**Healthy young adults mean**	**Difference of Means**	**CI 95% lower÷upper**	**AIS patients mean**	**Healthy young adults mean**	**Difference of Means**	**CI 95% lower÷upper**
|ASO| (mm)	|Average frontal spinal offsets|	8.1 ± 6.7	6.2 ± 5.1	1.84	−0.29 ÷ 3.96	7.3 ± 5.2	5.8 ± 4.6	1.44	−0.32 ÷ 3.21
|AGO| (mm)	|Average frontal global offsets|	12.4 ± 11.5	11.6 ± 8.4	0.82	−2.78 ÷ 4.43	10.8 ± 9.8	12.8 ± 8.7	−1.92	−5.26 ÷ 1.41
CA1 (degrees)	1°Cobb angle	15.1 ± 6.9	11.5 ± 5.4	**3.65***	1.45 ÷ 5.86	14.3 ± 7.0	10.4 ± 5.3	**3.89***	1.67 ÷ 6.11
CA2 (degrees)	2°Cobb angle	10.0 ± 5.9	7.2 ± 4.3	**2.72***	0.87 ÷ 4.56	10.2 ± 5.8	7.0 ± 4.7	**3.23***	1.33 ÷ 5.12
TKA (degrees)	"Thoracic" Kyphosis angle	47.3 ± 8.5	45.1 ± 8.9	2.23	−0.92 ÷ 5.38	38.5 ± 10.4	36.4 ± 8.4	2.04	−1.35 ÷ 5.43
LLA (degrees)	"Lumbar" Lordosis angle	39.7 ± 8.3	32.8 ± 8.1	**7.06***	4.09 ÷ 10.03	40.1 ± 10.0	32.3 ± 8.4	**7.81***	4.49 ÷ 11.13
|ΔASIS| (mm)	|ΔAnterior superior iliac spine|	10.1 ± 8.2	7.5 ± 5.3	**2.55***	0.09 ÷ 5.01	9.1 ± 7.1	7.6 ± 5.2	1.48	−0.74 ÷ 3.70
|ΔPSIS| (mm)	|ΔPosterior superior iliac spine|	6.5 ± 4.2	5.1 ± 2.2	**1.42***	0.23 ÷ 2.60	6.1 ± 3.9	5.1 ± 2.2	1.01	−0.13 ÷ 2.14
|PT| (mm)	|Pelvis torsion| = |(ΔASIS-ΔPSIS)|	6.7 ± 5.6	5.3 ± 4.5	1.25	−0.57 ÷ 3.07	6.6 ± 5.1	5.6 ± 4.8	1.00	−0.78 ÷ 2.78
SA (degrees)	Sacral angle	16.8 ± 5.6	15.7 ± 5.5	1.11	−0.88 ÷ 3.10	18.6 ± 5.0	16.8 ± 5.5	1.83	−0.06 ÷ 3.72
ASO SG (mm)	Average sagittal spinal offsets	−14.1 ± 12.8	−14.0 ± 12.4	−0.06	−4.60 ÷ 4.48	−21.7 ± 12.6	−17.4 ± 13.5	−4.22	−8.93 ÷ 0.50
AGO SG (mm)	Average sagittal global offsets	−10.4 ± 23.3	−10.2 ± 21.5	−0.24	−8.29 ÷ 7.81	−14.9 ± 24.5	−8.8 ± 19.4	−6.09	−14.00 ÷ 1.83
|ΔUL| (%BW)	|ΔUnderfoot load|	6.3 ± 5.2	4.5 ± 3.8	**1.74***	0.12 ÷ 3.37	6.9 ± 4.7	5.1 ± 4.5	**1.84***	0.17 ÷ 3.50

*The * associated with bold numbers indicates the statistically significant differences of means.*

TABLE 6 | Intra-subject statistical analysis comparison IO vs. ISCO posture: number of obtained for *Improvement*, *Worsening*, and *Unchanged* for each considered parameter reported, separately per genders, as percentages of the total AIS patients and healthy young adults.

		AIS patients males			**AIS patients females**			**Healthy young adults**		
Parameter	**Descriptions**	***Improvement***	***Worsening***	***Unchanged***	***Improvement***	***Worsening***	***Unchanged***	***Improvement***	***Worsening***	***Unchanged***
|ASO|	|Average frontal spinal offsets|	24.6%	15.8%	59.6%	33.3%	22.7%	44.0%	29.8%	20.7%	49.6%
|AGO|	|Average frontal global offsets|	24.6%	15.8%	59.6%	14.7%	16.0%	69.3%	26.4%	30.6%	43.0%
|ΔASIS|	|ΔAnterior superior iliac spine|	35.1%	17.5%	47.4%	28.0%	18.7%	53.3%	19.8%	14.0%	66.1%
|ΔPSIS|	|ΔPosterior superior iliac spine|	24.6%	10.5%	64.9%	22.7%	24.0%	53.3%	21.5%	19.0%	59.5%
CA1	1°Cobb angle	21.1%	12.3%	66.7%	33.3%	13.3%	53.3%	28.1%	23.1%	48.8%
CA2	2°Cobb angle	12.3%	22.8%	64.9%	34.7%	13.3%	52.0%	25.6%	26.4%	47.9%
|PT|	|Pelvis torsion| = |(ΔASIS-ΔPSIS)|	29.8%	29.8%	40.4%	21.3%	32.0%	46.7%	29.8%	35.5%	34.7%
SA	Sacral angle	42.1%	17.5%	40.4%	25.3%	28.0%	46.7%	35.5%	5.8%	58.7%
TKA	"Thoracic" Kyphosis angle	36.8%	36.8%	26.3%	29.3%	41.3%	29.3%	36.4%	27.3%	36.4%
LLA	"Lumbar" Lordosis angle	26.3%	24.6%	49.1%	29.3%	20.0%	50.7%	20.7%	12.4%	66.9%
|ΔUL|	|ΔUnderfoot load average|	23.3%	27.9%	48.8%	22.0%	40.7%	37.3%	22.5%	27.5%	50.0%
FPI	Frontal postural index	12.3%	3.5%	84.2%	17.3%	4.0%	78.7%	14.0%	9.9%	76.0%
SPI	Sagittal postural index	19.3%	14.0%	66.7%	14.7%	18.7%	66.7%	27.3%	10.7%	62.0%
GPI	Global postural index	7.0%	5.3%	87.7%	4.0%	2.7%	93.3%	6.6%	6.6%	86.8%

population (D'Amico et al., 2018a). The capability of such a method to properly reconstruct and measure the 3D spine shape was discussed for the first time in D'Amico et al. (1995). The agreement between the opto-electronic stereophotogrammetric spine shape reconstruction and x-ray evaluation on scoliotic patients was demonstrated in a comparative study in which both evaluations were performed within minutes of each other (D'Amico and Vallasciani, 1997). More recently, such a method was used to determine the baseline reference normative data of a healthy young adult population, i.e., the physiological standard for 30 selected quantitative 3D parameters that accurately capture and describe a full-skeleton, upright-standing attitude, including spine morphology and pelvic parameters. Such data demonstrated a high agreement with results obtained via other methods as presented in the existing literature. There is firm consistency with the results, especially concerning the spine, obtained via x-ray measurements which at this time are the "gold standard" (D'Amico et al., 2017b; Kinel et al., 2018). Other non-ionizing approaches, such as the rasterstereographic back-surface measurement technique or the recently introduced ultrasound measurement, were excluded because they raise concerns and questions that need further clarification about measurement accuracy and/or the need for the patient to keep a constrained position during the scanning measurement (Kotwicki et al., 2007; Frerich et al., 2012; Takács et al., 2014; Bassani et al., 2019; Wanke-Jellinek et al., 2019; Wu et al., 2020). To note, new recently introduced optical method and software tool (Ćuković et al., 2020) relying on the digitalized dorsal surface associated with a new 3D spine modeling (Ćuković et al., 2015), multiscale and registerable 3D generic spinal model complemented by CAD technologies show a new, hopefully promising technique to improve rastereographic clinical reliability.

Rehabilitation aims to improve the postural performance by stimulating, via proper motor exercises, the proper integration and management in all the components of the central nervous system controlling posture (Weiss et al., 2006; Czaprowski et al., 2014; Monticone et al., 2014, 2016; Kuru et al., 2016; Negrini et al., 2018, 2019; Schreiber et al., 2019). This study's outcomes support the thesis that postural training in AIS patients is needed because of the poor self-correction ability they demonstrate, and it must be individualized. In the group analysis, by considering **Table 4**, it is possible to notice that females present changes in five out of thirteen parameters (38.4%) during the ISCO task. However, for the primary Cobb angle (CA1), the value of change could be considered without clinical relevance resulting in about 1°Cobb angle. Thus, by adding this latter to the unchanged parameters, the *Unchanged* percentage increases to 69.23% of the considered postural parameters.

Moreover, when parameters exhibit statistically significant and clinically relevant value changes (**Table 4**), they show the tendency of a postural worsening. Both genders present a substantial TKA reduction (around 9° in males and 8° in females, respectively), but such reduction induces a further departure from normative values (**Table 5**). Furthermore, a forward unbalancing of both the trunk and global posture is highlighted by the values of SA, averaged spinal offset sagittal (ASO SG), and averaged global offset sagittal (AGO SG) for females parameters (D'Amico et al., 2018a). Conversely, unexpectedly the lumbar level seems to be entirely neglected, in terms of perception and motor control in both genders, in that minimal changes (−0.41° for males and −0.2° for females) occur in ISCO (**Table 4**). Significant modifications of TKA and SA in ISCO were found in healthy young adults (D'Amico et al., 2018a) and healthy adolescents as well (Czaprowski et al., 2014). We confirmed TKA and SA relevant modifications in AIS patients, but our results did not confirm females' better ability to modify their lumbar lordosis than males (Czaprowski et al., 2014). Indeed, we found that the lumbar spine proprioception and control are scarce in both sexes, either in AIS patients or healthy young adults. Statistically significant differences in six parameters over 13 (46.1%) showed a worse posture in AIS male patients than healthy young adults males in IO (**Table 5**). Conversely, AIS patients' females were worse than healthy young adults' females in only three parameters.

As expected, in the frontal plane, the largest and more clinically relevant discrepancies are related to spine deformities, while in the remaining parameters, AIS patients are not so different from healthy young adults, except for the underfoot load difference (|ΔUL|) in male AIS patients. Indeed, this result confirms that healthy young adults' posture is not optimal. Asymmetry (associated with unbalanced posture, uneven underfoot loads, slight spinal curvature in the frontal plane, and pelvis torsion) appears to be a standard in healthy young subjects. Differences in the underfoot distribution between AIS patients and age and BMI matched healthy subjects have been observed during gait, showing differences between feet asymmetries of COP patterns and COP velocities related to scoliosis severity (Gao et al., 2019).

Healthy young males have the same TKA as females but a lower LLA value (D'Amico et al., 2017b, 2018a). On the contrary, LLA in scoliotic males is higher than that in healthy young adult males, and its value is the same as that of AIS females.

On the other hand, scoliotic females have reduced TKA compared with healthy young adult females, but similar LLA. During the self-correction performance, the AIS patients present a different behavior by gender. In females, disparities observed in IO compared with healthy young adults increase in number, while in males, they decrease. Indeed, AIS females worsen their posture showing an increase in the trunk's forward leaning (ASO SG and SA) and an increased underfoot loading unbalancing (|ΔUL|). Conversely, the values of |ΔASIS| and |ΔPSIS| show that AIS males have good pelvis control. In fact, while in the IO, they presented more oblique pelvis than healthy young adults, they performed such a good self-correction that, during such maneuver, they showed no more differences in pelvis obliquity compared with healthy young adults.

Looking at summarizing indexes at intra-subject level analysis, as for healthy young adults (D'Amico et al., 2018a), a high percentage of AIS patients could not modify their 3D posture. These findings are relatively confirmed even when changes are analyzed separately in the frontal or sagittal planes. Remarkably, only 7% of males and 4% of females were able to reach a global improvement. However, when AIS patients performed self-correction maneuvers, they tended to improve those parameters related to scoliotic deformities, pelvic obliquity, and lateral leaning (i.e., where they showed worse disparities vs. healthy young adults in IO), but without reaching relevant clinical changes. Worth noting, such improvements are obtained at the cost of a clinically remarkable sagittal posture worsening: flattening in the trunk and forward posture unbalancing either in the trunk (both genders) or globally (females only).

Indeed, all the above demonstrate that, when changes occurred, participants could not focus and control their posture globally, but they could focus only on a few aspects at a time, individually. The best values of *Improvement* were obtained in the males group in SA (42.1%), TKA (36.8%), and |ΔASIS| (35.1%) while for the females in CA2 (34.7%), CA1 (33.3%), and |ASO| (33.3%). However, even *Worsening* scored high in some parameters. Curiously, males presented in TKA (36.8%) and |PT| (29.8%) the same percentages of *Improvements* and *Worsening*, respectively. Furthermore, for |ΔUL| (27.9% vs. 23.3%) and CA2 (22.8% vs. 12.3%) the *Worsening* outweighs the *Improvements*. For the females, it is possible to see in **Table 6** that the *Worsening* scored higher than improvements in six out of 11 considered postural parameters with TKA and |ΔUL| *Worsening* exceeding 40%. However, the percentage of *Improvement*/*Worsening* of summarizing indexes (FPI, SPI, and GPI) resulted far below those obtained for such single postural parameters. Thus, all these results lead to the deduction that posture perception and control are not an easy task, and it is differently perceived/managed at different parts of the body among participants. The lumbar level shows the largest unmodified behavior. Based on that, it can be argued that specific, focused work, and physical activity is needed (Moon et al., 2013; Monticone et al., 2014; Berdishevsky et al., 2016; Negrini et al., 2018, 2019; Mueller and Niederer, 2020). The same kind of postural control limitation was found in healthy young adults (D'Amico et al., 2018a). For this reason, it can be argued that AIS patients do not present impaired behavior either in proprioception or motor control compared with healthy young adults.

The 3D stereo-photogrammetric approach, together with the implemented 3D entire skeleton model, allows quantifying body posture and 3D spine shape with many numerical parameters. In this study, we chose to consider 13 numerical parameters (**Table 2**) describing the 3D posture and spine shape of AIS patients quantifying the spinal deformities in the frontal plane and the spine curves in the sagittal plane, the global and trunk offsets in the frontal and sagittal planes, the pelvis obliquity and torsion, and the underfoot load distribution.

This approach allows describing posture focusing attention on either specific aspects or at a more global level. The 3D stereo-photogrammetric approach accuracy leads the statistical analysis to discriminate, as statistically significant, differences related to subtle changes accounted for even only about 1°Cobb angle value in spine shape, far below the level of clinical significance.

Nevertheless, there are inherent limitations in the study because we compared populations at different ages, i.e., adolescents and young adults. Results may show different outcomes if healthy adolescent would be compared, so further studies are necessary. A further limitation relates to the fact that we could not include a direct comparison between patients undergoing treatment with PSSEs techniques and a control group treated with a traditional therapy approach in our study. This will be the subject of a future study.

CONCLUSION

The study's clinical relevance is related to the finding that, as found for healthy young adults, the self-correction maneuver is not instinctive in AIS patients but must be learned with specific postural training. Participants were, in general, not able to focus and control their posture globally, but only in a few aspects at a time in an individual way. In such characteristics, AIS patients are not so different from healthy young adults. Some perception of deformity is present in AIS patients for both planes, either frontal or sagittal. There is more attention to the postural control in the sagittal plane (in that relevant modifications are observed); nevertheless, self-correction maneuver led to a worsening in this plane.

Moreover, control on the lumbar level seems to be neglected in both genders. These findings support the necessity of customized PSSEs to treat AIS patients. The personalized PSSEs should aim to stimulate the individual's capacity to perceive and control his/her posture, and particularly the shape of the spine, to reduce spinal deformities, and the limitation of functional spinal units in order to prevent inappropriate posture and improve stability of the spine through voluntary intervention.

The 3D stereo-photogrammetric approach effectively described participants' posture, motor control, and proprioceptive capability. Its routine usage is recommended as a complementary tool for analyzing AIS patients to design a customized PSSE therapy and monitor the treatment efficacy in producing an improved proprioceptive ability.

DATA AVAILABILITY STATEMENT

The raw data supporting the conclusions of this article will be made available by the authors, without undue reservation.

ETHICS STATEMENT

The studies involving human participants were reviewed and approved by The Ethics Committee University of Medical Sciences, Poznan, Poland. Resolution number: 75/17. Written informed consent to participate in this study was provided by the participants' legal guardian/next of kin. Written informed consent was obtained from the minor(s)' legal guardian/next of kin for the publication of any potentially identifiable images or data included in this article.

AUTHOR CONTRIBUTIONS

All authors listed have made a substantial, direct and intellectual contribution to the work, and approved it for publication.

FUNDING

The authors received funding and support in the form of the GOALS System free use and publication fee (if any) coverage from the Bioengineering & Biomedicine Company Srl.

ACKNOWLEDGMENTS

The authors wish to acknowledge the Bioengineering & Biomedicine Company Srl, Italy, for providing the GOALS System use for free, letting the authors freely use it without any limitations to carry out the study measurements to the accomplishment of the present study. The authors wish to thank all the experts for the English language assistance.

SUPPLEMENTARY MATERIAL

The Supplementary Material for this article can be found online at: https://www.frontiersin.org/articles/10.3389/fbioe.2021.663394/full#supplementary-material

REFERENCES

Bańkosz, Z., and Barczyk-Pawelec, K. (2020). Habitual and ready positions in female table tennis players and their relation to the prevalence of back pain. *PeerJ.* 8:e9170. doi: 10.7717/peerj.9170

Bassani, T., Stucovitz, E., Galbusera, F., and Brayda-Bruno, M. (2019). Is rasterstereography a valid noninvasive method for the screening of juvenile and adolescent idiopathic scoliosis? *Eur. Spine J.* 28, 526–535. doi: 10.1007/s00586-018-05876-0

Berdishevsky, H., Lebel, V. A., Bettany-Saltikov, J., Rigo, M., Lebel, A., Hennes, A., et al. (2016). Physiotherapy scoliosis-specific exercises – a comprehensive review of seven major schools. *Scoliosis* 11:20. doi: 10.1186/s13013-016-0076-9

Ćuković, S., Devedžić, G., Luković, V., Anwer, N., Zecevic Lukovic, T., and Karuppasamy, S. (2015). 3D Modeling of Spinal Deformities Shapes Using 5Th Degree B-Splines. *J. Prod. Eng.* 18, 103–106.

Ćuković, S., Taylor, W. R., Heidt, C., Devedžić, G., Luković, V., and Bassani, T. (2020). "Transpositions of Intervertebral Centroids in Adolescents Suffering from Idiopathic Scoliosis Optically Diagnosed," in *Computer Methods, Imaging and Visualization in Biomechanics and Biomedical Engineering Lecture Notes in Computational Vision and Biomechanics*. eds G. A. Ateshian, K. M. Myers, and J. M. R. S. Tavares. (Cham: Springer International Publishing). doi: 10.1007/978-3-030-43195-2_10

Czaprowski, D., Pawłowska, P., Stoliński, L., and Kotwicki, T. (2014). Active self-correction of back posture in children instructed with "straighten

your back" command. *Man. Ther.* 19, 392–398. doi: 10.1016/j.math.2013.10.005

D'Amico, M., D'Amico, G., and Roncoletta, P. (1995). Algorithm for Estimation, Classification and Graphical Representation of Clinical Parameters in the Measurement of Scoliosis and Spinal Deformities by Means of Non-Ionising Device. *Three Dimens. Anal. Spinal Deform.* 15, 33–38. doi: 10.3233/978-1-60750-859-5-33

D'Amico, M., Kinel, E., D'Amico, G., and Roncoletta, P. (2017a). A 3D Spine and Full Skeleton Model for Opto-Electronic Stereo- Photogrammetric Multi-Sensor Biomechanical Analysis in Posture and Gait. Newyork: IEEE. doi: 10.5772/intechopen.68633

D'Amico, M., Kinel, E., and Roncoletta, P. (2017b). Normative 3D opto-electronic stereo-photogrammetric posture and spine morphology data in young healthy adult population. *PLoS One* 12:e0179619. doi: 10.1371/journal.pone.0179619

D'Amico, M., Kinel, E., and Roncoletta, P. (2018a). 3D quantitative evaluation of spine proprioceptive perception/motor control through instinctive self-correction maneuver in healthy young subjects' posture: an observational study. *Eur. J. Phys. Rehabil. Med.* 54, 428–439. doi: 10.23736/S1973-9087.17.04738-4

D'Amico, M., Kinel, E., Roncoletta, P., and D'Amico, G. (2018b). ASAP POSTURE. PLoS One. URL: https://www.protocols.io/view/asap-posture-q5zdy76 [Accessed June 22, 2018]

D'Amico, M., and Vallasciani, M. (1997). Non-ionising opto-electronic measurement and x-ray imaging. two complementary techniques for spinal deformities evaluation and monitoring: results of one year clinical activity. *Stud. Health Technol. Inform.* 37, 151–154. doi: 10.3233/978-1-60750-881-6-151

Day, J. M., Fletcher, J., Coghlan, M., and Ravine, T. (2019). Review of scoliosis-specific exercise methods used to correct adolescent idiopathic scoliosis. *Arch. Physiother.* 9:8. doi: 10.1186/s40945-019-0060-9

Faul, F., Erdfelder, E., Lang, A.-G., and Buchner, A. (2007). G*Power 3: a flexible statistical power analysis program for the social, behavioral, and biomedical sciences. *Behav. Res. Methods* 39, 175–191. doi: 10.3758/BF03193146

Frerich, J. M., Hertzler, K., Knott, P., and Mardjetko, S. (2012). Comparison of radiographic and surface topography measurements in adolescents with idiopathic scoliosis. *Open Orthop. J.* 6, 261–265. doi: 10.2174/1874325001206010261

Gao, C.-C., Chern, J.-S., Chang, C.-J., Lai, P.-L., and Lung, C.-W. (2019). Center of pressure progression patterns during level walking in adolescents with idiopathic scoliosis. *PLoS One* 14:e0212161. doi: 10.1371/journal.pone.0212161

Growth Charts - Clinical Growth Charts (2019). URL: https://www.cdc.gov/growthcharts/clinical_charts.htm [Accessed April 24, 2020].

Jung, K.-S., Jung, J.-H., In, T.-S., and Cho, H.-Y. (2020). Effects of Prolonged Sitting with Slumped Posture on Trunk Muscular Fatigue in Adolescents with and without Chronic Lower Back Pain. *Medicina* 57, 3. doi: 10.3390/medicina57010003

Kinel, E., D'Amico, M., and Roncoletta, P. (2018). Normative 3D opto-electronic stereo-photogrammetric sagittal alignment parameters in a young healthy adult population. *PLoS One* 13:e0203679. doi: 10.1371/journal.pone.0203679

Kotwicki, T., Kinel, E., Stryla, W., and Szulc, A. (2007). Discrepancy in clinical versus radiological parameters describing deformity due to brace treatment for moderate idiopathic scoliosis. *Scoliosis* 2:18. doi: 10.1186/1748-7161-2-18

Kuru, T., Yeldan, İ, Dereli, E. E., Özdinçler, A. R., Dikici, F., and Çolak, İ (2016). The efficacy of three-dimensional Schroth exercises in adolescent idiopathic scoliosis: a randomised controlled clinical trial. *Clin. Rehabil.* 30, 181–190. doi: 10.1177/0269215515575745

Monticone, M., Ambrosini, E., Cazzaniga, D., Rocca, B., and Ferrante, S. (2014). Active self-correction and task-oriented exercises reduce spinal deformity and improve quality of life in subjects with mild adolescent idiopathic scoliosis. Results of a randomised controlled trial. *Eur. Spine J.* 23, 1204–1214. doi: 10.1007/s00586-014-3241-y

Monticone, M., Ambrosini, E., Cazzaniga, D., Rocca, B., Motta, L., Cerri, C., et al. (2016). Adults with idiopathic scoliosis improve disability after motor and cognitive rehabilitation: results of a randomised controlled trial. *Eur. Spine J.* 25, 3120–3129. doi: 10.1007/s00586-016-4528-y

Moon, H. J., Choi, K. H., Kim, D. H., Kim, H. J., Cho, Y. K., Lee, K. H., et al. (2013). Effect of lumbar stabilization and dynamic lumbar strengthening exercises in patients with chronic low back pain. *Ann. Rehabil. Med.* 37, 110–117. doi: 10.5535/arm.2013.37.1.110

Mueller, J., and Niederer, D. (2020). Dose-response-relationship of stabilisation exercises in patients with chronic non-specific low back pain: a systematic review with meta-regression. *Sci. Rep.* 10:16921. doi: 10.1038/s41598-020-73954-9

Negrini, S., Donzelli, S., Aulisa, A. G., Czaprowski, D., Schreiber, S., de Mauroy, J. C., et al. (2018). 2016 SOSORT guidelines: orthopaedic and rehabilitation treatment of idiopathic scoliosis during growth. *Scoliosis* 13:3. doi: 10.1186/s13013-017-0145-8

Negrini, S., Donzelli, S., Negrini, A., Parzini, S., Romano, M., and Zaina, F. (2019). Specific exercises reduce the need for bracing in adolescents with idiopathic scoliosis: a practical clinical trial. *Ann. Phys. Rehabil. Med.* 62, 69–76. doi: 10.1016/j.rehab.2018.07.010

O'Sullivan, P. B. (2000). Masterclass. Lumbar segmental 'instability': clinical presentation and specific stabilizing exercise management. *Man. Ther.* 5, 2–12. doi: 10.1054/math.1999.0213

O'Sullivan, P. B., Grahamslaw, K. M., Kendell, M., Lapenskie, S. C., Möller, N. E., and Richards, K. V. (2002). The effect of different standing and sitting postures on trunk muscle activity in a pain-free population. *Spine* 27, 1238–1244.

O'Sullivan, P. B., Mitchell, T., Bulich, P., Waller, R., and Holte, J. (2006). The relationship beween posture and back muscle endurance in industrial workers with flexion-related low back pain. *Man. Ther.* 11, 264–271. doi: 10.1016/j.math.2005.04.004

Rencher, A. C. (2003). *Methods of Multivariate Analysis*. United States: John Wiley & Sons.

Schreiber, S., Parent, E. C., Hill, D. L., Hedden, D. M., Moreau, M. J., and Southon, S. C. (2019). Patients with adolescent idiopathic scoliosis perceive positive improvements regardless of change in the Cobb angle – Results from a randomized controlled trial comparing a 6-month Schroth intervention added to standard care and standard care alone. SOSORT 2018 Award winner. *BMC Musculoskelet Disord.* 20:319. doi: 10.1186/s12891-019-2695-9

Takács, M., Rudner, E., Kovács, A., Orlovits, Z., and Kiss, R. M. (2014). The Assessment of the Spinal Curvatures in the Sagittal Plane of Children Using an Ultrasound-Based Motion Analysing System. *Ann. Biomed. Eng.* 43, 348–362. doi: 10.1007/s10439-014-1160-z

Wanke-Jellinek, L., Heese, O., Krenauer, A., Würtinger, C., Siepe, C. J., Wiechert, K., et al. (2019). Is there any use? Validity of 4D rasterstereography compared to EOS 3D X-ray imaging in patients with degenerative disk disease. *Eur. Spine J.* 28, 2162–2168. doi: 10.1007/s00586-019-06082-2

Waongenngarm, P., Rajaratnam, B. S., and Janwantanakul, P. (2015). Perceived body discomfort and trunk muscle activity in three prolonged sitting postures. *J. Phys. Ther. Sci.* 27, 2183–2187. doi: 10.1589/jpts.27.2183

Weiss, H.-R., Hollaender, M., and Klein, R. (2006). ADL based scoliosis rehabilitation–the key to an improvement of time-efficiency? *Stud. Health Technol. Inform.* 123, 594–598.

Wu, H.-D., Liu, W., and Wong, M.-S. (2020). Reliability and validity of lateral curvature assessments using clinical ultrasound for the patients with scoliosis: a systematic review. *Eur. Spine J.* 29, 717–725. doi: 10.1007/s00586-019-06280-y

Conflict of Interest: MD'A and PR own shares of the Bioengineering & Biomedicine Company Srl. This does not alter our adherence to Frontiers in Bioengineering and Biotechnology policies on sharing data and materials. The Bioengineering & Biomedicine Company Srl did not play any direct role in the study design, data collection and analysis, decision to publish, or the manuscript preparation.

The remaining author declares that the research was conducted in the absence of any commercial or financial relationships that could be construed as a potential conflict of interest.

frontiers in Bioengineering and Biotechnology

ORIGINAL RESEARCH
published: 23 June 2021
doi: 10.3389/fbioe.2021.687323

Spinal Palpation Error and Its Impact on Skin Marker-Based Spinal Alignment Measurement in Adult Spinal Deformity

Pieter Severijns[1,2†], Thomas Overbergh[1†], Stefan Schmid[3], Lieven Moke[1,4] and Lennart Scheys[1,4]*

[1] Department of Development and Regeneration, Faculty of Medicine, Institute for Orthopaedic Research and Training, KU Leuven, Leuven, Belgium, [2] Department of Rehabilitation Sciences, KU Leuven, Leuven, Belgium, [3] Spinal Movement Biomechanics Group, Division of Physiotherapy, Department of Health Professions, Bern University of Applied Sciences, Bern, Switzerland, [4] Division of Orthopaedics, University Hospitals Leuven, Leuven, Belgium

OPEN ACCESS

Edited by:
Fabio Galbusera, Galeazzi Orthopedic Institute (IRCCS), Italy

Reviewed by:
Qiang Chen, Southeast University, China
Sabine Bauer, University of Koblenz and Landau, Germany

***Correspondence:**
Pieter Severijns
pieter.severijns@kuleuven.be

† These authors have contributed equally to this work and share first authorship

Specialty section:
This article was submitted to Biomechanics, a section of the journal Frontiers in Bioengineering and Biotechnology

Received: *29 March 2021*
Accepted: *31 May 2021*
Published: *23 June 2021*

Citation:
Severijns P, Overbergh T, Schmid S, Moke L and Scheys L (2021) Spinal Palpation Error and Its Impact on Skin Marker-Based Spinal Alignment Measurement in Adult Spinal Deformity. Front. Bioeng. Biotechnol. 9:687323. doi: 10.3389/fbioe.2021.687323

Spinal alignment measurement in spinal deformity research has recently shifted from using mainly two-dimensional static radiography toward skin marker-based motion capture approaches, allowing three-dimensional (3D) assessments during dynamic conditions. The validity and accuracy of such skin marker-based methods is highly depending on correct marker placement. In this study we quantified, for the first time, the 3D spinal palpation error in adult spinal deformity (ASD) and compared it to the error in healthy spines. Secondly, the impact of incorrect marker placement on the accuracy of marker-based spinal alignment measurement was investigated. 3D, mediolateral and inferosuperior palpation errors for thoracolumbar and lumbar vertebral levels were measured on biplanar images by extracting 3D positions of skin-mounted markers and their corresponding anatomical landmarks in 20 ASD and 10 healthy control subjects. Relationships were investigated between palpation error and radiographic spinal alignment (lordosis and scoliosis), as well as body morphology [BMI and soft tissue (ST) thickness]. Marker-based spinal alignment was measured using a previously validated method, in which a polynomial is fit through the marker positions of a motion trial and which allows for radiograph-based marker position correction. To assess the impact of palpation error on spinal alignment measurement, the agreement was investigated between lordosis and scoliosis measured by a polynomial fit through, respectively, (1) the uncorrected marker positions, (2) the palpation error-corrected (optimal) marker positions, and (3) the anatomically corrected marker positions (toward the vertebral body), and their radiographic equivalents expressed as Cobb angles (ground truth), using Spearman correlations and root mean square errors (RMSE). The results of this study showed that, although overall accuracy of spinal level identification was similar across groups, mediolateral palpation was less accurate in the ASD group (ASD_{mean}: 6.8 mm; $Control_{mean}$: 2.5 mm; $p = 0.002$). Significant correlations with palpation error indicated that determining factors for marker misplacement were spinal malalignment, in particular scoliotic deformity ($r = 0.77$; $p < 0.001$), in the ASD group and

body morphology [i.e., increased BMI (r_S = 0.78; p = 0.008) and ST thickness (r_S = 0.66; p = 0.038)] in healthy spines. Improved spinal alignment measurements after palpation error correction, shows the need for radiograph-based marker correction methods, and therefore, should be considered when interpreting spinal kinematics.

Keywords: spinal palpation error, adult spinal deformity, marker-based spinal alignment measurement, marker placement, thoracolumbar, lumbar, spinal level identification, motion analysis

INTRODUCTION

Spinal alignment measurement in spinal deformity research has recently shifted from using mainly two-dimensional (2D) static radiography (Schwab et al., 2012; Smith et al., 2013; Ailon et al., 2015) toward skin marker-based motion capture approaches. This allows three-dimensional (3D) assessment during both static positions and dynamic conditions, including daily life motor tasks (Schmid et al., 2016; Diebo et al., 2018; Severijns et al., 2020, 2021). However, the validity and accuracy of such skin marker-based methods is highly dependent on correct marker placement, which is known to be one of the main sources of variability in kinematic results (Della Croce et al., 2005; Gorton et al., 2009; McFadden et al., 2020). Nevertheless, information on spinal marker placement accuracy (i.e., palpation error) and its possible effect on spinal alignment measurements, in both healthy and deformed spines, is scarce.

Schmid et al. (2015) previously investigated the validity of skin marker-based spinal alignment measurement in adolescent idiopathic scoliosis (AIS) and observed systematic underestimations of the coronal curves. In addition, inaccurate marker placement was found to lead to an underestimation of spinous process-derived thoracolumbar and lumbar curves. Mean 2D palpation error over the entire spine in the inferosuperior and mediolateral direction was 8.2 mm and 1.3 mm, respectively (Schmid et al., 2015). Additionally, Severijns et al. (2020) recently introduced a method to quantify subject-specific spinal alignment in adult spinal deformity (ASD) allowing correction of the skin marker positions toward the positions of the corresponding vertebral bodies. They reported an underestimation of both sagittal and coronal curves when uncorrected skin marker positions were used. However, the impact of correcting the marker positions to their theoretical optimal skin position was not investigated (Severijns et al., 2020).

Data on the accuracy of identifying spinal structures (e.g., spinous processes) through manual palpation is also of importance in the treatment of spinal disorders, for instance to identify symptomatic levels, to assess intervertebral motion or to identify injection locations (Simmonds and Kumar, 1993; Broadbent et al., 2000; Nyberg and Russell Smith, 2013). However, even in non-deformed spines, results on the accuracy and reliability of these palpations are rather inconsistent, possibly due to differences in assessment methods (Haneline and Young, 2009; Kilby et al., 2012). Correct level identifications reported in the literature, varied from 29 to 71% and for mean palpation error values have been reported varying from 2.7 to 19.3 mm (Downey et al., 1999; Broadbent et al., 2000; Harlick et al., 2007; Kilby et al., 2012; Cooper et al., 2013). All these studies report 2D instead of 3D errors and, to the author's knowledge, the palpation error in deformed adult spines specifically has not yet been investigated.

This study therefore aimed at quantifying the 3D spinal palpation error in deformed adult spines and to compare it to the error in healthy non-deformed spines. Moreover, we sought to explore underlying reasons for palpation error by investigating associations with radiographic alignment and body morphology parameters, i.e., the body mass index (BMI) and soft tissue thickness (ST thickness) (Kawchuk et al., 2011). Finally, the impact of incorrect marker placement on marker-based spinal curvature measurement was investigated.

MATERIALS AND METHODS

Participants

Twenty patients with ASD were included from the local outpatient spinal clinic as well as 10 adults with normal spinal alignment (**Table 1**). Inclusion criteria for both groups were a minimum age of 18 years, whereas for the ASD group, participants had to present at least one of the following radiographically confirmed spinal deformity signs: pelvic tilt (PT) $\geq$20°, pelvic incidence minus lumbar lordosis (PI-LL) $\geq$10°, sagittal vertical axis (SVA) $\geq$4 cm, or coronal Cobb angle $\geq$20°. All subjects provided informed consent and the study protocol was approved by the local ethics committee (no. S58082).

Data Collection Procedures

A trained physiotherapist (5 years of experience in motion analysis) equipped all subjects, through manual palpation with the subject standing upright, with six single retro-reflective markers placed on the spinous processes of C7, T5, T9, T12, L3 and on the sacrum (in the middle between left and right posterior superior iliac spine) as well as six clusters, each consisting of three markers, placed on the spinous processes of T1, T3, T7, T11, L2, L4 (Overbergh et al., 2020; Severijns et al., 2020; **Figure 1**). All subjects underwent a full-spine biplanar radiographic examination (EOS imaging, Paris, France) in the finger-on-clavicle position. The subjects were positioned by an experienced staff member of our in-house radiology department, so that the subject coordinate system was as closely aligned as possible with the coordinate system of the EOS system. Subsequently, for all subjects a static motion capture trial was recorded in a standing position with the arms hanging alongside the body in the motion lab (Vicon, Oxford, United Kingdom).

The radiographic images were used to determine the sagittal spinopelvic alignment [PT, PI-LL, SVA and lumbar lordosis (LL)]

TABLE 1 | Subject characteristics, body morphology, and radiography.

	ASD (n = 20)	Control (n = 10)	p-value
Subject characteristics			
Age (year)	60.5 (13.5)	65.0 (8.3)	0.350
Gender (F/M)	14F/6M	7F/3M	1.000
Body morphology			
Height (cm)	163.8 (8.8)	167.5 (16.8)	0.719
Weight (kg)	66.5 (13.6)	63.7 (23.1)	0.510
BMI (kg/m^2)	24.4 (5.1)	22.5 (5.4)	0.281
ST thickness (mm)	21.5 (12.8)	16.9 (9.8)	0.373
Radiographic parameters			
PT (°)	25.1 (12.4)	19.5 (9.9)	0.267
SVA (mm)	31.3 (35.0)	8.8 (13.5)	**0.005**
PI-LL (°)	9.7 (28.0)	−0.4 (14.0)	**0.029**
Coronal (D/T/L/N)	7D/11L/2N	10N	**<0.001**

Medians and interquartile ranges are reported; Significance: $p < 0.05$. BMI, Body Mass Index; F, Female; M, Male; PT, Pelvic tilt; SVA, Sagittal vertical axis; PI, Pelvic incidence; LL, Lumbar lordosis; Coronal, SRS-Schwab Coronal classification; D, Double; T, Thoracic; L, Lumbar; N, No Major Coronal Deformity; ST, Soft tissue.

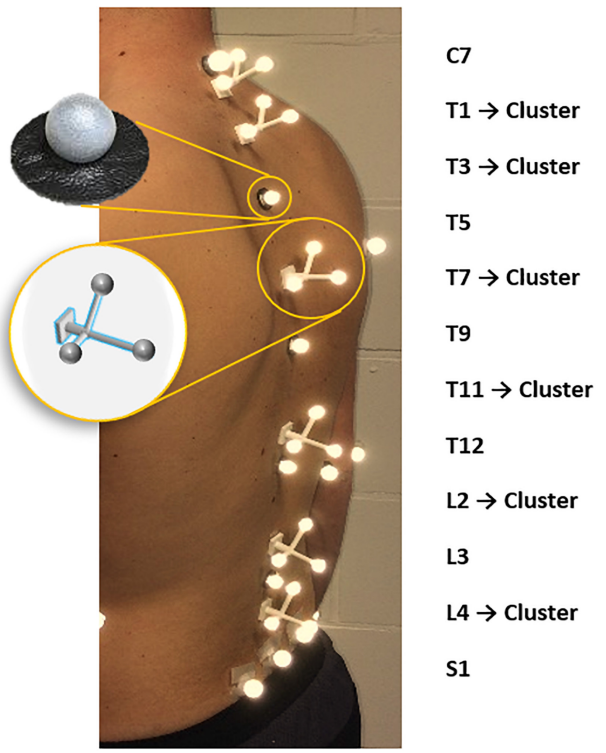

FIGURE 1 | Spinal marker protocol.

as well as the type and severity of the coronal deformation according to the SRS-Schwab coronal classification (Schwab et al., 2012) and the method of Cobb (scoliosis) (Cobb, 1948), respectively. The images also served as data source for the assessment of spinal palpation error (see section "Palpation Error Quantification"; **Figure 2**), whereas the obtained motion capture-based marker trajectories were used to quantify the impact of marker misplacement on spinal alignment measurement (see section "Marker-Based Spinal Alignment Measurement and Impact of Incorrect Marker Placement"; **Figure 3**).

Palpation Error Quantification

Palpation error was only evaluated for thoracolumbar (T11, T12) and lumbar (L2, L3, L4) levels instrumented with a marker, as thoracic spinous process identification on the sagittal radiographic images was restricted by superimposition of other structures, mainly the rib cage.

3D positions of both markers and anatomical landmarks were extracted from biplanar radiographic images. One single person, trained in analyzing radiographic images, manually identified the following three points from the sagittal and coronal radiographic images for each selected vertebral level (Overbergh et al., 2020; **Figure 2**):

A. Spinous process: The most posterior point of the spinous process identified on the sagittal image, as well as, on the same height, the midpoint of the spinous process identified on the coronal image.

B. Actual marker position: The midpoint of the base of the single marker (T12, L3) or marker cluster (T11, L2, L4) identified on both the sagittal and coronal images.

C. Optimal marker position: A theoretically optimal palpation would result in a marker placed as close as possible to the targeted anatomical landmark, i.e., the distance between the marker base and the landmark should be as small as possible to enable optimal tracking. We therefore defined the position on the skin at the closest distance from the spinous process point to the skin surface as the optimal marker position on the sagittal image. Thereto, a circle was centered on the spinous process point whereof the radius was enlarged until the circle edge reaches the skin surface (**Figure 2B**). The midpoint of the spinous process, in the same inferosuperior position as the sagittal defined position, was then defined as the corresponding optimal marker position in the coronal image.

Palpation error was defined as the 3D Euclidean distance between the actual (B.) and optimal (C.) marker positions, which further served as a basis for the calculation of mediolateral and inferosuperior palpation errors. All measurements were performed with respect to the EOS reference axis system. Palpation errors on each marker-instrumented level (T11, T12, L2, L3, L4), as well as the mean and maximum errors were reported. The 3D distance between the spinous process (A.) and the optimal marker position (C.) was used to quantify ST thickness. Maximal ST thickness was reported and used for further analysis (see section "Palpation Error Quantification and Correlations With Radiographic Parameters, BMI and ST Thickness").

When the lower/upper boundary of the marker was above/below the upper/lower boundary of the spinous process, the palpation was identified as an incorrect level identification (Schmid et al., 2016). These were counted per level and the total percentage of incorrect level identifications per group (ASD vs. Control) was calculated.

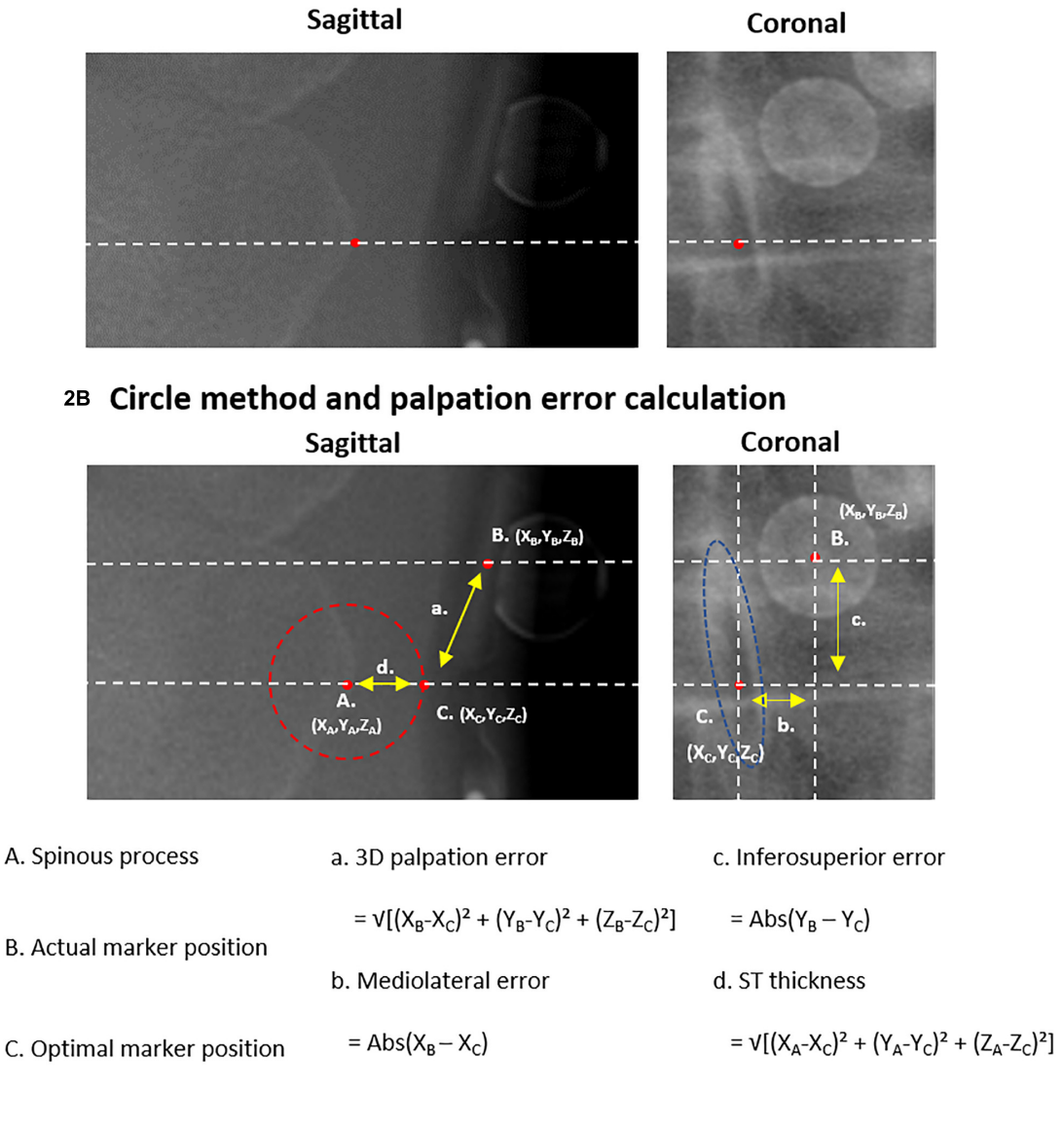

FIGURE 2 | Palpation error. **(A)** The identification of a landmark in the sagittal image with corresponding reference line and landmark identification in the coronal image is displayed. **(B)** Shows the circle-based method to define the theoretical optimal marker position ('C.'). The spinous process ('A.') serves as the center of the circle. The 3D distance between the actual marker position ('B.') and the optimal marker position ('C.') defines the palpation error. 3D, three-dimensional; X, mediolateral axis; Y, inferosuperior axis; Z, anteroposterior axis.

Marker-Based Spinal Alignment Measurement and Impact of Incorrect Marker Placement

Marker-based spinal alignment, namely LL and scoliosis, was measured using a previously validated method, in which a polynomial is fit through the marker positions of a motion trial (Severijns et al., 2020). The method allows for marker position correction using 3D coordinates of both the markers and anatomical landmarks derived from biplanar images (**Figure 3**). The polynomial order (2nd – 7th) was subject-specific and was identified through visual inspection of the best agreement with the corrected 3D marker positions (**Supplementary Figure 1**). More details on this method are reported elsewhere (Severijns et al., 2020). To assess the impact of palpation error on spinal alignment measurement, the agreement was investigated between LL and scoliosis measured by a polynomial fit through (1) the uncorrected marker positions, (2) the palpation error-corrected marker positions (toward the optimal marker position), and (3) the anatomically corrected marker positions

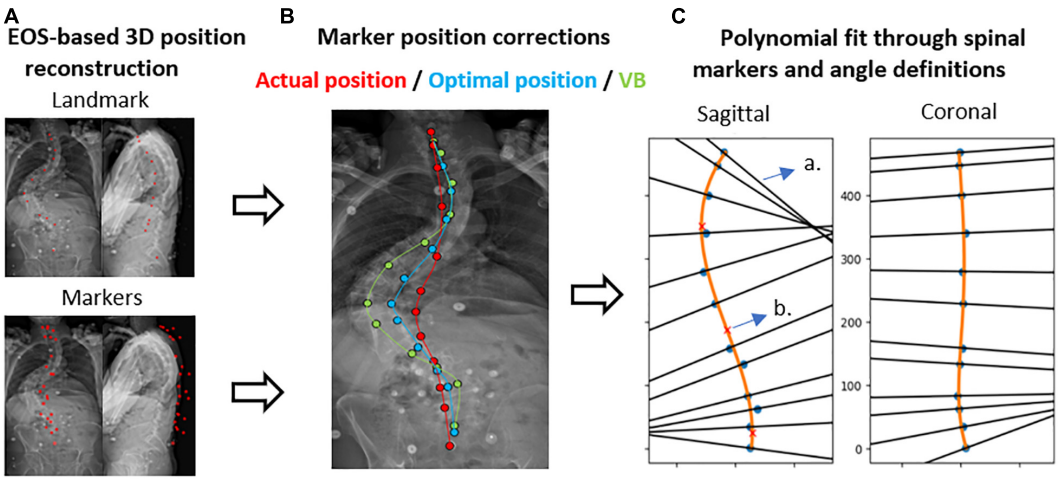

FIGURE 3 | Polynomial method with subject-specific marker position correction. **(A)** Displays the EOS-based 3D reconstruction of markers and (anatomical) landmarks. **(B)** The marker position correction method toward the actual/optimal marker position or the vertebral body (VB) is presented. **(C)** Shows the polynomial fit and spinal angle definitions. a. Normal to the polynomial; b. Inflection point of the curve [figure edited from Severijns et al. (2020)].

(toward the vertebral body), respectively, and their radiographic equivalents (ground truth) as measured with the method of Cobb (1948).

Statistical Analysis

Due to non-normality of a large part of the data (verified by the Shapiro–Wilk test), data were reported as medians and interquartile ranges and all statistical analyses were carried out using non-parametric methods. To compare the subject characteristics, radiographic parameters, palpation error and marker-based spinal alignment parameters between the ASD and control group, Mann–Whitney *U* tests were performed. To compare spinal alignment parameters between different methods within each group, Friedman tests were used. The relationship between marker-based and radiographic spinal alignment measurements were investigated using Spearman correlation coefficients (r_s) and root mean square errors (RMSE). In addition, Spearman correlation coefficients were used to investigate the relationship between the mean palpation error and radiographic parameters (LL and scoliosis), BMI and ST thickness, respectively. Correlation coefficients of less than 0.25 were thereby considered as little to no relationship, from 0.25 to 0.50 as fair, from 0.50 to 0.75 as moderate to good and above 0.75 as good to excellent (Portney and Watkins, 2009). SPSS 26 (IBM Corp., Armonk, NY, United States) was used for statistical analysis. The level of significance was set at $p < 0.05$.

RESULTS

Participants

The ASD and control groups did not differ in age, height, weight, BMI, and gender (**Table 1**). Radiographic parameters showed group differences for SVA (ASD: 31.3 mm; Control: 8.8 mm; $p = 0.005$), PI-LL (ASD: 9.7°; Control: −0.4°; $p = 0.029$), and coronal curve type ($p < 0.001$) but not for ST thickness.

Palpation Error Quantification and Correlations With Radiographic Parameters, BMI and ST Thickness

The 3D palpation error showed no differences between the two groups on any spinal level, nor did the mean or maximum 3D palpation errors (**Table 2**). Comparing the mediolateral and inferosuperior errors separately, on the other hand, revealed larger mediolateral errors in the ASD group for the mean (ASD: 6.8 mm; Control: 2.5 mm; $p = 0.002$) and maximum (ASD: 12.6 mm; Control: 5.0 mm; $p = 0.003$) errors, and more specifically, for the spinal levels T12 (ASD: 8.7 mm; Control: 2.9 mm; $p = 0.007$) and L3 (ASD: 5.8 mm; Control: 2.3 mm; $p = 0.015$). Inferosuperior palpation errors were comparable between the two groups. The percentage of incorrect level identification was 37% for the ASD group, whereby mostly the lumbar levels L2 – L4 were incorrectly identified. In the control group, 32% of the markers were at least one level off, with an equal distribution across all spinal levels.

In the ASD group, the mediolateral palpation error showed a good to excellent relation with scoliosis ($r_s = 0.77$; $p < 0.001$) (**Table 3**). In the control group, the mediolateral palpation error showed a good to excellent relation with BMI ($r_s = 0.78$; $p = 0.008$) and a moderate to good relation with ST thickness ($r_s = 0.66$; $p = 0.038$).

Impact of Marker Misplacement on Marker-Based Spinal Alignment Measurement

Due to problematic marker visibility on biplanar images, necessary for marker position correction, four subjects were excluded from the marker-based spinal alignment measurement.

TABLE 2 | 3D, mediolateral and inferosuperior palpation errors and incorrect level identifications.

	3D palpation error (mm)			Incorrect level identification	
Level	**ASD (*n* = 20)**	**Control (*n* = 10)**	***p*-value**	**ASD**	**Control**
T11	8.9 (16.8)	12.5 (11.4)	0.307	3/20	4/10
T12	15.6 (15.0)	15.2 (11.9)	0.983	3/20	3/10
L2	21.7 (12.9)	13.8 (12.9)	0.055	12/20	4/10
L3	14.0 (12.3)	11.6 (10.0	0.248	10/20	3/10
L4	11.7 (13.6)	11.6 (11.4)	0.914	9/20	2/10
Mean PE	15.5 (9.2)	14.0 (5.8)	0.502	Total:	
Max PE	25.4 (12.0)	19.4 (12.2)	0.100	37%	32%
	Mediolateral palpation error (mm)			**Inferosuperior palpation error (mm)**	
Level	**ASD**	**Control**	***p*-value**	**ASD**	**Control**	***p*-value**
T11	4.6 (8.8)	3.2 (4.6)	0.155	5.0 (6.9)	10.7 (14.3)	0.074
T12	8.7 (16.2)	2.9 (2.4)	**0.007**	8.2 (11.4)	12.6 (12.4)	0.100
L2	8.5 (14.3)	3.1 (3.5)	0.143	15.7 (13.9)	11.4 (7.7)	0.846
L3	5.8 (8.5)	2.3 (3.5)	**0.015**	9.1 (16.9)	10.6 (8.9)	0.530
L4	3.7 (6.2)	2.1 (5.1)	0.422	8.1 (11.5)	9.5 (10.7)	0.502
Mean PE	6.8 (9.1)	2.5 (1.9)	**0.002**	8.1 (9.2)	12.4 (6.1)	0.091
Max PE	12.6 (17.4)	5.0 (4.6)	**0.003**	18.5 (12.0)	18.4 (12.9)	0.948

Medians and interquartile ranges are reported. Significance: $p < 0.05$. 3D, Three-dimensional; PE, Palpation error; Mean, Mean palpation error over the different levels; Max, Maximal palpation error over the different levels.

TABLE 3 | Correlations between mean palpation error and radiographic parameters/body morphology.

	3D palpation error				Incorrect level identifications			
	ASD		**Control**		**ASD**		**Control**	
	r_s	***p*-value**	**r_s**	***p*-value**	**r_s**	***p*-value**	**r_s**	***p*-value**
LL (°)	−0.17	0.466	0.22	0.533	−0.03	0.907	−0.21	0.566
Scoliosis (°)	0.19	0.416	N.A.		−0.24	0.313	N.A.	
BMI (kg/m^2)	0.18	0.443	0.36	0.310	0.15	0.520	0.01	0.972
ST thickness	0.27	0.251	0.13	0.726	0.23	0.324	0.01	0.972
	Mediolateral palpation error				**Inferosuperior palpation error**			
LL (°)	0.34	0.141	−0.08	0.829	−0.22	0.359	0.12	0.751
Scoliosis (°)	0.77	**<0.001**	N.A.		−0.27	0.246	N.A.	
BMI (kg/m^2)	−0.08	0.734	0.78	**0.008**	0.14	0.548	0.26	0.467
ST thickness	0.33	0.158	0.66	**0.038**	0.04	0.865	0.08	0.829

Correlation coefficients are reported. Significance: $p < 0.05$.
3D, Three-dimensional; ASD, Adult Spinal Deformity; r_s, Spearman correlation coefficient; BMI, Body Mass Index; LL, Lumbar Lordosis; ST, Soft tissue; N.A., Not applicable.

The following results are therefore based on a group of 16 patients with ASD and compared to ten control subjects.

Although all methods were able to discriminate ASD from controls on LL measurement, significant differences between methods were observed (**Table 4**). A polynomial through both the uncorrected and palpation error-corrected marker positions resulted in significantly lower LL and scoliosis values compared to radiographic values ($p < 0.001$), except for palpation error-corrected LL values in control subjects.

For LL in the ASD group, a moderate correlation was found between corrected marker-based results and radiographic analysis ($r_s = 0.71$; $p = 0.002$), and a good correlation between uncorrected marker-based results and radiography ($r_s = 0.76$; $p = 0.001$) (**Table 5**). The RMSE was smaller for palpation error correction (RMSE = 21.48°) compared to no correction (RMSE = 27.18°). For scoliosis, correction for palpation error led to an excellent correlation with radiography ($r_s = 0.83$; $p < 0.001$) and a decreased RMSE (30.25°), compared to no correction ($r_s = 0.50$; $p = 0.034$; RMSE = 41.51°). For all parameters and in all groups, a polynomial through the vertebral body positions led to the highest correlation with radiography (LL_{ASD}: $r_s = 0.94$; $LL_{control}$: $r_s = 0.90$; Scoliosis: $r_s = 0.92$;

TABLE 4 | Spinal alignment measurement with radiography and marker-based polynomial measurement, with different levels of marker position correction.

Parameter	ASD (n = 16)	Control (n = 10)	p-value between groups
Lumbar lordosis (°)			
1. Radiography	45.7 (38.9)	59.9 (13.0)	**0.027**
2. Polynomial method:			
a. No correction	22.7 (26.9)	32.9 (9.3)	**0.003**
b. Palpation error correction	26.4 (26.7)	38.6 (11.9)	**0.003**
c. Vertebral body correction	42.6 (38.7)	60.6 (16.6)	**0.017**
p-value between methods	**<0.001**	**<0.001**	
	(2a vs. 1 and 2c) (2b vs. 1 and 2c)	(2a vs. 1 and 2c) (2b vs. 2c)	
Scoliosis (°)			
1. Radiography	48.3 (29.7)	*N/A*	*N/A*
2. Polynomial method:			
a. No correction	7.4 (9.6)	*N/A*	*N/A*
b. Palpation error correction	16.5 (16.4)	*N/A*	*N/A*
c. Vertebral body correction	44.8 (36.9)	*N/A*	*N/A*
p-value between methods	**<0.001**		
	(2a vs. 1 and 2c) (2b vs. 1)		

Median (interquartile range); N/A, Not applicable; Significance: $p < 0.05$.

TABLE 5 | Relation between marker-based spinal alignment measurement and radiographic measurement.

Polynomial method:	Group	Correlation coefficient r_s	p-value	RMSE
Lumbar lordosis (°)				
No correction	Control	0.32	0.365	27.11
	ASD	0.76	**0.001**	27.18
Palpation error correction	Control	0.33	0.347	23.03
	ASD	0.71	**0.002**	21.48
Vertebral body correction	Control	0.90	**<0.001**	4.34
	ASD	0.94	**<0.001**	7.21
Scoliosis (°)				
No correction	ASD	0.50	**0.034**	41.51
Palpation error correction	ASD	0.83	**<0.001**	30.25
Vertebral body correction	ASD	0.92	**<0.001**	9.31

r_s, Spearman correlation coefficient; RMSE, Root mean square error; Significance: $p < 0.05$.

$p < 0.001$), and the smallest RMSE (LL_{ASD}: 7.21; $LL_{control}$: 4.34; Scoliosis: 9.31).

DISCUSSION

In this study, the 3D spinal palpation error and its impact on marker-based spinal alignment measurement were investigated and compared between patients with ASD and healthy controls. The results showed differences in palpation accuracy between deformed and healthy spines, with mean and maximum mediolateral errors of 6.8 mm and 12.6 mm in the ASD group and 2.5 mm and 5.0 mm in the control group, respectively. Furthermore, the mediolateral palpation error showed high correlations with scoliosis in the ASD group, and with BMI and ST thickness in the control group.

The high positive correlation between the mean mediolateral error and scoliosis indicates that the underlying cause of these errors can be assumed to be the deformity itself. Scoliosis is a 3D deformity, including a shift of the vertebral column in the coronal plane and a rotation in the transverse plane (Kim et al., 2010). Consequently, this rotation turns the spinous processes more toward the concave side of the curve, making their location less predictable compared to non-deformed spines. The largest mediolateral palpation errors were observed for spinal levels T12, L2, and L3, which corresponds to the levels where the apex of thoracolumbar/lumbar scoliosis curves is typically located (Lenke, 2007). Since the apex is the point of the curve with the largest coronal shift and the most vertebral rotation, this indeed explains the large mediolateral palpation errors for these spinal levels (Kim et al., 2010).

Surprisingly, in the inferosuperior direction no differences in palpation error were observed between deformed and healthy spines. This was also reflected by the percentages of incorrect level identifications, which were quite similar between both groups (ASD: 37%; Controls: 32%). With 32% in healthy spines, incorrect level identification was lower compared to Harlick et al. (2007), reporting 53% in the lumbar spine, but similar to Cooper et al. (2013), reporting a 29% incorrect palpation of L4. Schmid et al. (2015) reported 42.3% incorrect inferosuperior palpation across all spinal levels and 40% in lumbar levels in AIS, which corresponds to the palpation accuracy in our study in ASD. Comparing palpation errors between studies is challenging due to the heterogeneous methodologies applied in the literature. In this study, a very strict procedure was used, in which one point was identified as the optimal marker location and any deviation from this point was addressed as an error. Since this is, to the best of our knowledge, the first study to assess the 3D distance between actual and optimal spinal marker positions, preventing direct comparisons with the literature, mediolateral and inferosuperior 2D distances were also calculated. Other studies indeed used less strict methods, in which any overlap between the marker and the boundaries of the spinous process was identified as correct palpation (Harlick et al., 2007; Cooper et al., 2013; Schmid et al., 2015). This might explain the differences in mean mediolateral errors between the lumbar results of Schmid et al. (2015) in AIS (0.9 mm) and this study (6.8 mm). Moreover, AIS is characterized by deformities mostly affecting the thoracic spine (Konieczny et al., 2013) in contrast with more thoracolumbar and lumbar deformities in ASD (Acaroğlu et al., 2016), possibly also contributing to the larger lumbar palpation errors in this study.

Although palpation error was found to be mainly related to radiographic parameters in the patient group, mediolateral error in healthy spines instead showed higher correlations

with BMI (r = 0.78) and ST thickness (r = 0.66). Such relation between BMI and ST thickness has been established previously (Kawchuk et al., 2011). Our results extrapolate and confirm the impact of higher BMI and larger ST thickness on palpation accuracy. Also in the ASD group, fair non-significant relations were found between palpation error and ST thickness. ST thickness is known to be increased in the lumbar spine compared to more proximal spinal levels, and changes depending on spinal position (Beaudette et al., 2017). As such, the combination of a lumbar deformity with increased lumbar ST thickness, might explain the relatively higher proportion of incorrect level identifications in the lumbar levels within the ASD group. Controls, having a neutrally positioned lumbar spine, had a more consistent ratio of incorrect level identification over thoracolumbar/lumbar levels. From a clinical perspective, these findings indicate that spinal palpation of lumbar levels for symptomatic level identification (Simmonds and Kumar, 1993) or intervertebral motion assessment (Nyberg and Russell Smith, 2013) is less accurate in deformed spines compared to non-deformed spines. The overall incorrect level identification results (ASD: 37%; Controls: 32%) also stress the importance of medical imaging guidance when identifying spinal levels for injections (Broadbent et al., 2000).

3D measurement of palpation error, allowed us to assess the impact of incorrect marker placement on marker-based spinal alignment measurement using a validated polynomial method with marker position correction (Severijns et al., 2020). As mentioned in the literature (Schmid et al., 2015; Severijns et al., 2020), skin marker-based curve measurement led to an underestimation of radiographic spinal alignment measurements. When correction of palpation error was performed, this underestimation decreased, resulting in higher LL and scoliosis values, and lower RMSEs. For scoliosis, palpation error correction also resulted in an excellent correlation with radiographic results. Although the results confirm that overall, correcting toward the vertebral body positions provides the most accurate results (Severijns et al., 2020), this study shows that incorrect marker placement impacts skin marker-based curve measurement, especially in the coronal plane, and should be considered in kinematic result interpretation when no marker position correction is or can be performed.

A first limitation of this study is that, except for T11 and T12, palpation error of thoracic levels was not investigated. The reason was the superimposition of other structures on radiographic images, mainly the ribcage, preventing a reliable identification of the thoracic spinous processes. Consequently, these levels were not corrected for palpation error in the marker-based spinal alignment measurement. However, since ASD is mainly characterized by thoracolumbar and lumbar deformity (Acaroğlu et al., 2016), the clinically most relevant spinal levels were included in this study. A second limitation is the difference in subject positioning during marker placement (arms alongside the body) and biplanar imaging (fingers on the clavicles), resulting in slight differences in lumbar position (Marks et al., 2009). Consequently, skin motion artifact (Mahallati et al., 2016) cannot be excluded of having led to small differences in marker location during imaging. Indeed, our study design did not allow investigating the effects of skin motion artifacts on marker-based spinal alignment measurement during motion. Future research assessing these artifacts during different positions (semi-static) (Overbergh et al., 2020) or during a range of clinically relevant dynamic movements is required, to further increase confidence in marker-based spinal kinematic results during motion.

In conclusion, this study showed that, although 3D palpation error was similar between deformed and healthy adult spines, mediolateral palpation was less accurate in the ASD group. Overall accuracy of spinal level identification was similar across groups, however, with a larger inaccuracy in lumbar levels within the ASD group. Determining factors for palpation error were spinal malalignment, in particular scoliotic deformity, in deformed spines and body morphology (i.e., increased BMI and ST thickness) in healthy spines. Improved spinal alignment measurements after palpation error correction, shows the need for radiograph-based marker correction methods, and therefore should be considered when interpreting kinematic results.

DATA AVAILABILITY STATEMENT

The raw data supporting the conclusions of this article will be made available by the authors, without undue reservation.

ETHICS STATEMENT

The studies involving human participants were reviewed and approved by the Commissie Medische Ethiek UZ KU Leuven/Onderzoek. The patients/participants provided their written informed consent to participate in this study.

AUTHOR CONTRIBUTIONS

PS collected the data, conceptualized the study, analyzed the data, and wrote the initial manuscript. TO collected the data, conceptualized the study, developed the technical tools necessary for data analysis, and edited the manuscript. SS conceptualized the study and edited the manuscript. LM conceptualized the study and was responsible for subject recruitment. LS conceptualized the study, edited the manuscript, and supervised the project. All authors contributed to the article and approved the submitted version.

FUNDING

This study was funded by the KU Leuven C2 funds, Medtronic, and a strategic basic research grant (SB/1S56017N) of the Research Foundation – Flanders (FWO). The funder had no role in study design and collection, analysis, and interpretation of the results.

ACKNOWLEDGMENTS

The authors would like to thank Kristel Van de Loock and Rowie De Buysscher for their participation in the data management and Michiel Brandt for his contribution to the data processing.

SUPPLEMENTARY MATERIAL

The Supplementary Material for this article can be found online at: https://www.frontiersin.org/articles/10.3389/fbioe.2021.687323/full#supplementary-material

REFERENCES

Acaroğlu, R. E., Dede, Ö, Pellisé, F., Güler, Ü. O., Domingo-Sàbat, M., Alanay, A., et al. (2016). Adult spinal deformity: a very heterogeneous population of patients with different needs. *Acta Orthop. Traumatol. Turc.* 50, 57–62. doi: 10.3944/AOTT.2016.14.0421

Ailon, T., Smith, J. S., Shaffrey, C. I., Lenke, L. G., Brodke, D., Harrop, J. S., et al. (2015). Degenerative spinal deformity. *Neurosurgery* 77, S75–S91. doi: 10.1227/NEU.0000000000000938

Beaudette, S. M., Zwambag, D. P., Bent, L. R., and Brown, S. H. M. (2017). Spine postural change elicits localized skin structural deformation of the trunk dorsum in vivo. *J. Mech. Behav. Biomed. Mater.* 67, 31–39. doi: 10.1016/j.jmbbm.2016.11.025

Broadbent, C. R., Maxwell, W. B., Ferrie, R., Wilson, D. J., Gawne-Cain, M., and Russell, R. (2000). Ability of anaesthetists to identify a marked lumbar interspace. *Anaesthesia* 55, 1122–1126. doi: 10.1046/j.1365-2044.2000.01547-4.x

Cobb, J. (1948). Outline for the study of scoliosis. *Am. Acad. Orthop. Surg. Instr. Course Lect.* 5, 261–275.

Cooper, K., Alexander, L., Hancock, E., and Smith, F. W. (2013). The use of pMRI to validate the identification of palpated bony landmarks. *Man. Ther.* 18, 289–293. doi: 10.1016/j.math.2012.10.005

Della Croce, U., Leardini, A., Chiari, L., and Cappozzo, A. (2005). Human movement analysis using stereophotogrammetry part 4: assessment of anatomical landmark misplacement and its effects on joint kinematics. *Gait Posture* 21, 226–237. doi: 10.1016/j.gaitpost.2004.05.003

Diebo, B. G., Shah, N. V., Pivec, R., Naziri, Q., Patel, A., Post, N. H., et al. (2018). From static spinal alignment to dynamic body balance: utilizing motion analysis in spinal deformity surgery. *JBJS Rev.* 6:e3. doi: 10.2106/JBJS.RVW.17.00189

Downey, B. J., Taylor, N. F., and Niere, K. R. (1999). Manipulative physiotherapists can reliably palpate nominated lumbar spinal levels. *Man. Ther.* 4, 151–156. doi: 10.1054/math.1999.0196

Gorton, G. E., Hebert, D. A., and Gannotti, M. E. (2009). Assessment of the kinematic variability among 12 motion analysis laboratories. *Gait Posture* 29, 398–402. doi: 10.1016/j.gaitpost.2008.10.060

Haneline, M. T., and Young, M. (2009). A review of intraexaminer and interexaminer reliability of static spinal palpation: a literature synthesis. *J. Manip. Physiol. Ther.* 32, 379–386. doi: 10.1016/j.jmpt.2009.04.010

Harlick, J. C., Milosavljevic, S., and Milburn, P. D. (2007). Palpation identification of spinous processes in the lumbar spine. *Man. Ther.* 12, 56–62. doi: 10.1016/j.math.2006.02.008

Kawchuk, G. N., Prasad, N., Parent, E., Chapman, S., Custodio, M., Manzon, M., et al. (2011). Spinal landmark depth in relation to body mass index. *Man. Ther.* 16, 384–387. doi: 10.1016/j.math.2011.01.007

Kilby, J., Heneghan, N. R., and Maybury, M. (2012). Manual palpation of lumbo-pelvic landmarks: a validity study. *Man. Ther.* 17, 259–262. doi: 10.1016/j.math.2011.08.008

Kim, H., Kim, H. S., Moon, E. S., Yoon, C.-S., Chung, T.-S., Song, H.-T., et al. (2010). Scoliosis imaging: what radiologists should know. *Radiographics* 30, 1823–1842. doi: 10.1148/rg.307105061

Konieczny, M. R., Senyurt, H., and Krauspe, R. (2013). Epidemiology of adolescent idiopathic scoliosis. *J. Child. Orthop.* 7, 3–9. doi: 10.1007/s11832-012-0457-4

Lenke, L. G. (2007). The lenke classification system of operative adolescent idiopathic scoliosis. *Neurosurg. Clin. N. Am.* 18, 199–206. doi: 10.1016/j.nec.2007.02.006

Mahallati, S., Rouhani, H., Preuss, R., Masani, K., and Popovic, M. R. (2016). Multisegment kinematics of the spinal column: soft tissue artifacts assessment. *J. Biomech. Eng.* 138:071003. doi: 10.1115/1.4033545

Marks, M., Stanford, C., and Newton, P. (2009). Which lateral radiographic positioning technique provides the most reliable and functional representation of a patient's sagittal balance? *Spine* 34, 949–954. doi: 10.1097/BRS.0b013e318199650a

McFadden, C., Daniels, K., and Strike, S. (2020). The sensitivity of joint kinematics and kinetics to marker placement during a change of direction task. *J. Biomech.* 101:109635. doi: 10.1016/j.jbiomech.2020.109635

Nyberg, R. E., and Russell Smith, J. (2013). The science of spinal motion palpation: a review and update with implications for assessment and intervention. *J. Man. Manip. Ther.* 21, 160–167. doi: 10.1179/2042618613Y.0000000029

Overbergh, T., Severijns, P., Beaucage-Gauvreau, E., Jonkers, I., Moke, L., and Scheys, L. (2020). Development and validation of a modeling workflow for the generation of image-based, subject-specific thoracolumbar models of spinal deformity. *J. Biomech.* 110:109946. doi: 10.1016/j.jbiomech.2020.109946

Portney, L. G., and Watkins, M. P. (2009). *Foundations of Clinical Research: Application to Practice*. Upper Saddle River, NJ: Prentice Hall.

Schmid, S., Studer, D., Hasler, C.-C., Romkes, J., Taylor, W. R., Brunner, R., et al. (2015). Using skin markers for spinal curvature quantification in main thoracic adolescent idiopathic scoliosis: an explorative radiographic study. *PLoS One* 10:e0135689. doi: 10.1371/journal.pone.0135689

Schmid, S., Studer, D., Hasler, C. C., Romkes, J., Taylor, W. R., Lorenzetti, S., et al. (2016). Quantifying spinal gait kinematics using an enhanced optical motion capture approach in adolescent idiopathic scoliosis. *Gait Posture* 44, 231–237. doi: 10.1016/j.gaitpost.2015.12.036

Schwab, F., Ungar, B., Blondel, B., Buchowski, J., Coe, J., Deinlein, D., et al. (2012). SRS-Schwab adult spinal deformity classification: a validation study. *Spine* 37, 1077–1082. doi: 10.1097/BRS.0b013e31823e15e2

Severijns, P., Moke, L., Overbergh, T., Beaucage-Gauvreau, E., Ackermans, T., Desloovere, K., et al. (2021). Dynamic sagittal alignment and compensation strategies in adult spinal deformity during walking. *Spine J.* doi: 10.1016/j.spinee.2021.02.017

Severijns, P., Overbergh, T., Thauvoye, A., Baudewijns, J., Monari, D., Moke, L., et al. (2020). A subject-specific method to measure dynamic spinal alignment in adult spinal deformity. *Spine J.* 20, 934–946. doi: 10.1016/j.spinee.2020.02.004

Simmonds, M. J., and Kumar, S. (1993). Health care ergonomics part II: location of body structures by palpation - a reliability study. *Int. J. Ind. Ergon.* 11, 145–151. doi: 10.1016/0169-8141(93)90008-2

Smith, J. S., Shaffrey, C. I., Fu, K.-M. G., Scheer, J. K., Bess, S., Lafage, V., et al. (2013). Clinical and radiographic evaluation of the adult spinal deformity patient. *Neurosurg. Clin. N. Am.* 24, 143–156. doi: 10.1016/j.nec.2012.12.009

Conflict of Interest: The authors declare that the research was conducted in the absence of any commercial or financial relationships that could be construed as a potential conflict of interest.

frontiers in Bioengineering and Biotechnology

ORIGINAL RESEARCH
published: 26 July 2021
doi: 10.3389/fbioe.2021.714292

Mechanical Parameters and Trajectory of Two Chinese Cervical Manipulations Compared by a Motion Capture System

Xuecheng Huang[1,2,3,4†], Dongxin Lin[1,2,3†], Zeyu Liang[1,2,3†], Yuping Deng[1,2,3], Zaopeng He[5], Mian Wang[1,2,3], Jinchuan Tan[1,2,3], Yikai Li[6], Yang Yang[1,2,3] and Wenhua Huang[1,2,3*]*

[1] National Key Discipline of Human Anatomy, School of Basic Medical Sciences, Southern Medical University, Guangzhou, China, [2] Guangdong Engineering Research Center for Translation of Medical 3D Printing Application, Southern Medical University, Guangzhou, China, [3] Guangdong Provincial Key Laboratory of Medical Biomechanics, Southern Medical University, Guangzhou, China, [4] Shenzhen Hospital of Guangzhou University of Chinese Medicine, Shenzhen, China, [5] Hand and Foot Surgery and Plastic Surgery, Affiliated Shunde Hospital of Guangzhou Medical University, Foshan, China, [6] School of Chinese Medicine, Southern Medical University, Guangzhou, China

OPEN ACCESS

Edited by:
Stefan Schmid,
Bern University of Applied Sciences, Switzerland

Reviewed by:
William Ray Reed,
University of Alabama at Birmingham, United States
Wenxin Niu,
Tongji University, China

***Correspondence:**
Yang Yang
15625055563@163.com
Wenhua Huang
huangwenhua2009@sina.com

† These authors have contributed equally to this work and share first authorship

Specialty section:
This article was submitted to Biomechanics, a section of the journal Frontiers in Bioengineering and Biotechnology

Received: 25 May 2021
Accepted: 29 June 2021
Published: 26 July 2021

Citation:
Huang X, Lin D, Liang Z, Deng Y, He Z, Wang M, Tan J, Li Y, Yang Y and Huang W (2021) Mechanical Parameters and Trajectory of Two Chinese Cervical Manipulations Compared by a Motion Capture System. Front. Bioeng. Biotechnol. 9:714292. doi: 10.3389/fbioe.2021.714292

Objective: To compare the mechanical parameters and trajectory while operating the oblique pulling manipulation and the cervical rotation–traction manipulation.

Methods: An experimental research measuring kinematics parameter and recording motion trajectories of two cervical manipulations were carried out. A total of 48 healthy volunteers participated in this study, who were randomly divided into two groups of 24 representing each of the two manipulations. A clinician performed two manipulations in two groups separately. A motion capture system was used to monitor and analyze kinematics parameters during the operation.

Results: The two cervical manipulations have similar thrust time, displacement, mean velocity, max velocity, and max acceleration. There were no significant differences in active and passive amplitudes between the two cervical rotation manipulations. The thrust amplitudes of the oblique pulling manipulation and the cervical rotation–traction manipulation were $5.735 \pm 3.041°$ and $2.142 \pm 1.742°$, respectively. The thrust amplitudes of the oblique pulling manipulation was significantly greater than that of the cervical rotation–traction manipulation ($P < 0.001$).

Conclusion: Compared with the oblique pulling manipulation, the cervical rotation–traction manipulation has a less thrust amplitudes.

Keywords: motion capture, cervical spondylotic radiculopathy, cervical rotation manipulation, thrust range of motion, active range of motion, passive range of motion

INTRODUCTION

Cervical spinal manipulation is proven to be effective in improving the range of motion of the cervical spine and relieve pain (Bronfort et al., 2004; Vernon and Humphreys, 2008), largely due to its high-speed and low-amplitude (HVLA) operating characteristics (Galindez-Ibarbengoetxea et al., 2017; Gómez et al., 2020). HVLA techniques can be defined as it uses low amplitude, high speed thrusts where the vertebrae are taken out of their normal physiological range of motion without surpassing the boundary of anatomical integrity (Giacalone et al., 2020). HVLA techniques

has a positive effect on reducing neck pain (Ruiz-Sáez et al., 2007), increasing cervical spine mobility (Martínez-Segura et al., 2006), and improving posture (Smith and Mehta, 2008) by acting on the facet joints and soft tissues including muscles and ligaments. However, manipulations are greatly diverse, and lack of diagnoses, therapeutic standards, and complete evaluation systems which are used for the mechanical parameters and safety indexes. This dilemma limits the development and communication of CSM and predisposes to serious complications of the various structures involved in cervical spine injury, mainly including soft tissue injury, aggravation of disk herniation, and even spinal cord injury (Gorrell et al., 2016; Nielsen et al., 2017; Kranenburg et al., 2017a,b).

Therefore, it is of considerable importance to determine the key biomechanical parameters of the operation (Herzog, 2010). Cervical rotation manipulation (CRM) is one of the cervical spine manipulation techniques, which has a long history and is widely used in China (Zhu et al., 2005). The oblique pulling manipulation (Zhang and Gu, 2014) and the rotation–traction manipulation (Huang et al., 2017) both are CRM, and they are commonly used operations in clinical practice (Anderst et al., 2018). From a kinematic point of view, the process of any CRMs involve first flexing and rotating the cervical spine to a specific angle and then applying a rotational force that causes slight displacement of adjacent tissues, such as vertebrae and disks in the space. Here, "force, direction, angle, speed, displacement, and time" constitute the essence of the manipulation effect. Consequently, quantifying the operational characteristics of the CRM will help to standardize it and indirectly ensure its therapeutic effect (Triano et al., 2003; Needham et al., 2016).

Motion capture is currently widely used in the animation industry and sport medical biomechanics (Menolotto et al., 2020). Optical systems have been considered the gold standard for motion capture in the literature (van der Kruk and Reijne, 2018). It is a precision device for accurately measuring, capturing, and recording the motion of moving objects in a spatial coordinate system that has emerged in the last decade. It can be used to extract and analyze trajectories and characteristics of movements during an operation, resulting in very accurate measurements of technical specifications that can guide clinicians and serve as the basis for mechanistic studies (Boser et al., 2018). When the motion capture object is a real person, the marker is typically a human anatomical bone process or joint, and the corresponding model and identification is localized (Liu et al., 2020). Motion capture devices can track and record motion data for each marker including the trajectory, speed, acceleration, and angle of each joint of the body. Therefore, we take the unique advantage of the optical motion capture system to compare the mechanical parameters and trajectories when operating the oblique pulling manipulation and the cervical rotation-traction manipulation.

MATERIALS AND METHODS

A total of 48 volunteers (20 women and 28 men) aged from 24 to 30 years old, who had no pathological changes after X-ray examination, were selected. They were randomly divided into the group of the oblique pulling manipulation and the group of the rotation–traction manipulation. A total of 24 subjects were in each group. A senior clinician was involved in the study. Before the experiment, the volunteers were massaged on the neck for 5–10 min to relax and were informed and familiar with the entire experimental process. All subjects signed informed consent before participation, and the project was approved by the Medical Ethics Committee of Shunde Hospital, Guangzhou Medical University.

Instrumentation

The digital motion capture system was composed of 12 sets of infrared motion capture cameras (model: Miqus M3, origin: Qualisys, Sweden; full view standard model: 2 million pixels, 340 FPS sampling rate; full view model: 500,000 pixels, 650 FPS sampling rate; 0.1 mm accuracy), which were placed throughout the room to collect the kinematics data. Visual 3D software (origin: C-Motion) was used to analyze and rebuild the three-dimensional images.

Procedures

Field Calibration

This study was implemented at the Southern Medical University of Basic Medicine. First, an L-shaped calibrator (including three points and two gradienters) was used to perform static calibration for the horizontal plane and the origin of coordinates. Then, a T-shaped calibrator (comprising three points) was used to perform the dynamic calibration by waving the calibrator constantly in the experimental site. The three-dimensional space Cartesian coordinate system was defined through the calibration of the horizontal, coordinate, and origin space. The *X*-axis represents the frontal axis, the *Y*-axis represents the sagittal axis, and the *Z*-axis represents the vertical axis.

Marker Fixation

After volunteers put on straitjackets and caps, 13 special marker points were placed in the head and trunk to establish three-dimensional models. The specific positions were as follows (as shown in **Figure 1**): five marker points were on the head (one point each on the bilateral temporal regions, one point on the forehead, one point on the vertex, and one point on the occipital region), four points on the shoulder and neck (one point each on the bilateral acromions and one point each on the midline bilateral clavicles), and a four points on the trunk (one point each on the bilateral pectoralis major muscles, one point under the xiphoid, and one point on the upper abdomen). The location of the marker points displayed in the motion capture system and the relationship and coordinate system between the head rigid body and the torso rigid body is shown in **Figure 2**.

Formal Experiment

Before the experiment, the first volunteer stood on the spot, arms outstretched for system calibration. The volunteers were manipulated in a upright seated position, and the clinician stood behind the volunteers. The two cervical spine manipulations we are comparing are non-fixed-point rotational manipulations.

FIGURE 1 | Position of marker points on the volunteers.

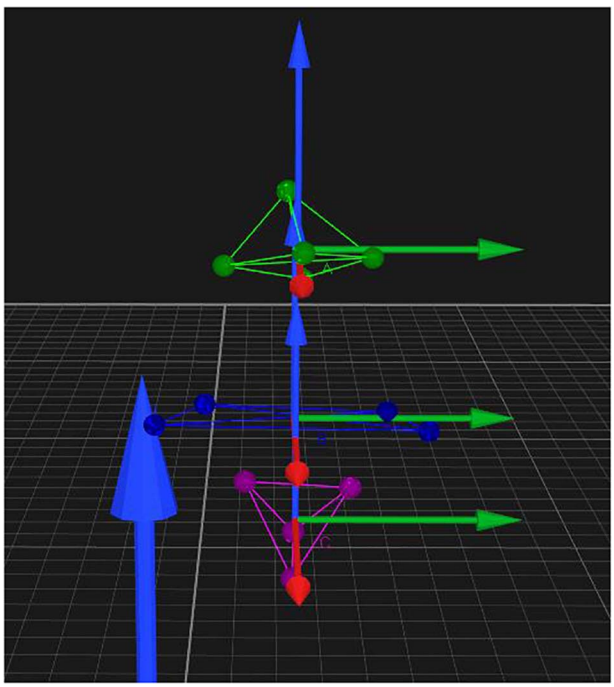

FIGURE 2 | Position of markers displayed in the motion capture system and the relationship and coordinate system between the head rigid body and the torso rigid body.

They are not performed on a specific cervical segment, but use the wrenching of the head to transmit force to the cervical spine to achieve a therapeutic effect. The clinician performs the oblique pulling and the rotation-traction manipulation on the left and right sides of the subjects by group. The oblique pulling manipulation was based on the manipulation rules formulated by Yao et al. (2012). Take the oblique pulling manipulation on the right as an example (shown in **Figure 3**). The specific steps were as follows. (A) Flexion: guide the subject's head into flexion. (B) Active Rotation: extreme rotation in the right direction. (C) Passive rotation: the practitioner uses the right elbow against the volunteer's left shoulder, the right hand against the back of the volunteer's neck, and the left hand against the volunteer's jaw to help the subject bend again to the right limit. (D) Transient pull: the clinician momentarily increases the force of rotation and then releases it. The oblique pulling manipulation is done with one hand against the participant's jawbone and the other hand against the neck, with the two hands exerting concerted force in opposite directions, allowing the neck to be mildly twisted to the point of apparent resistance. The rotation–traction manipulation was based on the manipulation rules formulated by Liguo et al. (2017). The right side of the rotation–traction manipulation is used as an example (shown in **Figure 4**). The specific steps were as follows. (A) Flex: the volunteer's head was guided to flex. (B) Rotary position: the head was rotated to the right direction limit, then the clinician helped the subjector to rotate to the right direction limit again. (C) Pretraction: the volunteer's mandible was held in the clinician's forearm and then pulled slowly upward for approximately 3–5 s. (D) Upward-thrust: the head was thrust upward rapidly after pretraction. The cervical rotation-traction manipulation is to use the clinician's elbow against the participant's jawbone, the other hand against the neck, and the elbow with a short force to quickly thrust upward. The manipulation procedure was captured dynamically by the motion capture system.

Data Analysis and Post-Processing

The saved data were analyzed and processed by Visual 3D analysis software. According to the anatomical features, the five points of the head are used as the rigid body of the head, and the four points of the shoulders and the four points of the upper abdomen are used as the rigid body of the trunk. The relative motion between the head rigid body and the trunk rigid body was calculated. We used the mean values of the data obtained from the left and right sides. Finally, the thrust time, thrust displacement, mean thrust velocity, maximum thrust velocity, maximum thrust acceleration, thrust angular displacement, active motion amplitude, and passive motion amplitude of the 48 volunteers obtained were analyzed using the statistical package SPSS 19.0. A two independent samples *t*-test was used to compare two groups of data.

RESULTS

Baseline information for the two groups is compared in **Table 1**, and there were no differences in gender distribution, subject age, height, or weight between the two groups to allow for a subject study.

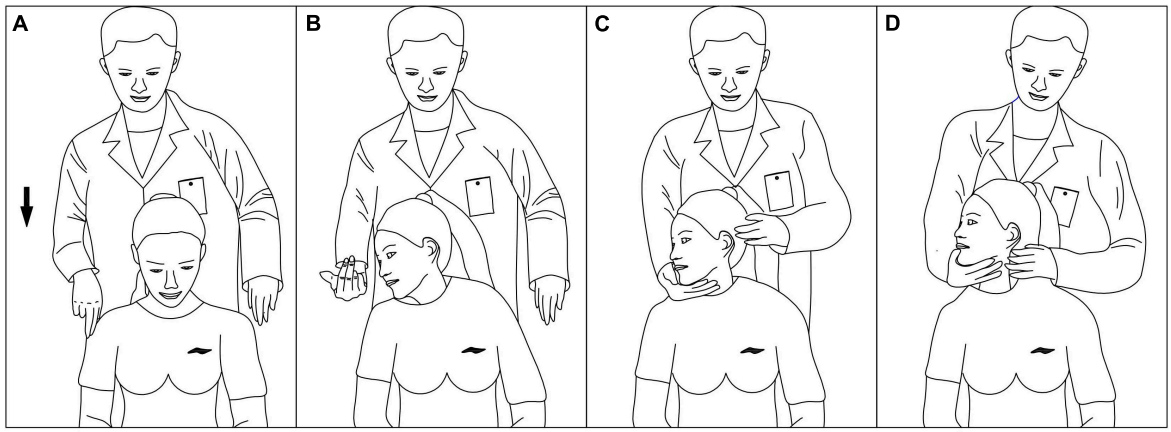

FIGURE 3 | Process of the oblique pulling manipulation. **(A)** Flex. **(B)** Active rotation. **(C)** Passive rotation. **(D)** Instant pull.

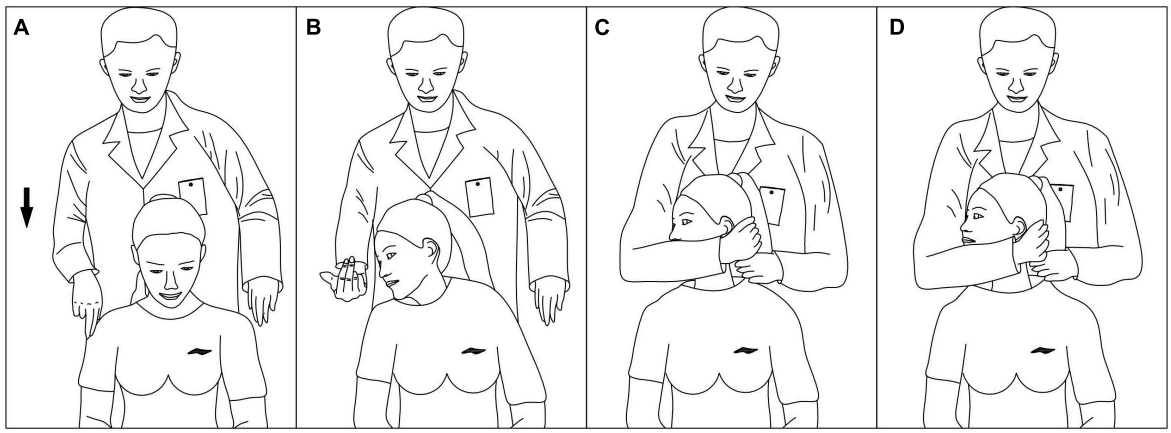

FIGURE 4 | Process of the cervical rotation–traction manipulation. **(A)** Flex. **(B)** Rotary position. **(C)** Pretraction. **(D)** Upward-thrust.

The kinematic parameters of the participants are listed in **Table 2**. The thrust time, thrust displacement, average thrust speed, max thrust speed, and max thrust acceleration all showed no significant difference between two manipulations ($P > 0.05$).

Table 3 presents the mean amplitude of active and passive motion during two manipulations. No significant difference is found between the oblique pulling manipulation and the cervical rotation–traction manipulation ($P > 0.05$).

The mean thrust angular displacement of two manipulations is shown in **Table 4**. The thrust amplitudes of the oblique pulling manipulation significantly greater than the cervical rotation–traction manipulation ($P < 0.001$).

DISCUSSION

This study adopts three-dimensional motion capture technology to conduct kinematic analysis of the operational characteristics of the two techniques, so as to conduct a comprehensive analysis of the techniques from the perspective of three-dimensional structure; to conduct a detailed and thorough study of the techniques by measuring the frequency, velocity, acceleration and other data of the techniques; and to make a convincing comparison of the safety of the two techniques. Therefore, using numerical or mechanical language to describe the mechanical characteristics of the Chinese manipulation will help standardize the manipulation and indirectly ensure the efficacy of the manipulation.

In motion capture systems, marker points must be placed in such a way that they not only represent head and torso

TABLE 1 | Comparison of baseline information between the two groups.

	Oblique pulling manipulation	Cervical rotation–tractionmanipulation	*P*
Age (y)	27.30 ± 4.28	26.90 ± 3.27	0.882
Height (cm)	173.00 ± 7.63	172.90 ± 9.56	0.980
Weight (kg)	67.93 ± 11.65	65.30 ± 13.31	0.602
BMI	22.72 ± 2.36	22.06 ± 3.29	0.892

BMI = Weight (kg)/Height (m^2).

TABLE 2 | Comparison of kinematic parameters of participants between the two groups.

	Oblique pulling manipulation	Cervical rotation–traction manipulation	*P*
Thrust time (s)	0.240 ± 0.054	0.252 ± 0.041	0.188
Thrust displacement (mm)	35.19 ± 14.67	34.65 ± 12.40	0.833
Average thrust speed (mm/s)	150.89 ± 67.71	138.20 ± 47.50	0.251
Maximum thrust speed (mm/s)	216.12 ± 91.45	193.88 ± 65.12	0.139
Maximum thrust acceleration (mm/s^2)	6399.49 ± 2115.26	5352.57 ± 3683.69	0.233

TABLE 3 | Comparion of active and passive motion amplitude between the two groups (°).

	Oblique pulling manipulation	Cervical rotation–traction manipulation	*P*
Active movement amplitude	67.18 ± 4.31	67.72 ± 3.83	0.485
Passive motion amplitude	77.74 ± 4.15	79.22 ± 4.16	0.059

TABLE 4 | Comparison of thrust angular displacement between the two groups (°).

	Oblique pulling manipulation	Cervical rotation–traction manipulation	*P*
Thrust angular displacement	5.735 ± 3.041	2.142 ± 1.724	0.000

movements, but also that they are not obscured by the clinician (Price et al., 2020). The head and torso are marker points placed according to anatomical bony landmarks, where the five points on the head constitute the rigid body of the head, and the four points on the shoulders and the four points on the upper abdomen constitute the rigid body of the torso. The relative motion between the rigid body of the head and the rigid body of the trunk indirectly reflects the motion of the cervical spine.

Van Zoest and Gosselin (2003) directly measured the three-dimensional interactions between physician limbs and patients during manipulation and showed a significant advantage of the presence of three-dimensional mechanical parameters over unidirectional mechanical parameters. However, they did not study the thrust velocity and acceleration. In this study, we successfully captured the mechanical parameters and the trajectory of two cervical manipulations. **Table 2** shows that the kinematic parameters of the two manipulations are more consistent when thrust. We observed that both manipulations meet the characteristics of HVLA cervical spine manipulation techniques by comparing with Zhu's experimental results (van der Kruk and Reijne, 2018; thrust velocity: 203.06 ± 49.95 mm/s; thrust acceleration: 3836.27 ± 1262.28 mm/s^2). Statistical analysis showed that the mechanical parameters of the two methods were not statistically significant. We confirmed that there were no significant differences in kinematic characteristics between the oblique pulling manipulation and the cervical rotation–traction manipulation.

Table 3 shows the active and passive motion amplitudes of the two groups. Active range of motion is when the volunteer actively flexes and rotates to the side to the limit. Passive range of motion is the volunteer first actively moves as far as possible and the clinical then passively continues the movement until the maximum passive ROM is reached. Both active and passive movements are within the range of physiological activity (Tousignant et al., 2006). The amplitude of active and passive motion for the oblique pulling manipulation was 67.18 ± 4.31° and 77.74 ± 4.15°, respectively. The amplitudes of cervical rotation–traction manipulation were 67.72 ± 3.83° and 79.22 ± 4.16°, respectively. The present experimental results are similar to the active and passive rotation values measured by Mei et al. (2010) using a laser scanner (global positioning system coordinates, accuracy 0.01°), at 68.37 ± 3.32° and 78.94 ± 4.46°. In addition, the present experiment is similar to the rotation angle data measured by Feipel et al. (1999) for the cervical spine in flexion, again validating the reliability of the data in this study. In summary, the amplitude of active and passive movements of the cervical spine is similar in both manipulations.

The thrust amplitude of the oblique pulling manipulation was more than twice of that the cervical rotation-traction manipulation as **Table 4** shown.

The Reason Why the Oblique Pulling Manipulation Has a Larger Thrust Amplitude Than the Cervical Rotation-Traction Manipulation

From the third and fourth pictures of **Figures 3**, **4**, it can be seen that the pretraction position of the cervical rotation-traction manipulation does not differ much from the position of the thrust process, whereas the oblique pulling manipulation undergoes a large change in position before and after the thrust. We may be able to analyze the reasons for this result in terms of the manipulative characteristics of the two manipulations by the motion capture system. The oblique pulling manipulation is divided into three main processes: active rotation of the subject to the limit, fixed angle after the clinician helps the subject reach the limit again with passive movement, and sudden pulling. While the main steps of the cervical rotational-traction manipulation involves active rotation of the subject to the limit. The clinician then pretracted the subject forward to a fixed angle and abruptly thrusted upward. The oblique pulling manipulation is dominated by rotation during traction and upward lifting. And the cervical rotational traction method is mainly upward lifting with rotation as an aid during traction. The different manipulative characteristics of the two methods of thrusting are directly responsible for the different thrust amplitudes. Zhu (van der Kruk and Reijne, 2018) used 12 digital motion capture lenses to dynamically capture the operation process of the CRM. The results show that the force direction of thrust is mainly vertically upward. In the mean time, the cervical rotation-traction manipulation makes a forward traction in preparation for the

thrust while reducing the thrust amplitude. In addition, the pre-traction of cervical spinal manipulation can enlarge the sagittal plane of the intervertebral foramen, reduce the internal pressure of the nucleus pulposus, help to avoid the secondary damage to the intervertebral disk caused by the pure rotational force, help to release the adhesions of the ligaments around the surrounding small joints, increase the mobility of the intervertebral joints, narrow the range of motion of the cervical spine during the thrust, and facilitate the safe operation of the manipulation (Li et al., 1998; Anderst et al., 2018). Through the photos we found that the cervical rotation-traction manipulation has a larger body contact area than the oblique pulling manipulation. We believe that the larger body contact area is to transmit the force to the hand through the torso, which can control the force better and the force emitted is more stable. Thereby its thrust amplitude is smaller.

The Hazards of Large Thrust Amplitudes

Cervical rotation manipulations produce thrusts that move the cervical spine out of its normal physiological range of motion without exceeding the limits of anatomical integrity (Chaibi and Benth, 2017). Klein et al. (2003) used a three-dimensional space-measuring instrument to measure motion parameters during the cervical spine rotation manipulation. They measured the three-dimensional range and amplitude of motion of the left and right cervical segments (C3 and C5). They found the maximum amplitude between the head and trunk during thrust did not exceed the physiological range of activity. Passmore et al. (Chaibi and Benth, 2017) used a cervical range-of-motion goniometer to measure improvement in mobility after cervical spine manipulation. They concluded that cervical rotation to the right resulted in a significant improvement in range of motion of 3.75 degrees.

However, at the same time, torsion is the most significant risk factor for disk injury, especially in the pathological state of the disk (Harvey-Burgess and Gregory, 2019). The intervertebral disk is the most critical part of the cervical spine load-bearing system. Torsional loading produces shear stresses in the horizontal and vertical planes of the disk, which are proportional to the distance between the axes of rotation. Biomechanical experiments (Schmidt et al., 2007; Veres et al., 2010) have shown that when the spine is flexed and the compound torque is rotated, the disk is subjected to large shear forces, and the compound motion of repeated flexion plus rotation may damage the disk. At this point, excessive rotation may lead to disk herniation or even prolapse. The intervertebral disk is viscoelastic tissue (González Martínez et al., 2017) that undergoes elastic changes in a physiological state after compression and is linear. Once subjected to larger shear forces or repeated excessive stresses it becomes non-linear which is a plastic change. It inhibits the synthesis of the disk matrix and decreases its content, leading to an increased risk of disk degeneration. While moderate stress is essential to maintain normal disk nutrition, an abnormally high stress environment is an important factor in disk degeneration, which can alter the surrounding environment of disk chondrocytes.

On the other hand, when the Luschka joint of the C3 to C4 vertebrae is in the coronal position, too much thrust force at this time can cause abnormal shear forces resulting in hook vertebral fractures. In addition, excessive thrust amplitude may cause cervical dislocation, small joint displacement, cervical instability and intervertebral joint disorder. Cervical spine manipulation is widely used in relieving cervical myofascial pain and increasing cervical spine mobility. In this experiment, we chose volunteers who were healthy and cervical spine manipulation was relatively safe to operate in normal subjects. However, when cervical spine manipulation is used to treat patients with cervical spondylotic radiculopathy, the wide range of rotation during retraction may aggravate cervical disk herniation and compress the nerve roots and cervical spinal cord.

LIMITATION

However, this study has some limitations. First of all, this study involved only one clinician, and the mechanical parameters of CRM may vary considerably between practitioners of different genders, sizes, and clinical experience. Secondly, the subjects were young, healthy individuals, so the results of the study may not be generalizable to other populations. Thirdly, only two subcategories of non-fixed-point rotational manipulation were explored in this study, and the mechanical parameters of non-fixed-point rotational manipulation cannot be directly extrapolated to fixed-point rotational manipulation. In order to further investigate the clinical efficacy and safety of CRM for cervical radiculopathy, the next step will be to select other techniques, such as fixed-point rotation, and recruit patients with varying degrees of cervical spondylosis as volunteers for basic research as well as practitioners with different gender, age and other influencing factors. Questions such as whether the kinematic characteristics of twisting and lifting techniques with smaller thrust amplitude displacements are regular, and whether they are common to different clincians in different subjects need further refinement.

CONCLUSION

In summary, the mechanical parameters and active and passive motion amplitudes of the oblique pulling manipulation are similar to those of the cervical rotational traction manipulation. However, in terms of thrust amplitude, the oblique pulling manipulation has a greater amplitude and therefore maybe poses a greater risk of potential cervical spine injury during manipulation than the cervical rotational traction manipulation.

DATA AVAILABILITY STATEMENT

The raw data supporting the conclusions of this article will be made available by the authors, without undue reservation.

ETHICS STATEMENT

The studies involving human participants were reviewed and approved by Research Ethics Association, Shunde Hospital Affiliated to Guangzhou Medical University. The patients/participants provided their written informed consent to participate in this study. Written informed consent was obtained from the individual(s) for the publication of any potentially identifiable images or data included in this article.

AUTHOR CONTRIBUTIONS

DL completed the experiment and wrote the manuscript. XH directed the design test and repaired manuscript. The rest of the authors were put forward valuable opinions in the whole subject design. All authors contributed to the article and approved the submitted version.

FUNDING

General Project of Nature Foundation of Guangdong Province (2020A151501998), the Science and Technology Project of Guangdong Province (2016B090917001 and 2017B090912006), Sanming Project of Medicine in Shenzhen (SZSM201612019), and Promote Innovation – Driven Power Engineering Projects in FoShan (2019012).

ACKNOWLEDGMENTS

We would like to thank my supervisor, Wenhua Huang, for providing support conditions and guidance for this experiment, the Human Anatomy Department of Southern Medical University for providing the experimental equipment, and every volunteer who participated in the experiment.

SUPPLEMENTARY MATERIAL

The Supplementary Material for this article can be found online at: https://www.frontiersin.org/articles/10.3389/fbioe.2021.714292/full#supplementary-material

REFERENCES

Anderst, W. J., Gale, T., LeVasseur, C., Raj, S., Gongaware, K., and Schneider, M. (2018). Intervertebral kinematics of the cervical spine before, during, and after high-velocity low-amplitude manipulation. *Spine J.* 18, 2333–2342. doi: 10.1016/j.spinee.2018.07.026

Boser, Q. A., Valevicius, A. M., Lavoie, E. B., Chapman, C. S., Pilarski, P. M., Hebert, J. S., et al. (2018). Cluster-based upper body marker models for three-dimensional kinematic analysis: comparison with an anatomical model and reliability analysis. *J. Biomech.* 72, 228–234. doi: 10.1016/j.jbiomech.2018.02.028

Bronfort, G., Haas, M., Evans, R. L., and Bouter, L. M. (2004). Efficacy of spinal manipulation and mobilization for low back pain and neck pain: a systematic review and best evidence synthesis. *Spine J.* 4, 335–356. doi: 10.1016/j.spinee.2003.06.002

Chaibi, A., and Benth, J. Š (2017). Tuchin PJ, Russell MB. Chiropractic spinal manipulative therapy for migraine: a three-armed, single-blinded, placebo, randomized controlled trial. *Eur. J. Neurol.* 24, 143–153. doi: 10.1111/ene.13166

Feipel, V., Rondelet, B., Le Pallec, J., and Rooze, M. (1999). Normal global motion of the cervical spine: an electrogoniometric study. *ClinBiomech (Bristol, Avon.)* 14, 462–470. doi: 10.1016/s0268-0033(98)90098-5

Galindez-Ibarbengoetxea, X., Setuain, I., Andersen, L. L., Ramírez-Velez, R., González-Izal, M., Jauregi, A., et al. (2017). Effects of cervical high-velocity low-amplitude techniques on range of motion, strength performance, and cardiovascular outcomes: a review. *J. Altern. Complement Med.* 23, 667–675. doi: 10.1089/acm.2017.0002

Giacalone, A., Febbi, M., Magnifica, F., and Ruberti, E. (2020). The effect of high velocity low amplitude cervical manipulations on the musculoskeletal system: literature review. *Cureus.* 12:e7682. doi: 10.7759/cureus.7682

Gómez, F., Escribá, P., Oliva-Pascual-Vaca, J., Méndez-Sánchez, R., and Puente-González, A. S. (2020). Immediate and Short-term effects of upper cervical high-velocity, low-amplitude manipulation on standing postural control and cervical mobility in chronic nonspecific neck pain: a randomized controlled trial. *J. Clin. Med.* 9:2580. doi: 10.3390/jcm9082580

González Martínez, E., García-Cosamalón, J., Cosamalón-Gan, I., Esteban Blanco, M., García-Suarez, O., and Vega, J. A. (2017). Biología y mecanobiologíadel disco intervertebral [Biology and mechanobiology of the intervertebral disc]. *Neurocirugia (Astur.)* 28, 135–140. doi: 10.1016/j.neucir.2016.12.002

Gorrell, L. M., Engel, R. M., Brown, B., and Lystad, R. P. (2016). The reporting of adverse events following spinal manipulation in randomized clinical trials-a systematic review. *Spine J.* 16, 1143–1151. doi: 10.1016/j.spinee.2016.05.018

Harvey-Burgess, M., and Gregory, D. E. (2019). The effect of axial torsion on the mechanical properties of the Annulus Fibrosus. *Spine* 44, E195–E201. doi: 10.1097/BRS.0000000000002803

Herzog, W. (2010). The biomechanics of spinal manipulation. *J. BodywMovTher.* 14, 280–286. doi: 10.1016/j.jbmt.2010.03.004

Huang, Y., Li, S., Feng, M., and Zhu, L. (2017). Cervical spine mechanism for reproduction of the biomechanical behaviours of the human neck during rotation-traction manipulation. *Appl. Bionics. Biomech.* 2017:5829048. doi: 10.1155/2017/5829048

Klein, P., Broers, C., Feipel, V., Salvia, P., Van Geyt, B., Dugailly, P. M., et al. (2003). Global 3D head-trunk kinematics during cervical spine manipulation at different levels. *ClinBiomech (Bristol Avon.)* 18, 827–831. doi: 10.1016/s0268-0033(03)00170-0

Kranenburg, H. A., Lakke, S. E., Schmitt, M. A., and Van der Schans, C. P. (2017a). Adverse events following cervical manipulative therapy: consensus on classification among Dutch medical specialists, manual therapists, and patients. *J. Man. ManipTher.* 25, 279–287. doi: 10.1080/10669817.2017.1332556

Kranenburg, H. A., Schmitt, M. A., Puentedura, E. J., Luijckx, G. J., and van der Schans, C. P. (2017b). Adverse events associated with the use of cervical spine manipulation or mobilization and patient characteristics: a systematic review. *MusculoskeletSciPract* 28, 32–38. doi: 10.1016/j.msksp.2017.01.008

Li, Y. K., Zhu, Q. A., and Zhong, S. Z. (1998). The effect of cervical traction combined with rotatory manipulation on cervical nucleus pulposus pressures. *J. Manipulative PhysiolTher.* 21, 97–100.

Liguo, Z., Minshan, F., Xunlu, Y., Shangquan, W., and Jie, Y. (2017). Kinematics analysis of cervical rotation-traction manipulation measured by a motion capture system. *Evid Based Complement Alternat. Med.* 2017:5293916. doi: 10.1155/2017/5293916

Liu, S., Zhang, J., Zhang, Y., and Zhu, R. (2020). A wearable motion capture device able to detect dynamic motion of human limbs. *Nat Commun* 11, 5615. doi: 10.1038/s41467-020-19424-2

Martínez-Segura, R., Fernández-de-las-Peñas, C., Ruiz-Sáez, M., López-Jiménez, C., and Rodríguez-Blanco, C. (2006). Immediate effects on neck pain and active range of motion after a single cervical high-velocity low-amplitude manipulation in subjects presenting with mechanical neck pain: a randomized

controlled trial. *J. Manipulative PhysiolTher.* 29, 511–517. doi: 10.1016/j.jmpt.2006.06.022

Mei, L., Li, Y. K., Fu, X. Y., and Wang, H. J. (2010). "Relationship between the wrenching direction of the cervical spine rotation maneuver and the cervical spine rotation angle. *J. Chin. Rehabil. Med.* 25, 9–12.

Menolotto, M., Komaris, D. S., Tedesco, S., O'Flynn, B., and Walsh, M. (2020). Motion capture technology in industrial applications: a systematic review. *Sensors* 20:5687. doi: 10.3390/s20195687

Needham, R., Stebbins, J., and Chockalingam, N. (2016). Three-dimensional kinematics of the lumbar spine during gait using marker-based systems: a systematic review. *J. Med. Eng. Technol.* 40, 172–185. doi: 10.3109/03091902.2016.1154616

Nielsen, S. M., Tarp, S., Christensen, R., Bliddal, H., Klokker, L., and Henriksen, M. (2017). The risk associated with spinal manipulation: an overview of reviews. *Syst. Rev.* 6:64. doi: 10.1186/s13643-017-0458-y

Price, M. A., LaPrè, A. K., Johnson, R. T., Umberger, B. R., and Sup, F. C. IV (2020). A model-based motion capture marker location refinement approach using inverse kinematics from dynamic trials. *Int. J. Numer. Method Biomed. Eng.* 36:e3283. doi: 10.1002/cnm.3283

Ruiz-Sáez, M., Fernández-de-las-Peñas, C., Blanco, C. R., Martínez-Segura, R., and García-León, R. (2007). Changes in pressure pain sensitivity in latent myofascial trigger points in the upper trapezius muscle after a cervical spine manipulation in pain-free subjects. *J. Manipulative PhysiolTher.* 30, 578–583. doi: 10.1016/j.jmpt.2007.07.014

Schmidt, H., Kettler, A., Heuer, F., Simon, U., Claes, L., and Wilke, H. J. (2007). Intradiscal pressure, shear strain, and fiber strain in the intervertebral disc under combined loading. *Spine* 32, 748–755. doi: 10.1097/01.brs.0000259059.90430.c2

Smith, L., and Mehta, M. (2008). "The effects of upper cervical complex high velocity low amplitude thrust technique and sub-occipital muscle group inhibition techniques on standing balance. *Int. J. Osteop. Med.* 11:162. doi: 10.1016/j.ijosm.2008.08.020

Tousignant, M., Smeesters, C., Breton, A. M., Breton, E., and Corriveau, H. (2006). Criterion validity study of the cervical range of motion (CROM) device for rotational range of motion on healthy adults. *J. Orthop. Sports Phys.Ther.* 36, 242–248. doi: 10.2519/jospt.2006.36.4.242

Triano, J. J., Rogers, C. M., Combs, S., Potts, D., and Sorrels, K. (2003). Quantitative feedback versus standard training for cervical and thoracic manipulation. *J. Manipulative PhysiolTher.* 26, 131–138. doi: 10.1016/S0161-4754(02)54105-1

van der Kruk, E., and Reijne, M. M. (2018). Accuracy of human motion capture systems for sport applications; state-of-the-art review. *Eur. J. Sport Sci.* 18, 806–819. doi: 10.1080/17461391.2018.1463397

Van Zoest, G. G., and Gosselin, G. (2003). Three-dimensionality of direct contact forces in chiropractic spinal manipulative therapy. *J. Manipulative PhysiolTher.* 26, 549–556. doi: 10.1016/j.jmpt.2003.08.001

Veres, S. P., Robertson, P. A., and Broom, N. D. (2010). The influence of torsion on disc herniation when combined with flexion. *Eur. Spine J.* 19, 1468–1478. doi: 10.1007/s00586-010-1383-0

Vernon, H., and Humphreys, B. K. (2008). Chronic mechanical neck pain in adults treated by manual therapy: a systematic review of change scores in randomized controlled trials of a single session. *J. Man ManipTher.* 16, E42–E52. doi: 10.1179/jmt.2008.16.2.42E

Yao, B. B., A, R., and Yu, T. Y. (2012). Clinical experience of Professor Yu Tianyuan in the treatment of neurogenic cervical spondylosis. *J. Trad. Chin. Med.* 27, 1160–1163.

Zhang, J., and Gu, F. (2014). "Progress in the study of cervical trigger method. *J. China Pharmaceutic. Herald* 11, 152–153.

Zhu, L. G., Yu, J., and Gao, J. H. (2005). An overview about cervical rotational manipulation of cervical spondyloticradiculopathy. *J. Tradition. Chin. Orthop. Traumatol.* 17, 69–73.

Conflict of Interest: The authors declare that the research was conducted in the absence of any commercial or financial relationships that could be construed as a potential conflict of interest.

Publisher's Note: All claims expressed in this article are solely those of the authors and do not necessarily represent those of their affiliated organizations, or those of the publisher, the editors and the reviewers. Any product that may be evaluated in this article, or claim that may be made by its manufacturer, is not guaranteed or endorsed by the publisher.

frontiers in Bioengineering and Biotechnology

ORIGINAL RESEARCH
published: 31 August 2021
doi: 10.3389/fbioe.2021.721042

Subject-Specific Alignment and Mass Distribution in Musculoskeletal Models of the Lumbar Spine

*Marie-Rosa Fasser [1,2], Moritz Jokeit [1,2], Mirjam Kalthoff [2], David A. Gomez Romero [2], Tudor Trache [1], Jess G. Snedeker [1,2], Mazda Farshad [1] and Jonas Widmer [1,2]**

[1]Department of Orthopaedics, Balgrist University Hospital, Zurich, Switzerland, [2]Institute for Biomechanics, ETH Zurich, Zurich, Switzerland

Musculoskeletal modeling is a well-established method in spine biomechanics and generally employed for investigations concerning both the healthy and the pathological spine. It commonly involves inverse kinematics and optimization of muscle activity and provides detailed insight into joint loading. The aim of the present work was to develop and validate a procedure for the automatized generation of semi-subject-specific multi-rigid body models with an articulated lumbar spine. Individualization of the models was achieved with a novel approach incorporating information from annotated EOS images. The size and alignment of bony structures, as well as specific body weight distribution along the spine segments, were accurately reproduced in the 3D models. To ensure the pipeline's robustness, models based on 145 EOS images of subjects with various weight distributions and spinopelvic parameters were generated. For validation, we performed kinematics-dependent and segment-dependent comparisons of the average joint loads obtained for our cohort with the outcome of various published *in vivo* and *in situ* studies. Overall, our results agreed well with literature data. The here described method is a promising tool for studying a variety of clinical questions, ranging from the evaluation of the effects of alignment variation on joint loading to the assessment of possible pathomechanisms involved in adjacent segment disease.

Keywords: spine biomechanics, musculoskeletal modelling, subject-specificity, upper body mass distribution, thoracolumbar alignment, automatized model generation, spine loading prediction, bi-planar radiography

OPEN ACCESS

Edited by:
Dennis E. Anderson, Harvard Medical School, United States

Reviewed by:
Hossein Mokhtarzadeh, The University of Melbourne, Australia
Tito Bassani, Galeazzi Orthopedic Institute (IRCCS), Italy

****Correspondence:***
Jonas Widmer
jonas.widmer@balgrist.ch

Specialty section:
This article was submitted to Biomechanics, a section of the journal Frontiers in Bioengineering and Biotechnology

Received: *05 June 2021*
Accepted: *06 August 2021*
Published: *31 August 2021*

Citation:
Fasser M-R, Jokeit M, Kalthoff M, Gomez Romero DA, Trache T, Snedeker JG, Farshad M and Widmer J (2021) Subject-Specific Alignment and Mass Distribution in Musculoskeletal Models of the Lumbar Spine. Front. Bioeng. Biotechnol. 9:721042. doi: 10.3389/fbioe.2021.721042

1 INTRODUCTION

The high incidence of back pain in the general population poses a socio-economic burden on society (Traeger et al., 2019; Hoy et al., 2014; Dagenais et al., 2008). Despite the increasing number of treatment options, self-assessed patient satisfaction stagnates (Friedly et al., 2010). This motivates the investigation of spinal biomechanics with the intention to improve diagnosis, treatment, and rehabilitation options (Widmer et al., 2020). Developing preventive measures and suitable treatment strategies for spinal pathology implies knowledge about the loading conditions within the spine and its muscles. The effect of physiologically pertinent mechanical loading conditions on various spinal tissues has been thoroughly studied *in vivo* (Polga et al., 2004; Daggfeldt and Thorstensson, 2003; Wilke et al., 2001; Sato et al., 1999) and *in vitro* (Rohlmann et al., 2009, 2001; Wilke et al., 2003). Although providing valuable insight into the spinal loading response, several disadvantages come along with experimental studies. The invasiveness of *in vivo*

measurements raises ethical concerns with respect to both healthy and pathological subjects. *In vitro* experiments allow the investigation of loading patterns in a well-controlled environment, but the lack of muscular activity acts as a limiting factor. To overcome constrained sample availability and variability, musculoskeletal models have been established as a non-invasive alternative to study the intricate processes in the healthy and pathological spine (Christophy et al., 2012; Bruno et al., 2015; Senteler et al., 2017). These multi-rigid body models can be used to simulate the neuromuscular activity of the human body through inverse kinematics and static optimization, providing muscle forces and joint loads as an output. Musculoskeletal models can be used to investigate the loading conditions and optimal posture during physiological activities, e.g., in the context of preventive or rehabilitative exercises. Furthermore, the use of these models has the potential to improve pre-operative planning by not only taking geometrical aspects into account but also by considering functional aspects. In addition to valuable direct information about spine loading, the output of a robust model can enhance patient-specificity in other modeling modalities, e.g., providing more physiological loading conditions in finite element models (Esat and Acar, 2004; Toumanidou and Noailly, 2015).

Thus far, a variety of musculoskeletal models with increasing complexity has been introduced in the literature (Damsgaard et al., 2006; de Zee et al., 2007; Delp et al., 2007; Christophy et al., 2012; Bruno et al., 2015; Malakoutian et al., 2018; Ignasiak et al., 2016a). Existing models that are validated against *in vivo* measurements, like the implementations by Christophy et al. (2012) and Bruno et al. (2015) serve as important references for the development of new approaches. However, these models are generic, based on data from few individuals, or they are a statistical representation of specific cohorts of people. Although it was shown that properties such as spinopelvic alignment, weight, and height affect the loading at intervertebral joints (Senteler et al., 2014; Han, 2013; Caprara et al., 2020), the extensive variability amongst individuals within the human population is hardly captured. This necessitates new modeling approaches that include individualized spinopelvic alignment and mass distribution. Furthermore, patient-specific model creation is tedious and time-consuming. For successful incorporation into the clinical workflow, subject-specificity, as well as automation of the process, is called for. Bassani et al. (2017) presented the first attempt towards semi-automatic model creation from annotated bi-planar x-ray images. However, the positioning of the center of mass for each segment was based on earlier literature findings. Building on this idea and previous research, the present work focuses on patient-specific scaling and alignment of the spinal geometry as well as an individualized mass distribution. To control all steps from geometric morphing to minimization of the quadratic muscle activity, the model was implemented in MATLAB, a programming framework widely adopted in the research community.

Overall, the aim of this work was to develop and validate a pipeline for the creation of semi-subject-specific musculoskeletal simulations which provides great flexibility in terms of future research questions to be studied. The following sections give a detailed description of the model's features and present results as well as the validation thereof. Subsequently, the advantages and limitations of the presented modeling approach are discussed.

2 MATERIALS AND METHODS

All steps associated with model generation, simulation, and results analysis were automatized and carried out with custom-written scripts in MATLAB (R2020b, TheMathWorks Inc., Natick, MA, United States).

2.1 Model Generation

2.1.1 Image Annotation

First, a defined set of anatomical landmarks are identified on bi-planar radiography images (EOS imaging, Paris, France; **Figure 1A**). In total, 112 and 109 points are marked on the frontal and sagittal planes, respectively. Annotated structures are the thoracic and lumbar vertebrae, the sacrum, the pelvis, the femoral head, the rib cage, and the body outline, as well as head and arms (**Figure 1B**). Thanks to the spatial calibration of the EOS system, the 2D anatomical landmarks derived from the simultaneously acquired orthogonal images can then be converted into 3D coordinates.

2.1.2 3D Model and Alignment

The proposed musculoskeletal model consists of seven functional segments: the rib cage, the five lumbar vertebrae, and the sacropelvic bone structures. Generic template models of vertebrae, ribs, sternum, pelvis, and sacrum are scaled and repositioned according to size and alignment represented in EOS images.

First, the coordinates of the vertebral body endplates (i.e., the four corners of the vertebral body detectable in the sagittal plane and four corners discernable in the frontal plane) are used to determine the scaling factors along all three axes of each vertebra. The width of the vertebra is scaled based on information from the frontal view image and height and depth, i.e. size in anteroposterior direction, are obtained from sagittal images.

The same landmarks are then used to fit a cubic spline through the centers of the vertebrae, from the uppermost thoracic level all the way down to the coccyx (**Figure 1C**). The resulting best-fit curve describes the patient-specific alignment of the spine and allows to keep the relative position of each bony segment constant (independently from the specifications resulting from imposed kinematics, **Section 2.2**). Correct arrangement of the scaled vertebral surface models along the spline is ensured by positioning the centroids of the template vertebral bodies on the respective centroids on the spline. Additionally, the vertebrae are rotated to align them with the orientation derived from landmarks in the sagittal and frontal planes. Next, the sternum and ribs are scaled and repositioned according to the location of the vertebrae and annotations of the ribcage (left, right, and anterior outline). Furthermore, pelvis and sacrum sizes are scaled to subject-specific dimensions based on the annotations of the femoral heads, the center of the sacral endplate, and the anterior superior iliac spines. The landmarks associated with the latter

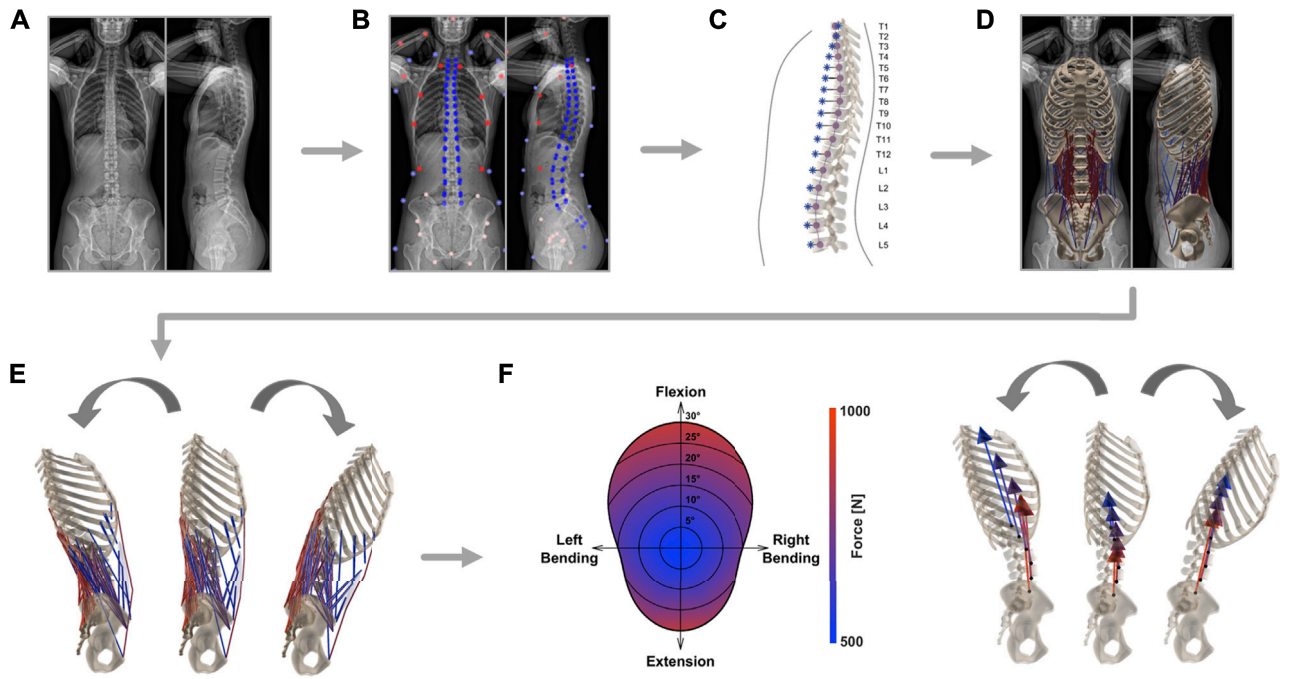

FIGURE 1 | Schematic depiction of the steps required for the generation of individualized musculoskeletal models. After EOS image acquisition **(A)**, the bi-planar radiographs were annotated by an experienced medical professional **(B)**. From the resulting landmarks, the alignment of the thoracolumbar spine (purple) and the segment-wise position of the center of mass (blue) were derived **(C)**. A model rendering subject anatomy was created and included the eight major muscle groups involved in stabilizing the lower spine **(D)**. Kinematic boundary conditions were set **(E)** and consequently magnitude and direction of joint load was computed based on static optimization **(F)**.

structures are used to rotate the pelvis and the sacrum in the frontal plane. The alignment within the sagittal plane relative to the longitudinal body axis is determined based on the vector from the center of the sacral endplate to the femoral heads for the pelvis and the vector to the caudal end of the coccyx for the sacrum. To achieve even better correspondence between 3D model geometry and the actual subject anatomy, the template pelvic bone is finally morphed onto the subject-specific landmarks using the *As-Rigid-As-Possible*-algorithm by Sorkine and Alexa (2007) (**Figure 1D**).

The alignment and dimensions of the thoracolumbar vertebrae within the sagittal and coronal plane (lumbar lordosis, thoracic kyphosis, sagittal vertical axis) are replicated in order to have a consistent placement of the center of masses, muscle attachment points, and center of rotations, which are all highly dependent on the subject's anatomy. The scaling and positioning of the sacropelvic components accurately reproduce the subject's anatomy and alignment (sacral slope, pelvic tilt, pelvic incidence) according to landmarks of the sacral endplate, the femoral heads, and the pelvis.

2.1.3 Mass Distribution

We use the body contour obtained from the bi-planar EOS scans to determine the position of the center of mass (COM) for each relevant segment. The sagittal image is used to determine the body delimitation towards the anterior and posterior and the coronal image is used to determine the left and right outline of the torso. Seven regularly-spaced landmarks are positioned along each of the outlines (anterior, posterior, left, and right, **Figure 1B**). Through each set of landmarks, a spline function is fitted to obtain a smooth and continuous body demarcation (**Figure 1C**). The torso is subdivided into seventeen segments, each associated with one thoracolumbar vertebra. Every segment is then further subdivided into 2 mm thick elliptically-shaped slices. For each body segment, the corresponding center of volume (COV) is computed as a mean of the COVs of all 2-mm slices contained in the segment. Homogeneous density distribution at each level was assumed. Therefore, the COM of the segments coincides with the COV in our models. The mass assigned to each level is based on experimentally derived percentage distribution (Pearsall et al., 1996). The COM of the ribcage is lumped to a single point computed from the COMs of the twelve thoracic segments, the head, and the arms, weighted by the respective percentage mass contribution (Pearsall et al., 1996; Bruno et al., 2015). These weighting parameters, together with the estimation of the volume and the experimentally derived mean values for density at each level, are used to extrapolate the body weight (BW) of the subjects (Pearsall et al., 1996). We tested the procedure for BW estimation with a dataset comprising 82 subjects with available bi-planar radiographs and of known weight (mean weight being 77 kg, ranging from 43 to 135 kg; unpublished data). The correlation between measured and predicted body weight was high (Pearson's correlation: $\rho = 0.89$, p-value > 0.0001). The mean absolute prediction error (MAE) was 7.0 Kg and the mean absolute percentage error (MAPE) was 9.0%.

TABLE 1 | Mean values of segment contribution to overall lumbar range of motion in flexion, extension, lateral bending, and axial rotation. The mean values of several *in-vivo* measurements are shown and were obtained from Widmer et al. (2019).

Segment	Flexion (%)	Extension (%)	Lateral bending (%)	Axial rotation (%)
L1L2	14	27	22	20
L2L3	19	21	26	23
L3L4	21	12	25	20
L4L5	25	9	17	20
L5S1	21	31	10	17

2.1.4 Joints and Muscles

The single rigid parts of the musculoskeletal model are connected through spherical joints, with the sacropelvic bone being fixed in space. The resulting six centers of rotation (COR) connecting the segments to each other are positioned in the middle of the respective intervertebral space. Each of the 230 model's muscle fibers is assigned to one of the following eight muscle groups: external abdominal oblique, internal abdominal oblique, latissimus dorsi, psoas major, quadratus lumborum, rectus abdominis, erector spinae, or multifidus. Every muscle fiber connects two or more rigid components. Muscle attachment points and muscle properties (pennation angle, optimal fiber length, tendon slack length, maximal isometric force) are implemented based on previously published generic models (Christophy et al. (2012); Bruno et al. (2015), **Figure 1D**). Consistent placement of insertion points is possible by defining them relative to the nodes of the template meshes. The displacement-dependent behavior of muscle fibers is described with a simplified Hill-model (Hill, 1938), where only the active force contribution of the fibers is modeled. A Gaussian function was used to describe the active force-length relationship (Thelen, 2003). The optimal fiber length of each muscle fiber was taken from Bruno et al. (2015) and scaled according to the ratio between the original resting length and the subject-specific resting length. The latter was computed after each muscle attachment point being positioned according to the scaled, translated, rotated, and morphed rigid body.

2.2 Model Analysis

Inverse kinematics allows to derive joint reaction forces (JRF) and muscle activation patterns based on prescribed displacements and imposed external loads. The segmental motion constraints for the rigid bodies are obtained from *in vivo* measurements (Widmer et al. (2019), **Table 1**). The tabularized values indicate the percentage contribution of each segment to prescribed overall rotation in the sagittal (flexion and extension), frontal (lateral bending), and transverse (axial rotation) plane (**Figure 1E**). The overall angle of rotation was measured between the thorax and the fixed sacrum.

To compute the JRFs and muscle activity, a static optimization approach is employed (**Figure 1F**). This necessitates the construction of the moment equations for each joint comprising active contributions from muscles, forces derived from body mass distribution, and the reaction force from the more cranially positioned joints. Due to the high number of actuators (muscle fibers) with respect to the degrees of freedom, an infinite number of solutions available to reach equilibrium exists. To reduce the space of possible solutions, maintenance of energy efficiency in human muscle activation is assumed (Hicks et al., 2015). This allows to solve the moment equilibrium by minimizing the squared sum of muscle activity, which was set to range between 0.01 and 1:

$$C = \sum_{i=1}^{m} a_i^2, \quad 0.01 \le a_i \le 1 \tag{1}$$

where C is the cost function, a_i is the activation of the muscle fiber i, and m is the total number of muscle fibers. Minimization of this cost function was achieved with the *Interior point* optimization algorithm embedded in the *fmincon* MATLAB function and the initial guess for muscle activity $a_{0,i}$ was set to 0.5 for all fibers. A muscle fiber activity of 0.01 is implemented as lower boundary for the optimization to partially compensate for neglecting muscle co-activation with the use of the cost function from **Eq. (1)**. The neutral posture (0° position) was set to the point of minimum load of pre-run simulations of pure flexion-extension movements.

TABLE 2 | Mean, standard deviation, and range (minimum-maximum) are specified for age, weight, and spinopelvic parameters of the subjects included in this study. Except for age, all the information were computed based on annotated EOS images.

	Mean	Standard deviation	Range (min–max)
Age (Years)	39	24	7–85
Weight (kg)	66.5	22.7	18.8–137.0
Pelvic Incidence (°)	46.9	12.9	15.4–89.2
Sagittal Vertical Axis (mm)	6.6	35.6	–96.4–124.6
Sacral Slope (°)	34.4	10.2	10.4–64.1
Pelvic Tilt (°)	12.5	9.0	–11.1–37.6
Lumbar Lordosis (°)	50.3	13.7	0.8–83.2
Thoracic Kyphosis (°)	33.1	11.4	5.5–63.6

2.3 Dataset

To test the procedure presented in the previous sections, a dataset comprising bi-planar radiography images of 145 subjects (76 females, 69 males) was examined. The images were acquired at Balgrist University Hospital between June 2012 and November 2020. Exclusion criteria were the presence of implants in the vicinity of the spine and scoliosis in the thoracolumbar region [Cobb's angle ≥10°, Cobb (1948)]. The anonymized images were annotated by a medical professional using a custom graphical

user interface. Based on the landmarks from the annotated images, the lateral spinopelvic parameters were computed for all subjects. Determination of pelvic incidence, sacral slope, and pelvic tilt followed the description expounded in Legaye et al. (1998). The sagittal vertical axis was defined as the horizontal distance between the plumb line and the posterior corner of the sacral endplate. The thoracic kyphosis angle was measured between the superior endplate of T1 and the inferior endplate of T12. Correspondingly, lumbar lordosis described the angle between the superior L1 endplate and the sacral endplate. An overview of the demographic data and the postural measurements is presented in **Table 2**.

Next, individualized musculoskeletal models were created for each subject following the procedure described in **Section 2.1**. Consequently, the muscle activity and the intersegmental load were evaluated through static optimization in standing position and during flexion (maximal 30°), extension (maximal 20°), lateral bending (maximal 20°), axial rotation (maximal 30°), as well as for combinations of angles in the transversal plane (**Section 2.2**).

The consistency of the landmark positioning (**Section 2.1.1**) was assessed by quantifying the intra-rater and inter-rater reliability of annotations with intraclass correlation coefficients (ICC). Alignment parameters, weight estimation, and representative model results, such as the magnitude of the joint loads integrated over all levels and the summed tension generated by all lumbar erector spinae muscle fibers (in neutral position), were compared. One rater annotated a set of images at two different time points (TT), while another rater annotated the same set of images once (MRF). Annotations from nineteen images were considered for ICC of the alignment parameters and weight estimation, while the annotations from five different images were used to compare the reliability of the obtained model results. The radiographs for reliability evaluation were randomly selected from the available 145 images.

The compression and the anteroposterior shear components of the joint load are computed based on the local coordinate system linked to every joint. The compression component acts along the local axial direction, which is defined by the vector linking the considered joint and the joint next to it in cranial direction. The anteroposterior shear acts along the axis within the sagittal plane that is perpendicular to the local axial direction. A positive anteroposterior shear component indicates a contribution towards the posterior vertebral structures.

2.4 Validation

To validate the overall modeling approach, the results computed for our subjects were compared with those obtained by various *in vivo* and *in situ* studies (Lund et al., 2012; Hicks et al., 2015; Galbusera and Wilke, 2018). Information about the published studies used for validation are summarized in **Supplementary Table S1**. Several upper body postures were simulated for the comparisons mentioned below: standing in a neutral position, flexion (30°), extension (15°), lateral bending (20°), and axial rotation (30°). For lateral bending and axial rotation, the average between the movement to the left and to the right was considered.

First, measurements in patients who had a telemeterized vertebral body replacement implanted at the L1 level (Rohlmann et al., 2008) were compared to the results of previously published musculoskeletal models (Han et al., 2012; Bruno et al., 2015) and to the outcome of our analysis. For this purpose, the average compressive joint reaction forces at the L1L2 joint of the entire cohort were considered, as well as the simulated load in a single subject (male, 74 years, 69 Kg) with weight and age properties matched to the experimental conditions (2 males, 62 and 71 years, 66 and 72 Kg). Results for flexion, extension, lateral bending, and axial rotation were normalized to upright standing.

Next, the intradiscal pressure (IDP) measured within the L4L5 disc of healthy subjects in three different *in vivo* studies (Wilke et al., 2001; Sato et al., 1999; Takahashi et al., 2006) was compared to the outcome of the simulations. To account for a varying (mean) cross-sectional area (CSA) of the L4L5 IVD in the different experimental studies, the various experimentally determined IDPs were multiplied by the respective CSA. This output could then be compared to the compression force acting on the L4L5 joint in the musculoskeletal models after adjusting for the relationship between IDP and compressive JRF (F_c) with the following published equation:

$$IDP \cdot CSA_{IVD} = \frac{F_c}{f}, \qquad [\mathrm{N}] \tag{2}$$

where CSA_{IVD} is the CSA of the IVD and the factor f was set to 0.66 according to literature findings (Nachemson, 1959; Bruno et al., 2015). The compared upper body positions between measurements and simulation results depended on the available experimental data (Wilke et al. (2001): standing, flexion, extension, lateral bending, and axial rotation; Sato et al. (1999): standing, flexion, extension; Takahashi et al. (2006); standing, flexion). Both, the average cohort results, as well as the results for a subject (male, 34 years, 74 Kg) with characteristics comparable to the experiments (**Supplementary Table S1**), were analyzed.

Finally, a segment-wise comparison of the magnitude of compressive forces during standing was performed between other modeling studies (Ignasiak et al., 2016a; Bassani et al., 2017; Bruno et al., 2017) and the current one. In the work of Bruno et al. (2017) musculoskeletal models were generated for 125 male subjects with broad ranges of alignment, weight, and age parameters (**Supplementary Table S1**). We compared the results of their models (scaled by subject weight and height, and incorporating subject-specific rendering of the spine curvature) with the predicted load acting on the joints of the subject-specific models generated for the current study.

3 RESULTS

3.1 Spinal Alignment and Mass Distribution

Musculoskeletal models were successfully generated based on the bi-planar images of 145 subjects (**Figure 2**). The intra-rater ICCs were computed to quantify the reliability of landmark positioning

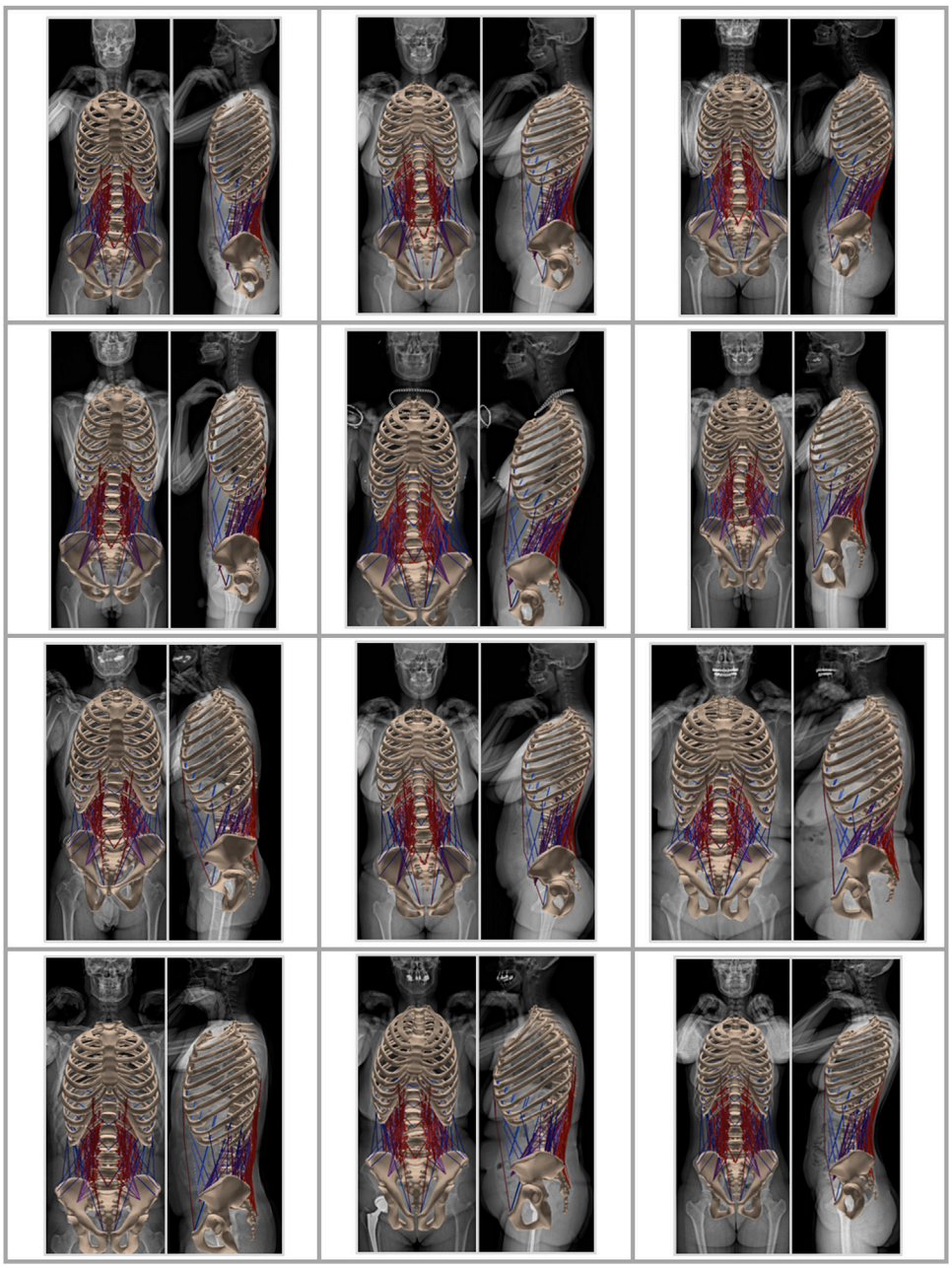

FIGURE 2 | Musculoskeletal models generated based on the EOS images of 12 subjects.

by a single rater at different time points in terms of the consistency of the obtained results (alignment, weight, and simulation results). All ICCs were greater than 0.90, except for those associated with the lumbar lordosis (ICC: 0.89; 95%: CI 0.74-0.96), pelvic incidence (ICC: 0.83; 95%: CI 0.60-0.93), and the sacral slope (ICC: 0.72; 95%: CI 0.41-0.88). Similar values were obtained for the assessment of inter-rater reliability, i.e., the comparison of annotations performed by two different raters (all ICC values and associated 95% CI are reported in **Supplementary Table S2**). **Figure 3A** depicts the thoracolumbar alignment of all subjects in the sagittal plane and with respect to the centroid of the L5 vertebra. As suggested by the values listed in **Table 2**, there are substantial variations amongst the curves and regarding the single alignment studied by Bruno et al. (2015). The average distance of the COM from the centroid of each vertebra diverged from previously reported computed tomography (CT)-derived measurements, particularly in the upper thoracic region and the lower lumbar spine (Pearsall et al., 1996, **Figure 3B**). The maximum relative distance towards the anterior from the vertebral center to the COM was determined at the L3 level

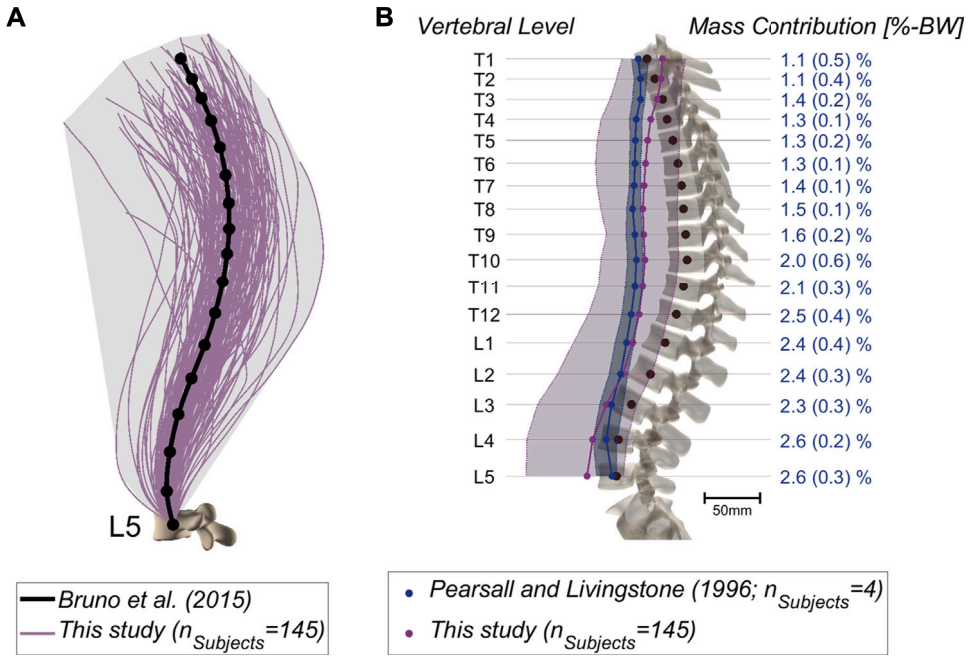

FIGURE 3 | (A) Alignments of the thoracolumbar spine derived from 145 patients based on cubic splines fitted through the vertebral centroids. Emphasis lies on the large variation compared to a generic model [Bruno et al. (2015); anatomy based on 25-years-old male, 50th percentile for height and weight, thoracic and lumbar curvature angles from average measurements]. **(B)** COM position relative to the vertebral centroids in the sagittal plane. The mean and range of the values (minimum-maximum) are depicted for the CT-derived measurements (blue) (Pearsall et al., 1996) and for our dataset (purple). Further, the percentage body weight concentrated at each segment was derived from literature and is indicated on the right (Pearsall et al., 1996).

with a magnitude of 85 mm, while a distance of 35 mm towards the posterior was measured at the uppermost thoracic vertebra.

3.2 Joint Reaction Forces

Figure 4 depicts the mean JRFs at different levels for the studied cohort (magnitude of compression and shear components are shown in **Supplementary Figure S1**). During flexion, the maximum load was found at the L5S1 joint, whereas extreme extension led to the highest joint loads at the T12L1 level. The heatmap-representation in **Figure 5** shows static optimization results as a mean for all subjects (segment-wise in **Figure 5A** and average of all levels in **Figure 5B**). It encompasses angular rotations around the axis normal to the sagittal plane (30° to −20°) and rotations along the axis normal to the frontal plane (15° to −15°), as well as combinations thereof. In general, the highest forces were observed when moving towards the extremities in the sagittal plane (high extension and most importantly, high flexion) and at the most caudally positioned joints (L4L5 and L5S1).

3.3 Validation

The magnitude of the computed compressive load at the L1L2 joint relative to standing for all subjects was compared to *in vivo*

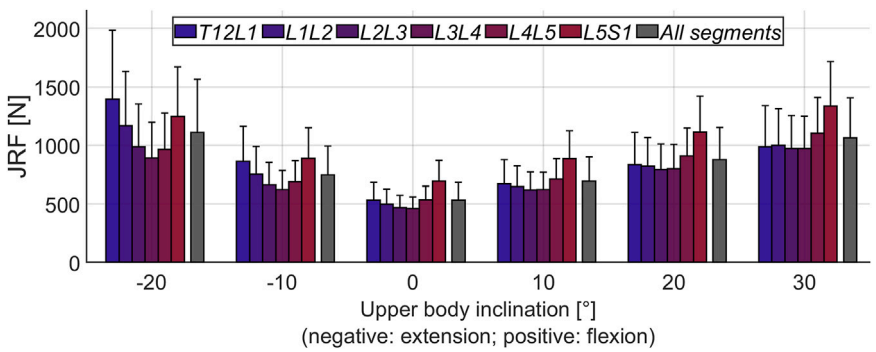

FIGURE 4 | Mean magnitude of JRFs during flexion-extension movement of the upper body. *All segments* refers to the average loading across the six considered joints (T12L1 to L5S1). The error bars indicate the standard deviation.

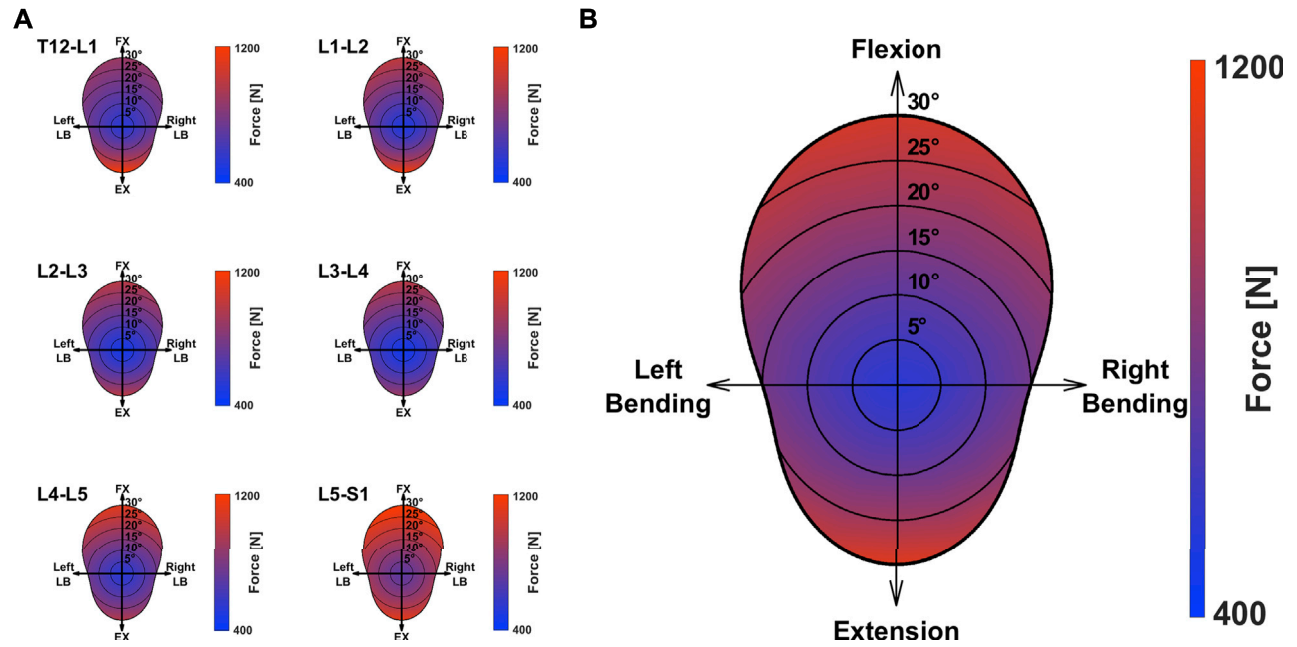

FIGURE 5 | Mean magnitude of JRF during movement around the axes perpendicular to the caudo-cranial axis. Values for the single segments **(A)** and the average loading over all considered joints **(B)** are depicted. FX: Flexion; EX: Extension; LB: Lateral Bending.

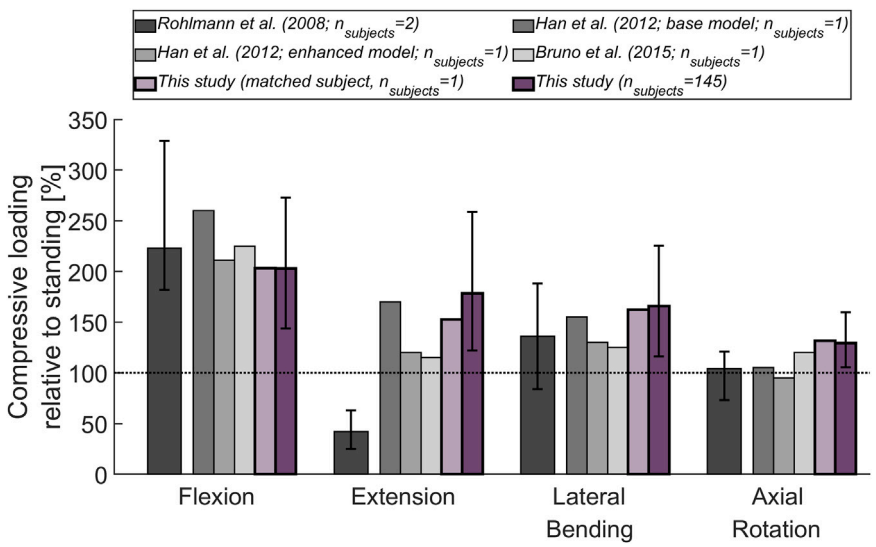

FIGURE 6 | Compressive load at L1L2 (relative to standing position) derived from *in vivo* measurements (Rohlmann et al., 2008) and from previously published thoracolumbar musculoskeletal models (Han et al., 2012; Bruno et al., 2015). These results are being compared to the mean compressive joint load obtained for the 145 subjects considered in this study (dark purple) and for a subject (male, 74 years, 69 kg; light purple) with age and weight properties comparable to those of the subjects in the experiments. The base model of Han et al. (2012) did not incorporate properties derived from passive elements or aspects of muscle dynamics, while these features were added in the enhanced model presented in the same publication. The error bars indicate the range between minimum and maximum values.

measurements of telemeterized L1 vertebral body implants (**Figure 6**). The relationship between loading during standing and loading after upper body rotations around the various body axes was similar for the cohort's average and the single subject matched to the experiment's participants in terms of sex, age and, weight. Except for flexion, there was a tendency for higher loads to be computed in the simulations, with a considerable discrepancy in extension. The difference between the

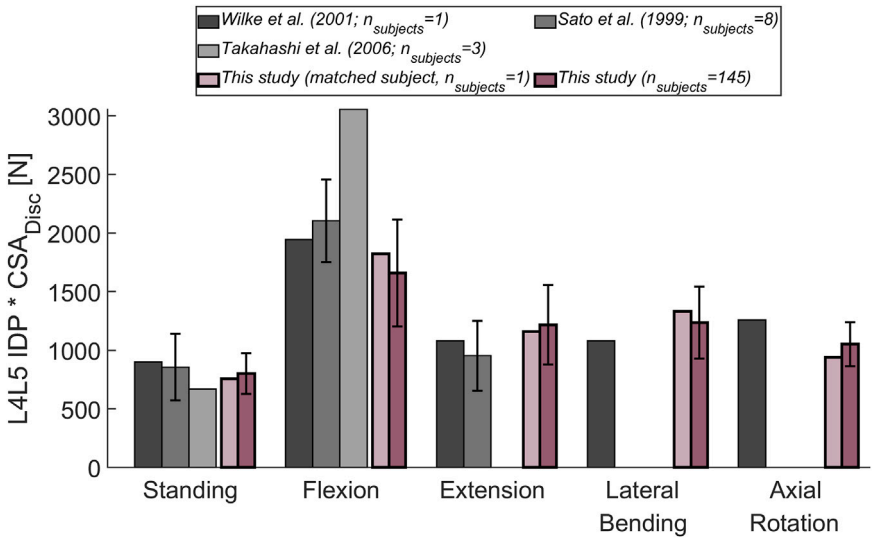

FIGURE 7 | Comparison between measured (Wilke et al., 2001; Sato et al., 1999; Takahashi et al., 2006) and computed IDP at the L4L5 joint. The following upper body positions were simulated: standing, flexion (30°), extension (15°), lateral bending (20°), and axial rotation (30°). To account for a varying CSA of the (mean) L4L5 IVD area in the different experimental studies, the experimentally determined IDP was multiplied by the respective CSA. The obtained results were compared to the mean results of the entire cohort considered in this study (dark purple). Additionally, the results for a subject (male, 34 years, 74 kg; light purple) with weight and age comparable to the subjects in the experimental studies, was depicted. Error bars indicate the standard deviation.

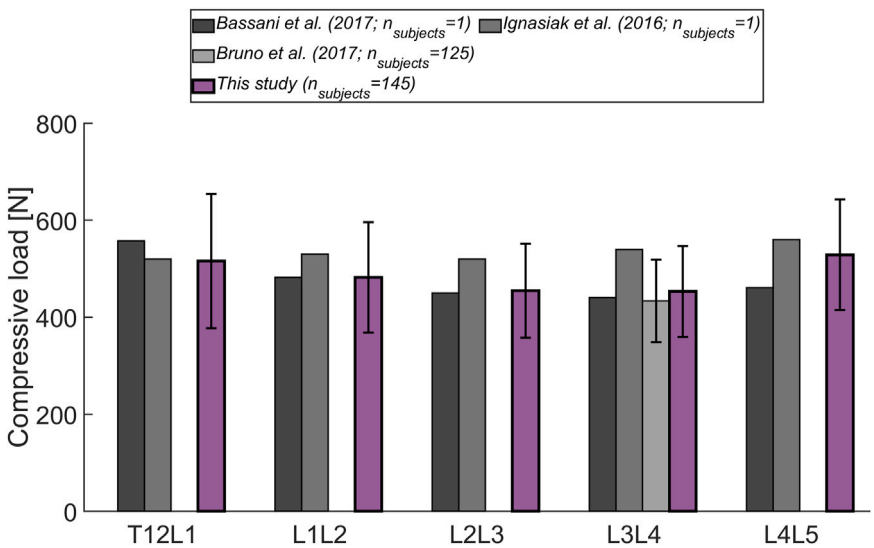

FIGURE 8 | Level-dependent comparison of the magnitude of compressive forces during standing with the outcome from other musculoskeletal models (Bassani et al., 2017; Ignasiak et al., 2016a; Bruno et al., 2017). Error bars indicate the standard deviation.

percentage values obtained with the subject-matched model and the results from the measurements were −20%, 110%, 26%, and 28% for flexion, extension, lateral bending, and axial rotation, respectively. These differences were comparable to those obtained with previously published musculoskeletal models replicating the *in vivo* conditions (Han et al. (2012); Bruno et al. (2015). **Figure 7** depicts IDP-related loading of the L4L5 disc for measurements and simulations performed at various upper body positions. Overall, the agreement between experimental results and simulations seems to be highest in standing position, while there is some underestimation seen with the simulation in flexion and lateral bending and slight overestimation of loading in extension and lateral bending. As shown in **Figure 7**, measured and estimated IDP values were similar, but there was a trend for the computed results to slightly overpredict the pressure within the disc. In terms of

compressive loading in the joints of the lower spine, the simulation results obtained in the current study are similar to those of previously published musculoskeletal models (Bassani et al. (2017); Ignasiak et al. (2016a); Bruno et al. (2017), **Figure 8**). Good agreement was achieved between the results of the study of Bruno et al. (2017) and those computed in this study for the compression at the L3L4 joint.

4 DISCUSSION

Previous studies on musculoskeletal models showed that biomechanical loads change considerably with spine alignment and tissue dimensions, along with a person's height and weight (Han, 2013; Bassani et al., 2017). Moreover, anatomical differences between male and female spinopelvic structures (pelvis, mass distribution, shape of lumbar curvature), as well as age-dependent variations, can be expected to affect the loading magnitude and distribution (Fon et al., 1980; Roussouly et al., 2005; Hay et al., 2015; Bassani et al., 2019). This highlights the necessity to accurately render these aspects when modeling the human spine. We, therefore, developed and validated a tool for the automatized generation of musculoskeletal models incorporating subject-specific alignment and mass distribution based on EOS images.

In contrast to CT and conventional X-ray imaging, the EOS system provides full-body scans in a weight-bearing posture with significantly lower radiation exposure (Dietrich et al., 2013). The use of bi-planar radiographs for musculoskeletal modeling is particularly favorable because these images are frequently acquired in clinical practice for the assessment of spine alignment.

To test the pipeline, models were generated for a cohort of 145 subjects without relevant spine deformations in the frontal plane. The results from the intra-rater and inter-rater reliability assessment of landmark positioning suggest that overall, the model properties and results can be well reproduced with the current annotation procedure (Koo and Li, 2016). The selected subjects formed a diverse cohort in terms of age, weight, and alignment (**Table 2**; **Figure 3**). This showed the robustness of the model creation approach and the cohort heterogeneity was reflected in the considerable range of computed joint loads (**Figure 4**). Furthermore, the average distance of COM from the corresponding vertebral centroid between our computations and the measurements of Pearsall et al. (1996) diverged towards the caudal and cranial ends of the thoracolumbar spine (**Figure 3B**). Our approach for determining the volume of transversal body sections was based on a simplification, namely fitting ellipses through just four landmarks delimiting the body extremity towards anterior, posterior, left, and right. However, there was also a large discrepancy in sample size, since Pearsall et al. (1996) only took measurements from four subjects, which might have limited the generalizability of their observations. Another factor limiting the comparability of relative COM position is the difference in posture during image acquisition (standing for the EOS images compared to supine in the CT scanner). Finally, this study focused on variations of alignment in the sagittal plane but the presented approach can be expected to similarly capture the fallout from alignment anomalies in the frontal plane (i.e. of scoliotic spines).

For model validation, mean results for the considered cohort were compared to normalized values from *in vivo* and *in situ* studies. The substantial deviation between measured and computed joint load in extended position (**Figure 6**) has already observed in other *in situ* studies (Han et al., 2012; Bruno et al., 2015). We hypothesize that this is caused by the load-carrying capacity of the facets, which might become more relevant during extension and hence, lead to a reduction of load exerted on the implant. The musculoskeletal models capture the force acting on the whole vertebra and do not differentiate between load transfer through posterior and anterior vertebral structures. Moreover, in addition to corpectomies at the L1 vertebra, the patients in the study of Rohlmann et al. (2008) had posterior spinal fixators in place, possibly causing parts of the load to be transferred across these additional implants. Furthermore, Rohlmann et al. (2008) did not specify the range of motion corresponding to the reported joint load. The level-dependent compressive loads agreed with the values derived from other musculoskeletal models (**Figure 8**). Also, the relative difference in loading observed between the joints was similar to the trend seen by Bassani et al. (2017) (highest forces were detected at the extremities of the lumbar spine).

Our study had several limitations. The analysis neglected thorax flexibility. As opposed to Bruno et al. (2015), the thorax was modeled as a rigid body and could therefore not account for relative rotations and joint reaction forces acting on the single thoracic vertebrae. However, according to Ignasiak et al. (2016b), this assumption does not considerably affect loading predictions in the lumbar spine. Further, the actual location of the COR hardly corresponds to the center of the intervertebral space, and the restriction of translational degrees of freedom through the use of spherical joints is a simplification. Rather, the COR in the lumbar spine has been described to be positioned more posteriorly and caudally with respect to the (upper) vertebral body. Moreover, the COR is not fixed but drifts during movement relative to the surrounding bony structures (Aiyangar et al., 2017). However, results obtained with another multi-rigid body model and sensitivity analysis performed with our model indicate that slight shifts in COR have no major influence on the results (Senteler et al., 2018). In this study, only the spine alignment in the frontal and sagittal plane was reproduced in the models, possible rotations of bony structures within the transverse plane were not taken into account. The impact on the results of this simplification is the subject of future investigations. Also, muscle properties were not derived from patient-specific measurements. The possibility to improve the models by incorporating image-based information or by using previously published regression models for the prediction of muscle parameters based on subject specifications (for example based on sex, age, height, and weight as proposed by Anderson et al. (2012)) needs to be assessed with a sensitivity analysis. So far, the lumbo-pelvic rhythm was not considered and we did not model the intra-abdominal pressure. According to previous investigations, the latter simplification, may have lead to an overestimation of joint loading (Arshad et al., 2016; Liu et al., 2019). Finally, the impact of passive structures (ligaments, intervertebral discs, facet joints) on spine behavior was not taken into account. It has been shown that the contribution to spine stabilization from these tissues becomes

especially relevant at positions further away from the neutral posture (Widmer et al., 2020). Consequently, when optimizing muscle activity at upper body positions increasingly further away from the standing position (0° around all axes), the aforementioned drawback can be expected to have a detrimental effect on the results. We, therefore, refrained from optimizing muscle activity at rotation angles greater than 30° around any axis. Despite these common modeling limitations, the framework represents a substantial advance in patient-specific modeling of the upper body and is likely to reveal novel insights into the biomechanics of the healthy and pathological spine.

5 CONCLUSION

Results obtained with spine multi-rigid body simulations are influenced by 1) the properties of the muscles, 2) the alignment of the CORs, and 3) the arrangement of the segments' COMs relative to the respective CORs. The present work showed that valuable information on subject-specific aspects concerning features 2) and 3) can be consistently gathered from EOS images. The modeling approach provides a robust tool for the automatized generation of individualized musculoskeletal models, importantly with accurate rendering of alignment and mass distribution. This powerful, high-throughput framework now enables the investigation of a variety of relevant clinical questions concerning the (lower) spine. Our overall aim is to enable studies on the impact of biomechanical aspects on the etiology and progression of pathologies and to perform subject-specific risk assessments. Specifically, we plan to evaluate the link between spine alignment and kinetics together with the possible clinical implications arising from this association.

DATA AVAILABILITY STATEMENT

The datasets presented in this article are not readily available because they are patient data.

ETHICS STATEMENT

The studies involving human participants were reviewed and approved by the Kantonale Ethikkommission, Kanton Zürich. Written informed consent to participate in this study was provided by the participants' legal guardian/next of kin.

AUTHOR CONTRIBUTIONS

M-RF contributed to the musculoskeletal model implementation, data analysis, results interpretation, writing of the manuscript. MJ contributed to the musculoskeletal model implementation, results interpretation, writing and editing of the manuscript. MK and DAG made large contributions to the implementation of the musculoskeletal model. TT annotated the EOS images. JGS and MF contributed to the interpretation of the results and editing of the manuscript. JW was responsible for the conception and design of the study, and contributed to the interpretation of the results, as well as writing and editing of the manuscript.

FUNDING

Financial support was provided by the Promedica Stiftung, Chur.

ACKNOWLEDGMENTS

The authors gratefully acknowledge the contribution of Kiran Kuruvithadam for his support in the development of the musculoskeletal model.

SUPPLEMENTARY MATERIAL

The Supplementary Material for this article can be found online at: https://www.frontiersin.org/articles/10.3389/fbioe.2021.721042/full#supplementary-material

REFERENCES

Aiyangar, A., Zheng, L., Anderst, W., and Zhang, X. (2017). Instantaneous Centers of Rotation for Lumbar Segmental Extension *In Vivo*. *J. Biomech.* 52, 113–121. doi:10.1016/j.jbiomech.2016.12.021

Anderson, D. E., D'Agostino, J. M., Bruno, A. G., Manoharan, R. K., and Bouxsein, M. L. (2012). Regressions for Estimating Muscle Parameters in the Thoracic and Lumbar Trunk for Use in Musculoskeletal Modeling. *J. Biomech.* 45, 66–75. doi:10.1016/j.jbiomech.2011.10.004

Arshad, R., Zander, T., Dreischarf, M., and Schmidt, H. (2016). Influence of Lumbar Spine Rhythms and Intra-abdominal Pressure on Spinal Loads and Trunk Muscle Forces during Upper Body Inclination. *Med. Eng. Phys.* 38, 333–338. doi:10.1016/j.medengphy.2016.01.013

Bassani, T., Casaroli, G., and Galbusera, F. (2019). Dependence of Lumbar Loads on Spinopelvic Sagittal Alignment: An Evaluation Based on Musculoskeletal Modeling. *PloS One* 14, e0207997. doi:10.1371/journal.pone.0207997

Bassani, T., Ottardi, C., Costa, F., Brayda-Bruno, M., Wilke, H.-J., and Galbusera, F. (2017). Semiautomated 3D Spine Reconstruction from Biplanar Radiographic Images: Prediction of Intervertebral Loading in Scoliotic Subjects. *Front. Bioeng. Biotechnol.* 5. doi:10.3389/fbioe.2017.00001

Bruno, A. G., Bouxsein, M. L., and Anderson, D. E. (2015). Development and Validation of a Musculoskeletal Model of the Fully Articulated Thoracolumbar Spine and Rib Cage. *J. Biomech. Eng.* 137, 081003. doi:10.1115/1.4030408

Bruno, A. G., Mokhtarzadeh, H., Allaire, B. T., Velie, K. R., De Paolis Kaluza, M. C., Anderson, D. E., et al. (2017). Incorporation of Ct-Based Measurements of Trunk Anatomy into Subject-specific Musculoskeletal Models of the Spine Influences Vertebral Loading Predictions. *J. Orthop. Res.* 35, 2164–2173. doi:10.1002/jor.23524

Caprara, S., Moschini, G., Snedeker, J. G., Farshad, M., and Senteler, M. (2020). Spinal Sagittal Alignment Goals Based on Statistical Modelling and Musculoskeletal Simulations. *J. Biomech.* 102, 109621. doi:10.1016/j.jbiomech.2020.109621

Christophy, M., Faruk Senan, N. A., Lotz, J. C., and O'Reilly, O. M. (2012). A Musculoskeletal Model for the Lumbar Spine. *Biomech. Model. Mechanobiol.* 11, 19–34. doi:10.1007/s10237-011-0290-6

Cobb, J. (1948). Outline for the Study of Scoliosis. *Instr. Course Lect AAOS* 5, 261–275.

Dagenais, S., Caro, J., and Haldeman, S. (2008). A Systematic Review of Low Back Pain Cost of Illness Studies in the United States and Internationally. *Spine J.* 8, 8–20. doi:10.1016/j.spinee.2007.10.005

Daggfeldt, K., and Thorstensson, A. (2003). The Mechanics of Back-Extensor Torque Production about the Lumbar Spine. *J. Biomech.* 36, 815–825. doi:10.1016/s0021-9290(03)00015-0

Damsgaard, M., Rasmussen, J., Christensen, S. T., Surma, E., and de Zee, M. (2006). Analysis of Musculoskeletal Systems in the AnyBody Modeling System. *Simulation Model. Pract. Theor.* 14, 1100–1111. doi:10.1016/j.simpat.2006.09.001

de Zee, M., Hansen, L., Wong, C., Rasmussen, J., and Simonsen, E. B. (2007). A Generic Detailed Rigid-Body Lumbar Spine Model. *J. Biomech.* 40, 1219–1227. doi:10.1016/j.jbiomech.2006.05.030

Delp, S. L., Anderson, F. C., Arnold, A. S., Loan, P., Habib, A., John, C. T., et al. (2007). OpenSim: Open-Source Software to Create and Analyze Dynamic Simulations of Movement. *IEEE Trans. Biomed. Eng.* 54, 1940–1950. doi:10.1109/tbme.2007.901024

Dietrich, T. J., Pfirrmann, C. W. A., Schwab, A., Pankalla, K., and Buck, F. M. (2013). Comparison of Radiation Dose, Workflow, Patient comfort and Financial Break-Even of Standard Digital Radiography and a Novel Biplanar Low-Dose X-ray System for Upright Full-Length Lower Limb and Whole Spine Radiography. *Skeletal Radiol.* 42, 959–967. doi:10.1007/s00256-013-1600-0

Esat, V., and Acar, M. (2004). A Finite Element Investigation of a Functional Spine Unit in Conjunction with a Multi-Body Model of the Lumbar Spine for Impact Dynamics. *ASMEDC* Vol. 2, 563–569. Manchester, England. doi:10.1115/esda2004-58527

Fon, G., Pitt, M., and Thies, A., Jr (1980). Thoracic Kyphosis: Range in normal Subjects. *Am. J. Roentgenology* 134, 979–983. doi:10.2214/ajr.134.5.979

Friedly, J., Standaert, C., and Chan, L. (2010). Epidemiology of Spine Care: The Back Pain Dilemma. *Phys. Med. Rehabil. Clin. North America* 21, 659–677. doi:10.1016/j.pmr.2010.08.002

Galbusera, F., and Wilke, H.-J. (2018). *Biomechanics of the Spine: Basic Concepts, Spinal Disorders and Treatments*. Academic Press.

Han, K.-S., Zander, T., Taylor, W. R., and Rohlmann, A. (2012). An Enhanced and Validated Generic Thoraco-Lumbar Spine Model for Prediction of Muscle Forces. *Med. Eng. Phys.* 34, 709–716. doi:10.1016/j.medengphy.2011.09.014

Han, K. S., Rohlmann, A., Zander, T., and Taylor, W. R. (2013). Lumbar Spinal Loads Vary with Body Height and Weight. *Med. Eng. Phys.* 35, 969–977. doi:10.1016/j.medengphy.2012.09.009

Hay, O., Dar, G., Abbas, J., Stein, D., May, H., Masharawi, Y., et al. (2015). The Lumbar Lordosis in Males and Females, Revisited. *PloS one* 10, e0133685. doi:10.1371/journal.pone.0133685

Hicks, J. L., Uchida, T. K., Seth, A., Rajagopal, A., and Delp, S. L. (2015). Is My Model Good Enough? Best Practices for Verification and Validation of Musculoskeletal Models and Simulations of Movement. *J. Biomechanical Eng.* 137, 0209051–02090524. doi:10.1115/1.4029304

Hill, A. V. (1938). The Heat of Shortening and the Dynamic Constants of Muscle. *Proc. R. Soc. Lond. B* 126, 136–195. doi:10.1098/rspb.1938.0050

Hoy, D., March, L., Brooks, P., Blyth, F., Woolf, A., Bain, C., et al. (2014). The Global burden of Low Back Pain: Estimates from the Global Burden of Disease 2010 Study. *Ann. Rheum. Dis.* 73, 968–974. doi:10.1136/annrheumdis-2013-204428

Ignasiak, D., Dendorfer, S., and Ferguson, S. J. (2016a). Thoracolumbar Spine Model with Articulated Ribcage for the Prediction of Dynamic Spinal Loading. *J. Biomech.* 49, 959–966. doi:10.1016/j.jbiomech.2015.10.010

Ignasiak, D., Ferguson, S. J., and Arjmand, N. (2016b). A Rigid Thorax assumption Affects Model Loading Predictions at the Upper but Not Lower Lumbar Levels. *J. Biomech.* 49, 3074–3078. doi:10.1016/j.jbiomech.2016.07.006

Koo, T. K., and Li, M. Y. (2016). A Guideline of Selecting and Reporting Intraclass Correlation Coefficients for Reliability Research. *J. Chiropractic Med.* 15, 155–163. doi:10.1016/j.jcm.2016.02.012

Legaye, J., Duval-Beaupre, G., Marty, C., and Hecquet, J. (1998). Pelvic Incidence: a Fundamental Pelvic Parameter for Three-Dimensional Regulation of Spinal Sagittal Curves. *Eur. Spine J.* 7, 99–103. doi:10.1007/s005860050038

Liu, T., Khalaf, K., Adeeb, S., and El-Rich, M. (2019). Numerical Investigation of Intra-abdominal Pressure Effects on Spinal Loads and Load-Sharing in Forward Flexion. *Front. Bioeng. Biotechnol.* 7, 428. doi:10.3389/fbioe.2019.00428

Lund, M. E., de Zee, M., Andersen, M. S., and Rasmussen, J. (2012). On Validation of Multibody Musculoskeletal Models. *Proc. Inst. Mech. Eng. H* 226, 82–94. doi:10.1177/0954411911431516

Malakoutian, M., Street, J., Wilke, H.-J., Stavness, I., Fels, S., and Oxland, T. (2018). A Musculoskeletal Model of the Lumbar Spine Using ArtiSynth - Development and Validation. *Computer Methods Biomech. Biomed. Eng. Imaging Visualization* 6, 483–490. doi:10.1080/21681163.2016.1187087

Nachemson, A. (1959). Measurement of Intradiscal Pressure. *Acta Orthopaedica Scand.* 28, 269–289. doi:10.3109/17453675908988632

Pearsall, D. J., Reid, J. G., and Livingston, L. A. (1996). Segmental Inertial Parameters of the Human Trunk as Determined from Computed Tomography. *Ann. Biomed. Eng.* 24, 198–210. doi:10.1007/BF02667349

Polga, D. J., Beaubien, B. P., Kallemeier, P. M., Schellhas, K. P., Lew, W. D., Buttermann, G. R., et al. (2004). Measurement of *In Vivo* Intradiscal Pressure in Healthy Thoracic Intervertebral Discs. *Spine* 29, 1320–1324. doi:10.1097/01.brs.0000127179.13271.78

Rohlmann, A., Graichen, F., Kayser, R., Bender, A., and Bergmann, G. (2008). Loads on a Telemeterized Vertebral Body Replacement Measured in Two Patients. *Spine* 33, 1170–1179. doi:10.1097/BRS.0b013e3181722d52

Rohlmann, A., Neller, S., Claes, L., Bergmann, G., and Wilke, H.-J. (2001). Influence of a Follower Load on Intradiscal Pressure and Intersegmental Rotation of the Lumbar Spine. *Spine* 26, E557–E561. doi:10.1097/00007632-200112150-00014

Rohlmann, A., Zander, T., Rao, M., and Bergmann, G. (2009). Applying a Follower Load Delivers Realistic Results for Simulating Standing. *J. Biomech.* 42, 1520–1526. doi:10.1016/j.jbiomech.2009.03.048

Roussouly, P., Gollogly, S., Berthonnaud, E., and Dimnet, J. (2005). Classification of the normal Variation in the Sagittal Alignment of the Human Lumbar Spine and Pelvis in the Standing Position. *Spine* 30, 346–353. doi:10.1097/01.brs.0000152379.54463.65

Sato, K., Kikuchi, S., and Yonezawa, T. (1999). *In Vivo* Intradiscal Pressure Measurement in Healthy Individuals and in Patients with Ongoing Back Problems. *Spine* 24, 2468. doi:10.1097/00007632-199912010-00008

Senteler, M., Aiyangar, A., Weisse, B., Farshad, M., and Snedeker, J. G. (2018). Sensitivity of Intervertebral Joint Forces to center of Rotation Location and Trends along its Migration Path. *J. Biomech.* 70, 140–148. doi:10.1016/j.jbiomech.2017.10.027

Senteler, M., Weisse, B., Rothenfluh, D. A., Farshad, M. T., and Snedeker, J. G. (2017). Fusion Angle Affects Intervertebral Adjacent Spinal Segment Joint Forces-Model-Based Analysis of Patient Specific Alignment. *J. Orthop. Res.* 35, 131–139. doi:10.1002/jor.23357

Senteler, M., Weisse, B., Snedeker, J. G., and Rothenfluh, D. A. (2014). Pelvic Incidence-Lumbar Lordosis Mismatch Results in Increased Segmental Joint Loads in the Unfused and Fused Lumbar Spine. *Eur. Spine J.* 23, 1384–1393. doi:10.1007/s00586-013-3132-7

Sorkine, O., and Alexa, M. (2007). As-rigid-as-possible Surface Modeling. *Symp. Geometry Process.* 4, 109–116.

Takahashi, I., Kikuchi, S.-i., Sato, K., and Sato, N. (2006). Mechanical Load of the Lumbar Spine during Forward Bending Motion of the Trunk-A Biomechanical Study. *Spine* 31, 18–23. doi:10.1097/01.brs.0000192636.69129.fb

Thelen, D. G. (2003). Adjustment of Muscle Mechanics Model Parameters to Simulate Dynamic Contractions in Older Adults. *J. Biomechanical Eng.* 125, 70–77. doi:10.1115/1.1531112

Toumanidou, T., and Noailly, J. (2015). Musculoskeletal Modeling of the Lumbar Spine to Explore Functional Interactions between Back Muscle Loads and Intervertebral Disk Multiphysics. *Front. Bioeng. Biotechnol.* 3, 111. doi:10.3389/fbioe.2015.00111

Traeger, A. C., Buchbinder, R., Elshaug, A. G., Croft, P. R., and Maher, C. G. (2019). Care for Low Back Pain: Can Health Systems Deliver? *Bull. World Health Organ.* 97, 423–433. doi:10.2471/BLT.18.226050

Widmer, J., Cornaz, F., Scheibler, G., Spirig, J. M., Snedeker, J. G., and Farshad, M. (2020). Biomechanical Contribution of Spinal Structures to Stability of the Lumbar Spine-Novel Biomechanical Insights. *Spine J.* 20, 1705–1716. doi:10.1016/j.spinee.2020.05.541

Widmer, J., Fornaciari, P., Senteler, M., Roth, T., Snedeker, J. G., and Farshad, M. (2019). Kinematics of the Spine under Healthy and Degenerative Conditions: A Systematic Review. *Ann. Biomed. Eng.* 47, 1491–1522. doi:10.1007/s10439-019-02252-x

Wilke, H.-J., Neef, P., Hinz, B., Seidel, H., and Claes, L. (2001). Intradiscal Pressure Together with Anthropometric Data - a Data Set for the Validation of Models. *Clin. Biomech.* 16, S111–S126. doi:10.1016/S0268-0033(00)00103-0

Wilke, H.-J., Rohlmann, A., Neller, S., Graichen, F., Claes, L., and Bergmann, G. (2003). ISSLS Prize Winner: A Novel Approach to Determine Trunk Muscle Forces during Flexion and Extension. *Spine* 28, 2585–2593. doi:10.1097/01.brs.0000096673.16363.c7

Conflict of Interest: The authors declare that the research was conducted in the absence of any commercial or financial relationships that could be construed as a potential conflict of interest.

frontiers in Bioengineering and Biotechnology

ORIGINAL RESEARCH
published: 01 September 2021
doi: 10.3389/fbioe.2021.720060

Subject-Specific Spino-Pelvic Models Reliably Measure Spinal Kinematics During Seated Forward Bending in Adult Spinal Deformity

Thomas Overbergh[1], Pieter Severijns[1], Erica Beaucage-Gauvreau[1], Thijs Ackermans[1], Lieven Moke[1,2], Ilse Jonkers[3] and Lennart Scheys[1,2]*

[1]Department of Development and Regeneration, Faculty of Medicine, Institute for Orthopaedic Research and Training (IORT), KU Leuven, Leuven, Belgium, [2]Division of Orthopaedics, University Hospitals Leuven, Leuven, Belgium, [3]Department of Movement Sciences, Human Movement Biomechanics Research Group, KU Leuven, Leuven, Belgium

OPEN ACCESS

Edited by:
Fabio Galbusera, Galeazzi Orthopedic Institute (IRCCS), Italy

Reviewed by:
Rizwan Arshad, Royal Military College of Canada, Canada
Tito Bassani, Galeazzi Orthopedic Institute (IRCCS), Italy

***Correspondence:**
Thomas Overbergh
Thomas.Overbergh@kuleuven.be

Specialty section:
This article was submitted to Biomechanics, a section of the journal Frontiers in Bioengineering and Biotechnology

Received: *03 June 2021*
Accepted: *17 August 2021*
Published: *01 September 2021*

Citation:
Overbergh T, Severijns P, Beaucage-Gauvreau E, Ackermans T, Moke L, Jonkers I and Scheys L (2021) Subject-Specific Spino-Pelvic Models Reliably Measure Spinal Kinematics During Seated Forward Bending in Adult Spinal Deformity. Front. Bioeng. Biotechnol. 9:720060. doi: 10.3389/fbioe.2021.720060

Image-based subject-specific models and simulations are recently being introduced to complement current state-of-the-art mostly static insights of the adult spinal deformity (ASD) pathology and improve the often poor surgical outcomes. Although the accuracy of a recently developed subject-specific modeling and simulation framework has already been quantified, its reliability to perform marker-driven kinematic analyses has not yet been investigated. The aim of this work was to evaluate the reliability of this subject-specific framework to measure spine kinematics in ASD patients, in terms of 1) the overall test-retest repeatability; 2) the inter-operator agreement of spine kinematic estimates; and, 3) the uncertainty of those spine kinematics to operator-dependent parameters of the framework. To evaluate the overall repeatability 1], four ASD subjects and one control subject participated in a test-retest study with a 2-week interval. At both time instances, subject-specific spino-pelvic models were created by one operator to simulate a recorded forward trunk flexion motion. Next, to evaluate inter-operator agreement 2], three trained operators each created a model for three ASD subjects to simulate the same forward trunk flexion motion. Intraclass correlation coefficients (ICC's) of the range of motion (ROM) of conventional spino-pelvic parameters [lumbar lordosis (LL), sagittal vertical axis (SVA), thoracic kyphosis (TK), pelvic tilt (PT), T1-and T9-spino-pelvic inclination (T1/T9-SPI)] were used to evaluate kinematic reliability 1] and inter-operator agreement 2]. Lastly, a Monte-Carlo probabilistic simulation was used to evaluate the uncertainty of the intervertebral joint kinematics to operator variability in the framework, for three ASD subjects 3]. LL, SVA, and T1/T9-SPI had an excellent test-retest reliability for the ROM, while TK and PT did not. Inter-operator agreement was excellent, with ICC values higher than test-retest reliability. These results indicate that operator-induced uncertainty has a limited impact on kinematic simulations of spine flexion, while test-retest reliability has a much higher variability. The definition of the intervertebral joints in the framework was identified as the most sensitive operator-dependent parameter. Nevertheless, intervertebral joint estimations had small mean 90% confidence intervals (1.04°–1.75°). This work will contribute to understanding the limitations of kinematic simulations in ASD patients, thus leading to a better evaluation of future hypotheses.

Keywords: spine kinematics, reliability, operator variability, adult spinal deformity, motion analysis, opensim model, subject-specific modeling and simulation, spine model

INTRODUCTION

Musculoskeletal (MS) models and associated simulations of motion are used to provide a better understanding of the complex biomechanics of, primarily, the healthy spine (Bruno et al., 2015; Ignasiak et al., 2018; Beaucage-Gauvreau et al., 2019). These simulation-based approaches provide parameters that are otherwise difficult, or even impossible, to measure non-invasively *in vivo*, such as intervertebral (IV) joint angles, IV disc loads (Bruno et al., 2017) and spinal muscle forces (Burkhart et al., 2017). Indeed, in healthy subjects these MS models have shown excellent test-retest reliability in terms of spine curvature estimation (expressed as lumbar lordosis and thoracic kyphosis) (Burkhart et al., 2020). More recently, these MS models and simulation-based approaches were introduced in pathological spine populations, such as adult spinal deformity (ASD) (Overbergh et al., 2020) and adolescent idiopathic scoliosis (AIS) (Schmid et al., 2016), to complement the current state-of-the-art mostly static assessments and on the longer term improve the often poor outcomes of surgical treatments (Smith et al., 2016). More specifically, a novel method based on biplanar radiography and computed tomography (CT) was developed to create subject-specific spino-pelvic rigid body models that allows inclusion of personalized spinal alignment, intervertebral joint definitions, and associated virtual skin markers for ASD patients (Overbergh et al., 2020). The resulting subject-specific models from this method can provide innovative, functional biomarkers of pathological spine biomechanics. This novel modeling method circumvents the traditional marker-based scaling step (Delp et al., 2007; Burkhart et al., 2020), which is applicable to healthy subjects, but not suitable for subjects with a spinal malalignment due to the lack of sufficient a priori information on the specific spinal deformity.

However, to improve the rigor and objectivity of the results prior to clinical interpretation, it is imperative to verify the simulation results of modeling methods both in terms of accuracy and reliability (Schwartz et al., 2004; Hicks et al., 2015). The accuracy of the above-mentioned subject-specific biplanar radiograph-based modeling method, as well as its accuracy in estimating spine kinematics, was validated previously (Overbergh et al., 2020).

Nevertheless, the subject-specific model creation method and the use of these subject-specific models to evaluate spinal kinematics remain susceptible to variability from different sources of errors and the impact thereof has not been investigated yet. Indeed, the creation of image-based subject-specific spino-pelvic models requires operator-dependent manual inputs to define virtual markers, spinal alignment, and IV joints (Overbergh et al., 2020), resulting in an extrinsic variability on the simulation outputs (Schwartz et al., 2004). The reliability of these operator-dependent inputs can be evaluated using an operator agreement analysis quantifying the robustness of the kinematic simulation results to this extrinsic variability (Hicks et al., 2015). In addition, the reliability of the kinematics of a subject is affected by intra-subject differences (i.e., within- or between-session variability), categorized as intrinsic variability (Schwartz et al., 2004). In relation to this intrinsic variability, the test-retest reliability of spino-pelvic parameterization through marker-based polynomial fitting of a sit-to-stance (STS) motion has already been investigated in an ASD population, and was reported to perform equally or even more reliable than conventional radiographic measurements (Severijns et al., 2020). However, the effect of these intra-subject differences in combination with image-based subject-specific models has not yet been investigated in an ASD population.

Specifically for biomechanical modeling and simulation research, the complex non-linear interactions between input and output parameters often require an extension to the conventional operator agreement analyses to obtain a representative range of output variability and identify the aspects of the modeling method that have the highest/lowest impact on the outputs (Hicks et al., 2015). Therefore, uncertainty analyses, such as Monte-Carlo probabilistic simulations, are commonly used to assess the simultaneous impact of uncertainties arising from multiple sources (Hicks et al., 2015; Myers et al., 2015). Monte-Carlo analyses allow computation of sensitivity factors (e.g., correlation coefficients) to determine relations between the input and output distributions (Hicks et al., 2015; Myers et al., 2015) to identify the modeling components with a high impact on the output for future improvements. Thereto, Monte Carlo analyses generate a large number of statistically probable variations of a baseline model, consisting of randomly combined perturbations of the operator-dependent parameters susceptible to uncertainty. These perturbations are sampled from a probability density function representative of the actual variability of the operator-dependent parameters (Valero-Cuevas et al., 2003; Hannah et al., 2017). The impact of these operator-dependent parameters on the simulation outputs can then be translated into confidence bounds on the baseline output (Ackland et al., 2012; Valente et al., 2014; Myers et al., 2015).

The aim of this study was to evaluate the reliability of a previously developed subject-specific spino-pelvic modeling method (Overbergh et al., 2020) to measure spine kinematics in an ASD population, in terms of 1) the overall test-retest repeatability and 2) the inter-operator agreement of spine kinematic estimates; and 3) the sensitivity of those spine kinematics to operator-dependent aspects of the underlying subject-specific modeling method.

MATERIALS AND METHODS

Participants and Data Collection

Five participants [2 males (51 and 72 years), 3 females (62, 69, and 70 years)] with varying degrees of spinal malalignment and one control subject (female) participated in this study following ethical approval and informed consent (S58082) (Overbergh et al., 2020). All data collection was performed in at the university hospital of Leuven (UZ Leuven, Belgium). All subjects underwent CT imaging from T1 to pelvis (BrightSpeed by GE Healthcare, with an inter-slice distance of 1.25 mm and a pixel size of 0.39 mm × 0.39 mm). Thereafter, an

experienced physiotherapist instrumented each subject with reflective markers according to the skin marker protocol described in Overbergh et al. (2020). Full-body radiographic (x-ray) images were then acquired using the biplanar radiography system (EOS Imaging, Paris, France), while the subject was wearing the markers and adopted the Scoliosis Research Society free-standing position (fingers-on-clavicle variation) (Wang et al., 2014). When the subjects arrived at the motion laboratory, they were asked to perform a maximal forward trunk flexion from a normal upright seated position, while the trajectories of the reflective markers were recorded (100 Hz) using a 10-camera Vicon system (VICON Motion systems, Oxford Metrics, United Kingdom). Four of the five ASD patients and the control subject repeated all data collections, apart from the CT imaging, after an average 2-week time interval (mean 14.2 ± 9.9 days, 6–33 days). One ASD patient (male) was excluded for the second data collection due to a surgical intervention, but remained part of the study because of a successful first data collection.

Test-Retest Reliability

To test the repeatability of our workflow for spinal kinematic evaluation, we performed a test-retest reliability analysis between the two repeated data collection sessions available for each of the four ASD subjects (one excluded) and the control subject. Two subject-specific spino-pelvic models were created by one single operator to prevent confounding inter-rater variability; one for the initial data collection and one for the repeated data collection, respectively (Overbergh et al., 2020). The resulting subject-specific spine models each consist of 18 bodies (12 thoracic vertebrae, 5 lumbar vertebrae and a sacrum/pelvis body), interconnected by 17 spherical joints [each with three rotational degrees of freedom (DOFs)] and have a total of 28 virtual model markers each, corresponding to the retroreflective markers placed on the skin of the subject (Overbergh et al., 2020). It should be noted that these aspects of the model (i.e., bodies, joints and markers) all required input from an operator (Overbergh et al., 2020). The maximal forward trunk flexion motion, recorded as three-dimensional (3D) marker trajectories in the motion laboratory, was processed using Vicon Nexus 2.11 (VICON Motion systems, Oxford Metrics, United Kingdom) and low-pass Butterworth filtered (6 Hz). For each subject and each session, the respective models were used to run an inverse kinematics analysis (Lu and O'Connor, 1999) in OpenSim 3.3 (Stanford University, United States) (Delp et al., 2007) of the corresponding forward trunk flexion motions. The kinematic outputs (i.e., 51 joint angles ranging from L5/Sacrum to T1/T2) were time-normalized (to 100 frames) and noise reduction was performed using a moving average filter with a three-frame width. The joint kinematics (i.e., relative motion at the joint between two interconnected bodies) were converted to body kinematics (i.e., absolute motion of a body expressed in the ground reference frame) to obtain six common spino-pelvic parameters in the sagittal plane based on a-priori identification of anatomical landmarks on the model: 1) lumbar lordosis (LL), 2) thoracic kyphosis (TK), 3) sagittal vertical axis (SVA), 4) pelvic tilt (PT), and 5) T1 and 6) T9 spino-pelvic inclination (T1-SPI, T9-SPI), (detailed in **Supplementary Appendix S1**). The ranges of motion (ROM) of each of these spino-pelvic parameters (defined as the absolute value of the difference between the start and the end of the motion, **Supplementary Appendix S1**) were used as an outcome parameter to determine the test-retest reliability. This test-retest reliability was expressed as intraclass correlation coefficients (ICC's) with a two-way random effects model for absolute agreement [ICC(2,1)] (SPSS 25, IBM Corp. Armonk, NY). ICC's were classified as poor (ICC <0.40), fair to good (0.40–0.75) or excellent (>0.75) (Shrout and Fleiss, 1979). Standard error of measurement (SEM) was calculated as:

$$SEM = SD\sqrt{1 - ICC}, \quad (1)$$

with SD the standard deviation of the absolute difference relative to the mean output; and the smallest detectable difference (SDD) (Shrout and Fleiss, 1979) as:

$$SDD = SEM \times 1.96\sqrt{2} \quad (2)$$

Inter-Operator Reliability

To assess the portion of variability of the modeling method on the kinematic results that can be attributed to operator-dependent inputs (Overbergh et al., 2020), three operator-dependent modeling components (and their associated parameters) were first identified (**Figure 1**): (A) virtual markers (position parameters): the reconstruction of virtual marker positions requires operators to identify and delineate retro-reflective markers on both biplanar radiographic images; (B) bodies (i.e., vertebrae and pelvis) (position and orientation parameters): the manual reconstruction of the 3D spinal alignment requires operators to match subject-specific vertebrae projections on biplanar radiographic images until visual agreement; (C) joints (position and orientation parameters): the IV joint definition requires operators to manually identify anatomical landmarks on the bodies connected by these joints. This results in a total of 294 operator-dependent parameters [(28 markers × 3 DOFs) + (18 bodies × 6 DOFs) + (17 joints × 6 DOFs)].

Three operators participated in this study. One operator (O1, 4 years of spine modeling experience and developer of the modeling method), trained two additional operators (O2 and O3 with 6 and 2 years of spinal research experience, respectively) on the required steps of the modeling workflow through a dedicated manual describing optimal use of the custom software. Next, radiographic data of a cadaver with known ground truth spinal alignment due to plastination, was used for acquainting with and training in spinal alignment personalization (Overbergh et al., 2020) (detailed in **Supplementary Appendix S2**), followed by a final collective, quantitative feedback session between the operators. Then, each operator created a subject-specific spinal model of three randomly selected subjects (S1, S2 and S3, **Figure 2**) from the ASD group while being blinded to the other operators. The models were created as described in the modeling workflow of Overbergh et al. (2020), with the exception of segmenting the individual bones from CT which was only performed only by O1.

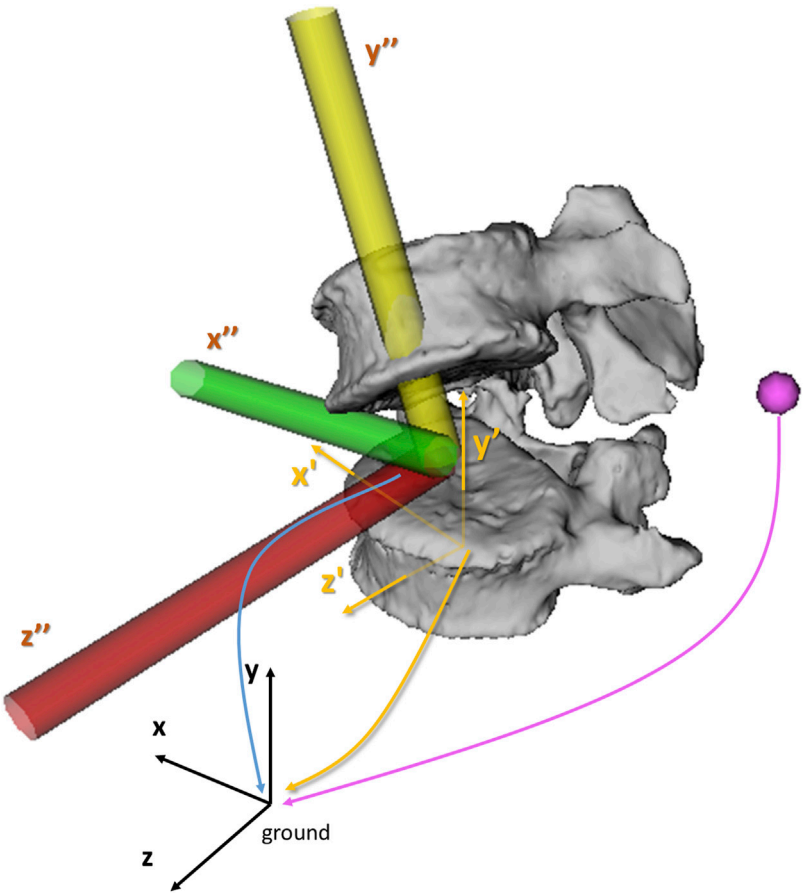

FIGURE 1 | Illustration of the three operator-dependent parameters components. The position of the virtual markers (pink sphere), the position and orientation of the bodies (yellow reference frame, x'y'z') and the position and orientation of the IV joints (yellow, green and red reference frame, x"y"z") are expressed in the ground reference frame (black, xyz). Within the model, positions of virtual markers, bodies and joints, are expressed in the x (mediolateral), y (inferosuperior) and z (posterior-anterior) directions. The orientations of the joints and bodies are expressed around the x (flexion-extension, FE), y (axial rotation, AR) and z-axis (lateroflexion, LF) using an xyz body-fixed sequence.

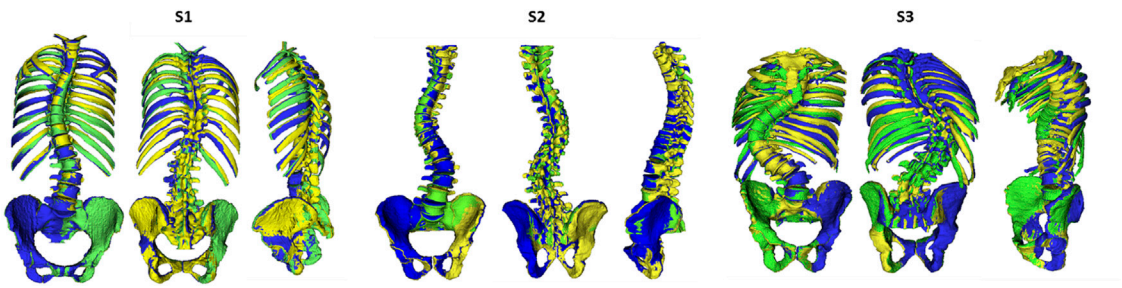

FIGURE 2 | Illustration of the alignment reconstruction for the three subjects [S1 (female), S2 (male) and S3 (male)] by the three operators: O1 (green), O2 (yellow) and O3 (blue).

Inter-Operator Agreement

Each of the nine created models was used to perform an inverse kinematics simulation of the subject's corresponding maximal forward flexion motion to obtain the ROM values for the six spino-pelvic parameters (LL, TK, SVA, PT, T1-SPI, T9-SPI). ICC's, SEM (**Formula 1**) and SDD (**Formula 2**) on these outcome values were used to assess inter-operator agreement.

Monte-Carlo Probabilistic Simulation

We performed a Monte-Carlo probabilistic simulation analysis to quantify the distributions of variations on simulated IV joint

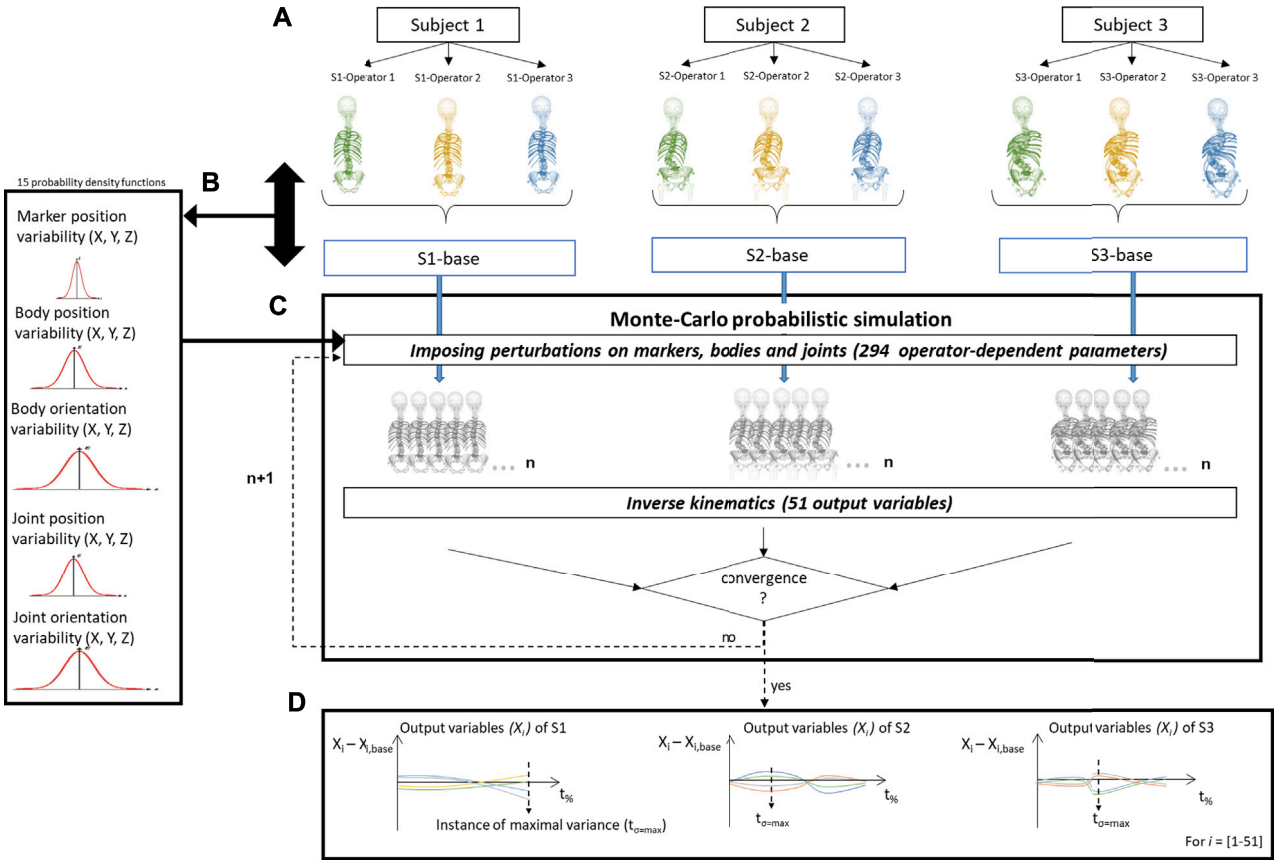

FIGURE 3 | Schematic representation of the determination of the inter-operator reliability of subject-specific modeling. **(A)** For each subject (S), a subject-specific model was created by each of the three operators (O). A baseline model (S-base) was then created for every subject by averaging these three respective models. **(B)** The variability in the operator-dependent parameters was calculated in relation to the respective baseline models, pooled together for all vertebral levels and subjects, and separated by direction. **(C)** In the Monte-Carlo probabilistic simulation, variations on the baseline model were created by imposing statistically probable error combinations on the operator-dependent parameters and then used to perform inverse kinematic simulations until the convergence criterion on the output variables (i.e., the joint angles) was reached. **(D)** The joint angles (X_i with i = 1...51) were then expressed relative to the joint angles of the corresponding baseline model ($X_{i,\,base}$) and time normalized ($t_{\%}$). $t_{\sigma=max}$ represents the time instance of maximal variance.

kinematics caused by operator variability, similar to the work by Valente et al. (2014). First, a baseline model (S-base) was determined for each of the three ASD subjects to avoid operator bias, by averaging the three operator-defined models (**Figure 3A**). These baseline models were considered as reference models to experimentally estimate the variability of the 294 operator-dependent model parameters. The variations of these operator-dependent components (marker, bodies, and joint) for the three models with respect to its respective baseline model were pooled into histograms over all vertebral levels and subjects, and separated by direction (x, y, z) for each parameter (position and orientation) (**Supplementary Appendix S3**). From these experimentally determined variability histograms, continuous probability density functions were estimated (MATLAB, The Mathworks Inc., MA) (**Supplementary Appendix S3**), and used as input to sample variations on the 294 operator-dependent model parameters (**Figure 3B**). This ensured statistically probable imposed perturbations according to a-priori experimentally determined inter-operator variability. To create a perturbed model, a value was sampled from the probability function for each operator-dependent model parameter and used to vary the value of that parameter in the baseline model. For each subject, every variation of the baseline model was then used to run an inverse kinematics analysis (Lu and O'Connor, 1999) (**Figure 3C**). The convergence criterion for the Monte-Carlo simulation was defined such that the mean and standard deviation of all output variables (here: joint angles averaged over the duration of the motion) over the last 10% of the simulations were within 2% of each final mean and standard deviation (**Supplementary Appendix S4**) (Valero-Cuevas et al., 2003; Ackland et al., 2012; Valente et al., 2013; Martelli et al., 2015).

Operator-Dependent Input Parameters

After assessing normality of the parameters of the model components (position and/or orientation of markers, bodies, joints), kernel functions were consistently used to estimate all distribution functions from their respective histograms

TABLE 1 | Results of the test-retest reliability analysis. ROM, range of motion; ICC, intraclass correlation coefficient; SD, standard deviation of the absolute differences between both sessions; SEM, standard error of measurement; SDD, smallest detectable difference. Significance level: $p < 0.05$ (bold). The confidence intervals for ICC's with a non-significant p value are not applicable.

Spino-pelvic parameter ROM	Test-retest ICC	95% confidence interval	p value	SD	SEM	SDD	Mean (range) ROM
LL (°)	0.86	0.032–0.985	**0.028**	5.5	2.1	5.7	20.5 (9.5–42.4)
TK (°)	0.12	—	0.460	6.2	5.8	16.1	19.8 (1.8–30.9)
SVA (cm)	0.91	0.363–0.991	**0.018**	0.9	0.3	0.7	30.0 (25.4–40.6)
PT (°)	0.80	—	0.095	5.3	2.4	6.6	53.9 (30.4–60.4)
T1-SPI (°)	0.91	0.226–0.990	**0.012**	4.7	1.4	4.0	66.7 (46.1–89.7)
T9-SPI (°)	0.91	0.360–0.990	**0.015**	4.7	1.4	3.9	60.6 (39.5–81.7)

(Distribution Fitter, MATLAB, The Mathworks Inc., MA) (**Supplementary Appendix S3**). To assess the variation of the operator-dependent inputs in the modeling method (markers, bodies and joints), we used the absolute value of the difference between each of the three operator-dependent models and its baseline model to determine the median and maximum values for each individual position and orientation parameter, in each direction.

To assess the robustness of the IV joint kinematics to variations in the operator-dependent model parameters, joint angles of the perturbed models were expressed relative to the joint angles of the baseline model's kinematics. For each subject, we then determined the 5–95% confidence bounds for each of the joint angles (17 joints with three rotational DOFs each), at each time frame of the performed spine flexion motion, which indicates a 90% probability that an estimated joint angle curve is within the confidence intervals with respect to the calculated reference curve (Myers et al., 2015; Navacchia et al., 2016). Thereafter, a box and whiskers plot was created at the time instance of respective maximal variance ($t_{\sigma=max,}$ **Figure 3D**) for every DOF at every joint (Ackland et al., 2012).

Sensitivity Factors

To quantify the sensitivity of simulated kinematics to variability in specific input parameters, sensitivity factors were determined as Pearson correlation coefficients (Myers et al., 2015) between the sampled perturbation values (for each of the 294 model parameter) and the corresponding absolute maximal difference of the IV joint kinematics with respect to the baseline model's IV joint kinematics (for each of the 51 DOFs), pooled for all three subjects (MATLAB).

RESULTS

Test-Retest Reliability

The test-retest reliability, expressed as ICCs of six spino-pelvic parameters in **Table 1**, was excellent (ICC>0.75) for the LL, SVA, PT (not significant), T1-SPI and T9-SPI. Nevertheless, high SEM and SDD were noted for TK, which presented with a poor reliability (ICC<0.40).

Inter-Operator Agreement

Excellent inter-operator agreement (ICCs ≥0.875) of the kinematics, expressed as spino-pelvic parameters, was noted for all analyzed parameters (**Table 2**).

Monte-Carlo Probabilistic Simulation

Operator-dependent Input Parameters

The median difference in the virtual marker positions with respect to the baseline models ranged between 0.120 and 0.122 mm (**Table 3**). For the 3D distance the median (maximal) difference was 0.262 mm (1.040 mm). The median differences with respect to the body positions and orientations of the baseline models ranged between 0.552 and 0.739 mm and 0.96°–1.68°, respectively (**Table 3**). Finally, the median differences with respect to the joint positions and orientations of the baseline models ranged between 0.566 and 1.058 mm and 1.16°–1.95°, respectively (**Table 3**). (See also **Supplementary Appendix S3** for the corresponding probability distributions.)

Kinematic Simulation Output

Convergence of the Monte-Carlo probabilistic simulations was reached at $n = 954$, $n = 814$ and $n = 894$ for subject S1, S2 and S3, respectively (detailed in **Supplementary Appendix S4**), where n is the number of iterations. For convenience, the minimal number of required iterations for convergence was rounded up to 1,000 and set equal for all subjects. **Figure 4** illustrates the 90%-confidence intervals (CIs) over the duration of the motion for S1.

The mean (maximum) of the 90%-CIs of the IV joint kinematics at their respective $t_{\sigma=max}$ were 1.04° (3.44° at L2/L3 lateroflexion [LF]), 1.14° (4.79° at L2/L3 LF) and 1.75° (11.72° at L2/L3 LF) for S1, S2 and S3 respectively (**Supplementary Figures S4.5–4.7** of **Supplementary Appendix S4**). The box and whisker plots show a higher variability at the lumbar and low thoracolumbar region compared to the upper thoracic region (**Figure 5**). Furthermore, S3 presents with larger CIs at the lumbar region than S1 and S2 (**Figure 4** and **Supplementary Figures S4.5–4.6** of **Supplementary Appendix S4**).

Sensitivity Factors

Calculating the sensitivity factors for all possible combinations of input (i.e., operator-dependent model parameters) and output (i.e., IV joint kinematics for every DOFs) variables, resulted in a 294 by 51 grid of correlations. Mean (maximal) sensitivity factors were 0.015 (0.15) for the marker positions, 0.015 (0.07) and 0.014 (0.06) for the body positions and orientations, respectively; and 0.022 (0.26) and 0.021 (0.47) for the joint positions and orientations, respectively.

TABLE 2 | Results of the inter-operator reliability analysis. ROM, range of motion; ICC, intraclass correlation coefficient, SD, standard deviation of absolute error relative to mean value; SEM, standard error of measurement; SDD, smallest detectable difference. Significance level: $p < 0.05$ (bold).

Spino-pelvic parameter ROM	Inter-operator ICC	95% confidence interval	*p* value	Mean SD	SEM	SDD
LL (°)	0.970	0.775–0.999	0.002	1.82	0.3	0.9
TK (°)	0.875	0.189–0.997	0.031	1.95	0.7	1.9
SVA (cm)	0.964	0.737–0.999	0.005	0.43	0.1	0.2
PT (°)	0.998	0.981–1.000	<0.001	0.13	0.0	0.0
T1-SPI (°)	1.000	0.999–1.000	<0.001	0.06	0.0	0.0
T9-SPI (°)	1.000	0.998–1.000	<0.001	0.07	0.0	0.0

TABLE 3 | Operator-dependent input parameters.

Input parameters	Median (max) X	Median (max) Y	Median (max) Z
Marker position (mm)	0.112 (0.584)	0.120 (0.717)	0.120 (1.039)
Body position (mm)	0.672 (4.71)	0.552 (3.79)	0.739 (14.74)
Body orientation (°)	1.19 (10.4)	1.68 (10.8)	0.96 (6.83)
Joint position (mm)	0.782 (4.44)	0.566 (14.32)	1.058 (12.18)
Joint orientation (°)	1.65 (16.4)	1.95 (9.97)	1.16 (7.09)

DISCUSSION

This study aimed at evaluating the kinematic variability associated with both intrinsic and extrinsic sources of error (Schwartz et al., 2004), of a subject-specific spino-pelvic modeling method previously developed to quantify intervertebral joint motion in ASD subjects (Overbergh et al., 2020).

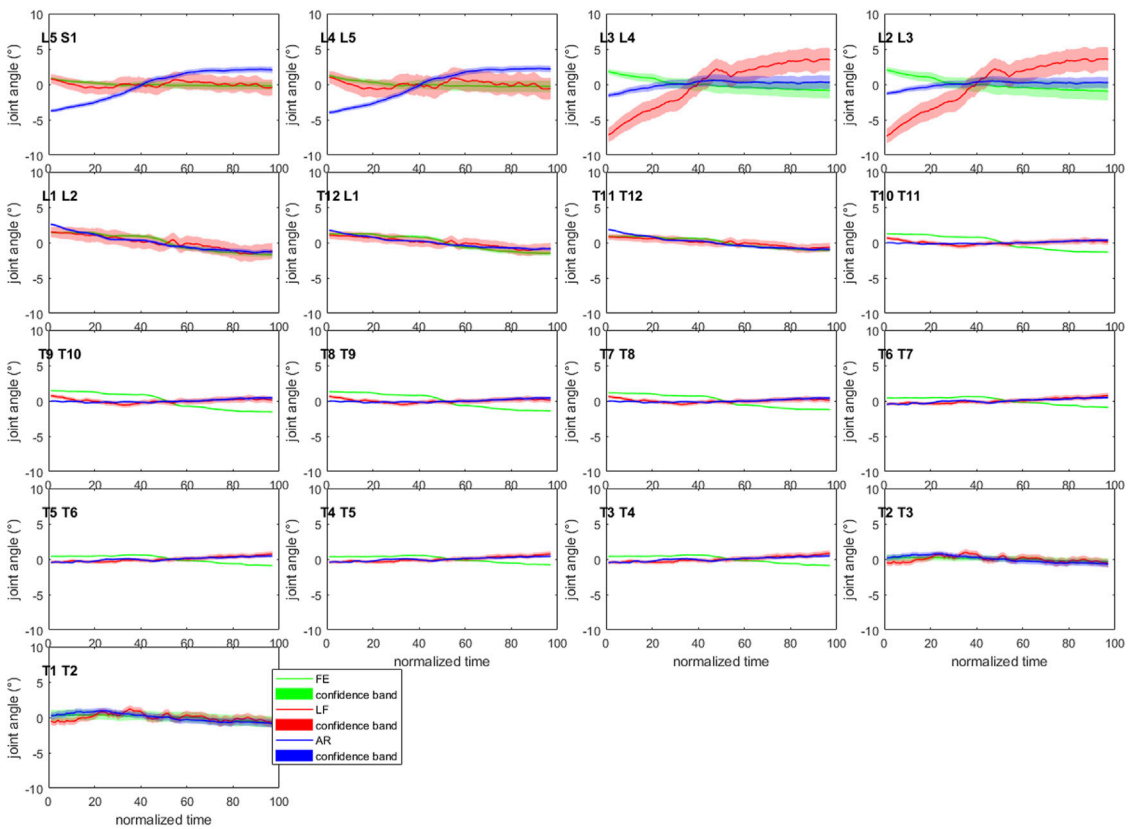

FIGURE 4 | Confidence bands (5–95%) for each of the joint angles of subject 1. All curves have been normalized to their mean value over the length of the motion to allow visualization within the −10°–10° joint angle range. AR: axial rotation; LF: lateroflexion; FE: flexion-extension (Graphs for S2 and S3 are available in **Supplementary Material S4.5–4.6** of **Supplementary Appendix S4**).

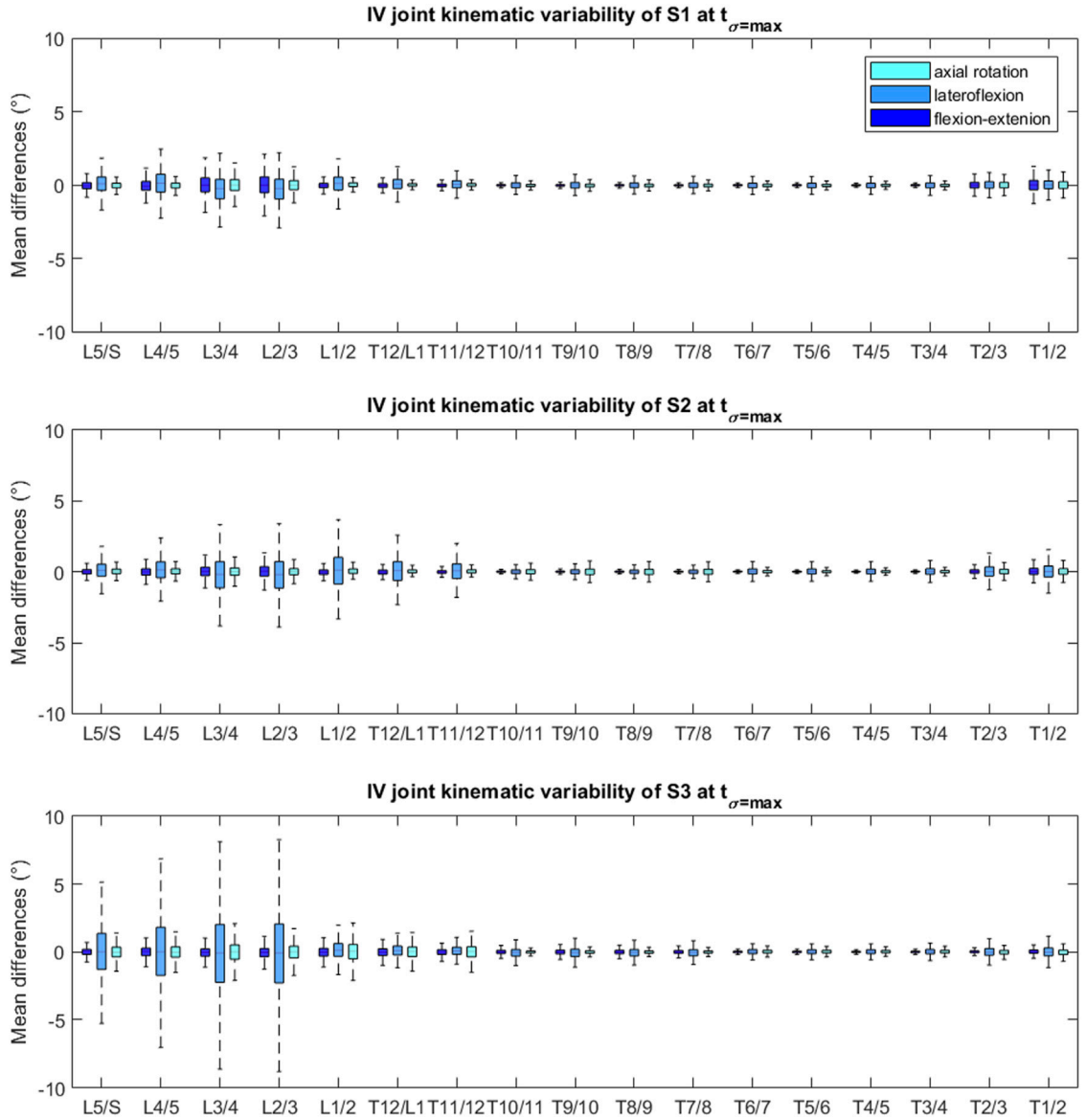

FIGURE 5 | Box and whisker plot of the joint values at $t_{\sigma=max}$ of each DOF, relative to the baseline model's joint angles, for each subject. The upper and lower edges of the box are the 75th and 25th percentiles, the horizontal bar in the box is the median (50th percentile) and the upper and lower bars are maximum and minimum values.

The test-retest reliability (intrinsic intra-subject and extrinsic intra-operator variability) of the kinematics within individual subjects was evaluated over a 2-week time interval. Although our method is capable of measuring spinal kinematics at the level of the IV joint, we gave priority to analyzing spino-pelvic parameters that are more commonly studied and used in clinical practice because of the lack of available literature on IV joint kinematic variability to compare to. Our results were similar to those previously reported in an ASD (Severijns et al., 2020) and healthy (Mousavi et al., 2018) population. Notably, we obtained a similar reliability for LL [ICC: 0.86 vs. 0.84 (Severijns et al., 2020) and 0.79 (Mousavi et al., 2018)] and SVA [ICC: 0.91 and 0.95 (Severijns et al., 2020)], but a lower reliability for TK [ICC: 0.12 vs. 0.95 (Severijns et al., 2020) and 0.78 (Mousavi et al., 2018)]. Although the skin marker set, pathology of the study population (ASD) and amount of subjects (5 and 8, respectively) are comparable to the study by Severijns et al. (2020), differences in the kinematic model (marker-driven subject-specific model vs. polynomial marker fit) along with the difference in motion performed by the subjects (trunk flexion [current work] vs. STS) may explain the notable difference in reliability of the TK parameter. Indeed, a maximal forward flexion is more challenging in terms of standardization compared to a STS movement. Furthermore, the thoracic region is typically more involved during maximal forward flexion compared to STS [mean ROM TK: 19.8° vs. 7.86° (Severijns et al., 2020)]. Lastly,

as the modeling method is more reliant on manual operator interaction compared to Severijns et al. (2020), the modeling method may present with a potentially higher intra-operator variability, which is part of the test-retest variability.

The inter-operator kinematic agreement was assessed to investigate the effects of extrinsic inter-operator variability specifically related to the modeling method. The operator agreement in terms of spino-pelvic parameters, was excellent with ICC values ranging from 0.875 (TK) to (almost) 1 (LL, SVA, PT, T1-SPI, T9-SPI), showing a high to very high agreement amongst the three operators. Compared to Severijns et al. (2020), we report higher ICC values for LL (0.97 vs. 0.92), but slightly lower for SVA (0.964 vs. 1.00) and TK (0.875 vs. 0.91). PT, T1-SPI and T9-SPI were in almost perfect agreement. The comparable, but still slightly higher, inter-operator reliability of Severijns et al. (2020) could possibly be explained by the limited amount of operator-dependent tasks (only marker identification) in their workflow, which can be done with high accuracy (Pillet et al., 2014) compared to the additional operator-dependent tasks (i.e., CT-segmentation, marker identification, body and joint reconstruction) required to create the fully subject-specific spino-pelvic models in this work. Nevertheless, only the latter allows analysis of individual IV joint angles.

To further quantify the probabilistic effects of subject-specific spino-pelvic modeling uncertainty on intervertebral kinematics in ASD patients, we used a Monte-Carlo probabilistic simulation. The variabilities in the operator-dependent modeling parameters (i.e., the virtual markers, bodies and IV joint definition) were thereto estimated within a small group of trained operators, each creating a model of the same three ASD subjects. The operator variability in segmenting the vertebrae from CT was excluded from this study [similarly to Valente et al. (2014)] due to its previously reported high level of operator precision for lumbar vertebrae (Cook et al., 2012) and the high time cost associated with segmentation. Variability in radiograph-based virtual marker identification was small and of similar magnitude than previously reported values for a similar study (Pillet et al., 2014). Likewise, the variability in spinal alignment reconstruction (i.e., bodies component) (median position and orientation variability between 0.55 and 0.74 mm and 0.96–1.68°, respectively) was similar to the previously reported accuracy when validated with a plastinated cadaver serving as ground truth (median accuracy between 0.57 and 1.57 mm and 1.02–2.20° for vertebral positions and orientations, respectively) (Overbergh et al., 2020). The IV joint definition is based on the position and orientation of the caudal vertebral bodies and on additional landmark identification by the operator; therefore resulting in a higher median variability for the positions and orientation of the joint component (0.57–1.06 mm, 1.16–1.95°), compared to the body component. With a mean 90% CI below 2° [1.04° (S1), 1.14° (S2) and 1.75° (S3)], IV joint kinematics were found to be reliable. This is in agreement with the high reliability of the spino-pelvic parameters in our inter-operator agreement analysis. Importantly, this indicates that the modeling method as well as the resulting kinematics during forward flexion are robust towards inter-operator variability. Although, for each subject, the imposed perturbations in the model variations were sampled from the same probability distributions, different IV joint variability can be noted. Interestingly, the largest variation was consistently noted at the lumbar region (especially L2/L3) for each of the three subjects (**Figure 5**). This could potentially be related to a higher ROM at this region, although preliminary analyses could not confirm this due to the low number of subjects. Notably, one subject (S3) presented with more than twice as large maximal CIs (lumbar region) compared to the other two subjects. Although we need more data to confirm, this may be due to the more severe deformity of S3 (**Figure 2**) and associated increased sensitivity of the kinematics to modeling error. Furthermore, kinematics demonstrated very low sensitivity to marker variability (maximal sensitivity factor: 0.15). Likely, this is due to the very limited marker variability in reconstruction from x-ray (largest noted variability of 1.04 mm) compared to the traditional error associated with marker-based motion capture systems (errors of 1–5 mm, (Hicks et al., 2015)) and considerably smaller than typical skin motion artefacts [up to 10 mm for human movement, (Hicks et al., 2015)]. Very low sensitivity factors were also found for the body positions and rotations (max: 0.07 and 0.06, respectively). This can be explained by the independence of the IV joint kinematics to the alignment, provided that changes to the alignment are isolated from changes to the joint definition and virtual marker positions. Overall, the imposed variability of the IV joint positions and orientations seemed to have the biggest effect on the IV joint kinematics, with maximal sensitivity factors of 0.26 and 0.47, respectively. Consequently, this study identifies modeling steps contributing to the reliable definition of the IV joints as a primary target for limiting kinematic variability.

There are some limitations associated with this study. Firstly, the input distributions of the probabilistic simulations can vary depending on the operators and subjects, thereby affecting the simulation outputs. In this study, operator-dependent parameters were grouped as model components (i.e., the marker positions, body and joint positions and orientations) to have a sufficient amount of samples to estimate a representative probability function based on the histograms, disregarding potential variations in variability within different vertebral levels. As part of future work, a larger group of subjects with different complexities of spinal malalignments would allow a more detailed analysis of the subject-, vertebral level- and direction-dependent variability distributions. Secondly, the type of simulated motion is expected to influence the kinematic variability. Besides its clinical relevance as a task of daily living (e.g., putting on shoes), maximal forward spine flexion was used here as a worst-case scenario because of its large spinal ROM. However, one should be careful with direct extrapolation of the results presented in this study to other motions such as gait, presenting with a lower spinal range of motion, or spinal lateroflexion and axial rotation, presenting with spinal coupling, which may provide additional important insights. This uncertainty analysis focused specifically on the operator-dependent components of the modeling method, thereby ignoring additional variability, for example originating from inter-rater variability in skin marker placement. Lastly, our

uncertainty analysis was limited to IV joint kinematics as outcome. However additional analyses should be done to assess the uncertainty propagation in possible subsequent simulation steps such as joint reaction forces or muscle activation (Myers et al., 2015; Burkhart et al., 2020).

Our systematic inter-operator approaches identified a limited impact of operator-induced variability on kinematic simulations of spine flexion in an ASD population. This excellent inter-operator agreement, compared to the lower test-retest reliability for the same motion, however, importantly indicates that the dominant portion of overall test-retest variability is only limitedly originating from aspects of the modeling (extrinsic), but rather from intra-subject differences (intrinsic) in motor task execution. Improved standardization of the maximal forward trunk flexion (e.g., pelvic fixation and/or targets) together with multiple acquisitions averaged per session, may thus improve the test-retest reliability.

In conclusion, although the current modeling method is dependent on manual inputs of the operators, causing additional variability in the simulation output, its isolated effect on the kinematics was very limited, indicating the modeling method to be highly reliable for kinematic analysis of spinal motion. In the future, this kinematic variability could likely be even further reduced by eliminating variability in operator-dependent model components through increased automation of the model creation procedures. Furthermore, this would also decrease the currently high time cost of subject-specific modeling (Aubert et al., 2019; Galbusera et al., 2020). Based on this study's results, the primary focus should hereby be on the intervertebral joint definition.

DATA AVAILABILITY STATEMENT

The raw data supporting the conclusion of this article will be made available by the authors, without undue reservation.

ETHICS STATEMENT

The studies involving human participants were reviewed and approved by S58082, University Hospital Leuven local ethics committee. The patients/participants provided their written informed consent to participate in this study. Written informed consent was obtained from the individual(s) for the publication of any potentially identifiable images or data included in this article.

AUTHOR CONTRIBUTIONS

TO collected patient data, was one of the operators creating models, conceptualized the study, developed the technical tools necessary for data analysis, processed the data, wrote the initial manuscript and edited the manuscript. PS collected patient data, conceptualized the study and edited the manuscript. EB-G was one of the operators creating models, conceptualized the study and edited the manuscript. TA was one of the operators creating models, conceptualized the study and edited the manuscript. LM conceptualized the study and was responsible for subject recruitment. IJ conceptualized the study and edited the manuscript. LS conceptualized the study, edited the manuscript and supervised the project.

FUNDING

This study was funded by KU Leuven C2 funds, Medtronic and a strategic basic research PhD grant (SB/1S56017N) of the Research Foundation–Flanders (FWO).

SUPPLEMENTARY MATERIAL

The Supplementary Material for this article can be found online at: https://www.frontiersin.org/articles/10.3389/fbioe.2021.720060/full#supplementary-material

REFERENCES

Ackland, D. C., Lin, Y.-C., and Pandy, M. G. (2012). Sensitivity of Model Predictions of Muscle Function to Changes in Moment Arms and Muscle-Tendon Properties: A Monte-Carlo Analysis. *J. Biomech.* 45, 1463–1471. doi:10.1016/j.jbiomech.2012.02.023

Aubert, B., Vazquez, C., Cresson, T., Parent, S., and de Guise, J. A. (2019). Toward Automated 3D Spine Reconstruction from Biplanar Radiographs Using CNN for Statistical Spine Model Fitting. *IEEE Trans. Med. Imaging* 38, 2796–2806. IEEE Trans. Med. Imaging. doi:10.1109/TMI.2019.2914400

Beaucage-Gauvreau, E., Robertson, W. S. P., Brandon, S. C. E., Fraser, R., Freeman, B. J. C., Graham, R. B., et al. (2019). Validation of an OpenSim Full-Body Model with Detailed Lumbar Spine for Estimating Lower Lumbar Spine Loads during Symmetric and Asymmetric Lifting Tasks. *Comp. Methods Biomech. Biomed. Eng.* 22, 451–464. doi:10.1080/10255842.2018.1564819

Bruno, A. G., Bouxsein, M. L., and Anderson, D. E. (2015). Development and Validation of a Musculoskeletal Model of the Fully Articulated Thoracolumbar Spine and Rib Cage. *J. Biomech. Eng.* 137, 1–10. doi:10.1115/1.4030408

Bruno, A. G., Burkhart, K., Allaire, B., Anderson, D. E., and Bouxsein, M. L. (2017). Spinal Loading Patterns from Biomechanical Modeling Explain the High Incidence of Vertebral Fractures in the Thoracolumbar Region. *J. Bone Miner. Res.* 32, 1282–1290. doi:10.1002/jbmr.3113

Burkhart, K., Grindle, D., Bouxsein, M. L., and Anderson, D. E. (2020). Between-session Reliability of Subject-specific Musculoskeletal Models of the Spine Derived from Optoelectronic Motion Capture Data. *J. Biomech.* 112, 110044. doi:10.1016/j.jbiomech.2020.110044

Burkhart, K. A., Bruno, A. G., Bouxsein, M. L., Bean, J. F., and Anderson, D. E. (2017). Estimating Apparent Maximum Muscle Stress of Trunk Extensor Muscles in Older Adults Using Subject-specific Musculoskeletal Models. *J. Orthop. Res.* 36, 498–505. doi:10.1002/jor.23630

Cook, D. J., Gladowski, D. A., Acuff, H. E., Yeager, M. S., and Cheng, B. C. (2012). Variability of Manual Lumbar Spine Segmentation. *Int. J. Spine Surg.* 6, 167–173. doi:10.1016/j.ijsp.2012.04.002

Delp, S. L., Anderson, F. C., Arnold, A. S., Loan, P., Habib, A., John, C. T., et al. (2007). OpenSim: Open-Source Software to Create and Analyze Dynamic Simulations of Movement. *IEEE Trans. Biomed. Eng.* 54, 1940–1950. doi:10.1109/tbme.2007.901024

Galbusera, F., Niemeyer, F., Bassani, T., Sconfienza, L. M., and Wilke, H.-J. (2020). Estimating the Three-Dimensional Vertebral Orientation from a Planar Radiograph: Is it Feasible?. *J. Biomech.* 102, 109328. doi:10.1016/j.jbiomech.2019.109328

Hannah, I., Montefiori, E., Modenese, L., Prinold, J., Viceconti, M., and Mazzà, C. (2017). Sensitivity of a Juvenile Subject-specific Musculoskeletal Model of the Ankle Joint to the Variability of Operator-dependent Input. *Proc. Inst. Mech. Eng. H* 231, 415–422. doi:10.1177/0954411917701167

Hicks, J. L., Uchida, T. K., Seth, A., Rajagopal, A., and Delp, S. L. (2015). Is My Model Good Enough? Best Practices for Verification and Validation of Musculoskeletal Models and Simulations of Movement. *J. Biomech. Eng.* 137, 020905. doi:10.1115/1.4029304

Ignasiak, D., Rüeger, A., Sperr, R., and Ferguson, S. J. (2018). Thoracolumbar Spine Loading Associated with Kinematics of the Young and the Elderly during Activities of Daily Living. *J. Biomech.* 70, 175–184. doi:10.1016/j.jbiomech.2017.11.033

Lu, T.-W., and O'Connor, J. J. (1999). Bone Position Estimation from Skin Marker Co-ordinates Using Global Optimisation with Joint Constraints. *J. Biomech.* 32, 129–134. doi:10.1016/s0021-9290(98)00158-4

Martelli, S., Valente, G., Viceconti, M., and Taddei, F. (2015). Sensitivity of a Subject-specific Musculoskeletal Model to the Uncertainties on the Joint Axes Location. *Comp. Methods Biomech. Biomed. Eng.* 18, 1555–1563. doi:10.1080/10255842.2014.930134

Mousavi, S. J., Tromp, R., Swann, M. C., White, A. P., and Anderson, D. E. (2018). Between-session Reliability of Opto-Electronic Motion Capture in Measuring Sagittal Posture and 3-D Ranges of Motion of the Thoracolumbar Spine. *J. Biomech.* 79, 248–252. doi:10.1016/j.jbiomech.2018.08.033

Myers, C. A., Laz, P. J., Shelburne, K. B., and Davidson, B. S. (2015). A Probabilistic Approach to Quantify the Impact of Uncertainty Propagation in Musculoskeletal Simulations. *Ann. Biomed. Eng.* 43, 1098–1111. doi:10.1007/s10439-014-1181-7

Navacchia, A., Myers, C. A., Rullkoetter, P. J., and Shelburne, K. B. (2016). Prediction of *In Vivo* Knee Joint Loads Using a Global Probabilistic Analysis. *J. Biomech. Eng.* 138, 4032379. doi:10.1115/1.4032379

Overbergh, T., Severijns, P., Beaucage-Gauvreau, E., Jonkers, I., Moke, L., and Scheys, L. (2020). Development and Validation of a Modeling Workflow for the Generation of Image-Based, Subject-specific Thoracolumbar Models of Spinal Deformity. *J. Biomech.* 110, 109946. doi:10.1016/j.jbiomech.2020.109946

Pillet, H., Sangeux, M., Hausselle, J., El Rachkidi, R., and Skalli, W. (2014). A Reference Method for the Evaluation of Femoral Head Joint center Location Technique Based on External Markers. *Gait & Posture* 39, 655–658. doi:10.1016/j.gaitpost.2013.08.020

Schmid, S., Studer, D., Hasler, C.-C., Romkes, J., Taylor, W. R., Lorenzetti, S., et al. (2016). Quantifying Spinal Gait Kinematics Using an Enhanced Optical Motion Capture Approach in Adolescent Idiopathic Scoliosis. *Gait & Posture* 44, 231–237. doi:10.1016/j.gaitpost.2015.12.036

Schwartz, M. H., Trost, J. P., and Wervey, R. A. (2004). Measurement and Management of Errors in Quantitative Gait Data. *Gait & Posture* 20, 196–203. doi:10.1016/j.gaitpost.2003.09.011

Severijns, P., Overbergh, T., Thauvoye, A., Baudewijns, J., Monari, D., Moke, L., et al. (2020). A Subject-specific Method to Measure Dynamic Spinal Alignment in Adult Spinal Deformity. *Spine J.* 20, 934–946. doi:10.1016/j.spinee.2020.02.004

Shrout, P. E., and Fleiss, J. L. (1979). Intraclass Correlations: Uses in Assessing Rater Reliability. *Psychol. Bull.* 86, 420–428. doi:10.1037/0033-2909.86.2.420

Smith, J. S., Klineberg, E., Lafage, V., Shaffrey, C. I., Schwab, F., Lafage, R., et al. (2016). Prospective Multicenter Assessment of Perioperative and Minimum 2-year Postoperative Complication Rates Associated with Adult Spinal Deformity Surgery. *Spi* 25, 1–14. doi:10.3171/2015.11.spine151036

Valente, G., Pitto, L., Testi, D., Seth, A., Delp, S. L., Stagni, R., et al. (2014). Are Subject-specific Musculoskeletal Models Robust to the Uncertainties in Parameter Identification?. *PLoS One* 9, e112625. doi:10.1371/journal.pone.0112625

Valente, G., Taddei, F., and Jonkers, I. (2013). Influence of Weak Hip Abductor Muscles on Joint Contact Forces during normal Walking: Probabilistic Modeling Analysis. *J. Biomech.* 46, 2186–2193. doi:10.1016/j.jbiomech.2013.06.030

Valero-Cuevas, F. J., Johanson, M. E., and Towles, J. D. (2003). Towards a Realistic Biomechanical Model of the Thumb: The Choice of Kinematic Description May Be More Critical Than the Solution Method or the Variability/uncertainty of Musculoskeletal Parameters. *J. Biomech.* 36, 1019–1030. doi:10.1016/s0021-9290(03)00061-7

Wang, M. Y., Lu, Y., Anderson, D. G., and Mummaneni, P. V. (2014). *Minimally Invasive Spinal Deformity Surgery*.

Conflict of Interest: The authors declare that the research was conducted in the absence of any commercial or financial relationships that could be construed as a potential conflict of interest.

Publisher's Note: All claims expressed in this article are solely those of the authors and do not necessarily represent those of their affiliated organizations, or those of the publisher, the editors and the reviewers. Any product that may be evaluated in this article, or claim that may be made by its manufacturer, is not guaranteed or endorsed by the publisher.

frontiers in Bioengineering and Biotechnology

ORIGINAL RESEARCH
published: 10 September 2021
doi: 10.3389/fbioe.2021.703144

Accounting for Biomechanical Measures from Musculoskeletal Simulation of Upright Posture Does Not Enhance the Prediction of Curve Progression in Adolescent Idiopathic Scoliosis

Tito Bassani[1]*, *Andrea Cina*[1], *Dominika Ignasiak*[2], *Noemi Barba*[3] and *Fabio Galbusera*[1]

[1]LABS-Laboratory of Biological Structures Mechanics, IRCCS Istituto Ortopedico Galeazzi, Milan, Italy, [2]Institute for Biomechanics, ETH Zurich, Zurich, Switzerland, [3]Department of Chemistry, Materials and Chemical Engineering "Giulio Natta", Politecnico di Milano, Milan, Italy

OPEN ACCESS

Edited by:
Dennis E Anderson,
Harvard Medical School,
United States

Reviewed by:
Navid Arjmand,
Sharif University of Technology, Iran
Virginie Lafage,
Hospital for Special Surgery,
United States
Erin Mannen,
Boise State University, United States

***Correspondence:**
Tito Bassani
tito.bassani@grupposandonato.it

Specialty section:
This article was submitted to Biomechanics, a section of the journal Frontiers in Bioengineering and Biotechnology

Received: 30 April 2021
Accepted: 26 August 2021
Published: 10 September 2021

Citation:
Bassani T, Cina A, Ignasiak D, Barba N and Galbusera F (2021) Accounting for Biomechanical Measures from Musculoskeletal Simulation of Upright Posture Does Not Enhance the Prediction of Curve Progression in Adolescent Idiopathic Scoliosis. Front. Bioeng. Biotechnol. 9:703144. doi: 10.3389/fbioe.2021.703144

A major clinical challenge in adolescent idiopathic scoliosis (AIS) is the difficulty of predicting curve progression at initial presentation. The early detection of progressive curves can offer the opportunity to better target effective non-operative treatments, reducing the need for surgery and the risks of related complications. Predictive models for the detection of scoliosis progression in subjects before growth spurt have been developed. These models accounted for geometrical parameters of the global spine and local descriptors of the scoliotic curve, but neglected contributions from biomechanical measurements such as trunk muscle activation and intervertebral loading, which could provide advantageous information. The present study exploits a musculoskeletal model of the thoracolumbar spine, developed in AnyBody software and adapted and validated for the subject-specific characterization of mild scoliosis. A dataset of 100 AIS subjects with mild scoliosis and in pre-pubertal age at first examination, and recognized as stable (60) or progressive (40) after at least 6-months follow-up period was exploited. Anthropometrical data and geometrical parameters of the spine at first examination, as well as biomechanical parameters from musculoskeletal simulation replicating relaxed upright posture were accounted for as predictors of the scoliosis progression. Predicted height and weight were used for model scaling because not available in the original dataset. Robust procedure for obtaining such parameters from radiographic images was developed by exploiting a comparable dataset with real values. Six predictive modelling approaches based on different algorithms for the binary classification of stable and progressive cases were compared. The best fitting approaches were exploited to evaluate the effect of accounting for the biomechanical parameters on the prediction of scoliosis progression. The performance of two sets of predictors was compared: accounting for anthropometrical and geometrical parameters only; considering in addition the biomechanical ones. Median accuracy of the best fitting algorithms ranged from 0.76 to 0.78. No differences were found in the classification performance by including or

neglecting the biomechanical parameters. Median sensitivity was 0.75, and that of specificity ranged from 0.75 to 0.83. In conclusion, accounting for biomechanical measures did not enhance the prediction of curve progression, thus not supporting a potential clinical application at this stage.

Keywords: spine, scoliosis, progression, musculoskeletal modelling, anybody, predictive modelling

INTRODUCTION

Adolescent idiopathic scoliosis (AIS) is a three-dimensional deformity of the spine occurring in the general population with prevalence between 2 and 3%. It begins at the time of the pubertal growth spurt and its cause is unclear (Weinstein et al., 2008; Nnadi and Fairbank, 2010). Approximately 10% of the diagnosed cases require conservative treatment and 0.1–0.3% operative correction (Negrini et al., 2018). A major clinical challenge is the difficulty of predicting curve progression at the initial presentation. The early detection of progressive curves can indeed offer the opportunity to better target effective non-operative treatments, reducing the need for surgery and the risks of related complications (Donzelli et al., 2020). The failure to accurately predict the risk of progression can lead to non-optimal treatment either by precluding timely, appropriate and efficient management or by generating unnecessary medical visits and radiographs. Moreover, uncertainty regarding curve progression and outcome can create anxiety in families and patients as well as unnecessary psychosocial stress associated with brace treatment (Weinstein et al., 2008).

Historically, curve magnitude, skeletal maturation and chronological age were considered as relevant risk factors of curve progression (Peterson and Nachemson, 1995; Kohashi et al., 1996; Lonstein and Carlson, 1984; Sanders et al., 2008; Noshchenko et al., 2015). Moreover, it was suggested that the three-dimensional shape of the scoliotic curve could be indicative of progression risk (Perdriolle and Vidal, 1981). Recently, predictive models for the early detection of the progression of scoliosis in subjects before growth spurt have been developed. Skalli et al. have proposed a severity index for classifying scoliosis as "stable" or "progressive" in subjects with mild scoliosis (Skalli et al., 2017; Vergari et al., 2019), the validation of which has been recently extended in a multicentric cohort of subjects (Vergari et al., 2021). The application requires the subjects to undergo radiographic examination by the EOS Imaging system (EOS Imaging, Paris, France), providing the simultaneous acquisition of the coronal and sagittal anatomical planes and allowing for the geometrical 3D reconstruction of the spine (Illes and Somoskeoy, 2012; Somoskeoy et al., 2012). Differently, Nault et al. evaluated mild and moderate cases and tried to predict the severity of scoliosis at full skeletal maturity (Nault et al., 2020). In both studies, the predictive models accounted for geometrical parameters describing the global spine, regional segments (scoliotic curve), or local descriptors of the curve (apex, cranial and caudal vertebrae), but neglected potential contributions from biomechanical measures.

In this regard, biomechanical parameters such as trunk muscle activation and intervertebral loading could provide additional advantageous information (Bassani et al., 2017; Schmid et al., 2020). Although not measurable *in vivo* due to the invasiveness of the procedures, such parameters can be obtained by numerical simulation based on musculoskeletal modelling approach, which allows for calculating the biomechanical loads in assigned kinematic conditions by means of inverse dynamic analysis (Dreischarf et al., 2016; Bassani and Galbusera, 2018). The present study exploits a thoracolumbar spine model with articulated ribcage, developed in AnyBody software (AnyBody Technology, Denmark) (Ignasiak et al., 2016a; Ignasiak et al., 2016b), and recently adapted and validated by our group for the subject-specific characterization of the scoliotic spine in mild severity cases (Barba et al., 2021). An existing dataset of 100 AIS subjects with mild scoliosis and in pre-pubertal age at first examination (acquired by EOS system), and recognized as stable or progressive after at least 6-months follow-up period is exploited. Anthropometrical data and geometrical parameters of the spine, as well as biomechanical parameters from musculoskeletal modelling, are accounted for as predictors of the progression of scoliosis. Six predictive modelling approaches based on different algorithms for the binary classification of stable and progressive cases are compared to find the best fitting ones. The identified models are exploited to evaluate the effect of accounting for the biomechanical parameters on the prediction of scoliosis progression. The classification performance between two sets of predictors is compared: accounting for anthropometrical and geometrical parameters, and considering in addition the biomechanical ones.

MATERIALS AND METHODS

The workflow of the study accounted for three consecutive steps (**Figure 1**): i) identification of the dataset of subjects and extraction of anthropometrical parameters; ii) computation of geometrical and biomechanical parameters; iii) evaluation of the effect of accounting for the biomechanical parameters on the prediction of the scoliosis progression.

Step i)

A retrospective search of the Picture Archiving and Communication System (PACS) of the IRCCS Istituto Ortopedico Galeazzi (Milan, Italy) was performed on anonymized data acquired in the period 2014–2020. Subjects with the following criteria were included: age ranging from 10 to 18 years; at least two radiographic examinations of the spine and pelvis acquired with the EOS system. Subjects with vertebral deformities or underwent operative correction were excluded, as well as those presenting non-standard position in biplanar radiography. The Cobb angle, quantifying the severity of scoliosis in the coronal plane, and the Risser sign, determining the skeletal maturity as state of ossification and fusion of the iliac

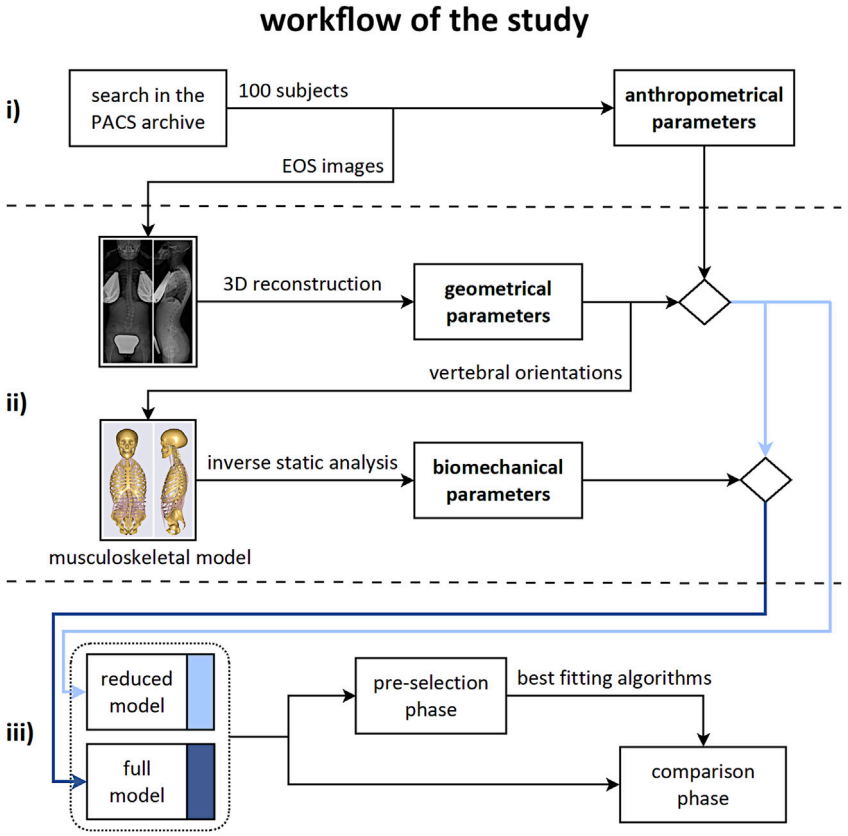

FIGURE 1 | Workflow of the study. Consecutive steps from top to bottom row: i) identification of the subjects dataset and extraction of the anthropometrical parameters; ii) computation of the geometrical and biomechanical parameters; iii) evaluation of the effect of accounting for the biomechanical parameters on the prediction of the scoliosis progression.

apophysis, by integer values ranging from 0 to 5 (Risser, 2010), were manually measured on the radiographic images under the supervision of an experienced spine surgeon. Subjects in the early adolescence (Risser sign ranging from 0 to 2) with mild scoliosis (Cobb angle ranging from 10 to 25) at first examination, and identified after at least 6-months follow-up period as "stable" (Risser>2, increase in Cobb angle <10) or "progressive" (Risser 0–2, increase in Cobb angle >10) were selected. According to that, a dataset of 100 subjects (60 stable and 40 progressive cases, respectively) was obtained. Age, sex, and Risser sign at first examination were accounted for as anthropometrical parameters.

Step ii)

Geometrical Parameters

The radiographic images acquired at first examination (in orthostatic position with arms raised and fingertips on cheekbones) were processed by a trained operator with sterEOS software, allowing for the reconstruction of the 3D orientations of the thoracolumbar vertebrae (from T1 to L5) and the pelvis in the anatomical planes, as well as for the identification of the scoliotic curves, characterized by Cobb angle larger than 10 (**Figures 2A,B**) (Illes and Somoskeoy, 2012; Somoskeoy et al., 2012; Melhem et al., 2016). The following geometrical parameters were obtained: thoracic kyphosis (TK) from T1 to T12, lumbar lordosis (LL) from L1 to S1, sacral slope (SS), pelvic incidence (PI), number of scoliotic curves, Cobb angle of the most severe curve, curve sagittal angle (measuring the relative angle between the upper and lower end vertebrae in the sagittal plane), and largest vertebral axial rotation inside the curve. The type of scoliosis was determined as well according to the Lenke scheme, which classifies the deformity into six different types depending on the location and number of curves (Lenke et al., 2001). In total, nine geometrical parameters were accounted for.

Biomechanical Parameters

The procedure for replicating the subject-specific spinal alignment with the AnyBody musculoskeletal model (**Figures 2C,D**), including the rearrangement of ribs and sternum, positioning of the vertebral centers of mass, preservation of the abdominal muscle structure, setting of the trunk muscle parameters, simulation of the load of the raised arms, and muscle co-activation in maintaining the upright posture, is reported in detail in (Barba et al., 2021). In brief, the pelvis is constrained to the ground and rigidly connected to the sacrum. The spinal alignment is replicated by setting the orientation of the sacrum in the sagittal plane and the rotation of the intervertebral spherical joints from T1 to L5, according to the vertebral

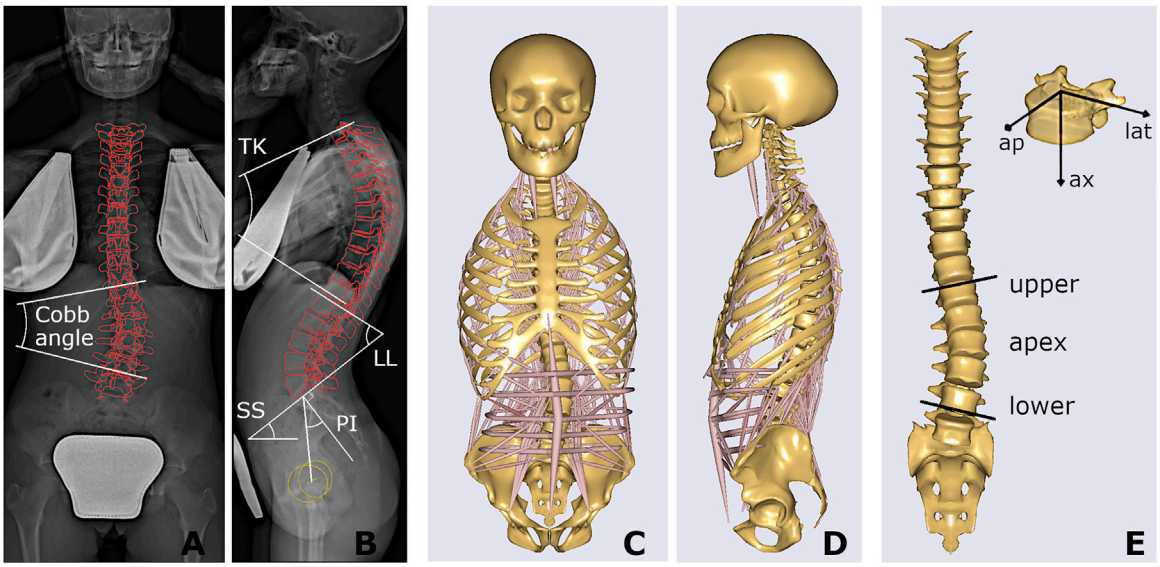

FIGURE 2 | Coronal and sagittal radiographic images of one stable subject, with projection of the reconstructed vertebrae and illustration of Cobb angle, spinal sagittal alignment (TK, LL) and spinopelvic angles (SS, PI) **(A,B)**; and corresponding musculoskeletal model **(C,D)**, also presented highlighting the scoliotic curve (apex, upper and lower end levels) with muscles and ribcage not shown, and the local vertebral reference system, i.e., anteroposterior (ap), lateral (lat), and axial (ax) component **(E)**.

orientations obtained from the geometrical reconstruction. Joint moments, representing the stiffness-related contribution of passive elements such as ligaments and facet joints, are assumed as zero to replicate neutral upright position. The physiological cross-section area of the trunk muscles is scaled according to reference values acquired in adolescent subjects and depending on age (Been et al., 2018). As regards the scaling of the body model, weight and height were predicted by exploiting linear regression models taking into account anthropometrical and geometrical parameters manually measured on the radiographic images (see Appendix section), since real data were not recorded together with the images in the PACS. These models were trained by another available dataset of 85 AIS subjects with comparable age range and scoliosis severity and known weight and height data, evaluated by our group in a previous study (Bassani et al., 2019). The predicted values were exploited to scale the body model by default length-mass-fat approach. Inverse static analysis was run to calculate muscle activation and intervertebral reaction force (F) in the assigned standing posture. The activity of each muscle fascicle ranged between 0 and 1, obtained by dividing the muscle force by the maximum force generating capacity (set as the product of the cross-section area and the assumed uniform muscle stress, 90 N/cm 2). The asymmetry of erector spinae (ES) and multifidus (MF) muscle activity, between the convex and concave side of the scoliotic curve, was calculated by the normalized activity ratio (nES, and nMF) at each vertebral level inside the curve. As explained in detail in (Barba et al., 2021), this parameter is calculated by accounting for the sum of the activations of the individual fascicles crossing the respective vertebral mid-plane. It measures the (convex − concave)/(convex + concave) activity at specific vertebral level, providing values near zero in correspondence of balanced activation, and positive and negative values (ranging from 0 to ±1) in case of larger activation in the convex and concave side, respectively. As regards F, the absolute value of the intervertebral lateral shear (F_{lat}), expressed in the local coordinate system of the vertebra (**Figure 2E**), was taken into account since expected as the most affected by lateral deviations of the spine in the coronal plane which characterize scoliosis. The following eleven biomechanical parameters were accounted for: F_{lat}, nES, and nMF calculated at apex, upper and lower end levels of the scoliotic curve (**Figure 2E**), and nES and nMF along the whole curve, obtained by summing the contributions at all levels (from upper to lower end) in the convex and concave side. The setting steps and the simulations were run in batch process using custom routines written in MATLAB (MathWorks Inc., Natick, MA, United States), as well as the procedures for predictive modelling and statistical analysis reported in the next sections.

Step iii)

Two sets of predictors for the binary classification of stable and progressive cases were defined. The "reduced" model accounted for 12 predictors: three anthropometrical and nine geometrical parameters (**Figure 1**, middle row). The "full" model accounted for the reduced set and for eleven biomechanical parameters in addition (23 predictors in total). Two consecutive processing phases were arranged: 'pre-selection' of the best classification approaches, and 'comparison' between the reduced and full model by exploiting the selected approaches (**Figure 1**, bottom row). Specifically, in the pre-selection phase six different algorithms for the binary classification of stable and progressive subjects were evaluated to find the best fitting

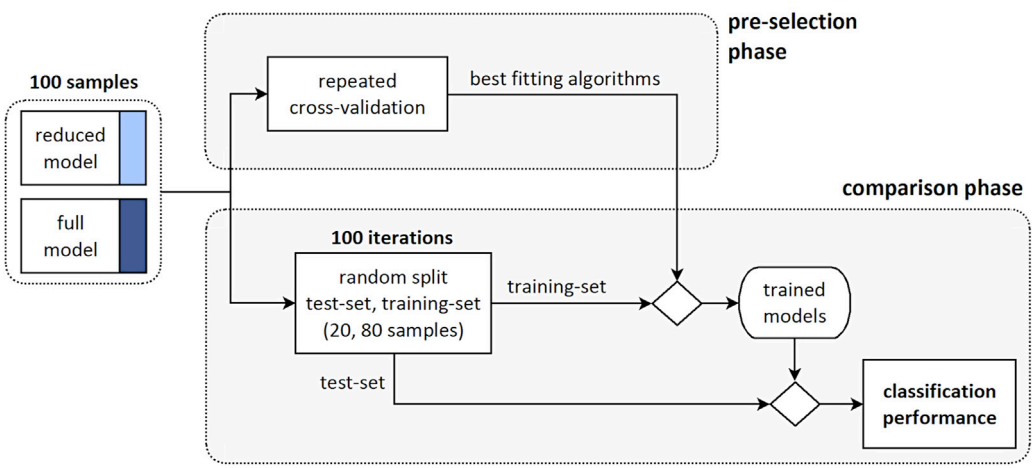

FIGURE 3 | Step iii) in detail. Diagram illustrating the pre-selection phase, providing the identification of the best fitting algorithms; and the comparison phase, providing the evaluation of the classification performance between the reduced and full model.

approaches, both in case of reduced and full model (**Figure 3**). Support vector machine (SVM), predictive discriminant analysis (PDA), naive Bayes classifier (BAY), decision tree (DET), k-nearest neighbors (KNN), and ensemble method (ENS) were considered (Scholz and Wimmer, 2021; Galbusera et al., 2019; Minasny, 2009; Harper, 2005). Preliminary tuning of the hyperparameters was performed (**Table1**). Features selection procedures, such as principal component analysis or assessment of the correlation between parameters and binary classification, were not applied because the comparison was specifically aimed to evaluate the effect of accounting for the whole sets of available measures. Data were processed in their original format, avoiding standardization, because found as generally providing slightly larger accuracy levels (i.e., the percentage of correct predictions). Sex and Lenke type were converted into dummy variables because characterized by categorical values. The model accuracy was evaluated for each classification algorithm according to repeated cross-validation approach, by performing 10 repetitions of 4-fold cross-validation procedure (Vanwinckelen and Blockeel, 2012). This approach is appropriate for small to modestly-sized datasets and simple linear models, to reduce the noise in the estimated performance (Kuhn and Kjell 2013). In each repetition, the original dataset (100 samples) was shuffled and split into four non-overlapping folds with 25 randomly assigned samples each, preserving the original proportion of stable and progressive cases (15 (60%) and 10 (40%), respectively). Three folds at a time were used as training-set to identify the model parameters (same set for all the approaches and predictors set), and the fourth fold was exploited to compute the model accuracy. In total, the procedure provided forty values of accuracy for each evaluated model. The best fitting approaches were identified as those providing the largest average (or median) accuracy level, and were then used in the subsequent phase.In the comparison phase, the effect of accounting for the biomechanical parameters on the prediction of the scoliosis progression was evaluated by comparing the classification performance between the reduced and full model. The original dataset was randomly split into training-set and test-set (80 and 20% of total samples, respectively, preserving the original proportion of stable and

TABLE 1 | Hyperparameters of the classification algorithms, with tested values (range and options) and best choice (providing the largest accuracy, and used in the study) reported underlined.

	Hyperparameters
SVM	*box constraint*: 1–100 (10); *kernel-function*: linear, Gaussian, polynomial (2–4 order), sigmoid (with gamma: 0.0001–10, and c: 0.1–100)
PDA	*discriminant type*: linear, quadratic; *gamma*: 0–1 (0.6)
BAY	*numerical predictors distribution*: normal, kernel; *kernel options*: normal, box, epanechnikov, triangle
DET	max *number of splits*: 1–10 (4); *split criterion*: Gini's diversity index, twoing, deviance; *prune*: on, off
KNN	*distance metric*: euclidean, cityblock, chebychev, minkowski; *distance weight*: equal, inverse, squaredinverse; *nearest neighbours*: 1–10 (7)
ENS	*method*: subspace, adaBoostM1, logitBoost, gentleBoost, RUSBoost, bag; *ensemble learning cycles*: 10–100 (30); *weak learner*: discriminant, KNN, tree

progressive cases). The training-set was used to identify the models parameters (same set for each best-fitting approach and predictors set). The test-set was exploited to compute the performance of the trained models in correctly identifying the progressive and stable subjects (i.e., sensitivity and specificity of the prediction, respectively). The procedure was iterated 100 times and the average (or median) value between the reduced and full model was compared for each approach. As regards the importance of the individual predictors in determining correct classification, it is worth noting that the considered approaches are not based on modelling a direct relationship between the predictors and the binary outcome, but on finding an optimal solution by mixing information from the whole set of predictors. In general, it is thus not possible to use the estimated coefficients of the models to analyze the importance of the predictors. However, an exception is represented by DET approach. In this case, the importance of each predictor can be estimated by summing changes in the mean squared error due to splits on every predictor and dividing the sum by the number of branch nodes (Breiman, 2001). The estimation provides a positive score, which is equal to zero in case of no impact, and exhibits larger value for larger importance of the predictor.

Statistical Analysis

As regards the anthropometrical, geometrical, and biomechanical parameters, the significance of the difference between stable and progressive cases was compared by unpaired t-test (or Wilcoxon rank sum test in case of non-normal distribution) if comparing numerical values, and chi-squared test (or Fisher exact test where necessary) in case of proportions. As regards the classification performance, in the majority of cases the distribution of the accuracy values (evaluated in the pre-selection phase), and those of sensitivity and specificity (comparison phase) was found to be non-normal. According to that, the difference in the median value of accuracy among the classification algorithms was tested by Kruskal-Wallis test (separately for reduced and full model) followed by post-hoc pairwise comparisons with Tukey-Kramer approach in case of overall significance (Bassani and Galbusera, 2020). In the comparison phase, the difference in the median value of sensitivity and specificity, between the reduced and full model, was tested according to Wilcoxon rank sum test for each considered algorithm. The strength of the relation between the geometrical and biomechanical parameters was evaluated by Pearson correlation coefficient or Spearman rank in case of non-normal distribution. The significance of the coefficients in being statistically different from zero was tested according to two-tailed t test or permutation distribution test, respectively. All the tests assumed 0.05 as significance level.

RESULTS

Subjects Parameters From Step i) and ii)

Overall, the comparison of the average values between progressive and stable subjects pointed out slight or rather moderate differences (**Table2**). Age was significantly lower in the progressive cases compared to stable ones (11.5 and 13.2, $p < 0.001$), as well as Risser sign (0.2 and 1.1, $p < 0.001$). No significant differences were exhibited for sex and the other geometrical parameters, except for the curve sagittal angle (16.4 and 22.1, $p = 0.04$). As regards the biomechanical parameters, F_{lat} was found significantly lower in the progressive cases at curve apex (14.2 and 26.4, $p < 0.01$), and at upper end (35.0 and 57.8, $p < 0.01$) and lower end (46.3 and 37.9, $p = 0.048$) levels, whereas no significant differences were recognized for nES and nMF muscle activity, which exhibited slightly positive values overall (ranging from 0.02 to 0.14). An example of the distribution of the intersegmental load F, and of nES, nMF, and F_{lat}, computed for a stable subject along the whole spine, is reported (**Figure 4**).

Classification Performance From Step iii)

In the pre-selection phase, the median accuracy of the reduced model was found significantly larger for PDA, BAY and ENS (0.76, 0.78 and 0.76, respectively) compared to SVM (0.68), DET (0.72), and KNN (0.70) (**Figure 5A** and **Table3**). Similar findings were observed with the full model: median accuracy of PDA, BAY and ENS equal to 0.72, 0.80, and 70.6, respectively, and lower values for SVM (0.64), DET (0.68), and KNN (0.64) (**Figure 5A** and **Table3**). Overall, the interquartile range (i.e., the difference between 75th and 25th percentiles) was similar among the considered conditions, with values ranging from 0.08 to 0.14. An example illustrating the ability in classifying true and false progressive cases, depicted by means of ROC curve, is reported for the reduced and full model (**Figures 5B,C**). The curves, obtained by processing a single selection of training- and test-set within a 4-folds split, pointed out larger values of the area under curve for PDA, BAY and ENS (ranging from 0.85 to 0.93) compared to SVM, DET, and KNN (ranging from 0.55 to 0.82). According to that, PDA, BAY and ENS algorithms were chosen as the best fitting approaches. In the comparison phase, no differences were found for sensitivity and specificity between the reduced and full model in each selected approach (**Figure 6**). As regards sensitivity, the same median value (0.75) was pointed out by PDA, BAY, and ENS, with larger interquartile range for ENS (0.25) compared to PDA and BAY (0.13). As regards specificity, the median value was significantly larger for ENS compared to PDA and BAY (0.83 and 0.75, $p < 0.05$), with similar interquartile range (0.16). The correlation coefficient between geometrical and biomechanical parameters was weak overall (lower than 0.3, **Table4**), and strong relationship (larger than 0.5) was found only between Cobb angle and F_{lat} at upper and lower end levels. As regards the importance of the predictors, that of chronological age, Risser sign, curve sagittal angle and F_{lat} at upper and lower end levels was larger compared to the other parameters (**Figure 7**).

DISCUSSION

The present study evaluated subjects with mild scoliosis at first examination and recognized as stable or progressive after at least 6-months follow-up period. Anthropometrical, geometrical and biomechanical parameters at first examination were extracted,

TABLE 2 | values of anthropometrical and geometrical parameters, and of biomechanical parameters, expressed as mean (SD) or number of cases, for stable and progressive subjects.

Anthropometrical and geometrical parameters			Biomechanical parameters		
	Stable	**Progressive**		**Stable**	**Progressive**
age [years]	13.2 (1.1)	11.5 (1.3)[a]	**F_{lat} upper** [N]	57.8 (41.2)	35.0 (21.4) [a]
sex [number of F/M subjects]	36/24	31/9	**F_{lat} apex** [N]	26.4 (22.2)	14.2 (11.6) [a]
Risser sign	1.1 (0.9)	0.2 (0.5)[a]	**F_{lat} lower** [N]	46.3 (23.4)	37.9 (20.2) [a]
TK [°]	44.0 (13.4)	41.4 (11.5)	**nES upper**	0.11 (0.22)	0.09 (0.19)
LL [°]	59.2 (9.8)	58.5 (9.9)	**nES apex**	0.12 (0.21)	0.1 (0.2)
SS [°]	39.6 (7.3)	39.6 (5.4)	**nES lower**	0.06 (0.19)	0.06 (0.18)
PI [°]	47.8 (7.8)	46.9 (7.5)	**nMF upper**	0 (0.19)	0.02 (0.11)
number of scoliotic curves	1.7 (0.6)	1.6 (0.5)	**nMF apex**	0.2 (0.29)	0.14 (0.22)
Cobb angle [°]	18.9 (6.1)	15.9 (5.1)	**nMF lower**	0.04 (0.25)	−0.03 (0.25)
curve sagittal angle [°]	22.1 (14.7)	16.4 (11.7)[a]	**nES curve**	0.11 (0.2)	0.08 (0.19)
largest axial rotation [°]	9.9 (5.6)	8.3 (5.0)	**nMF curve**	0.11 (0.22)	0.07 (0.18)
Lenke type [cases of type 1/2/3/4/5/6]	11/2/10/4/14/19	13/0/9/0/5/13	—	—	—

[a]*Indicates significant difference between stable and progressive group.*

and the effect of accounting for the biomechanical measures on the prediction of the scoliosis progression was assessed.

As regard the subjects' parameters, chronological age and skeletal maturation (Risser sign) were significantly lower in the progressive cases (**Table2**), confirming to be relevant risk factors of curve progression (Lonstein and Carlson, 1984; Sanders et al., 2008; Noshchenko et al., 2015) and indicating that the earlier is the onset of scoliosis the higher is the probability that the deformity will increase. According to that, these factors are evaluated by clinicians as essential indicators for the choice of conservative treatment by bracing (Negrini et al., 2018). Differently, the number of curves and the type of scoliosis (Lenke type) were found as not indicative of the risk of progression, as well as the three-dimensional shape of the primary scoliotic curve. In this regard, Cobb angle, curve sagittal angle, and largest axial rotation were similar overall, although the progressive cases exhibited slightly lower values, indicating a more flat spine in the scoliotic segment. However, the

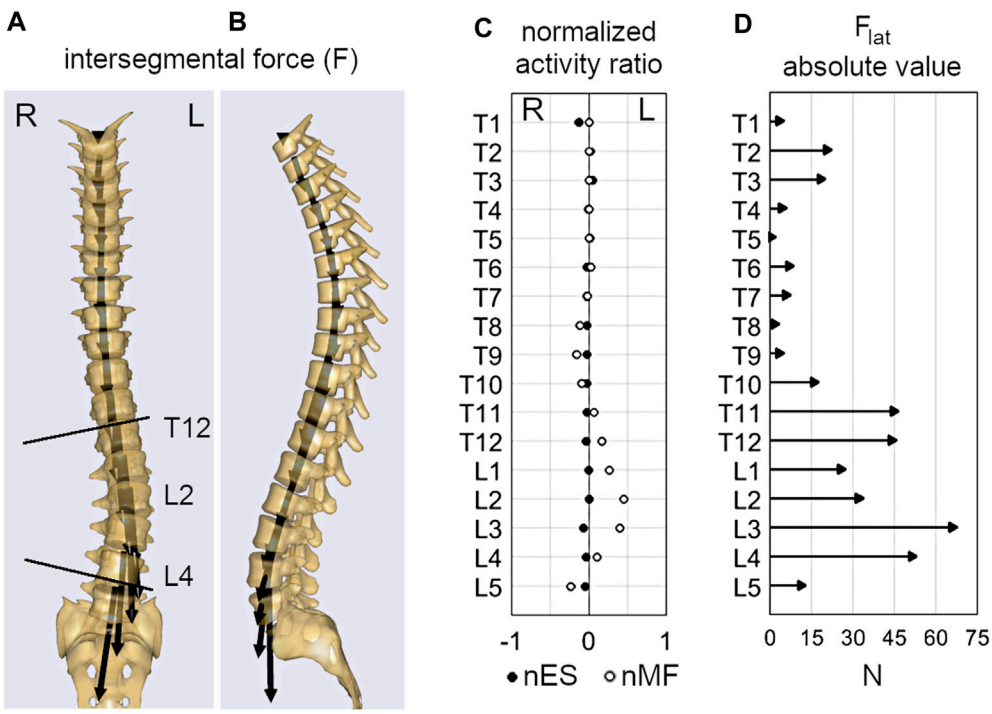

FIGURE 4 | Example of the biomechanical outcomes computed by inverse static analysis for the subject depicted in **Figure 2**. Intersegmental force vector, F **(A,B)**; normalized activity ratio of multifidus and erector spinae (nMF and nES) muscle **(C)**; absolute value of the lateral shear, F_{lat} **(D)**.

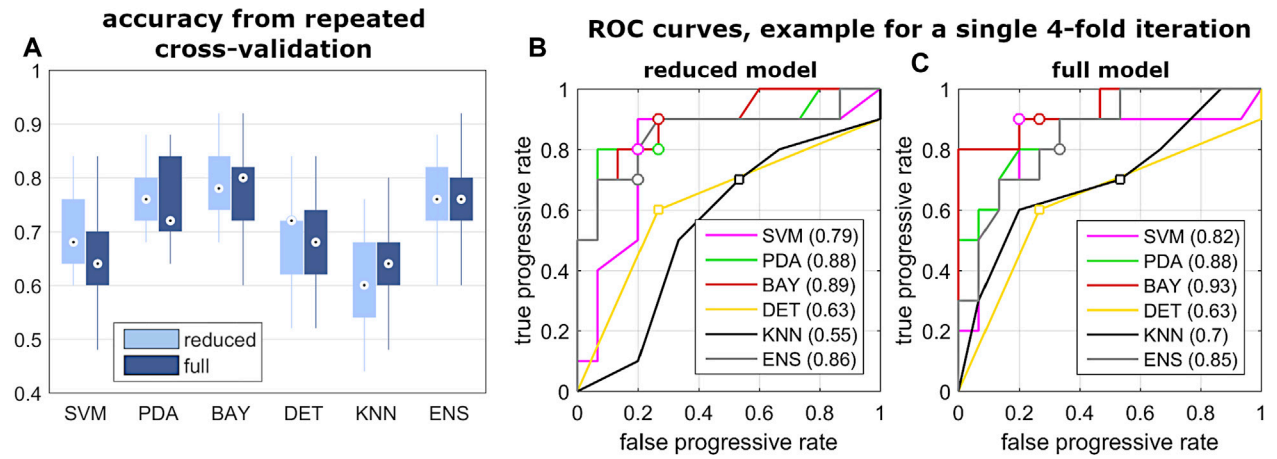

FIGURE 5 | Results from the pre-selection phase of step iii). Box and whiskers plot reporting the distribution of the accuracy values obtained by the evaluated classification algorithm **(A)**; and example of ROC curves calculated by exploiting one selection of training- and test-set of the 4-folds iteration, for reduced and full model **(B,C)**.

TABLE 3 | Accuracy (median and interquartile range), and statistical significance (*p*-value) of the post-hoc comparisons, among the classification algorithms (pre-selection phase, fig.5) for reduced and full model.

REDUCED MODEL						
	Accuracy	**Post-hoc comparisons**				
		PDA	**BAY**	**DET**	**KNN**	**ENS**
SVM	0.68 (0.12)	<0.01	<0.001	n.s.	<0.01	<0.01
PDA	0.76 (0.08)	—	n.s.	<0.01	<0.001	n.s.
BAY	0.78 (0.10)	—	—	<0.001	<0.001	n.s.
DET	0.72 (0.10)	—	—	—	<0.01	<0.001
KNN	0.60 (0.14)	—	—	—	—	<0.001
ENS	0.76 (0.10)	—	—	—	—	—
FULL MODEL						
	Accuracy	**post-hoc comparisons**				
		PDA	**BAY**	**DET**	**KNN**	**ENS**
SVM	0.64 (0.10)	<0.001	<0.001	n.s.	n.s.	<0.001
PDA	0.72 (0.14)	—	n.s.	<0.05	<0.001	n.s.
BAY	0.80 (0.10)	—	—	<0.001	<0.001	n.s.
DET	0.68 (0.12)	—	—	—	n.s.	<0.001
KNN	0.64 (0.08)	—	—	—	—	<0.001
ENS	0.76 (0.08)	—	—	—	—	—

n.s. indicates not significant p-*value.*

sagittal and the spinopelvic alignment (TK, LL, SS, and PI) were very similar between the groups, confirming that the risk of curve progression cannot be associated a priori with changes in the geometrical parameters at the onset. As regards the biomechanical parameters, the lateral component of the intervertebral load (F_{lat}) was generally lower in the progressive group at each considered level of the scoliotic curve (apex, and upper and lower end). This finding is in relation with the lower Cobb angle found for the progressive subjects compared to the stable ones (nearly significant difference, $p = 0.06$), and is in agreement with that recently observed by our group in a previous study (Barba et al., 2021). That study exploited the same musculoskeletal model to evaluate mild, moderate and severe subjects, and revealed F_{lat} as strongly correlated with scoliosis severity. In particular, the intervertebral force vector tends to be vertically oriented in the coronal plane despite the presence of deformity (see **Figure 4A**), whereas it is orthogonal to the vertebral upper endplate in the sagittal plane (**Figure 4B**). Larger deformity provides larger vertebral rotation in the coronal plane at upper and lower end levels of the scoliotic curve (**Figure 2E**), which results into larger contribution of the transferred load relatively to the lateral axis in the vertebral reference system (**Figure 2E**, upper right corner). As concerns the activation of MF and ES muscle, the slightly positive values (similar between groups) of the normalized activity ratio indicate a larger activation in the convex side of the scoliotic curve, in agreement with our previous findings (Barba et al., 2021) and with other numerical and experimental studies (Schmid et al., 2020; Cheung et al., 2005; Kwok et al., 2015). Overall, the biomechanical parameters did not provide a priori information about the risk of curve progression.

As regards the prediction of the scoliosis progression, the cross-validation analysis pointed out higher accuracy levels provided by PDA, BAY and ENS algorithm in the classification of stable and progressive cases (**Figure 5**), with median value ranging from 0.72 to 0.8 (**Table3**). This result was confirmed both in case of reduced predictors set (accounting for anthropometrical and geometrical parameters) and full set (accounting in addition for the biomechanical ones), revealing that neglecting or accounting for the biomechanical measure guaranteed very similar accuracy levels. This finding was statistically confirmed by comparing the level of sensitivity

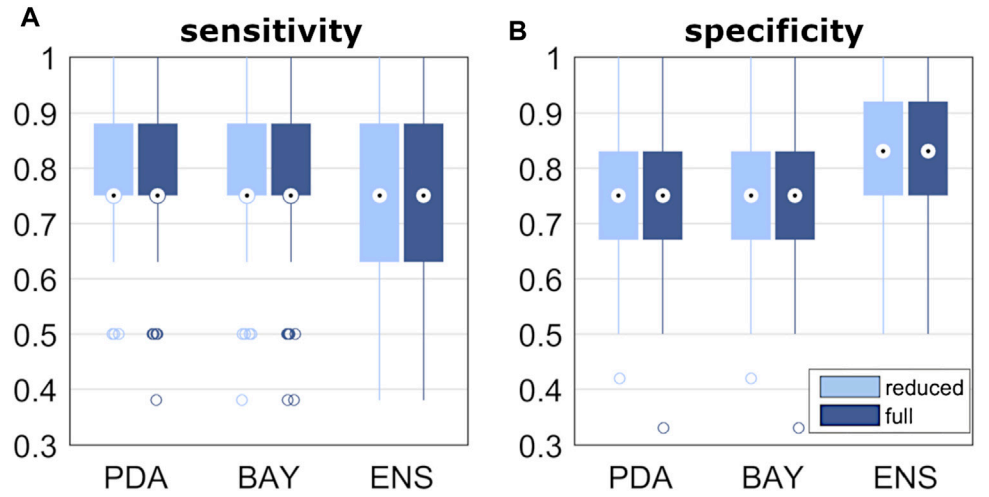

FIGURE 6 | Results of classification performance, from the comparison phase of step iii). Box and whiskers plot reporting the distribution of the sensitivity and specificity values **(A,B)** obtained by the best fitting algorithms.

and specificity between reduced and full model (**Figure 6**). The median values of sensitivity (0.75 for each algorithm) and specificity (0.75 for PDA and BAY, and 0.83 for ENS) were equal for the two models. According to that, the results demonstrated that accounting for the biomechanical measures was not sufficient for enhancing the prediction of the scoliosis progression. Such unexpected outcome could be explained by hypothesizing that in the evaluated conditions (mild scoliosis and replication of static standing posture), the information obtained from the musculoskeletal simulation may reflect those provided by the geometrical reconstruction, without representing an additional advantageous contribution. As well as the geometrical parameters, the biomechanical ones provide indeed information related to the three anatomical planes, since F_{lat} is calculated in the local vertebral reference system (**Figure 2**), and nES and nMF are computed by summing the activation of the individual muscle fascicles, the orientation of which depends on the 3D spinal alignment and the presence of deformity. However, the weak correlation found in general between the parameters (**Table4**), with strong relationship only between Cobb angle and F_{lat} and depending on the orientation of the intervertebral force vector as explained above, does not support the hypothesis of redundancy between geometrical and biomechanical parameters. As regards the importance of the individual predictors in correctly classifying the scoliosis progression, chronological age and Risser confirmed to be determining (**Figure 7**). The curve sagittal angle also demonstrated to have an impact and this is not unexpected, since it is well recognized that a deformity in the coronal plane implicates the flattening of the corresponding spine region in the sagittal plane (Kubat and Ovadia, 2020). The lateral shear at upper and lower end levels was found important as well, and can be explained as in relation with the differences in Cobb angle discussed above. However, the Cobb angle showed lower importance, suggesting that such analysis should be taken with caution overall, and that larger datasets should be considered to better consolidate the results.

In comparison to other studies, the classification performance was moderately lower: Skalli et al. reported 0.84 and 0.89 for sensitivity and specificity (Skalli et al., 2017), and Nault at al. 0.75 and 0.94, respectively, (Nault et al., 2020). However, it is

TABLE 4 | Correlation coefficient between geometrical and biomechanical parameters.

	F_{lat}			nES			nMF			nES along curve	nMF along curve
	Upper	Apex	Lower	Upper	Apex	Lower	Upper	Apex	Lower		
TK	−0.07	0.06	0.07	−0.01	−0.15	−0.03	0.05	−0.25[a]	−0.26[a]	−0.1	−0.2[a]
LL	−0.05	−0.01	0.1	0.01	-0.03	0.1	0.03	−0.24[a]	−0.4[a]	0.01	−0.22[a]
SS	0.01	0	0.09	0.15	0.12	0.12	0.01	−0.06	−0.17	0.13	−0.03
PI	0.05	0.02	0.06	0.08	0.13	0.18	0	−0.1	−0.24[a]	0.13	−0.1
Cobb angle	0.63[a]	0.29[a]	0.67[a]	−.01	0.01	0.02	0.12	0.36[a]	0.11	0.02	0.3[a]
curve sagittal angle	−0.29[a]	−0.05	−0.12	−0.05	−0.09	−0.07	−0.12	−0.12	−0.03	−0.07	−0.1
largest axial rotation	0.27[a]	0.12	0.53[a]	−0.08	−0.12	−0.04	0.2	0.34[a]	0.03	−0.12	0.32[a]

[a]*significantly different from zero.*

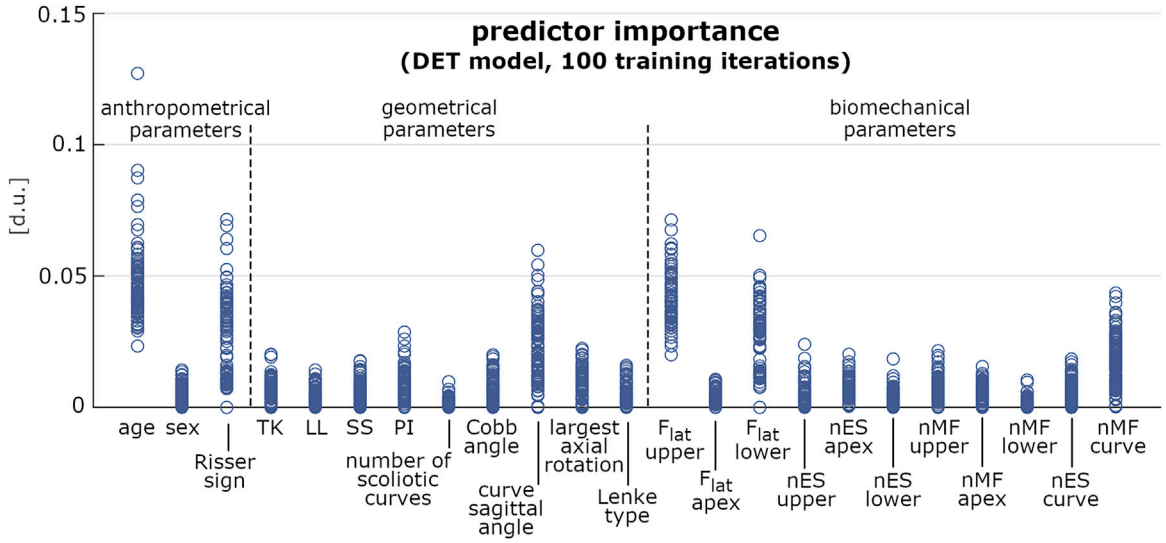

FIGURE 7 | Predictor importance (expressed in dimensionless units) of the anthropometrical, geometrical and biomechanical parameters, computed for 100 iterations of model training by DET approach. Each iteration accounted for 80 samples randomly chosen in the original dataset.

important to note that the results were obtained with different conditions of modelling strategy, number of evaluated subjects, and range of the reported results. Specifically, Skalli et al. exploited an approach based on PDA algorithm, which took into account six geometrical parameters of the primary scoliotic curve. The predictive model was trained by two control groups: non-scoliotic ones (53, stable), and cases with moderate and severe scoliosis (45, progressive). Another dataset of 65 subjects with mild scoliosis at first examination was processed by the model to determine the probability of being classified as stable or progressive, and then compared with the clinical evaluation in the follow-up. Nault at al. accounted for geometrical descriptors (more than twenty) of the global spine and scoliotic curve (Nault et al., 2014) in a dataset of 172 AIS subjects with mild and moderate scoliosis at first examination (Cobb angle ranging from 10 to 40). Their work was specifically devised to identify determinant predictors of the Cobb angle at final skeletal maturity. Descriptors found as not satisfactorily correlated with the measurement of the final Cobb angle were excluded, and an approach based on generalized linear model with backward selection was applied to find best predictors and interactions. The provided values of sensitivity and specificity were obtained as an example, by predicting those cases with final Cobb angle larger than 35. Differently from these studies, we calculated the classification performance in 100 random subsets of 20 subjects each (as described in Step iii section), and we compared the median value of sensitivity and specificity, the extent of which was found ranging from to 0.58 to 0.9 (median ± interquartile range, **Table 3**). As regards the evaluated predictors, we aimed to account for a list of descriptors expected as potentially related to the progression of scoliosis, avoiding similar additional parameters providing redundant information. For example, differently from that performed by Skalli et al. (2017) and Nault et al. (2020) the torsion index (the mean of the sum of the intervertebral axial rotations from lower end to apex and from apex to upper end of the scoliotic curve) was neglected in the present study. As expected, this index was found indeed significantly correlated with the largest axial rotation (0.6, $p < 0.001$), and the inclusion in the predictors set was verified as not improving the classification performance. In this respect, the index exhibited similar values in the stable and progressive group: 7.2 (4.2) and 7.1 (3.7), respectively.

The study has the following limitations. Only the relaxed upright posture was replicated, neglecting the simulation of more demanding tasks and motion activities. The development of such simulations implicates to deal with two major issues: how distributing the spine motion along the vertebral levels (i.e., the lumbar rhythm); how imposing the stiffness-related contribution of the passive elements during movements (joint moments). In this regard, reference data obtained *in vivo* or by experimental tests in AIS subjects are lacking in the literature. At this stage, we thus preferred to limit the simulation to the upright posture, although expected to provide lower spinal loads and muscle activities compared to the motion tasks (Dreischarf et al., 2016). According to that performed in previous similar works (Schmid et al., 2020; Barba et al., 2021), the evaluation of muscle activation as predictor of the scoliosis progression was limited to ES and MF. In this regard, additional groups such as quadratus lumborum, internal obliques, and latissimus dorsi could be considered as potential predictors in future developments simulating the motion of the trunk. No information about physical therapy or the prescription of bracing treatment in the period between the first examination and follow-up were available from the PACS search. The presence of that condition could represent a relevant factor since it is expected to counteract the progression of scoliosis, and neglecting such information could potentially bias the attribution of the subjects to stable or progressive group. In this regard, Skalli et al. accounted for the decision of bracing treatment in the clinical follow-up evaluation as a

criterion for identifying subject as progressive (Skalli et al., 2017). Conversely, the information was neglected by Nault et al. (2020), although in a preceding study, which accounted for subjects with Cobb angle ranging from 10 to 40 at first examination, they found that bracing treatment was more present in progressive cases compared to stable ones (58 and 45% of subjects, respectively, p = 0.13) (Nault et al., 2014). However, bracing is usually prescribed if either of the following two conditions are met: Cobb angle >25 and significant growth left until skeletal maturity; Cobb angle <25 but rapidly progressed at the 4–6-months follow-up appointment (Negrini et al., 2018). The first condition was not met in our dataset (Cobb angle <25 at first examination as inclusion criteria). Moreover, the follow-up time (minimum 6-months as inclusion criteria) was statistically similar between the stable and progressive group (27 (13) and 25 (12) months, respectively, as mean (SD), p = 0.44), thus reducing the probability of a potential bias. The exploited dataset accounted for a moderate number of subjects, and larger sets should be evaluated to refine the classification models and consolidate the results. As regards the reliability of the biomechanical measures, structural peculiarities and strengths and limitations of using musculoskeletal modelling approach for the characterization of the human spine have been extensively reviewed and discussed previously (Dreischarf et al., 2016; Dao, 2016; Bassani and Galbusera, 2018). In the context of the present study, the exploited body model has been previously validated for the replication of the spinal alignment in mild scoliosis (Cobb angle <30) (Barba et al., 2021). A potential limitation is represented by the scaling of the body model by exploiting predicted values of height and weight, due to the lack of real data. In this regard, a sensitivity analysis of model outcomes based on height and weight variation was not performed. However, the predicted values are expected to be well representative of the real ones, since low prediction errors were pointed out by the corresponding predictive models (see Appendix section). Indeed, the root-mean-square error, quantifying the goodness-of-fit between real and predicted data, was found to be equal to 3.9 kg and 4.3 cm for weight and height, respectively. In conclusion, accounting for biomechanical measures obtained with musculoskeletal modelling approach, replicating the static standing posture in subjects with mild scoliosis at first examination did not enhance the prediction of the scoliosis progression. The classification performance was found very similar by including or neglecting the biomechanical parameters, although no redundancy was observed overall between the geometrical and biomechanical measures. Therefore, a potential clinical application for the early detection of the progression of the deformity is not supported at this stage. Future developments will be aimed to consolidate the results by exploiting larger datasets of subjects, to obtain relevant information from the simulation of motion tasks, and to extend the classification perspective by exploiting multinomial approaches accounting for additional conditions such as non-scoliotic subjects and severe cases.

DATA AVAILABILITY STATEMENT

The raw data supporting the conclusions of this article will be made available by the authors, without undue reservation.

ETHICS STATEMENT

Ethical review and approval was not required for the study on human participants in accordance with the local legislation and institutional requirements. Written informed consent to participate in this study was provided by the participants' legal guardian/next of kin.

AUTHOR CONTRIBUTIONS

TB wrote the article and implemented the software procedures in MATLAB and AnyBody. AC analyzed the data, and gave substantial contributions to the application of the predictive modelling procedures. DI supported the application of the AnyBody routines and gave substantial contributions to the interpretation of the results. NB processed the radiographic images with sterEOS software, and implemented part of the procedures in AnyBody. FG gave substantial contributions to the conception and design of the work. All the authors critically revised the manuscript and approved the version to be published.

ACKNOWLEDGMENTS

The study was supported by the Italian Ministry of Health (Ricerca Corrente).

REFERENCES

Barba, N., Ignasiak, D., Villa, T. M. T., Galbusera, F., and Bassani, T. (2021). Assessment of Trunk Muscle Activation and Intervertebral Load in Adolescent Idiopathic Scoliosis by Musculoskeletal Modelling Approach. *J. Biomech.* 114, 110154. doi:10.1016/j.jbiomech.2020.110154

Bassani, T., and Galbusera, F. (2018). "Musculoskeletal Modeling," in *Biomechanics of the Spine*. Editors F. Galbusera, and H. Wilke (Academic Press), 257–277. doi:10.1016/b978-0-12-812851-0.00015-x

Bassani, T., and Galbusera, F. (2020). Statistics in Experimental Studies on the Human Spine: Theoretical Basics and Review of Applications. *J. Mech. Behav. Biomed. Mater.* 110, 103862. doi:10.1016/j.jmbbm.2020.103862

Bassani, T., Ottardi, C., Costa, F., Brayda-Bruno, M., Wilke, H.-J., and Galbusera, F. (2017). Semiautomated 3D Spine Reconstruction from Biplanar Radiographic Images: Prediction of Intervertebral Loading in Scoliotic Subjects. *Front. Bioeng. Biotechnol.* 5, 1. doi:10.3389/fbioe.2017.00001

Bassani, T., Stucovitz, E., Galbusera, F., and Brayda-Bruno, M. (2019). Is Rasterstereography a Valid Noninvasive Method for the Screening of Juvenile and Adolescent Idiopathic Scoliosis? *Eur. Spine J.* 28, 526–535. doi:10.1007/s00586-018-05876-0

Been, E., Shefi, S., Kalichman, L., F. Bailey, J., and Soudack, M. (2018). Cross-sectional Area of Lumbar Spinal Muscles and Vertebral Endplates: a Secondary Analysis of 91 Computed Tomography Images of Children Aged 2-20. *J. Anat.* 233, 358–369. doi:10.1111/joa.12838

Breiman, L. (2001). Random Forests. *Mach. Learn.* 45, 5–32. doi:10.1023/a:1010933404324

Cheung, J., Halbertsma, J. P. K., Veldhuizen, A. G., Sluiter, W. J., Maurits, N. M., Cool, J. C., et al. (2005). A Preliminary Study on Electromyographic Analysis of the Paraspinal Musculature in Idiopathic Scoliosis. *Eur. Spine J.* 14, 130–137. doi:10.1007/s00586-004-0780-7

Dao, T. T. (2016). Rigid Musculoskeletal Models of the Human Body Systems: A Review. *J. Musculoskelet. Res.* 19, 1630001. doi:10.1142/s0218957716300015

Donzelli, S., Zaina, F., and Negrini, S. (2020). Predicting Scoliosis Progression: a challenge for Researchers and Clinicians. *EClinicalMedicine* 18, 100244. doi:10.1016/j.eclinm.2019.100244

Dreischarf, M., Shirazi-Adl, A., Arjmand, N., Rohlmann, A., and Schmidt, H. (2016). Estimation of Loads on Human Lumbar Spine: A Review of *In Vivo* and Computational Model Studies. *J. Biomech.* 49, 833–845. doi:10.1016/j.jbiomech.2015.12.038

Galbusera, F., Casaroli, G., and Bassani, T. (2019). Artificial Intelligence and Machine Learning in Spine Research. *JOR Spine* 2, e1044. doi:10.1002/jsp2.1044

Harper, P. R. (2005). A Review and Comparison of Classification Algorithms for Medical Decision Making. *Health Policy* 71, 315–331. doi:10.1016/j.healthpol.2004.05.002

Ignasiak, D., Dendorfer, S., and Ferguson, S. J. (2016a). Thoracolumbar Spine Model with Articulated Ribcage for the Prediction of Dynamic Spinal Loading. *J. Biomech.* 49, 959–966. doi:10.1016/j.jbiomech.2015.10.010

Ignasiak, D., Ferguson, S. J., and Arjmand, N. (2016b). A Rigid Thorax assumption Affects Model Loading Predictions at the Upper but Not Lower Lumbar Levels. *J. Biomech.* 49, 3074–3078. doi:10.1016/j.jbiomech.2016.07.006

Illés, T., and Somoskeöy, S. (2012). The EOS Imaging System and its Uses in Daily Orthopaedic Practice. *Int. Orthop.* 36, 1325–1331. doi:10.1007/s00264-012-1512-y

Kohashi, Y., Oga, M., and Sugioka, Y. (1996). A New Method Using Top Views of the Spine to Predict the Progression of Curves in Idiopathic Scoliosis during Growth. *Spine* 21, 212–217. doi:10.1097/00007632-199601150-00010

Kubat, O., and Ovadia, D. (2020). Frontal and Sagittal Imbalance in Patients with Adolescent Idiopathic Deformity. *Ann. Transl. Med.* 8, 29. doi:10.21037/atm.2019.10.49

Kuhn, M., and Kjell, J. (2013). *Applied Predictive Modeling*. New York: Springer.

Kwok, G., Yip, J., Cheung, M. C., and Yick, K. L. (2015). Evaluation of Myoelectric Activity of Paraspinal Muscles in Adolescents with Idiopathic Scoliosis during Habitual Standing and Sitting. *Biomed. Res. Int.* 2015, 958450. doi:10.1155/2015/958450

Lenke, L. G., Betz, R. R., Harms, J., Bridwell, K. H., Clements, D. H., Lowe, T. G., et al. (2001). Adolescent Idiopathic Scoliosis. *J. Bone Jt. Surg. Am.* 83, 1169–1181. doi:10.2106/00004623-200108000-00006

Lonstein, J. E., and Carlson, J. M. (1984). The Prediction of Curve Progression in Untreated Idiopathic Scoliosis during Growth. *J. Bone Jt. Surg.* 66, 1061–1071. doi:10.2106/00004623-198466070-00013

Melhem, E., Assi, A., El Rachkidi, R., and Ghanem, I. (2016). EOS Biplanar X-ray Imaging: Concept, Developments, Benefits, and Limitations. *J. Child. Orthop.* 10, 1–14. doi:10.1007/s11832-016-0713-0

Minasny, B. (2009). The Elements of Statistical Learning. *Springer Series in Statistics*, 745.

Nault, M.-L., Beauséjour, M., Roy-Beaudry, M., Mac-Thiong, J.-M., de Guise, J., Labelle, H., et al. (2020). A Predictive Model of Progression for Adolescent Idiopathic Scoliosis Based on 3D Spine Parameters at First Visit. *Spine (Phila Pa. 1976)* 45, 605–611. doi:10.1097/brs.0000000000003316

Nault, M.-L., Mac-Thiong, J.-M., Roy-Beaudry, M., Turgeon, I., Deguise, J., Labelle, H., et al. (2014). Three-Dimensional Spinal Morphology Can Differentiate between Progressive and Nonprogressive Patients with Adolescent Idiopathic Scoliosis at the Initial Presentation. *Spine. (1976)* 39, E601–E606. doi:10.1097/brs.0000000000000284

Negrini, S., Donzelli, S., Aulisa, A. G., Czaprowski, D., Schreiber, S., de Mauroy, J. C., et al. (2018). 2016 SOSORT Guidelines: Orthopaedic and Rehabilitation Treatment of Idiopathic Scoliosis during Growth. *Scoliosis* 13, 3. doi:10.1186/s13013-017-0145-8

Nnadi, C., and Fairbank, J. (2010). Scoliosis: a Review. *Paediatr. Child. Health* 20, 215–220. doi:10.1016/j.paed.2009.11.009

Noshchenko, A., Hoffecker, L., Lindley, E. M., Burger, E. L., Cain, C. M., Patel, V. V., et al. (2015). Predictors of Spine Deformity Progression in Adolescent Idiopathic Scoliosis: A Systematic Review with Meta-Analysis. *World J. Orthop.* 6, 537–558. doi:10.5312/wjo.v6.i7.537

O'Neill, S., Kavanagh, R. G., Carey, B. W., Moore, N., Maher, M., and O'Connor, O. J. (2018). Using Body Mass index to Estimate Individualised Patient Radiation Dose in Abdominal Computed Tomography. *Eur. Radiol. Exp.* 2, 38. doi:10.1186/s41747-018-0070-5

Perdriolle, R., and Vidal, J. (1981). A Study of Scoliotic Curve. The Importance of Extension and Vertebral Rotation (Author's Transl). *Rev. Chir. Orthop. Reparatrice Appar. Mot.* 67, 25–34.

Peterson, L. E., and Nachemson, A. L. (1995). Prediction of Progression of the Curve in Girls Who Have Adolescent Idiopathic Scoliosis of Moderate Severity. Logistic Regression Analysis Based on Data from the Brace Study of the Scoliosis Research Society. *J. Bone Jt. Surg.* 77, 823–827. doi:10.2106/00004623-199506000-00002

Risser, J. C. (2010). The Classic: The Iliac Apophysis: an Invaluable Sign in the Management of Scoliosis. 1958. *Clin. Orthop. Relat. Res.* 468, 643–653. doi:10.1007/s11999-009-1096-z

Sanders, J. O., Khoury, J. G., Kishan, S., Browne, R. H., Mooney, J. F., 3rd, Arnold, K. D., et al. (2008). Predicting Scoliosis Progression from Skeletal Maturity: a Simplified Classification during Adolescence. *J. Bone Jt. Surgery Am.* 90, 540–553. doi:10.2106/jbjs.g.00004

Schmid, S., Burkhart, K. A., Allaire, B. T., Grindle, D., Bassani, T., Galbusera, F., et al. (2020). Spinal Compressive Forces in Adolescent Idiopathic Scoliosis with and without Carrying Loads: A Musculoskeletal Modeling Study. *Front. Bioeng. Biotechnol.* 8, 159. doi:10.3389/fbioe.2020.00159

Scholz, M., and Wimmer, T. (2021). A Comparison of Classification Methods across Different Data Complexity Scenarios and Datasets. *Expert Syst. Appl.* 168, 114217. doi:10.1016/j.eswa.2020.114217

Skalli, W., Vergari, C., Ebermeyer, E., Courtois, I., Drevelle, X., Kohler, R., et al. (2017). Early Detection of Progressive Adolescent Idiopathic Scoliosis. *Spine (Phila Pa. 1976)* 42, 823–830. doi:10.1097/brs.0000000000001961

Somoskeöy, S., Tunyogi-Csapó, M., Bogyó, C., and Illés, T. (2012). Accuracy and Reliability of Coronal and Sagittal Spinal Curvature Data Based on Patient-specific Three-Dimensional Models Created by the EOS 2D/3D Imaging System. *Spine J.* 12, 1052–1059. doi:10.1016/j.spinee.2012.10.002

Vanwinckelen, G., and Blockeel, H. (2012). "On Estimating Model Accuracy with Repeated Cross-Validation," in BeneLearn 2012: Proceedings of the 21st Belgian-Dutch Conference on Machine Learning, Ghent, Belgium, May 24–25, 2012, 39–44.

Vergari, C., Gajny, L., Courtois, I., Ebermeyer, E., Abelin-Genevois, K., Kim, Y., et al. (2019). Quasi-automatic Early Detection of Progressive Idiopathic Scoliosis from Biplanar Radiography: a Preliminary Validation. *Eur. Spine J.* 28, 1970–1976. doi:10.1007/s00586-019-05998-z

Vergari, C., Skalli, W., Abelin-Genevois, K., Bernard, J. C., Hu, Z., Cheng, J. C. Y., et al. (2021). Effect of Curve Location on the Severity index for Adolescent Idiopathic Scoliosis: a Longitudinal Cohort Study. *Eur. Radiol.* In press. doi:10.1007/s00330-021-07944-4

Weinstein, S. L., Dolan, L. A., Cheng, J. C., Danielsson, A., and Morcuende, J. A. (2008). Adolescent Idiopathic Scoliosis. *Lancet* 371, 1527–1537. doi:10.1016/s0140-6736(08)60658-3

Conflict of Interest: The authors declare that the research was conducted in the absence of any commercial or financial relationships that could be construed as a potential conflict of interest.

The handling editor DEA declared a past co-authorship with several of the authors TB and FG.

Publisher's Note: All claims expressed in this article are solely those of the authors and do not necessarily represent those of their affiliated organizations, or those of the publisher, the editors and the reviewers. Any product that may be evaluated in this article, or claim that may be made by its manufacturer, is not guaranteed or endorsed by the publisher.

APPENDIX

A procedure for predicting the subject's weight and height from anthropometrical data and geometrical parameters measured on the radiographic images was devised, based on that proposed by O'Neill et al. (O'Neill et al., 2018), who calculated the body mass index from the cross-sectional imaging of the abdomen. A dataset of 85 AIS subjects with known weight and height, underwent radiographic examination by EOS system and evaluated by our group in a previous study was exploited (Bassani et al., 2019). The subjects were checked to be characterized by the same age range and scoliosis severity (Cobb angle <25) of those evaluated in the present study (100 AIS subjects, **TableA1**). The procedure accounted for the identification of six landmarks (P1-P6, **Figure A1**), which were handpicked in sequence on the radiographic images to provide measurements expected as strongly related to the subject's weight and height. The points from P1 to P4 identified the maximum skin-to-skin anteroposterior and lateral diameter (D_{AP} and D_{LAT}, **Figure A1**) in correspondence of the upper endplate center of the L4 vertebra. The effective diameter, D_E, interpreting the diameter of the cross-sectional area at the considered level, was calculated as the square root of the product of D_{AP} and D_{LAT}. Points P5 and P6 identified the center of L5S1 and C7T1 intervertebral disc, respectively, and were exploited to calculate the vertical distance between the two discs. Two independent predictive models, based on multiple linear regression, were arranged to estimate weight and height. In each model, the following set of six predictive parameters was accounted for: age, sex (converted into dummy variable), TK and LL (**Figure 2B**), D_E, and discs vertical distance. The coefficients of the models were estimated by least mean squares approach (**TableA2**). The root-mean-square error (RMSE), quantifying the goodness-of-fit between real and predicted values, was found to be equal to 3.9 kg and 4.3 cm for weight and height, respectively. The estimated coefficients were exploited to process the six parameters as measured in the dataset of 100 AIS subjects, and to predict the corresponding values of weight and height. The distribution of the accounted parameters, as well as that of weight and height (real and predicted values, for the dataset of 85 and 100 AIS subjects, respectively), was verified to be comparable between the two datasets. In this regard, no significant differences were recognized (compared by *t*-test or Wilcoxon rank sum test) although the proportion between females and males was statistically lower in the present study (chi-square test) (**Table A1**). Data and image processing, and statistical analysis, were performed by custom routines written in MATLAB.

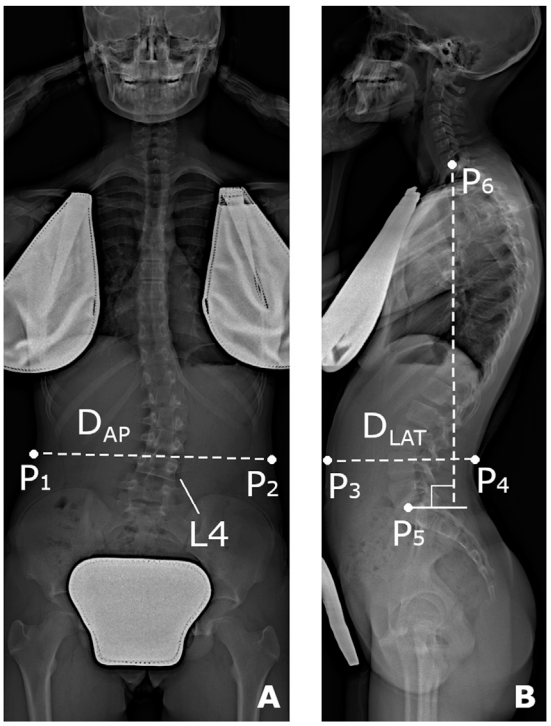

FIGURE A1 | Reference points (P1-P6) handpicked on the radiographic images in the coronal **(A)** and sagittal **(B)** plane for the prediction of subject's weight and height. Anteroposterior diameter (D_{AP}) calculated as the distance between P1 and P2, lateral diameter (D_{LAT}) as that between P3 and P4, and vertical distance between L5S1 and C7T1 disc center (P5 and P6, respectively).

TABLE A1 | values of the parameters, expressed as mean (SD) or number of cases, for the subjects evaluated in the present study and for the dataset with known weight and height values.

	Present study (N = 100)	Bassani et al. (2019) (N = 85)
age [years]	12.5 (1.5)	13.3 (1.2)
sex [F/M]	67/33	72/13>[a]
Cobb angle [°]	17.4 (5.9)	15.8 (11.4)
TK [°]	43.0 (12.7)	38.0 (12.3)
LL [°]	58.9 (9.8)	60.0 (11.0)
D_E [cm]	19.9 (1.9)	20.4 (2.0)
discs vertical distance [cm]	38.5 (3.2)	39.1 (3.3)
weight [kg]	44.5 (8.0) predicted	46.6 (9.0)
height [cm]	159.1 (10.3) predicted	159.3 (10.6)

[a]*indicates significant difference (p < 0.05) between the two study groups.*

TABLE A2 | Estimated coefficients of the linear regression models for the prediction of weight and height.

Predictor variable	Coefficient	
	Weight model	Height model
age [years]	0.8132	0.8038
sex [F/M]	–55.9553/–54.2006	45.5567/51.3015
TK [°]	0.0099	0.1886
LL [°]	0.0261	–0.0117
D_E [cm]	2.4337	0.5688
discs vertical distance [cm]	1.0201	2.1515

frontiers in Bioengineering and Biotechnology

ORIGINAL RESEARCH
published: 27 September 2021
doi: 10.3389/fbioe.2021.745837

A Reference Database of Standardised Continuous Lumbar Intervertebral Motion Analysis for Conducting Patient-Specific Comparisons

Alexander Breen[1], *Diana De Carvalho*[2], *Martha Funabashi*[3,4], *Greg Kawchuk*[5], *Isabelle Pagé*[4], *Arnold Y. L. Wong*[6] *and Alan Breen*[1,7]*

[1]AECC University College, Bournemouth, United Kingdom, [2]Division of Community Health and Humanities, Faculty of Medicine, Memorial University of Newfoundland, St. John's, NL, Canada, [3]Division of Research and Innovation, Canadian Memorial Chiropractic College, Toronto, ON, Canada, [4]Département de chiropratique, Université du Québec à Trois-Rivières, Trois-Rivières, QC, Canada, [5]Department of Physical Therapy, Faculty of Rehabilitation Medicine, University of Alberta, Edmonton, AB, Canada, [6]Department of Rehabilitation Sciences, The Hong Kong Polytechnic University, Hong Kong, SAR China, [7]Faculty of Science and Technology, Bournemouth University, Poole, United Kingdom

OPEN ACCESS

Edited by:
Babak Bazrgari, University of Kentucky, United States

Reviewed by:
Navid Arjmand, Sharif University of Technology, Iran
Ameet Krishnan Aiyangar, Swiss Federal Laboratories for Materials Science and Technology, Switzerland

***Correspondence:**
Alan Breen
breenalan@gmail.com

Specialty section:
This article was submitted to Biomechanics, a section of the journal Frontiers in Bioengineering and Biotechnology

Received: *22 July 2021*
Accepted: *08 September 2021*
Published: *27 September 2021*

Citation:
Breen A, De Carvalho D, Funabashi M, Kawchuk G, Pagé I, Wong AYL and Breen A (2021) A Reference Database of Standardised Continuous Lumbar Intervertebral Motion Analysis for Conducting Patient-Specific Comparisons. Front. Bioeng. Biotechnol. 9:745837. doi: 10.3389/fbioe.2021.745837

Lumbar instability has long been thought of as the failure of lumbar vertebrae to maintain their normal patterns of displacement. However, it is unknown what these patterns consist of. Research using quantitative fluoroscopy (QF) has shown that continuous lumbar intervertebral patterns of rotational displacement can be reliably measured during standing flexion and return motion using standardised protocols and can be used to assess patients with suspected lumbar spine motion disorders. However, normative values are needed to make individualised comparisons. One hundred and thirty-one healthy asymptomatic participants were recruited and performed guided flexion and return motion by following the rotating arm of an upright motion frame. Fluoroscopic image acquisition at 15fps was performed and individual intervertebral levels from L2-3 to L5-S1 were tracked and analysed during separate outward flexion and return phases. Results were presented as proportional intervertebral motion representing these phases using continuous means and 95%CIs, followed by verification of the differences between levels using Statistical Parametric Mapping (SPM). A secondary analysis of 8 control participants matched to 8 patients with chronic, non-specific low back pain (CNSLBP) was performed for comparison. One hundred and twenty-seven asymptomatic participants' data were analysed. Their ages ranged from 18 to 70 years (mean 38.6) with mean body mass index 23.8 kg/m^2 48.8% were female. Both the flexion and return phases for each level evidenced continuous change in mean proportional motion share, with narrow confidence intervals, highly significant differences and discrete motion paths between levels as confirmed by SPM. Patients in the secondary analysis evidenced significantly less L5-S1 motion than controls ($p < 0.05$). A reference database of spinal displacement patterns during lumbar (L2-S1) intersegmental flexion and return motion using a standardised motion protocol using fluoroscopy is presented. Spinal displacement patterns in asymptomatic individuals were found to be distinctive and consistent for

each intervertebral level, and to continuously change during bending and return. This database may be used to allow continuous intervertebral kinematics to drive dynamic models of joint and muscular forces as well as reference values against which to make patient-specific comparisons in suspected cases of lumbar spine motion disorders.

Keywords: back pain, videofluoroscopy, lumbar spine, intervertebral motion, kinematics, reference database, instability

INTRODUCTION

Pathological spinal motion, or lumbar instability, has long been thought of as the failure of the lumbar spine to maintain its normal pattern of displacement (Panjabi, 1992). However, it is currently unclear what this normal pattern actually consists of, as the motion segments of the spine are sited deep within the body, making them practically impervious to objective biomechanical measurement in living people. This tends to deny clinicians the tools to investigate relationships between symptoms and intrinsic biomechanics and constrains the identification of biomechanical markers for spinal pain. Given that the spine has a complex dynamic role in the normal activities of daily living, recent proposals for future directions in spine biomechanics research have included the recommendation that *"The dynamic properties of the* (functional spinal unit) *FSU . . . should be a focus of future research efforts as they are likely very relevant to the in vivo situation."* (Oxland, 2016). As non-invasive, *in vivo* measurement of the dynamic properties of the FSU generally requires imaging, precision imaging measurement of *in vivo* segmental spine dynamics is critical for gaining an understanding of spine biomechanics that could be applied in patient-specific assessments.

Spine biomechanics also increasingly involves biomechanical modelling, where *"the importance of verification, validation and sensitivity testing in computational studies within the field of biomechanical engineering"* has been highlighted (Jones and Wilcox, 2008). These models are sometimes utilized to estimate muscle and inter-joint forces within the lumbar spine, as they provide a relatively inexpensive and efficient method to estimate specific characteristics that are not otherwise possible or practical to measure *in-vivo*. However, while there are studies that provide *in vivo* information about intradiscal pressures, forces, and moments transmitted *via* instrumented vertebral implants, there is a lack of reference information with respect to multilevel continuous intervertebral motion for use in dynamically modelling loads (Dreischarf et al., 2016).

Although thorax and pelvis kinematics, used to drive such models, have often been measured using skin-based motion capture, the inherent errors associated with the proper identification of underlying bony landmarks mean that skin-based tracking is rarely used for measuring the motion of individual vertebrae (Eskandari et al., 2017). Instead, the kinematics of the lumbar vertebrae are often approximated from their segmental contributions to flexion motion based on static end-of-range radiographs. These contributions are then applied to the measured kinematics of the thorax-pelvis to estimate joint motion in the lumbar spine. However, it has been questioned as to whether this accurately represents vertebral orientation, for example, during dynamic bending tasks (Nagel et al., 2014; Aiyangar et al., 2015).

In addition, "Despite RoM being a simple metric that could be easily estimated within a clinical setting, it does not convey the contribution over time of the related segments/joints to the movement performed, compensatory actions nor the movement variability, thus limiting our understanding of movement strategies" (Papi et al., 2018). However, lumbar segmental contributions to motion, sometimes referred to as "spinal rhythms", have been demonstrated to change during simple tasks such as controlled flexion and return motion, (Aiyangar et al., 2015; Breen and Breen, 2020), and even during passive movement, where there is no measurable muscle activation (Breen and Breen, 2018). As such, physical and computational models that are validated using only end range of motion data may not accurately reproduce dynamic *in vivo* motion. Indeed, this may be one of the major causes of the large differences found in inter-joint and muscle forces when comparing models driven by generic patterns of rotational displacement in the lumbar spine and those based on kinematics acquired from dynamic imaging techniques (Eskandari et al., 2017; Byrne et al., 2020).

With advancements in imaging and object tracking technologies, continuous assessment of intersegmental spine motion during bending using quantitative fluoroscopy (QF) has been demonstrated to be relatively accurate and repeatable (Breen et al., 2019b). Thus, using QF for inter-image vertebral body tracking to quantify spine motion has allowed continuous intervertebral lumbar motion measurement *in-vivo*. However, the precision (and therefore the application) of dynamic models that integrate anthropometric and kinematic data will be limited if there is uncontrolled variation in subjects' motion behaviour (Magee, 2015).

In previous work using QF, where both the motion task and the analysis were highly standardised for range and velocity, some intervertebral motion sharing characteristics in the lumbar spine were found to be significantly different in chronic, nonspecific back pain (CNSLBP) patients compared with asymptomatic controls, indicating their eligibility to be considered as pain biomarkers (Breen and Breen, 2018; Breen and Breen, 2020). As some of these measurements were found to be relatively stable over 6 weeks in an asymptomatic population, this made these measures potentially suitable for use in outcome and prognostic studies. This, however, highlights the need for a reference database of normal values against which individuals could be compared (Breen et al., 2019a; Breen et al., 2019b). As the differences between patients and controls found in these

studies were in terms of continuous proportional motion sharing parameters, it was decided to formulate a normative Reference Database of these as information against which patient-specific comparisons could be made.

The present study therefore aimed to create a normative set of values for flexion and return dynamic lumbar segmental rotational contributions from a sizeable population base that could be used to drive future models. To support future patient-specific comparative studies and inform such musculoskeletal models, the project aimed to employ a standardised protocol, rather than a free-bending one, and to identify the intersegmental contributions to motion from L2-S1 during weight bearing flexion and return in asymptomatic individuals.

Given that more recent studies have focused on the return paths of lumbar flexion separately, to support dynamic loading models during lifting (Aiyangar et al., 2015; Pavlova et al., 2018), the motion was separated into the flexion phase, and the return to neutral phase for analysis. In addition, as proportional motion has been found to discriminate patients and controls in the past (Breen and Breen, 2018; Breen et al., 2018; Breen and Breen, 2020) but has not yet been analysed across the time series, this analysis protocol was also applied in a further secondary analysis of a matched Patient-control subgroup.

MATERIALS AND METHODS

The methods used for image acquisition and analysis in this project were agreed by an international forum of QF users in 2009 (Breen et al., 2012), and applied in the present Reference Database study. The participants in the Forum were the only four groups of QF users known to the authors in 2009, who all employed automated image registration and/or tracking for extracting vertebral kinematics data and used well documented data collection protocols. The focus of the Forum was to agree a standard protocol for data collection and analysis that could be employed efficiently for investigating and comparing symptomatic and asymptomatic participants for clinical investigations and research.

Participants

A convenience sample of 131 asymptomatic volunteer participants was recruited to the Reference Database study from staff, students and visitors at the AECC University College (Bournemouth, United Kingdom) between July 2011 and July 2020. Participants were included based on the following inclusion criteria: between 21 and 80 years old, self-reported body mass index less than 30 kg/m^2 (to ensure image quality), free of pain on the day of testing, free of any back pain that limited normal activity for more than 1 day in the previous year, no history of abdominal surgery or spondylolisthesis, no medical radiation exposure of >8 mSv in the previous 2 years (self-identified by pre-study questionnaire detailing recent medical imaging), and not currently pregnant. Ethical approval was obtained from the United Kingdom National Research Ethics Service (SouthWest 3, 10/H0106/65) and written Informed consent was obtained from all participants prior to inclusion in the study.

For the Patient-control subgroup study, 8 patients without any obvious mechanical disruption (for example surgery or spondylolisthesis), who had been referred for QF imaging to investigate CNSLBP using the same imaging protocol, were recruited. Their imaging results were compared to those of 8 of the asymptomatic controls, following written informed consent to inclusion on the study. The controls were chosen from the Reference Database as being of similar age, sex and BMI to the patients. Their demographic information is shown in **Table 1**.

Reference Database Study Sample Size

The design criterion for determining the sample size needed to establish a credible 95% reference interval (RI) is the ratio of the confidence interval (CI) width on the RI cut-point to the RI width. Practical values for this ratio suggested by Linnet range from 0.1 to 0.3 (Linnet, 1987). Using a conservative ratio of 0.15, with a 90% cut-off CI and a single 95% upper RI cut-point, we required 134 participants (SSS software v.1, Wiley-Blackwell, Chichester United Kingdom). To allow for tracking failure in approximately 10% of sequences, we rounded the sample size up to 148. However, assuming a non-Gaussian distribution for at least some of the reference data, we employed the non-parametric RI methodology recommended in the Clinical Laboratory Standards Institute guidelines, for which the minimum recommended sample size is 120 (CLSI, 2008). This was therefore selected as the minimum population for the Reference Database study.

Data Collection

The QF protocol for image acquisition and analysis procedures as been detailed in previous studies (Breen et al., 2012; Breen and Breen., 2018; du Rose et al., 2018; Breen and Breen, 2020). In brief however, participants were guided through a standard active weight-bearing flexion and return motion task. This was designed to reduce behavioural variations in participant bending, while controlling the speed and range of motion in a reproducible way. During this controlled motion, low dose fluoroscopic recordings of L2-S1 levels during continuous motion were acquired using a Siemens Arcadis Avantic digital C-arm fluoroscope (Siemens GMBH) at 15 frames per second. To achieve this, participants stood with their right-hand side next to a motion testing platform (Atlas Clinical Ltd. Lichfield, United Kingdom), which guided them through a 60° bending arc at 6°/s during both flexion and return phases (**Figure 1**). Participants were positioned in a comfortable upright stance with the centre of rotation of the motion platform in line with the disc space between the third and fourth lumbar vertebrae (This position was confirmed by single short pulse fluoroscopic images and the use of radiopaque markers temporarily aligned with the platform's centre of rotation.) A sacral brace and a belt around the hips of participants were used to minimise pelvic motion and keep the spine in the field of view throughout the bending sequence. This was to ensure the best field of view for all the segments to be conveniently imaged throughout the whole range of motion.

Before the acquisition of the QF images, participants undertook 3 practice bends. These standing movements,

TABLE 1 | Participant characteristics (mean and SD).

Reference database		Subgroup study		
		Controls	Patients	2-tailed p
N	127	8	8	
Females (%)	62 (48.8)	3 (38.8)	3 (38.8)	0.99
Age (years)	38.6 (13.8)	48.1 (13.4)	48.8 (14.4)	0.93
Height (m)	1.73 (0.09)	1.70 (0.1)	1.70 (0.1)	0.71
Weight (kg)	71.6 (12.7)	74.5 (12.7	75.4 (10.5)	0.41
BMI	23.8 (2.9)	25.8 (6.5)	25.3 (5.3)	0.42

SD: standard deviation; m: meters; kg: kilograms; BMI: body mass index.

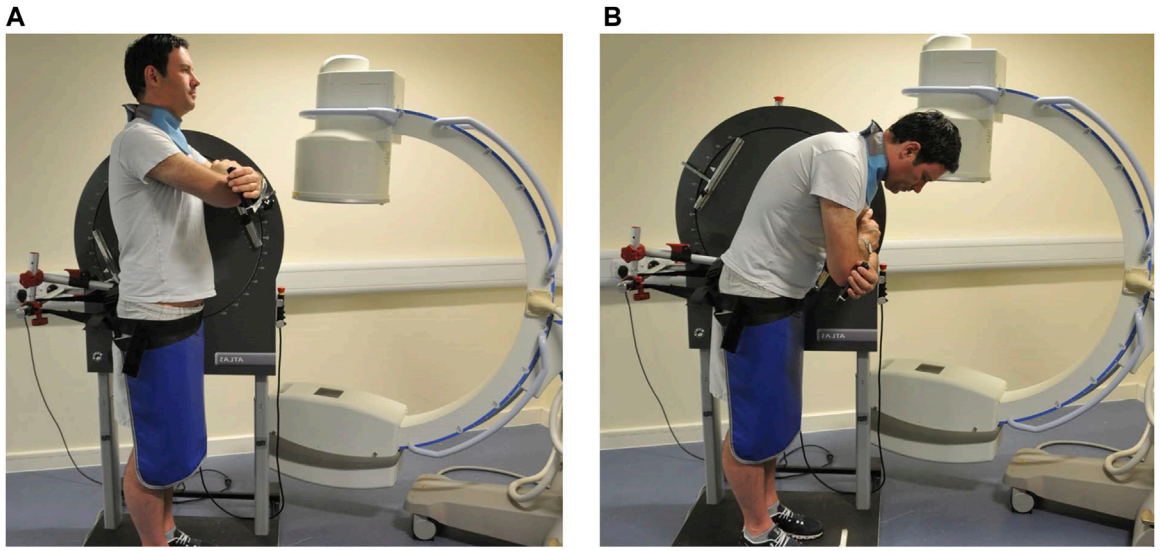

FIGURE 1 | Motion protocol used for fluoroscopic image acquisition (Courtesy Atlas Clinical Ltd., Lichfield, United Kingdom) **(A)** upright **(B)** flexed.

bending to 20° flexion and return, were followed by 40-degree and 60-degree bends. This ensured that participants could perform their recorded motion confidently and smoothly.

Intervertebral Motion Analysis

A previously validated semi-automated tracking process was used to determine the position of each vertebra (L2, L3, L4, L5 and S1) within each image recorded during the flexion and return trials (Breen et al., 2012). This process has been shown to have an accuracy for measuring intervertebral RoM of 0.52°, (du Rose and Breen, 2016), inter-and intra-observer repeatability ranging from ICC 0.94–0.96 and SEM 0.23°–0.61° and acceptable intra-subject repeatability (ICC 0.96, MDC over 6 weeks, 60%) (Breen et al., 2006; du Rose and Breen, 2016; Breen et al., 2019b).

Rotations were extracted from the positions for each of the tracked vertebrae (L2, L3, L4, L5 and S1, **Figure 2**) in each of the QF images throughout the flexion and return movement. Changes in the intervertebral angle from the starting position at each level (L2-L3, L3-L4, L4-L5, and L5-S1) over time were then computed. The motion outputs were separated into two phases, the flexion phase, and the return to neutral phase. To standardise the representation of motion across all participants, the L2-S1 angle was normalized to a percentage of its range of motion (RoM). Thus, during the flexion phase, standing was defined as 0% RoM and maximum flexion as 100% RoM, while in the return phase, 0% RoM was defined as maximum flexion and 100% RoM as being returned to the original reference position.

Changes in intervertebral angles were then interpolated to obtain each intervertebral motion segment's rotation for every 1% increment of the L2–S1 RoM. The segmental contribution of each intervertebral level as a percentage of the change in L2–S1 angle was then computed at every increment.

Statistical Analysis

For the Reference Database study, the share of intervertebral segmental motion was calculated for all participants for each level throughout the bending task. Statistical Parametric Mapping (SPM) was then used to compare the whole kinematic time-series between levels' contributions to motion for both the flexion and return sequences (Friston et al., 2007). SPM analysis is an open-source spm1d package (available from www.spm1d.org) based on Random Field Theory, and has been validated for 1D data (Adler et al., 2007; Pataky et al., 2016; Pataky, 2016). Following normality testing, custom Python programs (Python

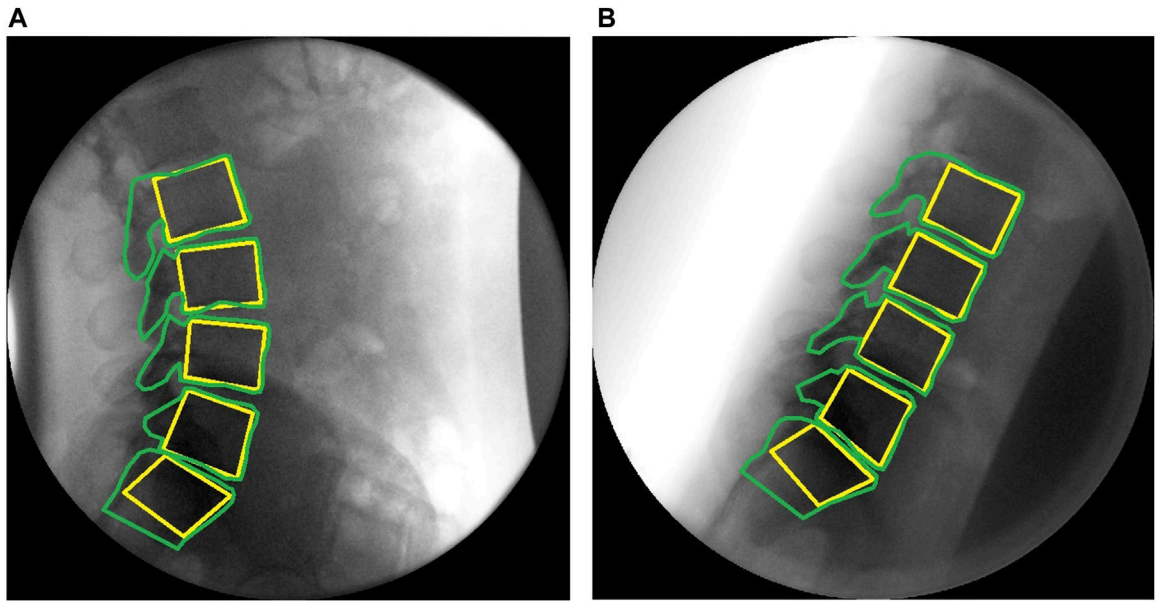

FIGURE 2 | Sagittal plane fluoroscopic images of the lumbar spine with computer templates **(A)** upright **(B)** flexed.

version 3.8) were used to conduct parametric two-tailed, two-sample t-tests across the time series. Statistical significance occurs when the SPM curves cross the critical threshold node at any time, taking into account that each time point is related to those on either side (Friston et al., 2007; Papi et al., 2020). Where multiple adjacent points of the SPM curves exceeded the critical threshold, the associated *p*-values were calculated using Random Field Theory.

For the Patient-control secondary analysis, SPM analysis was conducted using non-parametric two tailed t-tests. This compared segmental contributions to bending between patients and controls throughout the motion. Previous measures of segmental contribution have been shown to have high observer reliability and acceptable intrasubject repeatability over 6 weeks (Breen et al., 2019b; To et al., 2020).

RESULTS

For the Reference study, 131 participants were imaged. Four participants were excluded due to tracking errors of at least 1 vertebra. Full data sets were therefore obtained from 127 participants. Tables containing the Reference Database, detailing the mean and 95%CI for the continuous proportional segmental motion for flexion and return motion plus the Patient-Control secondary analysis data can be found in **Supplementary Material I**.

Reference Database study participants received a mean (upper third quartile) effective dose of 0.27 mSv (0.31) while secondary analysis patients received 0.26 mSv (0.30) for this investigation. These values are approximately one quarter of the dose of a conventional plain radiographic examination of the lumbar spine (Mellor et al., 2014).

For the Patient-control sub-study, 8 chronic back pain patients and 8 controls were imaged (43.8% female, mean age 48.1 (controls) and 48.8 years (patients). Thus, the sub-study participants were approximately 10 years older than those in the Reference Database study who had a mean age of 38.6. This was the only substantial difference between the studies.

Kinematics

The maximum intervertebral ranges throughout flexion and return motion (means) for the Reference Database study group and the Patient-control sub-study group are shown in **Table 2**. Maximum change in L5-S1 RoM was significantly less than the controls in the Patient-control sub-study.

Figure 3 shows statistically significant differences in contributions to bending during the motion, both between and within levels. Each intervertebral level had its own characteristic motion signature across the Reference Database study population, with significant differences ($p < 0.05$, noted from the lack of overlap of the 95%CI bands) between each level's contribution throughout most of the motion. It is also notable that these paths are in a state of constant change as the motion progresses, although all levels exhibit more uniform motion sharing in the return phase than in the flexion phase. In addition, there is a negative contribution to motion of L5-S1 at the beginning of flexion (**Figure 3A**). This is expected as participants attempt to move their hips back to keep the centre of mass over the feet.

The SPM analysis reported in **Figure 4** reveals these differences to be highly significant ($p < 0.001$) between levels for almost all data points across the motion for both flexion and return in the Reference Database study cohort, confirming the presence of discrete motion paths for each motion segment. During the outward flexion phase of movement, the superior

TABLE 2 | Mean maximum intervertebral rotational ranges (mean and SD).

Reference database		Subgroup study		
		Controls	Patients	2-tailed p
RoM L2-3	9.5 (3.87)	10.2 (1.4)	8.9 (5.2)	0.46
RoM L3-4	10.6 (2.96)	11.5 (2.8)	10.1 (2.8)	0.21
RoM L4-5	10.4 (3.93)	11.9 (3.5)	8.7 (1.1)	0.21
RoM L5-S1	5.7 (5.60)	7.2 (3.9)	3.2 (2.9)	0.05

RoM: range of motion (degrees)

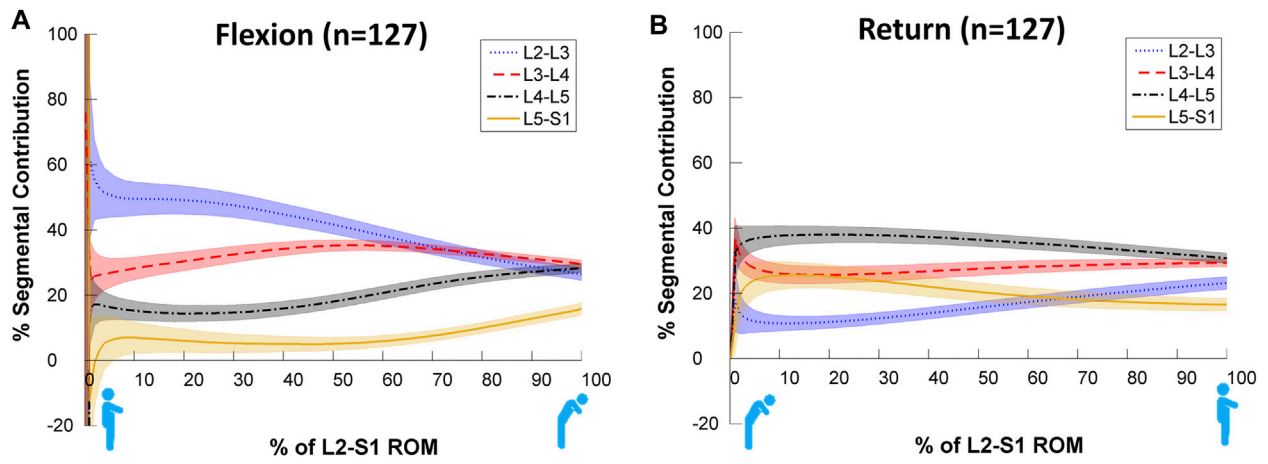

FIGURE 3 | Average segmental contribution to lumbar flexion [**(A)**: Flexion and **(B)**: return to standing] with 95% confidence intervals (shaded areas) in the Reference Database cohort.

lumbar motion segment of each pair (**Figure 4**) consistently contributed more to the range of motion, exceeding the critical value for 50–99% of the task. In addition, the L2-3 vs. L3-4 motion segment combination also had a supra-threshold cluster at the end of flexion where the *inferior* motion segment contributed more ($p = 0.008$).

During the return to upright position phase of the task, in 3 of the 6 inter joint combinations, the inferior motion segment of the pair constantly contributed significantly more to the return phase of bending ($p < 0.001$). The exceptions were "L3-4 vs. L5-S1" and "L4-5 vs. L5-S1", where the superior motion segment contributed a greater amount ($p < 0001$), and at "L2-3 vs. L5-S1", where initially (between 5–40% of the RoM) L5-S1 contributed more ($p < 0.001$). In the late stages of bending (at approximately 100% of RoM), L2-3 contributed more ($p < 0.001$).

Patient-Control Secondary Analysis

The motion contributions in the secondary analysis are shown in **Figure 5**. These subjectively demonstrate differences in the motion sharing patterns between patients and controls, especially at L5-S1. Verification of these differences can be seen in the non-parametric SPM analysis provided in **Supplementary Material III**.

Figure 6 compares the motion sharing patterns for all 8 patients and 8 controls in the secondary analysis. There was little difference between patients and controls in terms of motion sharing at most intervertebral levels, although these have been found to differentiate patients from controls in passive recumbent studies (Breen and Breen, 2018). However, SPM analyses reveals that there are statistically significant differences between the groups' motion share at L2-L3 during the return to neutral phase of the task ($p < 0.001$) and at the end range of L5-S1 motion (Flexion $p = 0.012$ and Return $p = 0.004$) (**Figure 6**).

DISCUSSION

Reference Study

To the best of the authors' knowledge this study reports the largest database of continuous intersegmental lumbar spine kinematics during weight bearing *in-vivo* flexion and return, providing normative reference values for making patient-specific kinematic comparisons, for informing dynamic FE loading models, and to help identify biomarkers for CNSLBP (Zanjani-Pour et al., 2018; Breen and Breen, 2020). The Reference Database study used an established standardised protocol to measure the intersegmental contributions to motion from L2-S1 during weight bearing flexion and return bending–unlike most conventional recording of lumbar flexion, which depends on participant co-ordination for its consistency. Using this protocol, continuous change in mean proportional motion share was observed during both the flexion

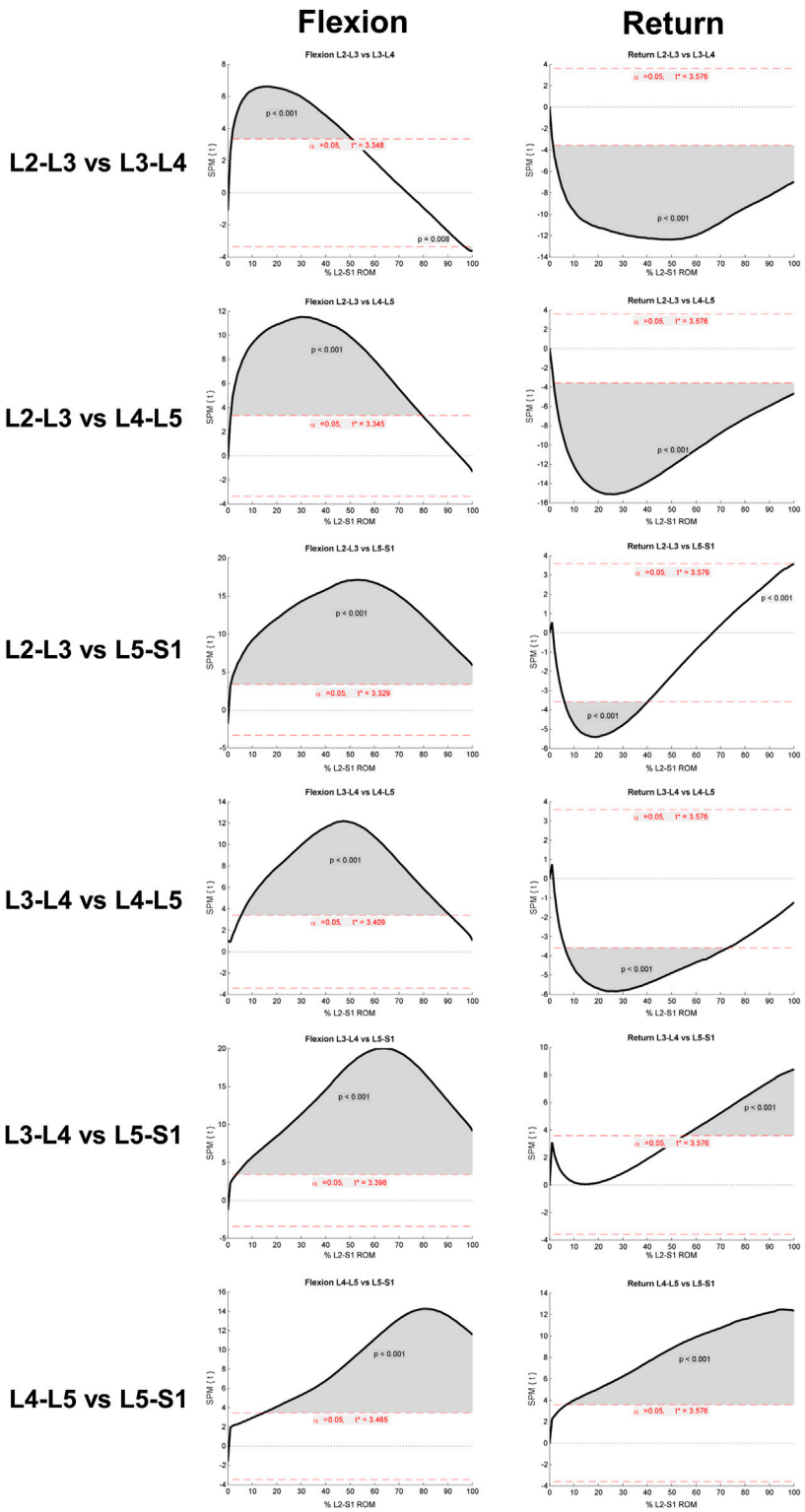

FIGURE 4 | Results of SPM parametric paired t-test (SPM{t}). Each row refers to a different intervertebral joint combination. Supra-threshold clusters indicate significance differences between joint contributions to motion and are shown in grey. The critical threshold is shown as a red dashed line. *Versions of these figures alongside the mean and 95%CI bands can be found in* **Supplementary Material II**.

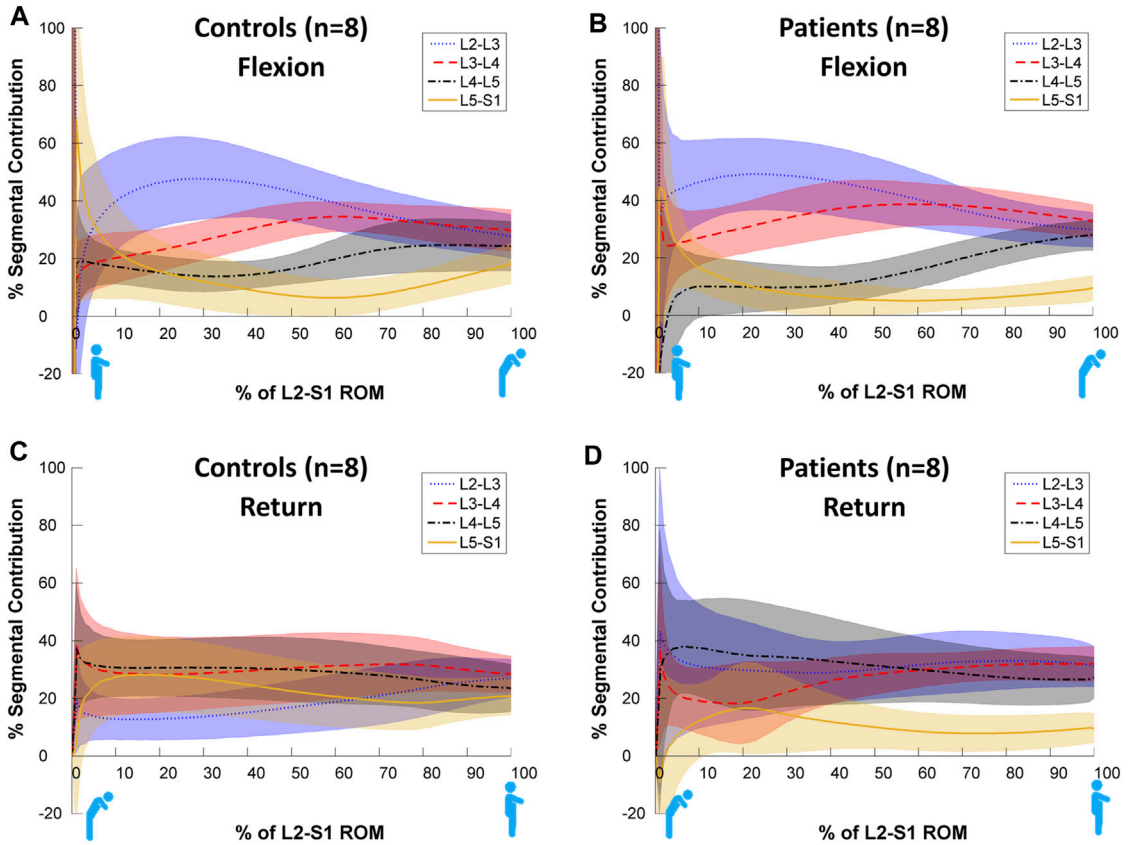

FIGURE 5 | Average segmental contribution to return from flexion with 95% confidence intervals (shaded areas) in the Patient-control sub-study cohorts. **(A)**: Control Flexion, **(B)**: Patient Flexion, **(C)**: Control Return, **(D)**: Patient Return.

and return phases and revealed significant differences in the motion paths between levels. In addition, while the similarity between this study's measures of lumbar segmental contributions and previous measures of lumbo-pelvic rhythms are interesting, these are not the same and should not be confused.

It would be appropriate to compare this database with previous fluoroscopy studies, however no one study has applied all the criteria required. We could find only four that attempted to employ completely continuous motion analysis (Okawa et al., 1998; Harada et al., 2000; Nagel et al., 2014; Aiyangar et al., 2015). This may, in part, account for the failure of studies that reported only quasi-static intersegmental motion to detect variations in the contributions of individual segments during bending (Wong et al., 2006). Only three used proportional motion (Teyhen et al., 2007; Nagel et al., 2014; Aiyangar et al., 2015), and none applied the degree of standardisation of participant motion during imaging used in the present study (Breen et al., 2012). Return phase motion (which is not represented as flexion in reverse) was reported in only 4 (Okawa et al., 1998; Harada et al., 2000; Teyhen et al., 2007; Aiyangar et al., 2015), while only 5 measured all levels from L2-S1 (Takayanagi et al., 2001; Lee et al., 2002; Wong et al., 2006; Ahmadi et al., 2009; Aiyangar et al., 2015). However, when comparing the segmental contributions derived from moderate or maximal flexion studies with continuous intervertebral motion studies, the distribution of sharing was found to be similar (Breen and Breen, 2020). Thus, the quasi-static spine kinematics literature, as reviewed by Widmer et al. (2019) exhibits a degree of consistency with more recent continuous motion studies in terms of lumbar intervertebral motion sharing.

The above considerations, plus the large number of participants in the Reference Database study, may account for the remarkably consistent motion sharing patterns during both outward and return continuous motion, despite some heterogeneity in participant characteristics. Although the age range in our sample was wide (21–70 years), body weight had an upper reference range of only 96 Kg, while weights of up to 119 Kg have been shown to be associated with substantially increased L5-S1 compression in flexed postures (Hajihosseinali et al., 2015). This may affect the segmental contribution at that level and was also noted in relation to RoM in the Widmer et al. (2019) review and in modelling studies by Zander et al. (2002). However, segmental contributions, once thought to be RoM-dependent, did not exhibit this in our Reference Database study, nor in other studies that included all segments from L2 to S1 (Miyasaka et al., 2000; Ahmadi et al., 2009; Aiyangar et al., 2015). Contribution patterns were also distinctly different in flexion and return, as one would expect with different phasing of trunk muscle activation (Ouaaid et al., 2013).

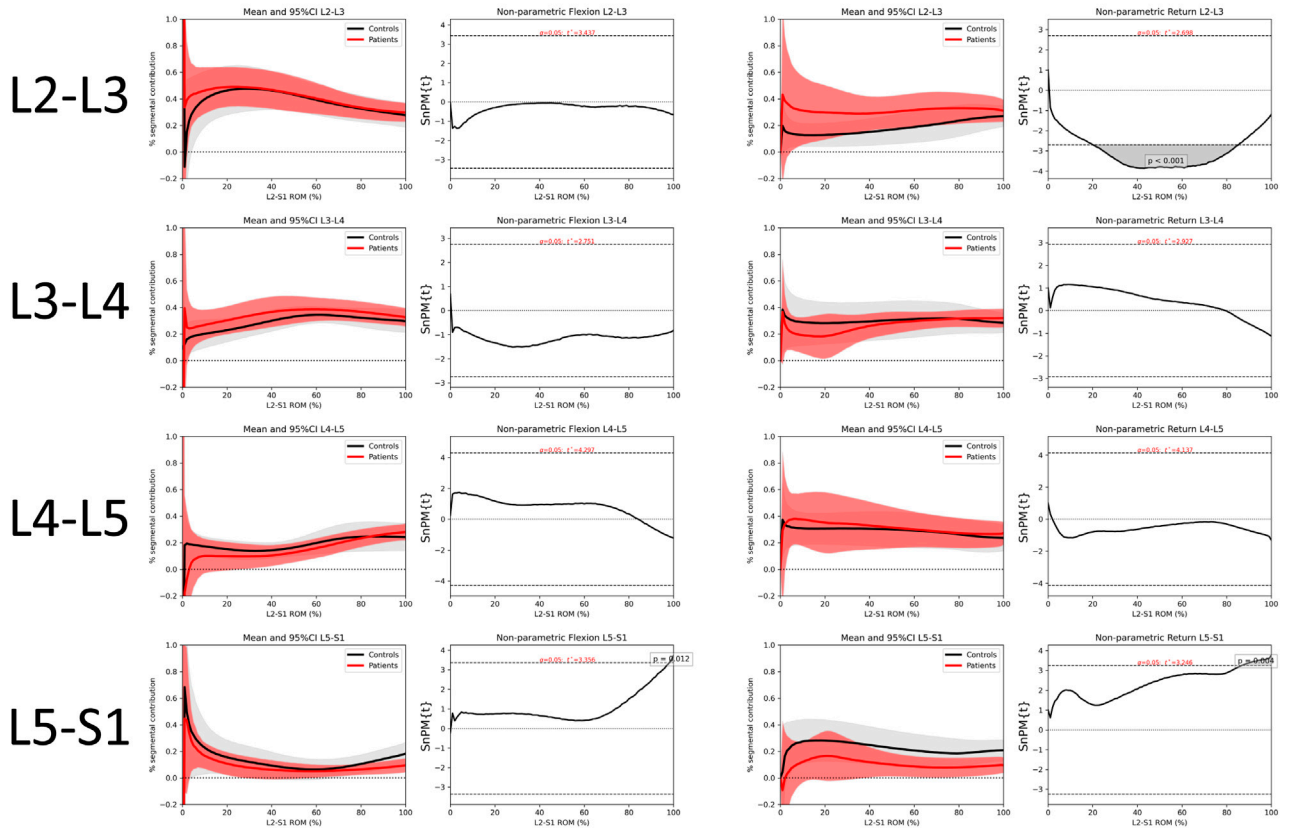

FIGURE 6 | Comparison of intervertebral motion sharing patterns between patients and controls at individual levels for flexion and return with 95% confidence intervals and SPM. Comparisons for all inter-joint combinations are shown in **Supplementary Material III**.

Patient-Control Sub-Study

The differences between patient and control subgroups in the return phase also seem to complement those previously found in weight bearing studies that combined outward and return motion (Breen and Breen, 2020). Moreover, the standardised image acquisition protocol would seem to make it unlikely that abnormal patterns are attributable to artefact rather than motion pathology. However, it also raises the possibility that other individual factors, such as lumbar geometry, may have an influence, making clinical assessments based on motion sharing patterns alone inadvisable.

The differences between patients and controls in the secondary analysis may reflect differences in the respective roles of the deep multifidus and erector spinae muscle groups in people with CNSLBP (Wallwork et al., 2009) and/or passive tissue restraint. Two trends are particularly apparent in this study of weight bearing motion. Firstly, L5-S1 shares less motion in patients, albeit non-significantly until the end of range. This is also reflected in the reduced RoM of L5-S1. Secondly, L2-3 shares significantly more motion in patients during the return phase, although this is only apparent in the mid-ranges and would not be measurable when merely investigating segmental range. Alterations in the readiness of lumbar joints to move in CNSLBP patients is also reflected clinically in the Kinesiopathological Model of low back pain, and is considered to be an important factor in rehabilitation (Van Dillen et al., 2013).

Strengths and Limitations

This is the largest dataset available to date to present normative values for continuous segmental contributions to motion in the lumbar spine using variables that have been shown to distinguish patients with CNSLBP from asymptomatic controls (Ahmadi et al., 2009; Breen and Breen, 2020). Moreover, the Patient-control sub-study provides further evidence of a kinematic biomarker for nonspecific back pain. However, standardising the motion protocol involves a trade-off between natural motion and the repeatability necessary to make patient-specific comparisons. In terms of the latter, the methodology used has undergone extensive validation in terms of precision and validity (Breen et al., 2006; Breen and Breen, 2016; Breen et al., 2019b) and has previously been used in preliminary dynamic loading studies using FE modelling (Zanjani-Pour et al., 2018). Thus, further subject-specific estimates of joint loading using dynamic imaging may be expected to improve the sensitivity of subject-specific model-based lumbar spinal loading estimates (Byrne et al., 2020). However, like many other biomechanical studies

that compare patients to controls, the sample size of our sub-study was small, which is a limitation that may be mitigated by further replication. In addition, while evidence suggests that magnitude of loading (beyond body weight), *in vivo*, does not have any significant effect on individual segmental contribution to motion (Aiyangar et al., 2015), biomechanical modelling should exercise caution if using this database to model unloaded or excessive loading states.

It would also have been useful for future biomechanical modelling studies if it had been possible to include the whole lumbar spine, but this could not be done owing to the limited image intensifier diameter. This is a problem with most current intensifiers which will be overcome as flat panel machines become more plentiful.

Future Studies

Further studies are needed, not only to replicate the present study's findings, but also to explore the effects of other variables, as well as coronal plane motion and passive recumbent motion, where body mass and muscular contractions are mitigated. However, there is still considerable scope for elaboration of motion sharing studies of weight bearing flexion and return. For example, variations in pelvic tilt may be an important source of heterogeneity in light of the variations in the motion segment flexibility that the QF procedure aims to measure (Retailleau and Colloud, 2020).

The specialised motion frame apparatus used in the current work, in addition to standardising the velocity and range of bending, also partially stabilises the sacrum. This increases to varying degrees, the contribution of the lumbar spine to the flexion motion, regardless of the degree of lordosis or sacral inclination. Although the degree of this restraint is not standardised and depends on the individual's natural lumbo-pelvic contribution to bending, this does not seem to disrupt the consistency of the resulting motion sharing patterns. Nevertheless, there is likely to be some relationship between lumbar sagittal shape and the motion contribution, albeit within the boundaries of the normative ranges of variation. This should be explored. Given that spine shape has been shown to influence a person's preference for squatting or stooping during lifting tasks, it would be useful to determine the relationships between spine shape and dynamic loading stresses at individual levels based on their contributions to flexion and return motion (Pavlova et al., 2018).

It would also be useful to explore other kinematic indices in terms of motion contributions, as the present database provides only rotational data, and there is evidence that the translational component, although small, also affects inter-segment rotational stiffness (Affolter et al., 2020). However, in a previous study, we did not find it to differentiate nonspecific back pain patients from controls (Breen et al., 2018).

Finally, it is now timely to explore possible relationships between the motion variants that seem to be associated with CNSLBP and possible sources of nociception. As these may not necessarily involve disco-ligamentous micro-strain, it may be useful to explore muscular metabolic pain as a mechanism by including blood flow studies with those of motion contributions during bending.

CONCLUSION

In asymptomatic people, provided a standardised QF imaging protocol for measuring continuous proportional lumbar intervertebral motion is used, consistent intervertebral motion patterns are revealed where each level follows its own discrete, level-specific path that changes significantly during the motion. This is proposed to represent the human normative phenotype when using the present imaging protocol. These paths constantly and consistently change as the bending motion progresses, although levels exhibit more uniform motion sharing in the return phase than in the flexion phase. Patients with CNSLBP showed a significantly greater contribution at L2-3 and a significantly smaller contribution at L5-S1 during the return phase.

DATA AVAILABILITY STATEMENT

The original contributions presented in the study are included in the article/**Supplementary Material**. Further inquiries can be directed to the corresponding author.

ETHICS STATEMENT

The studies involving human participants were reviewed and approved by the United Kingdom National Research Ethics Service (South West 3). The patients/participants provided their written informed consent to participate in this study.

AUTHOR CONTRIBUTIONS

AB and AxB contributed to the conception and design of the study and data collection. AxB organized the database, performed the statistical analysis, and wrote the first draft of the manuscript. AB provided interpretation of the outcomes. DDC, MF, GK, IP, and AW, contributed to the validation, writing the original draft and critical revisions of the article. All authors read, contributed to manuscript revision, and approved the submitted version.

SUPPLEMENTARY MATERIAL

The Supplementary Material for this article can be found online at: https://www.frontiersin.org/articles/10.3389/fbioe.2021.745837/full#supplementary-material

Supplementary Material I | Proportional intervertebral motion of individual level L2-S1 motion during forward bending and return in the Reference Database and Patient-control studies.

Supplementary Material II | SPM of inter-joint contributions to motion from the Reference Database, together with mean and 95% confidence intervals for each combination.

Supplementary Material III | Differences in the motion sharing patterns for all joint combinations between patients and controls analysed by 95% confidence intervals and SPM.

REFERENCES

Adler, R. J., Taylor, J. E., and Worsley, K. J. (2007). *Applications of Random fields and Geometry: Foundations and Case Studies*. Netherlands: Springer.

Affolter, C., Kedzierska, J., Vielma, T., Weisse, B., and Aiyangar, A. (2020). Estimating Lumbar Passive Stiffness Behaviour from Subject-specific Finite Element Models and *In Vivo* 6DOF Kinematics. *J. Biomech.* 102, 109681. doi:10.1016/j.jbiomech.2020.109681

Ahmadi, A., Maroufi, N., Behtash, H., Zekavat, H., and Parnianpour, M. (2009). Kinematic Analysis of Dynamic Lumbar Motion in Patients with Lumbar Segmental Instability Using Digital Videofluoroscopy. *Eur. Spine J.* 18, 1677–1685. doi:10.1007/s00586-009-1147-x

Aiyangar, A., Zheng, L., Anderst, W., and Zhang, X. (2015). Apportionment of Lumbar L2-S1 Rotation across Individual Motion Segments during a Dynamic Lifting Task. *J. Biomech.* 48 (13), 3709–3715. doi:10.1016/j.jbiomech.2015.08.022

Breen, A., and Breen, A. (2016). Accuracy and Repeatability of Quantitative Fluoroscopy for the Measurement of Sagittal Plane Translation and Finite centre of Rotation in the Lumbar Spine. *Med. Eng. Phys.* 38, 607–614. doi:10.1016/j.medengphy.2016.03.009

Breen, A., and Breen, A. (2020). Dynamic Interactions between Lumbar Intervertebral Motion Segments during Forward Bending and Return. *J. Biomech.* 102, 109603. doi:10.1016/j.jbiomech.2020.109603

Breen, A., and Breen, A. (2018). Uneven Intervertebral Motion Sharing Is Related to Disc Degeneration and Is Greater in Patients with Chronic, Non-specific Low Back Pain: an *In Vivo*, Cross-Sectional Cohort Comparison of Intervertebral Dynamics Using Quantitative Fluoroscopy. *Eur. Spine J.* 27 (1), 145–153. doi:10.1007/s00586-017-5155-y

Breen, A., Claerbout, E., Hemming, R., Ayer, R., and Breen, A. (2019a). Comparison of Intra Subject Repeatability of Quantitative Fluoroscopy and Static Radiography in the Measurement of Lumbar Intervertebral Flexion Translation. *Sci. Rep.* 9, 19253. doi:10.1038/s41598-019-55905-1

Breen, A. C., Muggleton, J. M., and Mellor, F. E. (2006). An Objective Spinal Motion Imaging Assessment (OSMIA): Reliability, Accuracy and Exposure Data. *BMC Musculoskelet. Disord.* 7 (1), 1–10. doi:10.1186/1471-2474-7-1

Breen, A. C., Teyhen, D. S., Mellor, F. E., Breen, A. C., Wong, K. W. N., and Deitz, A. (2012). Measurement of Intervertebral Motion Using Quantitative Fluoroscopy: Report of an International Forum and Proposal for Use in the Assessment of Degenerative Disc Disease in the Lumbar Spine. *Adv. Orthop.* 2012, 1–10. doi:10.1155/2012/802350

Breen, A., Hemming, R., Mellor, F., and Breen, A. (2019b). Intrasubject Repeatability of *In Vivo* Intervertebral Motion Parameters Using Quantitative Fluoroscopy. *Eur. Spine J.* 28 (2), 450–460. doi:10.1007/s00586-018-5849-9

Breen, A., Mellor, F. E., and Breen, A. C. (2018). Aberrant Intervertebral Motion in Patients with Treatment-Resistant Nonspecific Low Back Pain: a Retrospective Cohort Study and Control Comparison. *Eur. Spine J.* 27, 2831. doi:10.1007/s00586-018-5666-1

Byrne, R. M., Aiyangar, A. K., and Zhang, X. (2020). Sensitivity of Musculoskeletal Model-Based Lumbar Spinal Loading Estimates to Type of Kinematic Input and Passive Stiffness Properties. *J. Biomech.* 102, 109659. doi:10.1016/j.jbiomech.2020.109659

CLSI (2008). *Defining, Establishing and Verifying Reference Intervals in the Clinical Laboratory; Approved Guideline*. 3rd Edn. Wayne, PA: Clinical Laboratory Standards Institute.

Dreischarf, M., Shirazi-Adl, A., Arjmand, N., Rohlmann, A., and Schmidt, H. (2016). Estimation of Loads on Human Lumbar Spine: A Review of *In Vivo* and Computational Model Studies. *J. Biomech.* 49, 833–845. doi:10.1016/j.jbiomech.2015.12.038

du Rose, A., and Breen, A. (2016). Relationships between Lumbar Inter-vertebral Motion and Lordosis in Healthy Adult Males: a Cross Sectional Cohort Study. *BMC Musculoskelet. Disord.* 17 (121), 121. doi:10.1186/s12891-016-0975-1

du Rose, A., Breen, A., and Breen, A. (2018). Relationships between Muscle Electrical Activity and the Control of Inter-vertebral Motion during a Forward Bending Task. *J. Electromyogr. Kinesiol.* 43, 48–54. doi:10.1016/j.jelekin.2018.08.004

El Ouaaid, Z., Shirazi-Adl, A., Plamondon, A., and Larivière, C. (2013). Trunk Strength, Muscle Activity and Spinal Loads in Maximum Isometric Flexion and Extension Exertions: A Combined In Vivo-computational Study. *J. Biomech.* 46, 2228–2235. doi:10.1016/j.jbiomech.2013.06.018

Eskandari, A. H., Arjmand, N., Shirazi-AdlFarahmand, A. F., and Farahmand, F. (2017). Subject-specific 2D/3D Image Registration and Kinematics-Driven Musculoskeletal Model of the Spine. *J. Biomech.* 57, 18–26. doi:10.1016/j.jbiomech.2017.03.011

Friston, K. J., Ashburner, J. T., Kiebel, S. J., Nichols, T. E., and Penny, W. D. (2007). *Statistical Parametric Mapping: The Analysis of Functional Brain Images*. London: Elsevier.

Hajihosseinali, M., Arjmand, N., and Shirazi-Adl, A. (2015). Effect of Body Weight on Spinal Loads in Various Activities: A Personalized Biomechanical Modeling Approach. *J. Biomech.* 48, 276–282. doi:10.1016/j.jbiomech.2014.11.033

Harada, M., Abumi, K., Ito, M., and Kaneda, K. (2000). Cineradiographic Motion Analysis of normal Lumbar Spine during Forward and Backward Flexion. *Spine* 25, 1932–1937. doi:10.1097/00007632-200008010-00011

Jones, A. C., and Wilcox, R. K. (2008). Finite Element Analysis of the Spine: Towards a Framework of Verification, Validation and Sensitivity Analysis. *Med. Eng. Phys.* 30 (10), 1287–1304. doi:10.1016/j.medengphy.2008.09.006

Lee, S.-w., Wong, K. W. N., Chan, M.-k., Yeung, H.-m., Chiu, J. L. F., and Leong, J. C. Y. (2002). Development and Validation of a New Technique for Assessing Lumbar Spine Motion. *Spine* 27 (8), E215–E220. doi:10.1097/00007632-200204150-00022

Linnet, K. (1987). Two-stage Transformation Systems for Normalization of Reference Distributions Evaluated. *Clin. Chem.* 33 (3), 381–386. doi:10.1093/clinchem/33.3.381

Magee, J. (2015). Three Dimensional Digital Modelling of Human Spine Anthropometrics and Kinematics from Meta-Analysis. How Relevant Is Existing Anatomical Research? *J. Spine* 4 (1), 251–257. doi:10.4172/2165-7939.1000205

Mellor, F. E., Thomas, P., and Breen, A. (2014). Moving Back: The Radiation Dose Received from Lumbar Spine Quantitative Fluoroscopy Compared to Lumbar Spine Radiographs with Suggestions for Dose Reduction. *Radiography* 20, 251–257. doi:10.1016/j.radi.2014.03.010

Miyasaka, K., Ohmori, K., Suzuki, K., and Inoue, H. (2000). Radiographic Analysis of Lumbar Motion in Relation to Lumbosacral Stability. *Spine* 25 (6), 732–737. doi:10.1097/00007632-200003150-00014

Nagel, T. M., Zitnay, J. L., Barocas, V. H., and Nuckley, D. J. (2014). Quantification of Continuous *In Vivo* Flexion-Extension Kinematics and Intervertebral Strains. *Eur. Spine J.* 23, 754–761. doi:10.1007/s00586-014-3195-0

Okawa, A., Shinomiya, K., Komori, H., Muneta, T., Arai, Y., and Nakai, O. (1998). Dynamic Motion Study of the Whole Lumbar Spine by Videofluoroscopy. *Spine* 23 (16), 1743–1749. doi:10.1097/00007632-199808150-00007

Oxland, T. R. (2016). Fundamental Biomechanics of the Spine-What We Have Learned in the Past 25 Years and Future Directions. *J. Biomech.* 49 (6), 817–832. doi:10.1016/j.jbiomech.2015.10.035

Panjabi, M. M. (1992). The Stabilizing System of the Spine. Part I. Function, Dysfunction, Adaptation, and Enhancement. *J. Spinal Disord.* 5 (4), 383–389. doi:10.1097/00002517-199212000-00001

Papi, E., Bull, A. M. J., and McGregor, A. H. (2020). Alteration of Movement Patterns in Low Back Pain Assessed by Statistical Parametric Mapping. *J. Biomech.* 100, 109597. doi:10.1016/j.jbiomech.2019.109597

Papi, E., Bull, A. M. J., and McGregor, A. H. (2018). Is There Evidence to Use Kinematic/kinetic Measures Clinically in Low Back Pain Patients? A Systematic Review. *Clin. Biomech.* 55, 53–64. doi:10.1016/j.clinbiomech.2018.04.006

Pataky, T. C. (2016). rft1d: Smooth One-Dimensional Random Field Upcrossing Probabilities inPython. *J. Stat. Soft.* 71, i07. doi:10.18637/jss.v071.i07

Pataky, T., Vanrenterghem, J., and Robinson, M. A. (2016). The Probability of False Positives in Zero-Dimensional Analyses of One-Dimensional Kinematic, Force and EMG Trajectories. *J. Biomech.* 49, 1468. doi:10.1016/j.jbiomech.2016.03.032

Pavlova, A. V., Meakin, J. R., Cooper, K., Barr, R. J., and Aspden, R. M. (2018). Variation in Lifting Kinematics Related to Individual Intrinsic Lumbar Curvature: an Investigation in Healthy Adults. *BMJ Open Sport Exerc. Med.* 4, e000374. doi:10.1136/bmjsem-2018-000374

Retailleau, M., and Colloud, F. (2020). New Insights into Lumbar Flexion Tests Based on Inverse and Direct Kinematic Musculoskeletal Modeling. *J. Biomech.* 105, 109782. doi:10.1016/j.jbiomech.2020.109782

Takayanagi, K., Takahashi, K., Yamagata, M., Moriya, H., Kitahara, H., and Tamaki, T. (2001). Using Cineradiography for Continuous Dynamic-Motion Analysis of the Lumbar Spine. *Spine* 26 (17), 1858–1865. doi:10.1097/00007632-200109010-00008

Teyhen, D. S., Flynn, T. W., Childs, J. D., Kuklo, T. R., Rosner, M. K., Polly, D. W., et al. (2007). Fluoroscopic Video to Identify Aberrant Lumbar Motion. *Spine* 32 (7), E220–E229. doi:10.1097/01.brs.0000259206.38946.cb

To, D., Breen, A., Breen, A., Mior, S., and Howarth, S. J. (2020). Investigator Analytic Repeatability of Two New Intervertebral Motion Biomarkers for Chronic, Nonspecific Low Back Pain in a Cohort of Healthy Controls. *Chiropr Man. Therap* 28 (62), 1–9. doi:10.1186/s12998-020-00350-5

Van Dillen, L. R., Sahrmann, S. A., and Norton, B. J. (2013). "The Kinesiopathological Model and Mechanical Low Back Pain," in *Spinal Control: The Rehabilitation of Low Back Pain*. Editors P.W. Hodges, J. Cholewicki, and J. Van Dieen (Edinburgh: Churchill Livingstone Elsevier), 89–98. doi:10.1016/b978-0-7020-4356-7.00008-2

Wallwork, T. L., Stanton, W. R., Freke, M., and Hides, J. A. (2009). The Effect of Chronic Low Back Pain on Size and Contraction of the Lumbar Multifidus Muscle. *Man. Ther.* 14 (5), 496–500. doi:10.1016/j.math.2008.09.006

Widmer, J., Fornaciari, P., Senteler, M., Roth, T., Snedeker, J. G., and Farshad, M. (2019). Kinematics of the Spine under Healthy and Degenerative Conditions: a Systematic Review. *Ann. Biomed. Eng.* 47, 1491–1522. doi:10.1007/s10439-019-02252-x

Wong, K. W. N., Luk, K. D. K., Leong, J. C. Y., Wong, S. F., and Wong, K. K. Y. (2006). Continuous Dynamic Spinal Motion Analysis. *Spine* 31 (4), 414–419. doi:10.1097/01.brs.0000199955.87517.82

Zander, T., Rohlmann, A., Klöckner, C., and Bergmann, G. (2002). Comparison of the Mechanical Behavior of the Lumbar Spine Following Mono- and Bisegmental Stabilization. *Clin. Biomech.* 17, 439–445. doi:10.1016/s0268-0033(02)00040-2

Zanjani-Pour, S., Meakin, J. R., Breen, A., and Breen, A. (2018). Estimation of *In Vivo* Inter-vertebral Loading during Motion Using Fluoroscopic and Magnetic Resonance Image Informed Finite Element Models. *J. Biomech.* 70, 134–139. doi:10.1016/j.jbiomech.2017.09.025

Conflict of Interest: The authors declare that the research was conducted in the absence of any commercial or financial relationships that could be construed as a potential conflict of interest.

frontiers in Bioengineering and Biotechnology

ORIGINAL RESEARCH
published: 18 October 2021
doi: 10.3389/fbioe.2021.724854

Biomechanical Evaluation of the Effect of Minimally Invasive Spine Surgery Compared with Traditional Approaches in Lifting Tasks

John Rasmussen[1]*, *Kristoffer Iversen*[2], *Bjørn Keller Engelund*[2] and *Sten Rasmussen*[3]

[1]Department of Materials and Production, Aalborg University, Aalborg, Denmark, [2]AnyBody Technology A/S, Aalborg, Denmark, [3]Department of Clinical Medicine, Aalborg University and Aalborg University Hospital, Aalborg, Denmark.

Fusion of spinal vertebrae can be accomplished by different surgical approaches. We investigated Traditional Open Spine Surgery (TOSS) versus Minimally Invasive Spine Surgery (MISS). While TOSS sacrifices spine muscles originating or inserting on the affected vertebrae, MISS seeks to minimize the approach-related morbidity and preserve the tendon attachments of the muscles in the area. We captured 3-D motions of the full body of one healthy subject performing a variety of 10 kg box lifting operations representing activities-of-daily-living that are likely to challenge the spine biomechanically. The motion data were transferred to a full-body biomechanical model with a detailed representation of the biomechanics of the spine, and simulations of the internal spine loads and muscle forces were performed under a baseline configuration and muscle configurations typical for TOSS respectively MISS for the cases of L3/L4, L4/L5, L5/S1, L4/S1 and L3/L5 fusions. The computational model was then used to investigate the biomechanical differences between surgeries. The simulations revealed that joint reaction forces are more affected by both surgical approaches for lateral lifting motions than for sagittal plane motions, and there are indications that individuals with fused joints, regardless of the approach, should be particularly careful with asymmetrical lifts. The MISS and TOSS approaches shift the average loads of different muscle groups in different ways. TOSS generally leads to higher post-operative muscle loads than MISS in the investigated cases, but the differences are smaller than could be expected, given the differences of surgical technique.

Keywords: spine fusion, biomechanics, surgery, simulation, joint loads, muscles

OPEN ACCESS

Edited by:
Lennart Scheys,
KU Leuven, Belgium

Reviewed by:
Tito Bassani,
Galeazzi Orthopedic Institute IRCCS, Italy
Rizwan Arshad,
Royal Military College of Canada, Canada

***Correspondence:**
John Rasmussen
jr@mp.aau.dk

Specialty section:
This article was submitted to Biomechanics, a section of the journal Frontiers in Bioengineering and Biotechnology

Received: *14 June 2021*
Accepted: *04 October 2021*
Published: *18 October 2021*

Citation:
Rasmussen J, Iversen K, Engelund BK and Rasmussen S (2021) Biomechanical Evaluation of the Effect of Minimally Invasive Spine Surgery Compared with Traditional Approaches in Lifting Tasks. Front. Bioeng. Biotechnol. 9:724854. doi: 10.3389/fbioe.2021.724854

INTRODUCTION

Lumbar spinal fusion is a surgical procedure, where two or more of the spinal vertebrae are fused by means of mechanical devices and bone grafts. The indications include a variety of degenerative lumbar spinal diseases. Mobbs et al. (2015) provided a comprehensive review of evidence, indications and surgical approaches.

Presuming that the recovered patient will resume activities of daily living, the motion that previously took place between the fused vertebrae will be redistributed among adjacent spinal joints, which therefore will sustain increased articulation to accommodate the same overall motion of the lumbar spine. The relationship between articulation and net joint reaction is not immediately

obvious, but a positive correlation between the two has been hypothesized, and larger articulation with high certainty will cause higher material strain in the disk, and there is clinical evidence for the possibility of adjacent degeneration (Nagata et al., 1993; Aota et al., 1995; Chow et al., 1996; Guigui et al., 1997; Hambly et al., 1998; Etebar and Cahill, 1999; Kumar et al., 2001). On the other hand, the fused joint will transfer moments that were previously balanced by muscles. Thus, the fusion is likely to redistribute the loads on muscles and joints in the region depending on surgical approaches, which might therefore affect the health and longevity of the operated spine.

We shall refer in the following to Traditional Open Spine Surgery with a posterior approach as TOSS. In this approach, access to the affected vertebrae involves resection of a major part of the musculature surrounding the site. Fascicles of the spinal musculature, such as m. erector spinae and m. multifidus that originate or insert on the fused bones, are generally sacrificed, and the same is often the case for fascicles of m. multifidus that cross the site at oblique angles, because they cannot be displaced sufficiently during the surgery. In the presence of a fused, rigid connection between the formerly articulating vertebrae, which supports the joint moments that were previously balanced by muscle actions, it is tempting to think that the local musculature is redundant and that its resection has little or no consequence. However, the spinal muscle configuration is complex with a multitude of fascicles spanning single or multiple joints to articulate and stabilize the spinal column in a statically indeterminate system (Hansen et al., 2006). It is therefore likely that resection of the local muscles has consequences beyond the site.

Minimally Invasive Spine Surgery (MISS) has gained popularity in the past decades (McAfee et al., 2010; Härtl, 2020), based on the reasoning that trauma minimization is generally beneficial for the patient (Kim, 2010), especially since traditional open spine surgery (TOSS) has several reported drawbacks including blood loss, muscle pain and infection risk. Minimally invasive insertion systems are designed to minimize the approach-related morbidity of traditional lumbar pedicle fixation. Depending on the surgical technique, MISS allows for an almost complete preservation of the local musculature.

The consequences of MISS versus TOSS can be assessed retrospectively between patient populations. Favorable results regarding morbidity and infection (Altshuler et al., 2021), readmission and reoperation (Altshuler et al., 2020), and perioperative outcome (Goldstein et al., 2016) for MISS have been reported (Kim et al., 2005). In particular, reduction of surgical trauma in MISS seems obvious and has been confirmed (Stevens et al., 2006). However, reduction of fat infiltration in muscles post-surgery was also investigated and fell below statistical significance (Min et al., 2009), and meta studies (Fourney et al., 2010) failed to show reduction of complications in MISS versus TOSS. Thus, clinical evidence for the biomechanical advantage of MISS over TOSS remains somewhat inconclusive.

The aforementioned clinical studies do not have the resolution to distinguish between the details of the surgery and conditions in the individual patients, and statistics offer little to the causality of observed complications for each patient. Consequently, computer models have been used to make in-silico comparison of TOSS versus MISS. Bresnahan et al. (2010) used a computer model of nominal spine flexion and lateral flexion to confirm the dependency of post-operative muscle activity on the surgical technique in L3/L4 and L4/L5 fusion, and Malakoutian et al. (2016) computed that muscle damage typical of TOSS increases compression loads in adjacent joints in an upright posture. Benditz et al. (2018) simulated the influence of different sagittal alignments in standing postures. Localized tissue models based on finite element analysis (Rijsbergen et al., 2018) have simulated the resulting process of disk degeneration. They draw upon the advantage of detailed geometrical and material description but typically have the disadvantage of absence of simulation of muscle actions, which leaves them to investigate nominal loads. Park et al. (2015) used a finite element model to investigate tissue loads in nine single- and multi-joint fusions under nominal follower loads and moments. Previous computer models have therefore added to the knowledge in the field, but they cover either relatively few fusion sites and/or idealized load cases.

Musculoskeletal models with active muscles as well as experimental techniques to measure human motions have evolved since the aforementioned works in terms of anatomical detail and experimental accessibility. They enable systematic investigation of combinations of real-life load cases and surgical approaches. Computer models also offer the opportunity to investigate all-things-equal situations, where the influence of specific parameters can be computed in the absence of measurement inaccuracies and inter-subject variation. The aim of this paper is therefore to exploit new modeling opportunities to investigate the biomechanical advantages and disadvantages of MISS versus TOSS.

METHODS

A single, healthy subject (male, age 29, stature 1.89 m, body weight 82 kg) was recruited for the data collection and signed an informed consent form. The subject lifted boxes weighing 10 kg from the floor to two different heights of (A) 59 cm and (B) 158 cm respectively in a sagittal plane motion, and subsequently (C) from the floor to 59 cm height in a movement from left to right. The test subject was instructed to perform the task naturally and with a technique of his own choice. Before recording the motion, the subject had the opportunity to perform familiarization trials. The three motions, A, B and C, are illustrated in **Figure 1**.

The motions were recorded with the Xsens Awinda system (Xsens Technologies B.V., Enschede, Netherlands). This is a wearable technology based on inertial measurement units and sensor fusion (Koning et al., 2015), and its suitability for recording musculoskeletal model input has been verified previously (Karatsidis et al., 2018). The sensor positions are on the feet, the lower legs, the upper legs, the pelvis, the sternum, the shoulders, the upper arms, the forearms, the hands and the head.

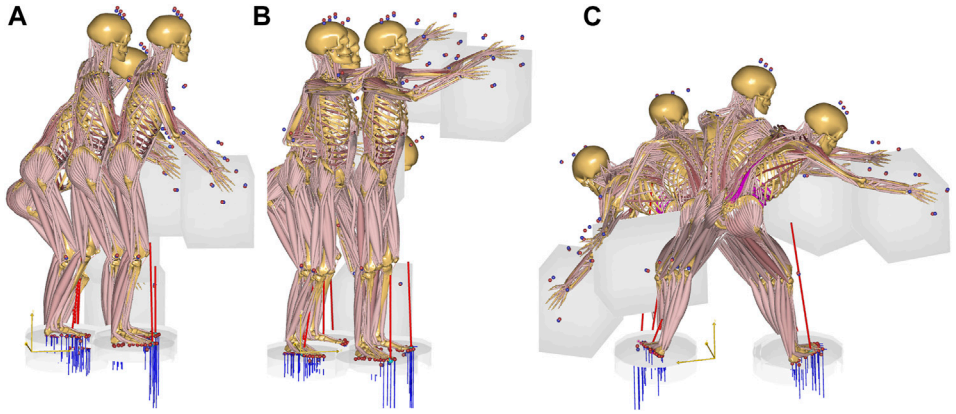

FIGURE 1 | The three box lifting cases. **(A)**: from the floor to 59 cm height. **(B)**: from the floor to 158 cm height. **(C)**: laterally from the floor to 59 cm height.

The motions were transferred via a BVH file to the AnyBody Modeling System version 7.3 (AnyBody Technology A/S, Aalborg, Denmark) (Damsgaard et al., 2006). The baseline model was the AnyScript Managed Model repository version 2.3.1 comprising lower extremities, pelvis and lumbar spine, a rigid thoracic spine and rib cage segment, an articulated cervical spine, shoulder complex, upper arms, forearms and rigid hand segments. The model comprises about 1,000 individually activated muscle fascicles. Muscle fascicles are modeled with individual cross sectional areas representing their strength, but the model does not take activation and contraction dynamics into account and its validity is therefore limited to relatively slow and voluntary movements. The model used inverse dynamics and solved for individual muscle forces with a quadratic recruitment criterion.

The lumbar spine model (de Zee et al., 2007) contains the lumbar vertebrae, the sacrum and the pelvis. The disk connections are idealized as spherical joints in the baseline, non-fused condition. The model comprises a total of 178 spinal muscle fascicles distributed over the groups: multifidi, erector spinae, psoas major, quadratus lumborum, semispinalis and spinalis. The model also comprises the abdominal musculature and its connection with the intra-abdominal pressure, which works to extend the lumbar spine as necessary. Scaling of the model to subject-specific dimensions happens on the segment level in response to the processing of the kinematics data, and segment inertial parameters are similarly scaled (Lund et al., 2015). The muscle strengths are scaled according to the BMI using the length-mass-fat scaling law (Rasmussen et al., 2005). The entire musculoskeletal model is continuously updated and published (Lund et al., 2020).

General validation of musculoskeletal models is difficult for a variety of reasons (Lund et al., 2012). For the case of the spine, intradiscal pressures in the intact structure and detailed joint force information from instrumented implants in operated structures have been obtained experimentally and were reviewed in detail by Dreischarf et al. (2016). They lend themselves to comparison with simulated values, and several independent research groups have corroborated the lumbar spine model used in this study (Han et al., 2012; Arshad et al., 2016; Bassani et al., 2017, 2020).

Analysis was performed on a baseline model representing the intact body, in single joint fusions of L3/L4, L4/L5, L5/S1, and in multiple joint fusions of L4/S1 and L3/L5, respectively, in MISS and TOSS configurations, resulting in a total of 33 combinations of analysis. In the MISS configurations, the musculature was intact, and the affected joints were fused to disable mutual motion and allow transfer of force and moment across them, i.e. the fused joints were changed from spherical to rigid joint assumptions and transferred any necessary moment across the fusion without the need for muscle actions. Except from the fusions, the spine model does not contain passive stiffness, i.e. all joint moments are balanced by muscle forces. The spine model's kinematic rhythm (Hansen et al., 2006) is mathematically equivalent to a movement distribution between the joints according to stiffness, i.e. as if the spine were a discretized elastic beam. This method was proposed by Stokes et al. (2002) based on *in-vitro* measurements of spine deflection. In the current, inverse dynamics model, the kinematics is resolved before kinetics, and the elastic beam assumption leads to a third-order polynomial, spatial spline shape, whose continuous deflection is collected in the discrete joints as flexion/extension, lateral flexion and axial rotation respectively. The third order polynomial for each of these articulations has four unknown coefficients, which are resolved from the four conditions of positional and slope continuity over the connections between the sacrum and the pelvis and T12/L1, respectively. This functional relationship between articulations enters the kinematic problem as constraints. In the presence of rigid, fused joint(s), this constraint set is augmented by high-weight conditions of no articulation between the fused vertebrae, and the resulting over-constrained system is solved by the method of Andersen et al. (2009). The consequence is that the previous articulations of fused joints will transfer to the remaining non-fused joints, which will behave as if the non-fused sections of the spine were discretized elastic beams. In the TOSS scenarios, the joints were also fused, and sacrificed muscle fascicles were removed from the model, leading to redistribution of their force contributions between the remaining muscles

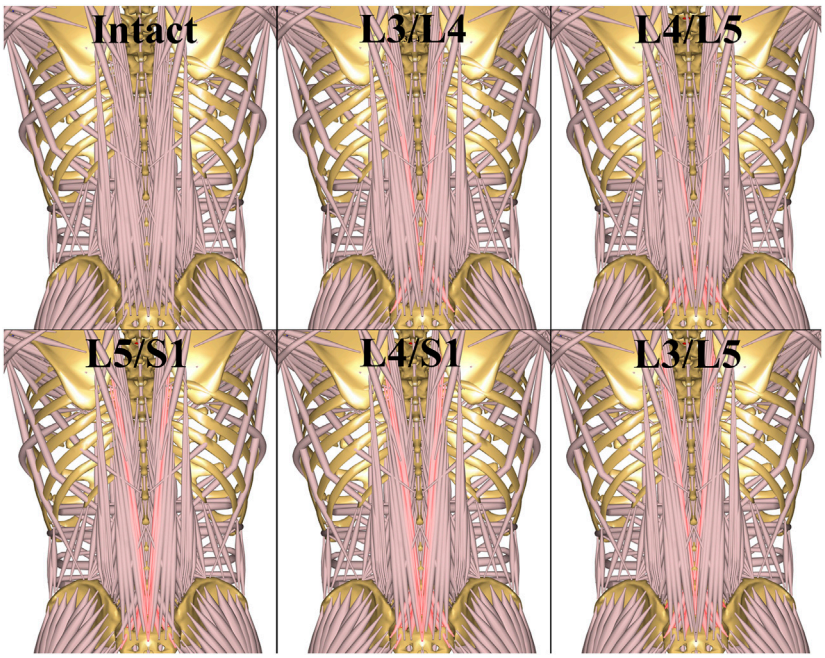

FIGURE 2 | TOSS muscle configurations for different fusions. The resected muscle fascicles for each case are highlighted and concisely listed in **Table 1**.

TABLE 1 | Resected fascicles of m. erector spinae and m. multifidus in TOSS at each lumbar fusion level. The systematic fascicle names refer to origin and insertion points in the published model (Lund et al., 2020). The mentioned fascicles are resected symmetrically on both sides.

	Lumbar fusion levels				
Muscle group	**L3/L4**	**L4/L5**	**L5/S1**	**L4/S1**	***L3/L5***
Erector Spinae	LTptT6S1 LTptT5L5	LTptT6S1	LTptT8S3 LTptT7S2 LTptT6S1	LTptT8S3 LTptT7S2 LTptT6S1 LTptT5L5	LTptT6S1 LTptT5L5 LTptT4L4
Multifidi	MFtsL3Ligament MFdL4S1 MFmL3S1 MFdL3L5	MFtsL3Ligament MFmL4Sacrum MFtsL4Sacrum MFmL5Sacrum MFdL5S1	MFtsL4Sacrum MFtsL5Sacrum MFmL4Sacrum MFmL5Sacrum MFdL5S1	MFtsL4Sacrum MFtsL5Sacrum MFmL4Sacrum MFmL5Sacrum MFdL5S1 MFtsL3Ligament MFdL4S1	MFtsL4Sacrum MFtsL3Ligament MFmL4Sacrum MFdL5S1 MFtstL2SIPS MFtsL2S1 MFtsL2L5MFmL3S1 MFdL3L5 MFdL4S1MFmL5Sacrum

according to the recruitment criterion. Thus, joint kinematics were identical for the MISS and TOSS cases, but MISS and TOSS kinematics were different from the baseline case. The muscle configuration was identical for the baseline and MISS cases, and different for each TOSS case.

Removal of muscle fascicles for each TOSS case was based on the surgical experience of the fourth author and performed interactively in a simulated "virtual surgery" performed on the 3-D graphical representation provided by the AnyBody Modeling System. The intact and resected muscle configurations are illustrated in **Figure 2**, and the resected muscle fascicles for each case are listed in **Table 1**, referring to the systematic naming conventions of the baseline model (Hansen et al., 2006; de Zee et al., 2007; Lund et al., 2020).

We report resultant reaction forces, i.e. the norm of the force vector, across the joints for the entire movement, to assess how different surgical combinations affect the loads on the spinal disks in different postures during the lifts. Muscle activity in the following means the percentage force to assumed isometric strength in a given muscle fascicle. To investigate the redistribution of loads between the muscle groups resulting from different fusions and resections, we computed the activity of each muscle group as the average over its fascicles. For each of the resulting average group activity curves, we found the maximum over the movement and computed the shift in percent compared to the baseline case. Resected muscles were completely removed from the model and therefore not included in the average.

RESULTS

This section presents resulting joint reaction forces, which acted on the spinal disks, and changes of muscle group activities in response to fusion and approach combinations.

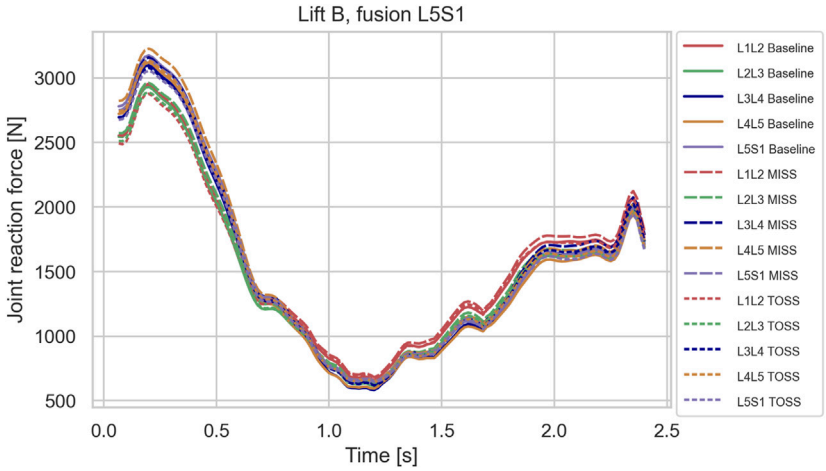

FIGURE 3 | Joint reaction forces in lifting case B for the baseline case and fusion of L5S1 in MISS and TOSS cases respectively. Baseline: solid lines. MISS: long dashes. TOSS: short dashes.

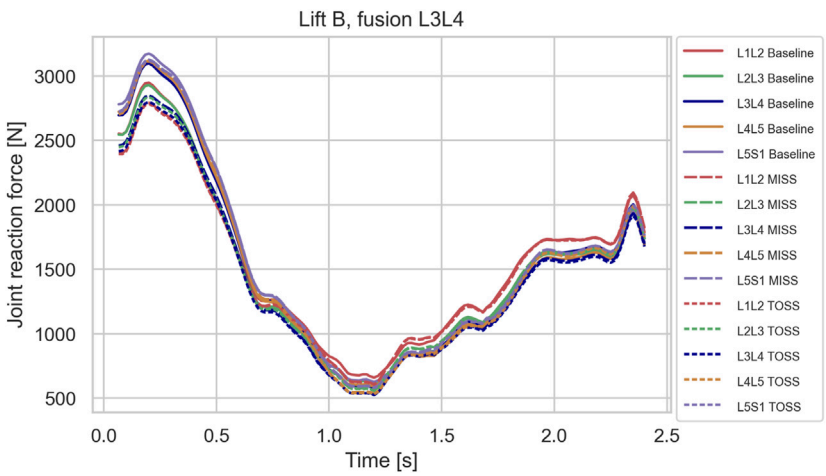

FIGURE 4 | Joint reaction forces in lifting case B for the baseline case and fusion of L3L4 in MISS and TOSS cases respectively. Baseline: solid lines. MISS: long dashes. TOSS: short dashes.

1. Joint reaction forces

In the sagittal plane lifts, A and B, the maximum lumbar loads over the motion were in the range 2800–3200 N and occurred when picking up the box in the beginning of the motion where spine flexion was at maximum. Since the initial posture was similar for the two lifts, the maximal spinal loads were also similar for these two cases. For these lifts, the differences in joint reaction forces between baseline and the two surgical approaches showed no clear pattern. L4L5 and L3L4, sustained 5–10% higher loads in the initial, flexed posture compared with L2L3 and L1L2, and this applied to baseline as well as both surgical approaches. **Figures 3–5** show case B for baseline and selected fusions.

Contrary to the sagittal lifts A and B, the lateral lift, C, did show a clear separation between fused cases and the baseline towards the end of the motion where the subject was reaching laterally to place the box. The load in this posture peaked approximately at $t = 1.75$ s as shown in **Figures 6–8**, which depict typical examples. **Table 2** summarizes the increase of joint load for each fusion case, MISS and TOSS respectively, and each joint relative to the baseline. Spinal loads in the asymmetrical posture of lift C were generally higher in the fused cases than in the baseline case, and more so for the superior fusion sites and for multi-joint fusions. Averaged over all fusion cases and all joints, the TOSS and MISS cases peak at 18 and 21% higher joint force, respectively, in this posture compared with baseline.

2. Muscle loads

Figure 9 shows the average activity within each muscle group for lift C in the baseline configuration. The graphs confirm the importance of m. erector spinae for lifting the box from the floor initially, where m. erector spinae fascicles sustained a mean

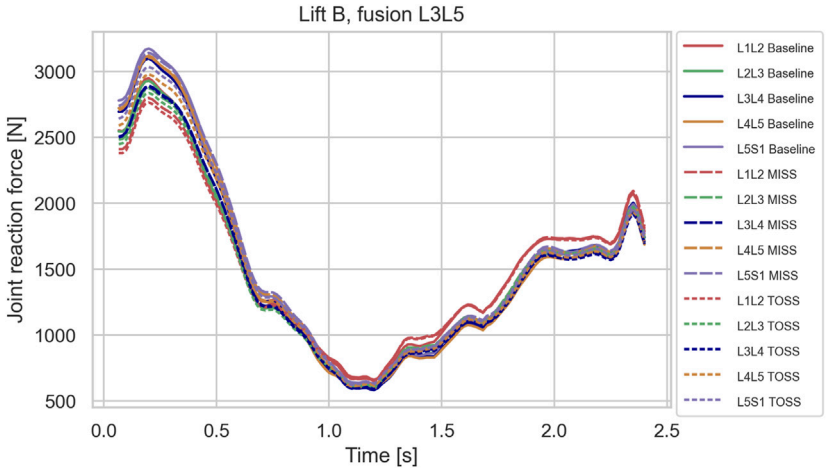

FIGURE 5 | Joint reaction forces in lifting case B for the baseline case and fusion of L3L5 in MISS and TOSS cases respectively. Baseline: solid lines. MISS: long dashes. TOSS: short dashes.

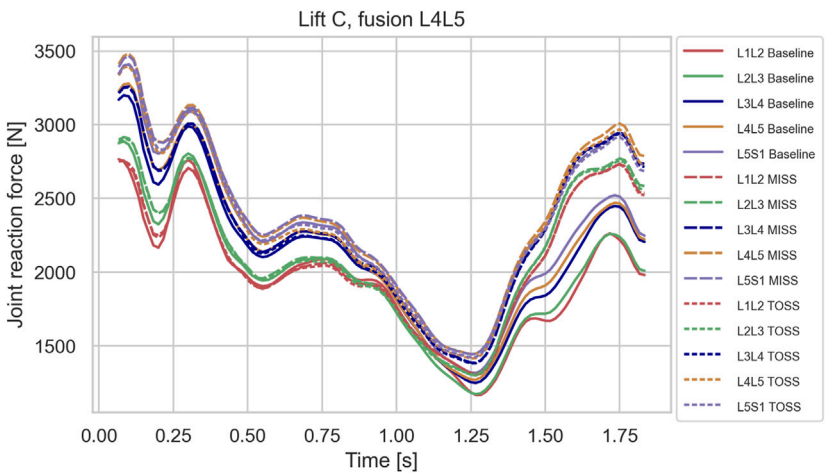

FIGURE 6 | Joint reaction forces in lifting case C for the baseline case and fusion of L4L5 in MISS and TOSS cases respectively. Baseline: solid lines. MISS: long dashes. TOSS: short dashes.

activity of 40%. As the box was moved laterally towards its final position, m. semispinalis fascicles were loaded up to 42% and other muscle groups up to about 30%.

Relative changes compared with the baseline case of maximum activity levels over the motion for the groups of m. quadratus lumborum (QL), m. erector spinae (ES) and m. multifidus (MTF) for each combination of lifting case (A, B and C), surgical technique (MISS or TOSS) and fusion sites (L3L4, L4L5, L5S1, L3L5 and L4S1) are presented in **Figure 10**. Each column of plots represents a lifting case, each row represents a fusion case, and the bars are color-coded for MISS and TOSS. Negative values signify an offloading on the average of the muscle group in question by the specified surgery.

The abdominal pressure contributes to the spine extension in the model and therefore works in synergy with the spine extensors. Averaged over the TOSS cases in lift B, the peak abdominal pressure increases by 2.7% compared with the baseline. However, it is primarily the cases involving fusion of the L5S1 joint that contribute, with 8.9% increase for the L4S1 fusion, 6.2% increase for the L5S1 case. The L3L5 fusion for this case reduces the abdominal pressure by −3.2%. The corresponding figures for MISS show a reduction of peak abdominal pressure for all fusions with an average of −1.7%.

DISCUSSION

Simulated joint forces for sagittal plane lifts (**Figures 3–5**) are in good agreement with Takahashi et al. (2006), who measured intradiscal pressures for similar lifts of 10 kg in four subjects and

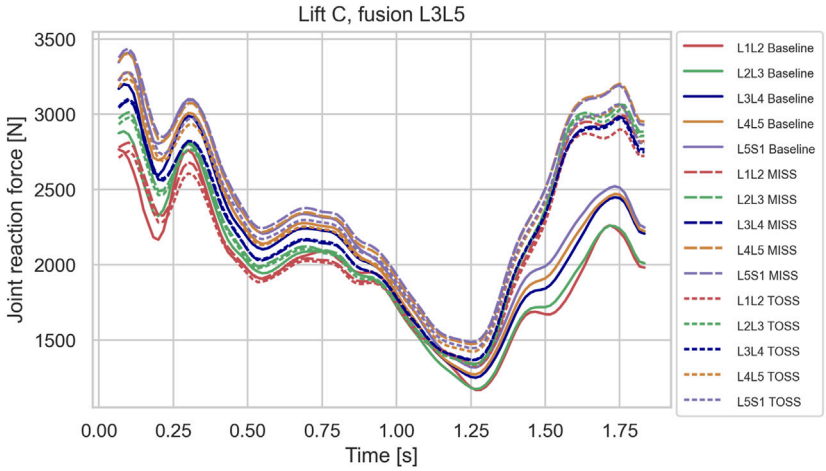

FIGURE 7 | Joint reaction forces in lifting case C for the baseline case and fusion of L3L5 in MISS and TOSS cases respectively. Baseline: solid lines. MISS: long dashes. TOSS: short dashes.

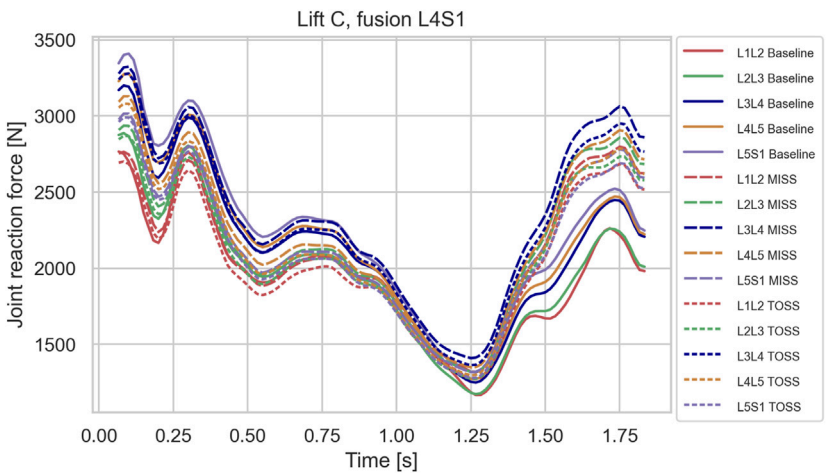

FIGURE 8 | Joint reaction forces in lifting case C for the baseline case and fusion of L4S1 in MISS and TOSS cases respectively. Baseline: solid lines. MISS: long dashes. TOSS: short dashes.

calculated disk compression forces from the measured pressures. They found increasing compression with flexion angle up to a maximum about 3 kN. The present model predicts maximum joint forces in the range of 2.8–3.2 kN for lifts A and B.

While it is clinically obvious that MISS reduces the surgical trauma compared with TOSS, mixed results regarding the biomechanical consequences of the two approaches have been reported, as mentioned in the introduction. On the one hand, MISS preserves musculature that is sacrificed by TOSS and, on the other hand, the importance of the resected musculature might diminish, when the joint is fused. We see from **Figures 3–5** that spinal joint reaction forces in the sagittal plane lifts A and B were not much influenced neither by the fusion site nor by the surgical approach. This is in agreement with previous clinical and meta studies (Stevens et al., 2006; Min et al., 2009), which have failed to show significant differences between the approaches. Somewhat contrary to our findings, Malakoutian et al. (2016) reported increased adjacent segment loads resulting from muscle weakening and triple-joint fusion in a simulation model. However, this model considered only upright standing and not flexion or lifting.

Figures 6–8, depicting the joint reaction forces in the lateral lift C, show a separation of the curves towards the end of the motion with higher joint reaction forces in the fused cases compared with baseline, regardless of surgical approach. This indicates that the load increase is governed more by the modified kinematics of the partially fused spine than by the altered muscle configuration resulting from the TOSS approach. Previously, finite element models without detailed muscle representations (Park et al., 2015; Rijsbergen et al., 2018) have indicated risk of

TABLE 2 | Increase of the joint forces relative to baseline in Lift C in the lateral posture near time t = 1.75 s for each fusion case.

Joint		Fusion						
		L3L4 (%)	L4L5 (%)	L5S1 (%)	L4S1 (%)	L3L5 (%)	MISS mean	TOSS mean
L1L2	MISS	29	21	7	24	32	23%	
	TOSS	29	21	1	19	28		19%
L2L3	MISS	32	23	9	26	36	25%	
	TOSS	31	22	4	21	34		22%
L3L4	MISS	18	20	10	25	22	19%	
	TOSS	16	20	5	21	21		17%
L4L5	MISS	28	22	10	18	30	21%	
	TOSS	27	20	4	13	24		18%
L5S1	MISS	25	17	1	10	27	16%	
	TOSS	25	16	−4	7	22		13%
Mean		26	20	5	18	28	21%	18%

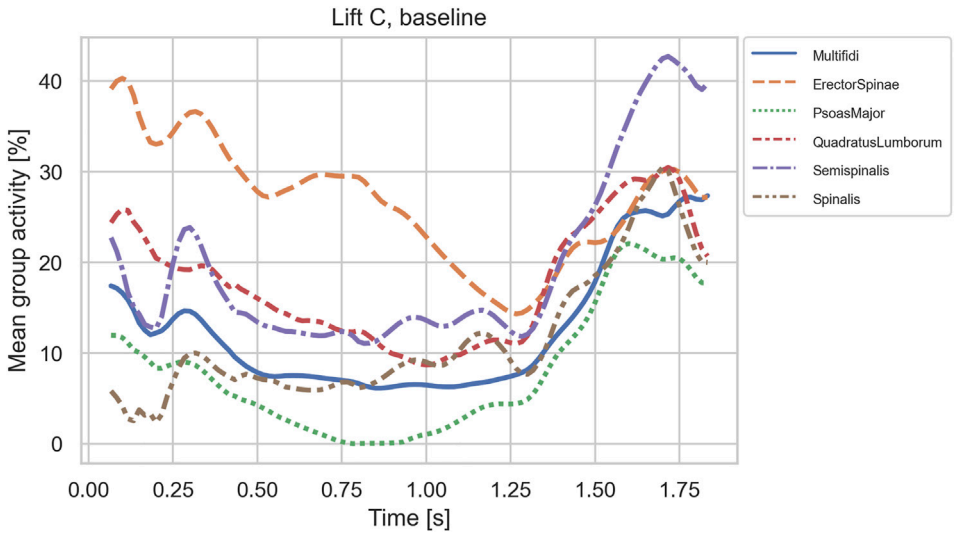

FIGURE 9 | Mean activities of muscle group fascicles in case C on the baseline anatomy.

adjacent disk degeneration following spinal joint fusion. The present model simulates the joint reaction force but not how this force is distributed to the disk. The aforementioned finite element models, on the other hand, take the disk deformation into account, including a possible concentration of stresses caused by the redistributed articulation in adjacent joints. Ideally, the detailed muscle forces and joint articulations simulated in the present model should be transferred to finite element models for computation of tissue stresses, thus exploiting the strengths of both model types.

Figure 10 summarizes the influence of surgical approaches on muscle loads for different fusion cases for the three lifts. Comparing these results column-wise, we see that cases A and B behaved similarly, and case C was different from the other two. The similarity of lifts A and B is because the larger spine loads occur in the more flexed postures, and this part of the movement was common to the two cases. For the sagittal lifts A and B, the changes of muscle activity were larger for the TOSS case compared to MISS, which is not surprising, given that the MISS approach leaves an intact musculature. The load on m. quadratus lumborum increased generally and more for TOSS than for MISS. It is remarkable that the TOSS approach offloaded m. multifidi for the L4L5 and L3L5 fusions. Closer investigation reveals that this was due to elimination of a few multifidi fascicles in the vicinity of the fusion site. The lost extension moment of these fascicles was compensated for by the moment transferred in the fused joint and by fascicles of m. erector spinae, which was also found previously (Bresnahan et al., 2010) for nominal movements with a previous version of the model used in this study. M. erector spinae is the primary spine extensor and has a larger baseline activity, so a given relative increase of its activity in **Figure 10** can compensate for a larger relative decrease of m. multifidi fascicles. It is also worth noting that a decrease of the muscular capacity for spine extension due to muscle resection will lead to a larger proportion of the extension moment to be provided by the abdominal pressure. This was shown as an average increase of peak abdominal pressure in the TOSS case. The abdominal pressure causes a distraction force on the vertebrae and can therefore reduce the joint compression forces, provided that the core musculature is capable of producing the additional pressure.

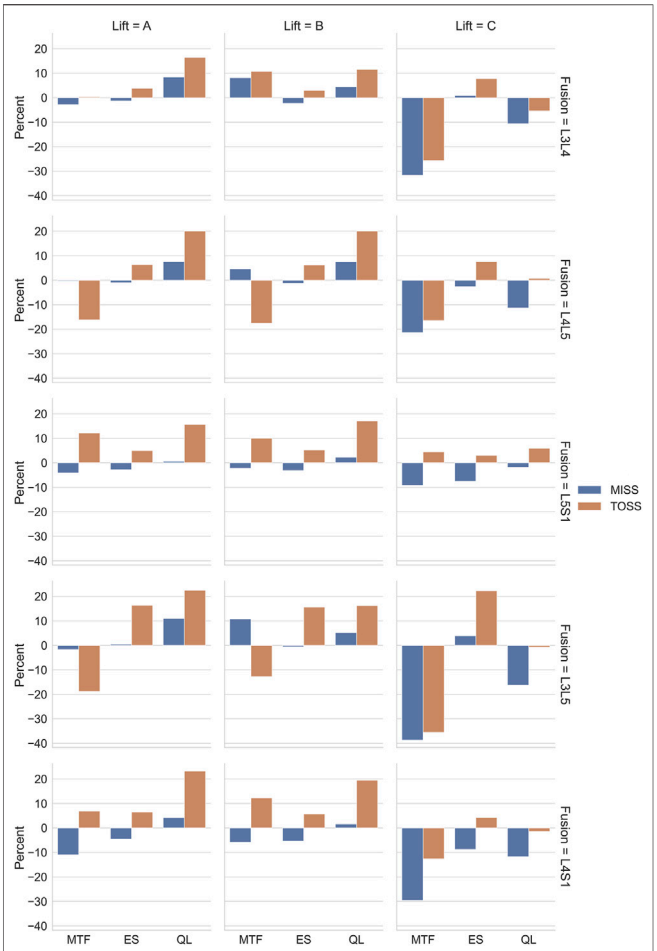

FIGURE 10 | Relative changes of mean loads of different muscle groups for the three lifting cases, A, B and C, as a consequence of different fusions and surgical approaches. Muscle groups: MTF, multifidus, ES, erector spinae, QL, quadratus lumborum.

For lift C, m. multifidus was offloaded considerably by all the fusions except L5S1, verifying this muscle group's role in axial rotation of the spine. The offloading effect was generally larger for MISS than for TOSS. For m. erector spinae, the load increases were smaller for MISS compared to TOSS, and offloading effects were larger for MISS compared to TOSS.

Row-wise comparison in **Figure 10** reveals that changes in average muscle activation were larger for higher single joint fusion sites, e.g., L3L4 compared with L5S1, and generally larger for multiple joint fusions, L3L5 and L4S1, than for single joint fusions. **Table 2** reveals a similar tendency for the joint loads in lift C. It is remarkable that fusion tended to offload the average m. multifidus activity for MISS and TOSS alike while, as shown in **Figures 6–8**; **Table 2**, fusion increased the joint reaction forces in the latter part of the motion. For the TOSS case, the reduced activity in m. multifidi fascicles was compensated for by an asymmetrical addition to m. erector spinae activity. In the MISS case, the joint fusion offloaded some fascicles of the intact musculature at the fusion site, while adjacent fascicles had to exert more force.

The biomechanical conclusions are that spinal fusion regardless of approach type has little influence on spinal joint reaction forces in sagittal plane lifts, but leads to increased loads in lateral lifts regardless of surgical approach. In terms of muscle loads, the spinal fusion can increase loads or offload different muscle groups, but the postoperative loads on the muscular system are generally smaller for MISS than for TOSS approaches.

In a clinical perspective, the results add biomechanical support for the case of MISS versus TOSS, but perhaps less than expected when considering the changes of muscle configuration involved in TOSS. Individuals with fused joints, regardless of the approach, should be advised to be particularly careful with asymmetrical lifts. Although this recommendation is accepted ergonomics practice, there appears to be biomechanical reasons to emphasize the recommendation to this patient group.

Human biomechanics is quite complicated, and simulation results should be used with caution. Most of the output variables in the present investigation are infeasible to measure *in-situ* on test subjects, and this challenge represents simultaneously the motivation for using models and the difficulty in terms of validating them. Known model limitations should therefore be borne in mind: The present spine model is limited to the lumbar and cervical sections, while the thoracic section and rib cage are considered as a single, rigid body. The model includes the extension effect of the abdominal pressure and its connection with m. transversus abdominis activation, but its implementation does not comprise the complexities of the diaphragm and pelvic floor. These shortcomings are the subject of ongoing research, and the results of this paper should be reevaluated continuously as models with higher fidelity become available.

It is a limitation of the study that input data were collected from a single, able-bodied individual performing only three different but related tasks. Generalization to patient populations would require data that account for variation in terms of anthropometry, motion patterns, gender, age and possibly other variables. The three lifting tasks are hardly representative for activities-of-daily living in general, and the finding that joint load tendencies are different for the two types of lifts, i.e., A/B versus C, indicates the necessity to perform biomechanical evaluation on a larger variety of activities-of-daily-living. Research to identify such a representative set of activities, against which biomechanical evaluation of spinal surgery can be performed, would be a valuable contribution towards *in-silico* models with clinical fidelity.

DATA AVAILABILITY STATEMENT

The raw data supporting the conclusion of this article will be made available by the authors, without undue reservation.

ETHICS STATEMENT

Ethical review and approval was not required for the study on human participants in accordance with the local legislation and institutional requirements. The patients/participants provided their written informed consent to participate in this study.

AUTHOR CONTRIBUTIONS

KI and BE designed and conducted the experiments and built the baseline biomechanical model. SR and JR developed the muscle configuration models representing the variations of surgical combinations. JR drafted the article, performed the simulations and programmed the data post processing. All authors contributed to the editing and proof reading of the article.

REFERENCES

Altshuler, M., Mueller, K. B., MacConnell, A., Wirth, P., Sandhu, F. A., and Voyadzis, J.-M. (2020). Reoperation, Readmission, and Discharge Disposition for Patients with Degenerative Lumbar Pathology Treated with Either Open or Minimally Invasive Techniques: A Single-Center Retrospective Review of 1435 Cases. *Neurosurgery* 87, 1199–1205. doi:10.1093/neuros/nyaa246

Altshuler, M., Mueller, K., MacConnell, A., Wirth, P., Sandhu, F., and Voyadzis, J.-M. (2021). Does Minimally Invasive Spine Surgery Reduce the Rate of Perioperative Medical Complications? A Retrospective Single-center Experience of 1435 Degenerative Lumbar Spine Surgeries. *Eur. Spine J.* 30, 122–127. doi:10.1007/s00586-020-06536-y

Andersen, M. S., Damsgaard, M., and Rasmussen, J. (2009). Kinematic Analysis of Over-Determinate Biomechanical Systems. *Comput. Methods Biomech. Biomed. Eng.* 12, 371–384. doi:10.1080/10255840802459412

Aota, Y., Kumano, K., and Hirabayashi, S. (1995). Postfusion Instability at the Adjacent Segments after Rigid Pedicle Screw Fixation for Degenerative Lumbar Spinal Disorders. *J. spinal Disord.* 8, 464–473. doi:10.1097/00002517-199512000-00008

Arshad, R., Zander, T., Dreischarf, M., and Schmidt, H. (2016). Influence of Lumbar Spine Rhythms and Intra-Abdominal Pressure on Spinal Loads and Trunk Muscle Forces during Upper Body Inclination. *Med. Eng. Phys.* 38, 333–338. doi:10.1016/j.medengphy.2016.01.013

Bassani, T., Stucovitz, E., Qian, Z., Briguglio, M., and Galbusera, F. (2017). Validation of the AnyBody Full Body Musculoskeletal Model in Computing Lumbar Spine Loads at L4L5 Level. *J. Biomech.* 58, 89–96. doi:10.1016/j.jbiomech.2017.04.025

Bassani, T., Stucovitz, E., Quian, Z., Briguglio, M., and Galbusera, F. (2020). Assessment of the Anybody Full Body Musculoskeletal Model in Computing Spine Loads at Lumbar Level: Comparison with *In Vivo* Values Obtained during Exercise Tasks. *ScienceOpen Posters*. doi:10.14293/S2199-1006.1.SOR-.PPIVBHK.v1

Benditz, A., Auer, S., Spörrer, J. F., Wolkerstorfer, S., Grifka, J., Suess, F., et al. (2018). Regarding Loads after Spinal Fusion, Every Level Should Be Seen Separately: A Musculoskeletal Analysis. *Eur. Spine J.* 27, 1905–1910. doi:10.1007/s00586-018-5476-5

Bresnahan, L., Fessler, R. G., and Natarajan, R. N. (2010). Evaluation of Change in Muscle Activity as a Result of Posterior Lumbar Spine Surgery Using a Dynamic Modeling System. *Spine* 35, E761–E767. doi:10.1097/BRS.0b013e3181e45a6e

Chow, D. H. K., Luk, K. D. K., Evans, J. H., and Leong, J. C. Y. (1996). Effects of Short Anterior Lumbar Interbody Fusion on Biomechanics of Neighboring Unfused Segments. *Spine* 21, 549–555. doi:10.1097/00007632-199603010-00004

Damsgaard, M., Rasmussen, J., Christensen, S. T., Surma, E., and de Zee, M. (2006). Analysis of Musculoskeletal Systems in the AnyBody Modeling System. *Simulation Model. Pract. Theor.* 14, 1100–1111. doi:10.1016/j.simpat.2006.09.001

de Zee, M., Hansen, L., Wong, C., Rasmussen, J., and Simonsen, E. B. (2007). A Generic Detailed Rigid-Body Lumbar Spine Model. *J. Biomech.* 40, 1219–1227. doi:10.1016/j.jbiomech.2006.05.030

Dreischarf, M., Shirazi-Adl, A., Arjmand, N., Rohlmann, A., and Schmidt, H. (2016). Estimation of Loads on Human Lumbar Spine: A Review of *In Vivo* and Computational Model Studies. *J. Biomech.* 49, 833–845. doi:10.1016/j.jbiomech.2015.12.038

Etebar, S., and Cahill, D. W. (1999). Risk Factors for Adjacent-Segment Failure Following Lumbar Fixation with Rigid Instrumentation for Degenerative Instability. *J. Neurosurg. Spine* 90, 163–169. doi:10.3171/spi.1999.90.2.0163

Fourney, D. R., Dettori, J. R., Norvell, D. C., and Dekutoski, M. B. (2010). Does Minimal Access Tubular Assisted Spine Surgery Increase or Decrease Complications in Spinal Decompression or Fusion? *Spine* 35, S57–S65. doi:10.1097/BRS.0b013e3181d82bb8

Goldstein, C. L., Macwan, K., Sundararajan, K., and Rampersaud, Y. R. (2016). Perioperative Outcomes and Adverse Events of Minimally Invasive versus Open Posterior Lumbar Fusion: Meta-Analysis and Systematic Review. *J. Neurosurg. Spine* 24, 416–427. doi:10.3171/2015.2.SPINE14973

Guigui, P., Lambert, P., Lassale, B., and Deburge, A. (1997). Long-Term Outcome at Adjacent Levels of Lumbar Arthrodesis. *Rev. Chir Orthop. Reparatrice Appar Mot.* 83, 685–696.

Hambly, M. F., Wiltse, L. L., Raghavan, N., Schneiderman, G., and Koenig, C. (1998). The Transition Zone Above a Lumbosacral Fusion. *Spine* 23, 1785–1792. doi:10.1097/00007632-199808150-00012

Han, K.-S., Zander, T., Taylor, W. R., and Rohlmann, A. (2012). An Enhanced and Validated Generic Thoraco-Lumbar Spine Model for Prediction of Muscle Forces. *Med. Eng. Phys.* 34, 709–716. doi:10.1016/j.medengphy.2011.09.014

Hansen, L., de Zee, M., Rasmussen, J., Andersen, T. B., Wong, C., and Simonsen, E. B. (2006). Anatomy and Biomechanics of the Back Muscles in the Lumbar Spine with Reference to Biomechanical Modeling. *Spine* 31, 1888–1899. doi:10.1097/01.brs.0000229232.66090.58

Härtl, R. (2020). The 6 T's of Minimally Invasive Spine Surgery. *Glob. Spine J.* 10, 5S–7S. doi:10.1177/2192568220911617

Karatsidis, A., Jung, M., Schepers, H. M., Bellusci, G., de Zee, M., Veltink, P. H., et al. (2018). Predicting Kinetics Using Musculoskeletal Modeling and Inertial Motion Capture. arXiv preprint arXiv:1801.01668.

Kim, C. W. (2010). Scientific Basis of Minimally Invasive Spine Surgery. *Spine* 35, S281–S286. doi:10.1097/BRS.0b013e3182022d32

Kim, D.-Y., Lee, S.-H., Chung, S. K., and Lee, H.-Y. (2005). Comparison of Multifidus Muscle Atrophy and Trunk Extension Muscle Strength. *Spine* 30, 123–129. doi:10.1097/01.brs.0000148999.21492.53

Koning, B. H. W., van der Krogt, M. M., Baten, C. T. M., and Koopman, B. F. J. M. (2015). Driving a Musculoskeletal Model with Inertial and Magnetic Measurement Units. *Comput. Methods Biomech. Biomed. Eng.* 18, 1003–1013. doi:10.1080/10255842.2013.867481

Kumar, M., Baklanov, A., and Chopin, D. (2001). Correlation between Sagittal Plane Changes and Adjacent Segment Degeneration Following Lumbar Spine Fusion. *Eur. Spine J.* 10, 314–319. doi:10.1007/s005860000239

Lund, M. E., Andersen, M. S., de Zee, M., and Rasmussen, J. (2015). Scaling of Musculoskeletal Models from Static and Dynamic Trials. *Int. Biomech.* 2, 1–11. doi:10.1080/23335432.2014.993706

Lund, M. E., de Zee, M., Andersen, M. S., and Rasmussen, J. (2012). On Validation of Multibody Musculoskeletal Models. *Proc. Inst. Mech. Eng. H* 226, 82–94. doi:10.1177/0954411911431516

Lund, M. E., Tørholm, S., Jensen, B. K., Galibarov, P. E., Dzialo, C. M., Iversen, K., et al. (2020). *The AnyBody Managed Model Repository (AMMR) (2.3.1)*. Zenodo. doi:10.5281/zenodo.3932764

Malakoutian, M., Street, J., Wilke, H.-J., Stavness, I., Dvorak, M., Fels, S., et al. (2016). Role of Muscle Damage on Loading at the Level Adjacent to a Lumbar Spine Fusion: a Biomechanical Analysis. *Eur. Spine J.* 25, 2929–2937. doi:10.1007/s00586-016-4686-y

McAfee, P. C., Phillips, F. M., Andersson, G., Buvenenadran, A., Kim, C. W., Lauryssen, C., et al. (2010). Minimally Invasive Spine Surgery. *Spine (Phila Pa 1976)* 35, S271–S273. doi:10.1097/BRS.0b013e31820250a2

Min, S.-H., Kim, M.-H., Seo, J.-B., Lee, J.-Y., and Lee, D.-H. (2009). The Quantitative Analysis of Back Muscle Degeneration after Posterior Lumbar Fusion: Comparison of Minimally Invasive and Conventional Open Surgery. *Asian Spine J.* 3, 89. doi:10.4184/asj.2009.3.2.89

Mobbs, R. J., Phan, K., Malham, G., Seex, K., and Rao, P. J. (2015). Lumbar Interbody Fusion: Techniques, Indications and Comparison of Interbody Fusion Options Including PLIF, TLIF, MI-TLIF, OLIF/ATP, LLIF and ALIF. *J. Spine Surg.* 1, 2–18. doi:10.3978/j.issn.2414-469X.2015.10.05

Nagata, H., Schendel, M. J., Transfeldt, E. E., and Lewis, J. L. (1993). The Effects of Immobilization of Long Segments of the Spine on the Adjacent and Distal Facet Force and Lumbosacral Motion. *Spine* 18, 2471–2479. doi:10.1097/00007632-199312000-00017

Park, W. M., Choi, D. K., Kim, K., Kim, Y. J., and Kim, Y. H. (2015). Biomechanical Effects of Fusion Levels on the Risk of Proximal Junctional Failure and Kyphosis in Lumbar Spinal Fusion Surgery. *Clin. Biomech.* 30, 1162–1169. doi:10.1016/j.clinbiomech.2015.08.009

Rasmussen, J., de Zee, M., Damsgaard, M., Christensen, S. T., Marek, C., and Siebertz, K. (2005). "A General Method for Scaling Musculo-Skeletal Models," in *2005 International Symposium on Computer Simulation in Biomechanics*. Cleveland, OH, United States: International Society of Biomechanics, Case Western Reserve University.

Rijsbergen, M. v., van Rietbergen, B., Barthelemy, V., Eltes, P., Lazáry, Á., Lacroix, D., et al. (2018). Comparison of Patient-Specific Computational Models vs. Clinical Follow-Up, for Adjacent Segment Disc Degeneration and Bone Remodelling after Spinal Fusion. *PLOS ONE* 13, e0200899. doi:10.1371/journal.pone.0200899

Stevens, K. J., Spenciner, D. B., Griffiths, K. L., Kim, K. D., Zwienenberg-Lee, M., Alamin, T., et al. (2006). Comparison of Minimally Invasive and Conventional Open Posterolateral Lumbar Fusion Using Magnetic Resonance Imaging and Retraction Pressure Studies. *J. Spinal Disord. Tech.* 19, 77–86. doi:10.1097/01.bsd.0000193820.42522.d9

Stokes, I. A., Gardner-Morse, M., Churchill, D., and Laible, J. P. (2002). Measurement of a Spinal Motion Segment Stiffness Matrix. *J. Biomech.* 35, 517–521. doi:10.1016/S0021-9290(01)00221-4

Takahashi, I., Kikuchi, S.-I., Sato, K., and Sato, N. (2006). Mechanical Load of the Lumbar Spine during Forward Bending Motion of the Trunk-A Biomechanical Study. *Spine* 31, 18–23. doi:10.1097/01.brs.0000192636.69129.fb

Conflict of Interest: Authors KI and KE were employed by the company AnyBody Technology A/S.

The remaining authors declare that the research was conducted in the absence of any commercial or financial relationships that could be construed as a potential conflict of interest.

frontiers in Bioengineering and Biotechnology

ORIGINAL RESEARCH
published: 04 November 2021
doi: 10.3389/fbioe.2021.769117

From Stoop to Squat: A Comprehensive Analysis of Lumbar Loading Among Different Lifting Styles

Michael von Arx[1], *Melanie Liechti*[1], *Lukas Connolly*[2,3,4], *Christian Bangerter*[1], *Michael L. Meier*[2,3] *and Stefan Schmid*[1,5]*

[1]Spinal Movement Biomechanics Group, Division of Physiotherapy, School of Health Professions, Bern University of Applied Sciences, Bern, Switzerland, [2]Integrative Spinal Research, Department of Chiropractic Medicine, Balgrist University Hospital, University of Zurich, Zurich, Switzerland, [3]University of Zurich, Zurich, Switzerland, [4]Department of Health Science and Technology, ETH Zurich, Zurich, Switzerland, [5]Faculty of Medicine, University of Basel, Basel, Switzerland

Lifting up objects from the floor has been identified as a risk factor for low back pain, whereby a flexed spine during lifting is often associated with producing higher loads in the lumbar spine. Even though recent biomechanical studies challenge these assumptions, conclusive evidence is still lacking. This study therefore aimed at comparing lumbar loads among different lifting styles using a comprehensive state-of-the-art motion capture-driven musculoskeletal modeling approach. Thirty healthy pain-free individuals were enrolled in this study and asked to repetitively lift a 15 kg-box by applying 1) a freestyle, 2) a squat and 3) a stoop lifting technique. Whole-body kinematics were recorded using a 16-camera optical motion capture system and used to drive a full-body musculoskeletal model including a detailed thoracolumbar spine. Continuous as well as peak compressive, anterior-posterior shear and total loads (resultant load vector of the compressive and shear load vectors) were calculated based on a static optimization approach and expressed as factor body weight (BW). In addition, lumbar lordosis angles and total lifting time were calculated. All parameters were compared among the lifting styles using a repeated measures design. For each lifting style, loads increased towards the caudal end of the lumbar spine. For all lumbar segments, stoop lifting showed significantly lower compressive and total loads (–0.3 to –1.0BW) when compared to freestyle and squat lifting. Stoop lifting produced higher shear loads (+0.1 to +0.8BW) in the segments T12/L1 to L4/L5, but lower loads in L5/S1 (–0.2 to –0.4BW). Peak compressive and total loads during squat lifting occurred approximately 30% earlier in the lifting cycle compared to stoop lifting. Stoop lifting showed larger lumbar lordosis range of motion (35.9 ± 10.1°) than freestyle (24.2 ± 7.3°) and squat (25.1 ± 8.2°) lifting. Lifting time differed significantly with freestyle being executed the fastest (4.6 ± 0.7 s), followed by squat (4.9 ± 0.7 s) and stoop (5.9 ± 1.1 s). Stoop lifting produced lower total and compressive lumbar loads than squat lifting. Shear loads were generally higher during stoop lifting, except for the L5/S1 segment, where anterior shear loads were higher during squat lifting. Lifting time was identified as another important factor, considering that slower speeds seem to result in lower loads.

Keywords: spine, biomechanics, freestyle lifting, musculoskeletal modeling, motion capture, spinal loading, posture

OPEN ACCESS

Edited by:
Marwan El-Rich, Khalifa University, United Arab Emirates

Reviewed by:
Francesco Travascio, University of Miami, United States
Ray Daniel, United States Army Aeromedical Research Lab, United States

***Correspondence:**
Stefan Schmid
stefanschmid79@gmail.com

Specialty section:
This article was submitted to Biomechanics, a section of the journal Frontiers in Bioengineering and Biotechnology

Received: *01 September 2021*
Accepted: *20 October 2021*
Published: *04 November 2021*

Citation:
von Arx M, Liechti M, Connolly L, Bangerter C, Meier ML and Schmid S (2021) From Stoop to Squat: A Comprehensive Analysis of Lumbar Loading Among Different Lifting Styles. Front. Bioeng. Biotechnol. 9:769117. doi: 10.3389/fbioe.2021.769117

INTRODUCTION

The importance of the correct lifting posture is believed to be strongly connected to the prevention of low back pain (LBP) (Balagué et al., 2012; Caneiro et al., 2019). Even healthcare professionals associate a flexed spine during lifting with danger and therefore seem to influence how people lift every day (Nolan et al., 2018). While lifting has been identified as a main risk factor for LBP, research fails to establish a clear connection between LBP, lifting posture and danger to the spine (Van Dieën et al., 1999; Balagué et al., 2012; Schaafsma et al., 2015; Saraceni et al., 2020). It is widely believed that a flexed spine causes higher spinal loads that could result in structural damage or lead to back complaints in the long-term. Furthermore, the interaction between shear and compressive loads and spine tolerance is still poorly understood (Bazrgari et al., 2007; Gallagher and Marras, 2012), and many of the assumptions regarding load tolerances of the spine are solely based on *in vitro* studies (Gallagher and Marras, 2012).

Van Dieën et al. (1999) concluded in their review that there was not enough evidence to support advocating the squat technique as a means of preventing LBP. In addition, more recent research suggests that differences in spinal loads among various lifting styles are relatively small and a straight back (spine in a neutral position) might not always be the optimal position (Kingma et al., 2010; Wang et al., 2012; Dreischarf et al., 2016; van der Have et al., 2019; Khoddam-Khorasani et al., 2020). Some suggest that a single optimal position for all situations does not exist (Burgess-Limerick, 2003) and that the lifting technique should be adapted to the lifted weight (Wang et al., 2012). Despite these facts, however, squat lifting still remains the recommended technique (Bazrgari and Shirazi-Adl, 2007; van der Have et al., 2019), which spurs a call for more comprehensive investigations of spinal loading during lifting.

Motion capture-driven musculoskeletal spine modeling is a reliable and non-invasive analysis tool, which allows the calculation of spinal loads in an environment close to the natural movement of the spine. However, many of the available models are highly simplified by using lumped segment models or generic spinal alignments, which limits the accuracy for simulating intersegmental spinal loading during functional activities. To overcome such shortcomings, Schmid et al. (2021) recently introduced a novel approach for modeling subject-specific spinal alignment based on the external back profile obtained from skin marker-based motion capture data, allowing simulations of spinal loading using models with fully articulated thoracolumbar spines.

Furthermore, the currently available studies investigating spinal loading during object lifting solely focused on the analysis of predetermined discrete parameters such as peak forces and none of them included quantitative analyses of data over time. Using such 0-dimensional scalar parameters means that only particular instances of the measurement domain are taken into account, whereby differences during other instances along the time dimension might be missed (regional focus bias) (Papi et al., 2020). To address these issues, Statistical Parametric Mapping (SPM) can be applied (Pataky et al., 2013) which uses Random Field Theory (Adler and Taylor, 2007) to identify statistical interference over 1-dimensional continuous vectors.

For these reasons, this study aimed at comparing compressive, anterior-posterior shear and total loads of the lumbar spine between freestyle, squat and stoop lifting using a novel subject-specific musculoskeletal modeling approach of the spine as well as advanced statistical methods for analyzing continuous data. Furthermore, lumbar lordosis angles as well as lifting movement duration were investigated for supporting the interpretation of the loads. Such comprehensive knowledge might help to shed more light into the question of how different lifting techniques affect spinal loading.

MATERIALS AND METHODS

Study Population

Thirty healthy pain-free adults (20 males and 10 females; age: 31.8 ± 8.5 years; body height: 175.3 ± 7.5 cm; body mass: 71.7 ± 10.2 kg; BMI: 23.3 ± 2.4 kg/m^2; sporting activities per week: 5.3 ± 4.3 h) were included in this cross-sectional, observational study. Recruitment took place in the personal and workplace environment of the investigators. Inclusion criteria were: aged between 18 and 65 years, ability to perform the required lifting tasks as well as sufficient understanding of the German language. Individuals were excluded in case of any history of LBP in the past 6 months, injuries or operations on the spine, hip, knee or ankle as well as any comorbidities or circumstances (e.g., pregnancy) that could limit the lifting capabilities. In addition, weightlifters, CrossFit athletes, physical therapists and nurses were not eligible due to a potential bias regarding lifting techniques. The local ethics committee provided exemption for this study (Kantonale Ethikkommission Bern, Req-2020-00364) and all participants provided written informed consent prior to collecting any personal or health related data.

Data Collection

Subject Preparation and Instrumentation

Data collection procedures were defined in a detailed case report form (CRF) and carried out in the same manner for each subject by the same two experienced physical therapists. Socio-economic and biometric information such as profession and physical activity level as well as age, sex, body mass, and body height were collected prior to any biomechanical measurements.

Subsequently, participants were equipped with 58 retro-reflective markers according to the configuration described by Schmid et al. (2017) (**Figure 1**). To enable detailed tracking of spinal motion, the configuration included markers placed on the spinous processes of the vertebrae C7, T3, T5, T7, T9, T11, L1-L5 and the sacrum (S1). Kinematic data were recorded using a 16-camera optical motion capture system (Vicon, Oxford, United Kingdom; sampling frequency: 200 Hz). In addition, ground reaction forces were recorded using an embedded force plate (AMTI BP400600, Advanced medical technology Inc., Watertown, MA, United States).

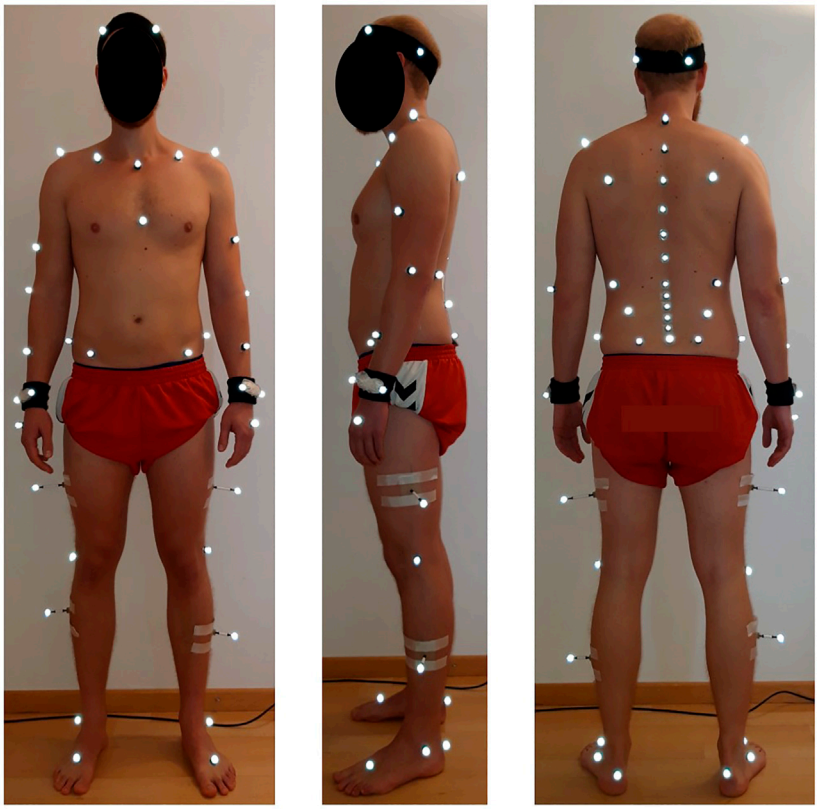

FIGURE 1 | Placement of the retro-reflective skin markers according to the configuration described by Schmid et al. (2017).

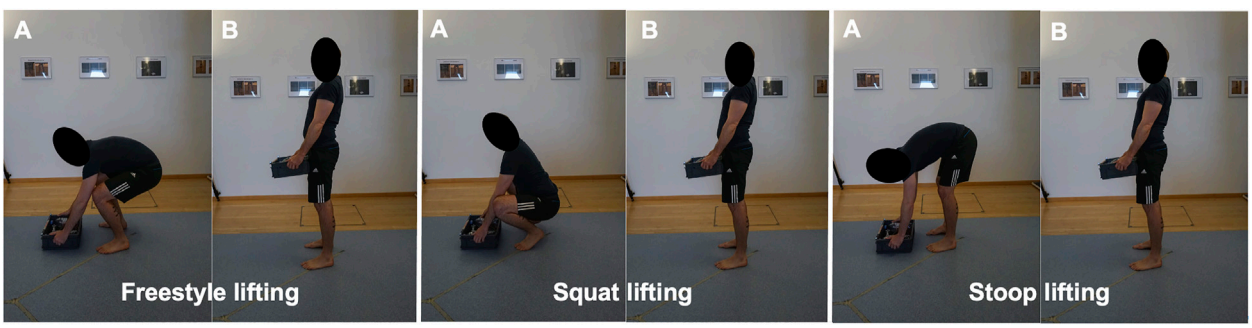

FIGURE 2 | Start **(A)** and end positions **(B)** of a lifting-up cycle for all three styles. The section of interest spanned from the moment the box left the floor until the subject reached a stable upright standing position.

Lifting Tasks

Subjects were asked to repetitively lift up a 15 kg-box from the floor using a 1) freestyle, 2) squat and 3) stoop lifting technique (**Figure 2**). The uniform weight of 15 kg was chosen based on Swiss national guidelines [Swiss National Accident Insurance Fund (SUVA), 2016], which consider the lifting of weights up to 15 kg as safe for adults of all genders. For comparison, the NIOSH guidelines [The National Institute for Occupational Safety and Health (NIOSH), 2007] consider weights of up to 51 pounds (about 23 kg) as safe for workers. Participants were given up to 5 min of practice time until the execution of the lifting technique matched the investigators demands.

For each lifting style, subjects had to perform five valid repetitions. A number of key characteristics were defined for each lifting technique, which were closely observed by the investigators during each repetition. All three lifting styles started with the feet parallel about hip width apart and 15 cm behind the box. The box had to be grabbed with both hands (height of the handles: 8 cm

above floor level), lifted up with the elbows extended or slightly flexed (height of the handles in upright standing position: about hip/pelvis height) and placed back on the same place. Participants were allowed short resting periods between the five repetitions and longer resting periods between the three different styles. This amounted to a measurement time of about 5 min per style and 20–30 min in total. To ensure that the participants did not experience muscle fatigue, subjective exertion levels were verbally assessed after each set of lifts. The vertical distance of the box travelled and the lifting frequency did thereby not exceed the limits of 3 feet (about 90 cm) and five lifts per min, respectively, which would be considered risk factors for musculoskeletal diseases by the NIOSH guidelines [The National Institute for Occupational Safety and Health (NIOSH), 2007]. Only the lifting up sections were used for analysis.

Instructions for freestyle lifting were simply to lift the box in the most comfortable manner, while keeping the feet in place and grabbing the box with both hands. Instructions for squat and stoop lifting were based on Dreischarf et al. (2016). Squat lifting was thereby characterized as lifting with the back kept as straight as possible and with mainly flexing the knees and the hips. Participants were asked to keep the feet flat on the ground if possible. If ankle mobility was insufficient for keeping the feet flat, subjects were tolerated to raise their heels and to stand on the forefoot in order to comply with the instruction of keeping the back as straight as possible. Stoop lifting was characterized by bending forward with a clear flexion of the spine and with the knees kept as straight as possible while bending in the hips. Subjects that were able to perform this lift with a straight back and straight legs by solely flexing in the hips were reminded to clearly flex their lumbar spine for the lift to count as valid.

Data Reduction

Data was pre-processed with the Nexus software (version 2.6, Vicon United Kingdom, Oxford, United Kingdom), which included the reconstruction and labeling of the markers as well as filtering of the trajectories. Additionally, temporal events were manually set to identify the sections of interest, i.e., the sections containing the lifting up movements. For detection of the exact start and end points, a custom MATLAB routine (R2020b; MathWorks, Inc., Natick Massachusetts, United States) was used. In brief, the start of the movement was defined as the point where the vertical velocity of the C7 marker initially exceeded 5% of the maximal vertical velocity, and the end of the movement was defined as the point where the vertical velocity fell below this 5% threshold (Schmid et al., 2021).

For determining spinal loading, we used previously introduced OpenSim-based female and male musculoskeletal full-body models including a detailed and fully articulated thoracolumbar spine (Schmid et al., 2021) (**Figure 3**). To enable subject-specific simulations, we used the OpenSim Scaling Tool to scale segment lengths and masses based on the marker data and total body mass, respectively. In addition, a custom MATLAB algorithm was applied to adjust the sagittal plane spinal curvatures based on the markers placed on the spinous processes, the head and the sacrum (Schmid et al., 2021). Simulations were driven by kinematic (derived from the marker data using the OpenSim Inverse Kinematics Tool) and ground reaction force data and solved using static optimization with a cost function that minimizes the sum of squared muscle activation (Herzog, 1987). Intersegmental joint forces were computed using OpenSim Joint Reaction Analysis.

Lumbar lordosis angles were calculated using a custom MATLAB routine as described in Schmid et al. (2017). In brief, we applied a combination of a quadratic polynomial and a circle fit function to the sagittal plane trajectories of the markers placed on the spinous processes of L1-S1 and used the central angle to express the lumbar lordosis angle.

Primary outcome variables were continuous as well as peak compressive forces, anterior-posterior (AP) shear forces and total forces (resultant force vector of the compressive and AP shear force vectors) for the segments T12/L1 to L5/S1 [expressed as a factor of body weight (BW)]. Secondary outcome variables included lumbar lordosis angle range of motion (RoM; expressed in degrees) as well as lifting movement duration [time between start and end points of lifting-up phase, expressed as dimensionless number according to Hof (1996)].

Statistical Analysis

Statistical analysis was performed using MATLAB with the package "spm1d" for one-dimensional Statistical Parametric Mapping (SPM; www.spm1d.org) for continuous data and RStudio (version 1.3.1093, R foundation for statistical computing, Vienna, Austria) for discrete parameters. Normal distribution was verified using the SPM-function "spm1d.stats.normality.anova1rm" for continuous data and the Shapiro Wilk test and Q-Q-plot inspection for discrete parameters. Differences among the three lifting styles were investigated using the SPM-functions "spm1d.stats.anova1rm" and "spm1d.stats.ttest_paired" for continuous data as well as repeated measures analyses of variance (ANOVA) with paired t-tests for post hoc analyses for discrete parameters. The alpha level was set at 0.05 for the ANOVAs and 0.017 (Bonferroni-corrected) for the post hoc tests.

RESULTS

For three participants, musculoskeletal simulations were not conducted due to insufficient marker recognition in the anterior thorax region, leaving a sample of 27 for the spinal loading parameters. The calculation of lumbar lordosis angle and lifting movement duration, on the other hand, was based on all 30 participants. Means and standard deviations as well as *p*-values of the statistical analyses for the continuous and peak spinal loads can be found in the **Supplementary Material**.

Continuous Loads

ANOVAs showed significant differences between lifting styles for all segments and load types. Results showed increasing loads towards the caudal end of the lumbar spine for all styles (**Figures 4–6**). Significant differences between styles occurred predominantly during the first 50% of the lifting cycle and got smaller towards the end of the cycle.

The analysis of total and compressive loads revealed that stoop lifting produced significantly smaller loads compared to both other styles in all segments and that the loads for freestyle and

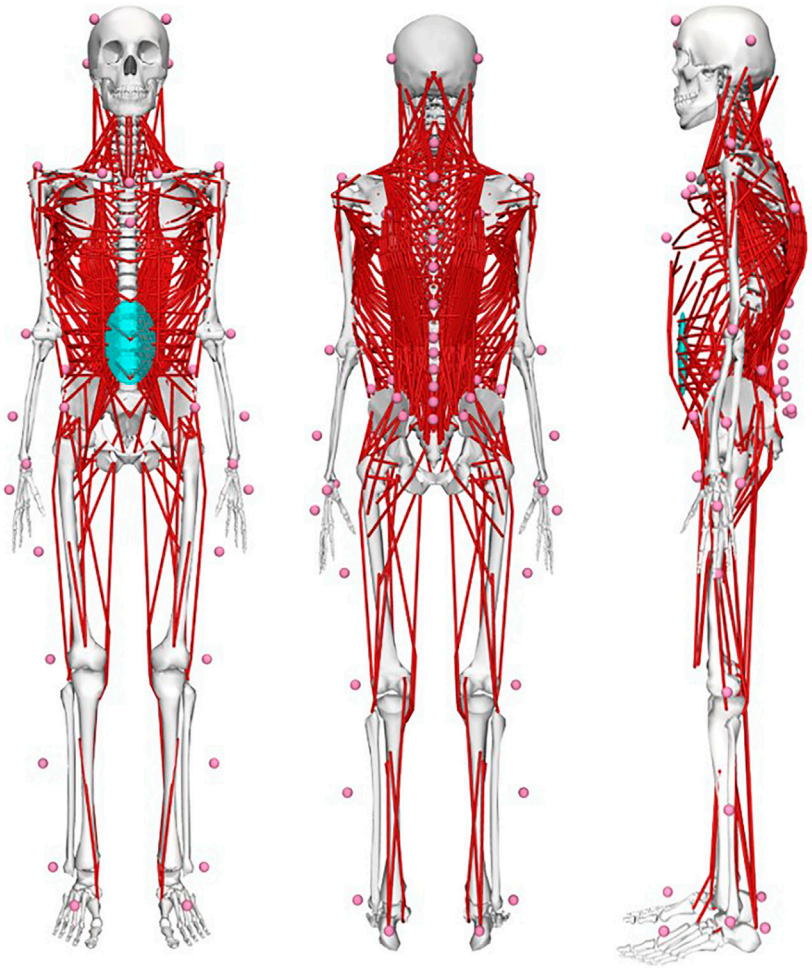

FIGURE 3 | OpenSim-based musculoskeletal full-body models including a detailed and fully articulated thoracolumbar spine and 58 virtual skin markers to allow for subject-specific model scaling as well as comprehensive simulation of spinal loading during dynamic functional activities using motion capture data.

squat lifting were mostly similar, with only few differences in the L4/L5 and L5/S1 segments for short sections of the lifting movement (**Figures 4**, **5**). Moreover, the onset of peak total loading occurred later in the cycle for stoop lifting when compared to squat and freestyle lifting.

AP shear loads analysis showed significant differences between all styles in all lumbar segments (**Figure 6**). Stoop lifting produced generally higher shear loads, except in the L5/S1 segment, where shear forces were smaller compared to the other lifting styles.

Peak Loads

ANOVAs showed significant differences between lifting styles for all segments and load types. For all styles and all three load types, peak loads increased towards the caudal end of the spine with the largest loads occurring in the L5/S1 segment (**Figures 7**–**9**). In addition, there was a trend for smaller differences in compressive and peak loads between styles towards the lower end of the spine, indicating that differences between styles are more pronounced in the upper part of the lumbar spine.

Peak total and compressive loads for stoop lifting were significantly smaller in every segment, when compared to both other styles (**Figures 7**, **8**). No significant differences in total and compressive loads were found between squat and freestyle lifting in the segments T12/L1 to L2/L3, while in the segments L3/L4 to L5/S1, freestyle produced significantly larger loads than both other styles.

Peak AP shear loads in the L5/S1 segment for all styles were up to 23 times larger as in the other segments (**Figure 9**). Stoop lifting resulted in significantly larger shear loads throughout the lumbar spine, except for the segment L5/S1. For the segments T12/L1 to L4/L5, squat lifting produced significantly smaller shear loads than both other styles.

Lumbar Lordosis Angle RoM and Lifting Movement Duration

The analysis of the lumbar lordosis angle RoM showed mean values of 24.2 ± 7.3° for freestyle, 25.1 ± 8.2° for squat and 35.9 ± 10.1° for stoop lifting. ANOVA revealed significant differences

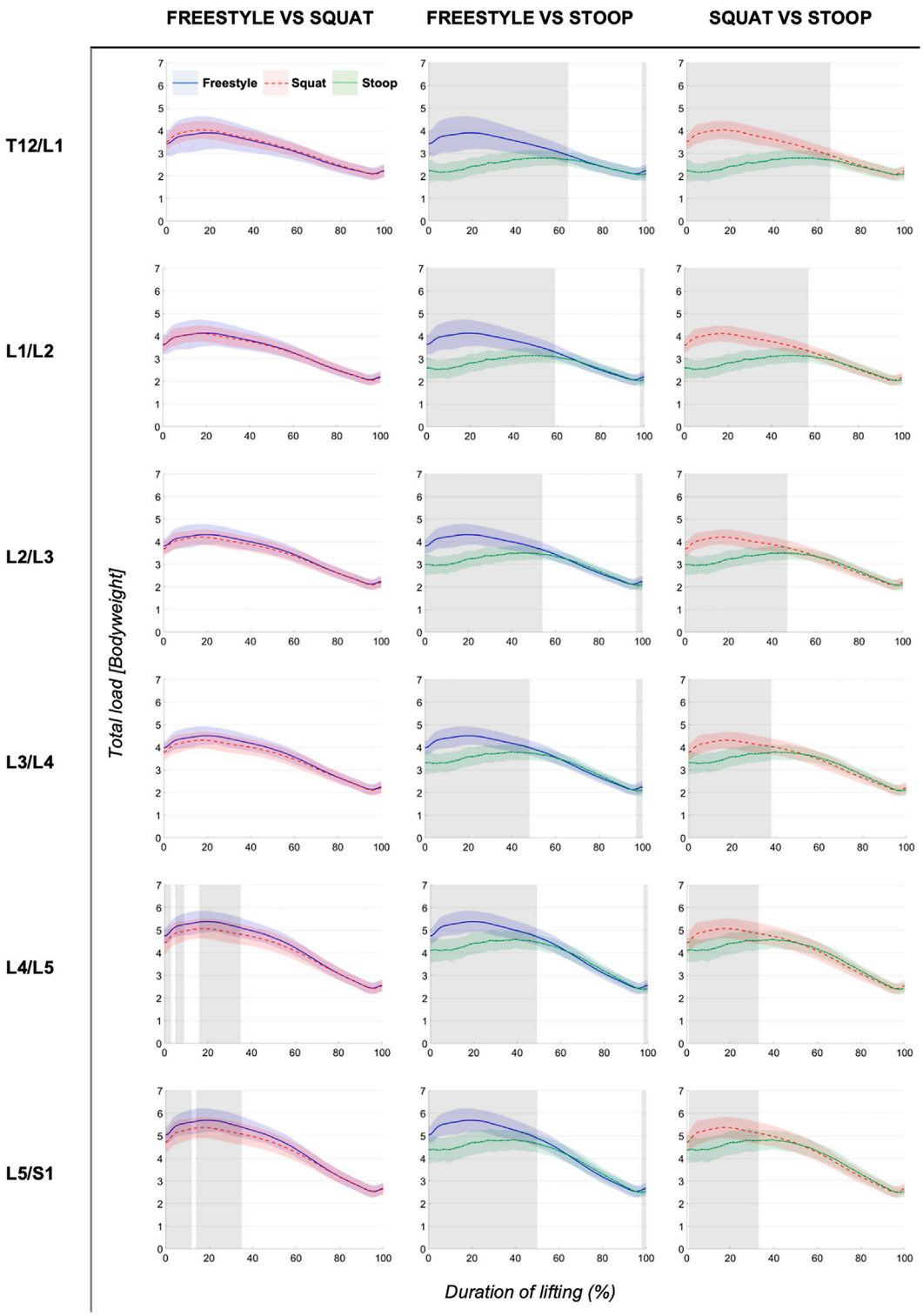

FIGURE 4 | Continuous total loads graphs arranged by compared styles and spinal segment. Curves depict the respective total loads throughout the lift up cycle, starting when the box leaves the ground (0%) to upright standing position (100%). Colored areas above and below the curves indicate the SD and the greyed sectors in the graphs indicate the parts of the lifting cycle where significant differences between styles were detected.

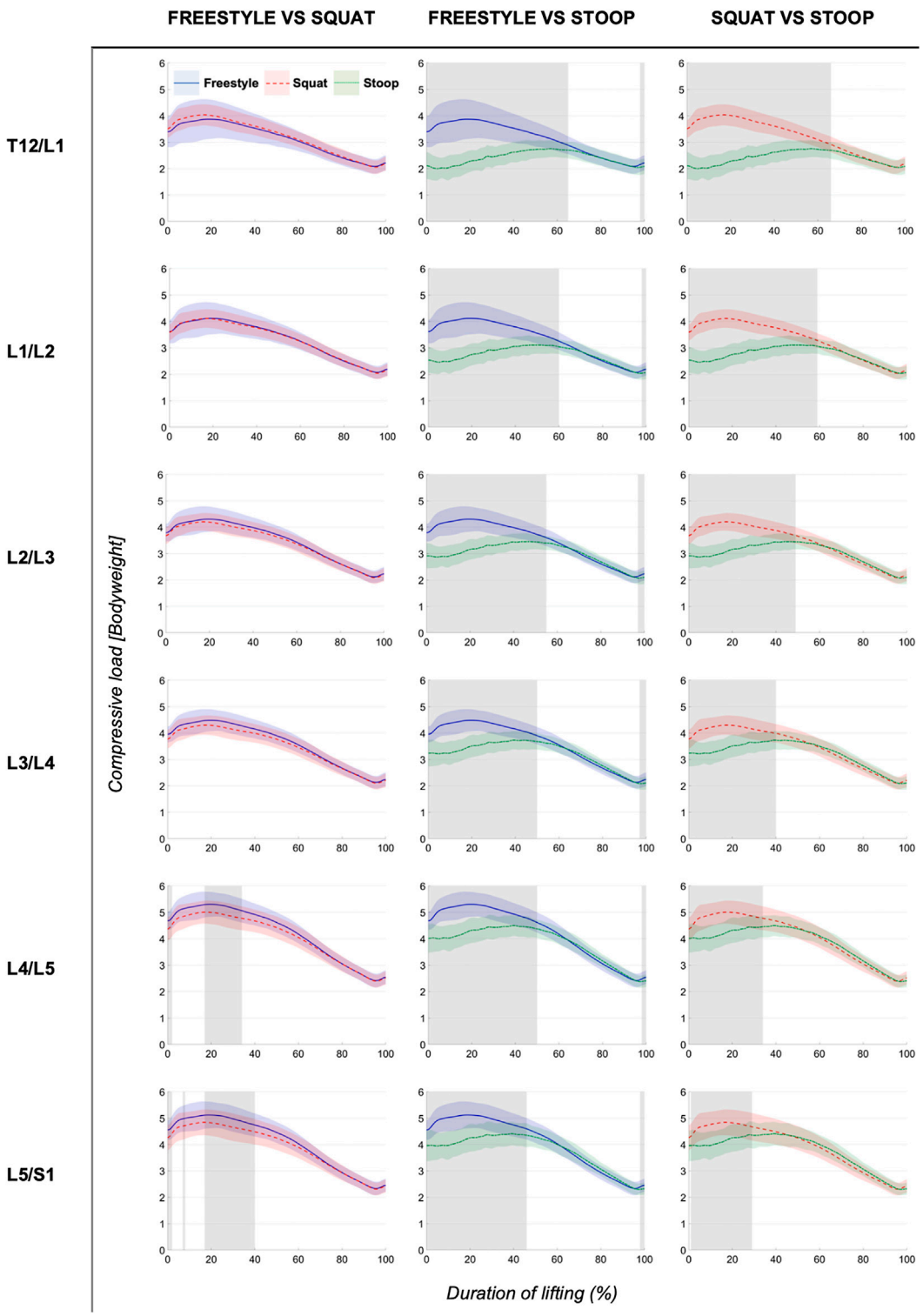

FIGURE 5 | Continuous compressive loads graphs arranged by compared styles and spinal segment. Curves depict the respective compressive loads throughout the lift up cycle, starting when the box leaves the ground (0%) to upright standing position (100%). Colored areas above and below the curves indicate the SD and the greyed sectors in the graphs indicate the parts of the lifting cycle where significant differences between styles were detected.

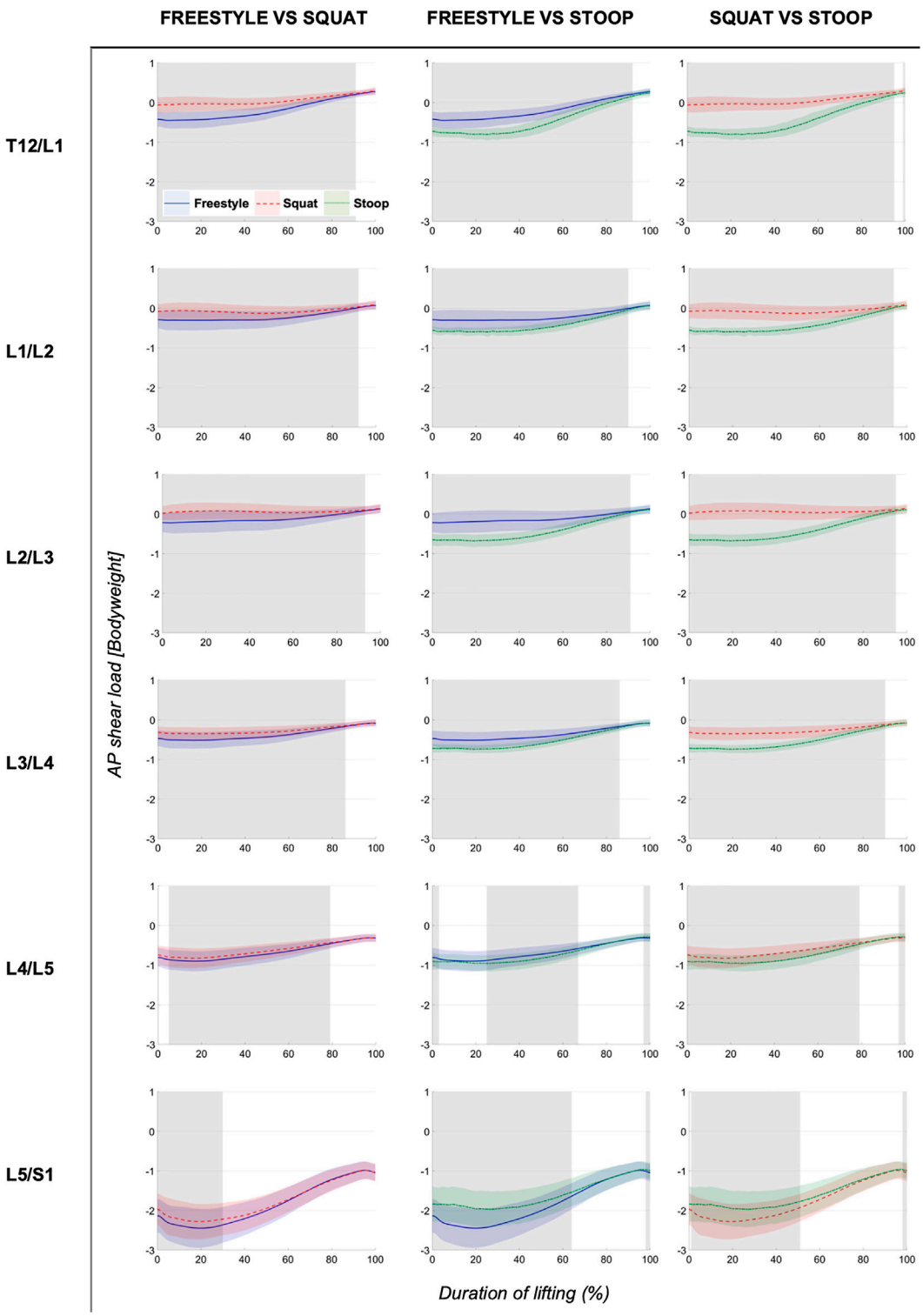

FIGURE 6 | Continuous AP shear loads graphs arranged by compared styles and spinal segment. Curves depict the respective AP shear loads throughout the lift up cycle, starting when the box leaves the ground (0%) to upright standing position (100%). Colored areas above and below the curves indicate the SD and the greyed sectors in the graphs indicate the parts of the lifting cycle where significant differences between styles were detected.

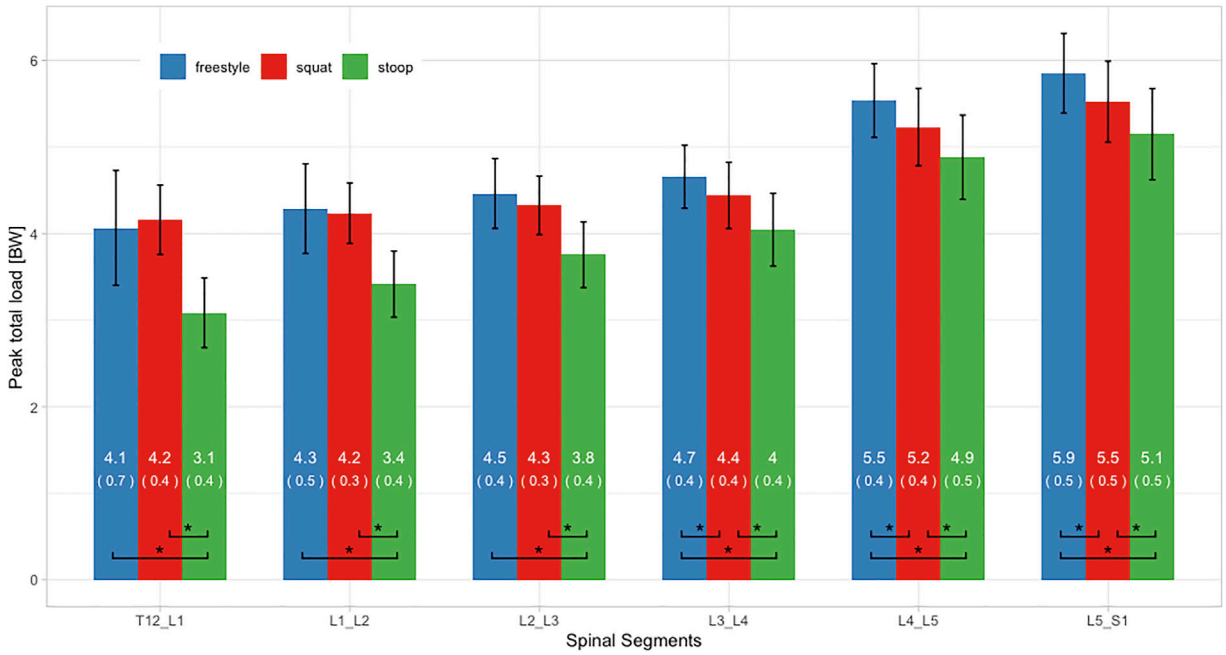

FIGURE 7 | Peak total loads of all three lifting styles grouped by spinal segments. Bars represent the mean loads normalized to bodyweight (BW). Mean and SD values are listed in the bar centers. Horizontal parentheses at the bottom of bar groups indicate comparisons for which a significant difference (*) was detected in the post hoc analysis. Lines at the bar ends indicate SD.

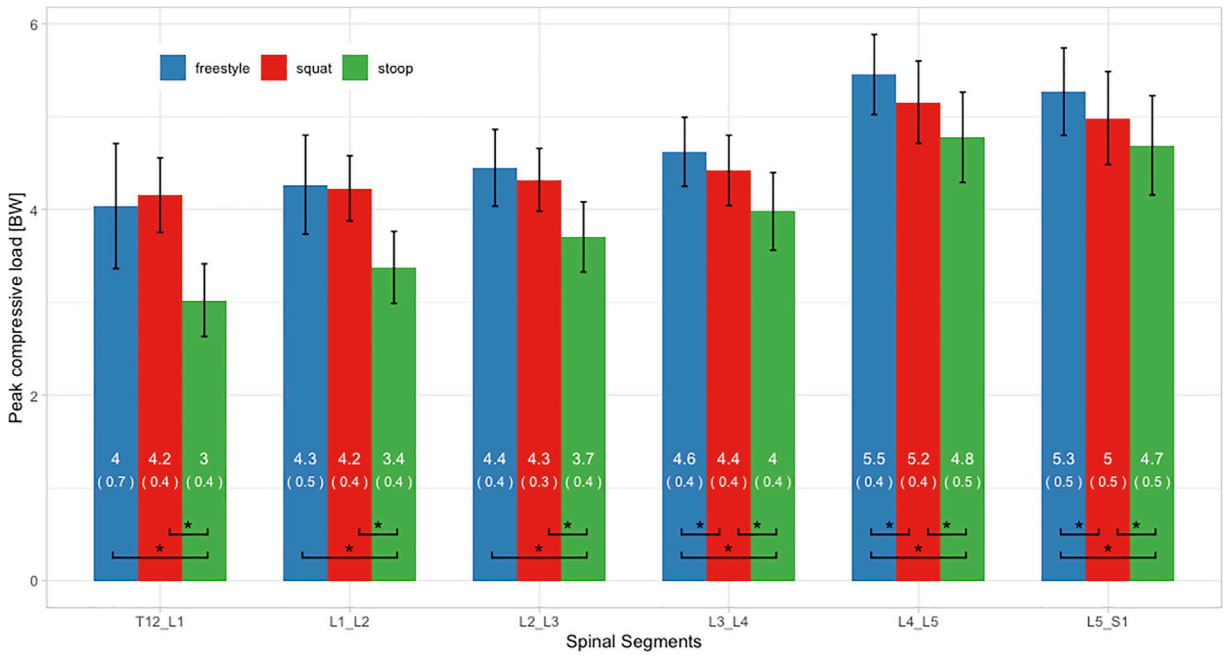

FIGURE 8 | Peak compressive loads of all three lifting styles grouped by spinal segments. Bars represent the mean loads normalized to bodyweight (BW). Mean and SD values are listed in the bar centers. Horizontal parentheses at the bottom of bar groups indicate comparisons for which a significant difference (*) was detected in the post hoc analysis. Lines at the bar ends indicate SD.

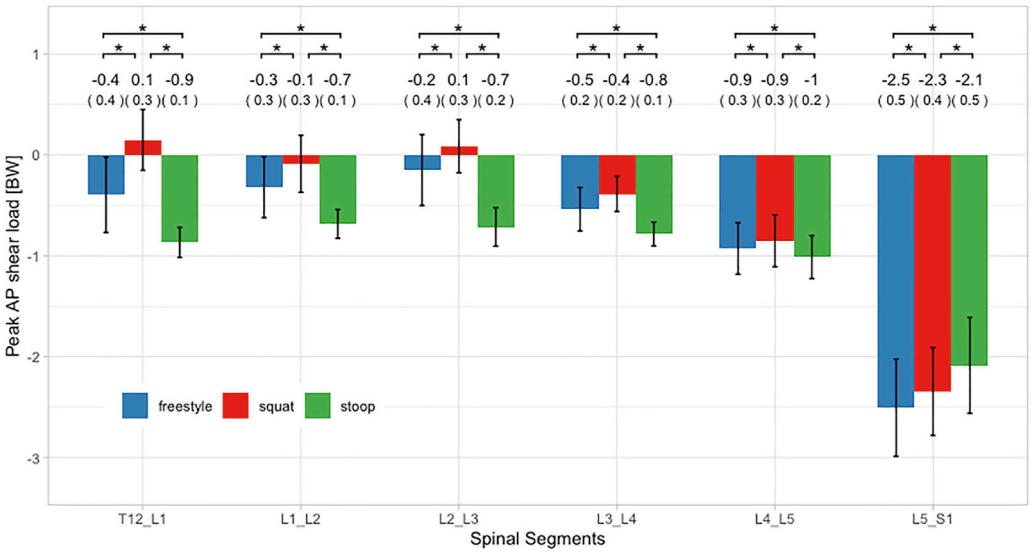

FIGURE 9 | Peak AP shear loads of all three lifting styles grouped by spinal segments. Bars represent the mean loads normalized to bodyweight (BW). Mean and SD values are listed above the bars. Horizontal parentheses above bar groups indicate comparisons for which a significant difference (*) was detected in the post hoc analysis. Lines at the bar ends indicate SD.

between styles ($p < 0.001$). Post hoc analysis revealed significant differences between stoop and squat lifting ($p < 0.001$) as well as between stoop and freestyle lifting ($p < 0.001$). No significant difference was found between squat and freestyle lifting.

Regarding lifting movement duration, freestyle lifting was performed the fastest with a mean duration of 4.6 ± 0.7, followed by squat lifting with 4.9 ± 0.7 and stoop lifting with 5.9 ± 1.1. The statistical analysis indicated significant differences between freestyle and squat lifting ($p = 0.004$), freestyle and stoop lifting ($p < 0.001$) as well as squat and stoop lifting ($p < 0.001$). Additional analyses showed trends for negative relationships between spinal loads and lifting movement duration (see **Supplementary Material**).

DISCUSSION

This study aimed at exploring differences in lumbar spine loading between freestyle, squat and stoop lifting using a comprehensive motion capture-driven musculoskeletal full-body modeling approach. Results demonstrated that stoop lifting produced smaller total and compressive loads compared to squat lifting. Moreover, stoop lifting generally resulted in higher AP shear loads, except for the L5/S1 segment, where AP shear loads were the smallest compared to the other lifting styles.

The fact that stoop lifting produced smaller compressive loads is consistent with Potvin et al. (1991), Kingma et al. (2004), Khoddam-Khorasani et al. (2020) and Leskinen et al. (1983). On the other hand, the findings partially disagree with Bazrgari et al. (2007), Anderson and Chaffin (1986) and Faber et al. (2009), who found that stoop lifting resulted in larger L5/S1 compressive loads than squat lifting. Furthermore, Hwang et al. (2009), Kingma et al. (2010), Dreischarf et al. (2016) and Troup et al. (1983) reported no significant difference in spinal compression between squat and stoop lifting. Reasons for such inconsistent findings could be differences in the experimental settings as well as the underlying models. Changes in lifting style execution, variations in lowering depth or horizontal distance of the weight to S1 might considerably influence spinal loading. This issue was also mentioned by Van Dieën et al. (1999) and could be addressed in the future with better standardization in the experimental designs.

While compressive loads in this study were up to 43 times larger than shear loads, shear forces are still a subject of great interest. Gallagher and Marras (2012) reported that especially spines of younger individuals (less than 30 years) might be particularly susceptible to shear loads due to higher disc elasticity. For all lifting styles evaluated in this study, AP shear loads reached magnitudes of about 2.5 BW in the L5/S1 segment, which was consistent with Kingma et al. (2004), Khoddam-Khorasani et al. (2020) and Bazrgari et al. (2007). The 180% increase in peak L4/L5 shear load during stoop compared to squat lifting reported by Potvin et al. (1991) was not reproduced in our experiment. Nonetheless, our simulations showed shear load increases ranging from 100% (L3/L4) to 800% (T12/L1) in segments above L4/L5. No significant differences in L5/S1 shear loads between stoop and squat lifting were reported by Kingma et al. (2004) and Kingma et al. (2010). In this study, L5/S1 was the only segment where shear loads were larger during squat compared to stoop lifting (about 10%). This is a particularly important finding when considering that about 90% of all spondylolisthesis and herniated discs occur in the L5/S1 segment (Gagnet et al., 2018; Donnally et al., 2021). In contrast, Bazrgari et al. (2007) found larger shear for this segment during stoop lifting. Shear forces appear to be highly dependent on the model used (Van Dieën et al., 1999). Kingma

et al. (2004) explained the lack of significant differences between lifting styles with a high between-subject variance of the shear forces. Reasons for such differing results could be different horizontal distances of the lifted weight to S1, different lumbar flexion angles or other confounding variables such as variations in lifting style execution or differences in starting positions (grip height).

Potvin et al. (1991) suggested, that shear loads are more strongly influenced by lumbar flexion angles than lifted weight. Compressive loads behave differently in this aspect as they increase linearly with added weight (Potvin et al., 1991; Marras et al., 1999). This would imply that lumbar flexion angles are a confounding variable when comparing shear loads, if not controlled for.

In this study, freestyle lifting generated larger spinal loads than squat lifting. This agrees with results of Kingma et al. (2010) where freestyle produced larger peak L5/S1 compression and shear forces than squat or stoop, although differences were not statistically significant. Moreover, Dolan et al. (1994b) reported that freestyle lifting generated larger net moments than both other styles but suspected this result to be mainly due to a faster execution of the freestyle lifts. In the studies by (Kingma et al., 2004) and (Khoddam-Khorasani et al., 2020), spinal loads during freestyle lifting fell in between those during squat and stoop lifting. Reason for these differences could be the variations in the experimental setting or the used models. In our study and the study conducted by Kingma et al. (2010) participants lifted a box from the floor, while in the study by Khoddam-Khorasani et al. (2020) participants were measured in isometrically held positions of 40 and 65° forward upper trunk inclination with and without holding a weight.

While loads increased for all lifting styles towards the caudal end of the lumbar spine, differences between lifting styles seemed more pronounced in the upper lumbar spine. Similar results were found by Khoddam-Khorasani et al. (2020), suggesting that differences between lifting styles become less relevant towards the caudal end of the spine.

Time related analysis revealed that peak loads occur at different time segments for squat lifting and stoop lifting. During squat lifting, the highest loads occurred within the first 30% of the lifting cycle, whereas during stoop lifting, peak loads were indicated between 40 and 70% of the lifting cycle. Faber et al. (2009) reported an early onset of peak loading but did not differentiate further between styles or within the lifting cycle. Referring to the strain rate dependency of vertebral discs (Kemper et al., 2007), a slower onset of peak loading during stoop lifting might result in less stress on the spine.

It has to be considered that at least a part of the differences in spinal loading between the lifting styles might have been due to differences in lifting movement duration. Stoop lifting was executed about 20% slower than squat lifting and about 30% slower than freestyle lifting. These slower lifting speeds are consistent with the findings of van der Have et al. (2019) but not with those of Straker (2003), who stated that stoop lifting is generally performed faster and is therefore less fatiguing than squat lifting. Trunk movement speed was shown to have a direct influence on spinal loading (Dolan et al., 1994a; Bazrgari et al., 2007). Faster lifting speeds thereby lead to larger net moments, suggesting that dynamic factors might have a larger impact on spinal loading than lifting technique (Kjellberg et al., 1998). Frost et al. (2015) demonstrated that movement strategies change when the same task is repeated with different speeds. van der Have et al. (2019) therefore suggested that faster lifting speeds should be favored as it might reduce muscle fatigue.

The lumbar lordosis angle RoMs measured in this study are consistent with previously reported findings (Potvin et al., 1991; Kingma et al., 2004; Kingma et al., 2010). Although RoM angles were smaller during squat lifting compared to stoop lifting, there is a considerable amount of lumbar flexion occurring even when specifically asked to keep a straight back. Pavlova et al. (2018) even suggested that individuals alter their lifting style primarily by altering knee joint flexion, while retaining similar lumbar spine motion as during freestyle lifting. Nevertheless, the fact that the spine never stays truly neutral when lifting should be kept in mind when discussing lumbar posture and lifting.

Limitations of this study include the specific biometric profile of the test group (age, fitness level and gender distribution), which makes the results not transferrable to a general population. In addition, not randomizing the sequence of lifting styles might have influenced the execution of the tasks (e.g., stoop lifting always performed last could have resulted in a slower execution). Methodological limitations include possible artifacts arising from the relative movement between the soft tissue (mainly skin, subcutaneous fat and muscles) and the vertebral bodies. However, an earlier MRI-based evaluation of the soft tissue artifacts associated with the currently used skin marker configuration indicated that sagittal plane spinal motion could be estimated with fairly high accuracy, comparable to that of lower extremity motion tracking (Zemp et al., 2014). Furthermore, it should be considered that the models were solved using static optimization, which means that muscle activations were estimated rather than measured. Possible atypical muscle activations patterns such as increased co-contractions would therefore not have been considered for the calculation of joint loading. The models also included several artificial torque generators (so called coordinate actuators), which were added to the intervertebral joints to account for the contribution of passive structures such as the thoracolumbar fascia but were not considered for the calculation of joint loading. Since the maximum activation levels of these actuators were kept relatively low (Schmid et al., 2021), however, we assume that they did not have a significant impact on the results.

Future research should include broadening the demographic and biometric parameters and include more diverse sample groups or explore lumbar loads among different lifting styles in combination with different lifting speeds. In addition, weights might be adjusted to individual strength levels of the participants. Kingma et al. (2010) reported that when using a 15 kg weight, the impact of trunk inclination outweighed the influence of the weight. In this experiment some subjects reported that the 15 kg box felt heavy, while others considered it light. Increasing the weight close to a subject's individual maximum should pronounce the effect of weight in relation to trunk inclination. Another topic for further research could be the interaction of shear loads in relation to different lumbar flexion angles and different weights.

The reason why squat lifting often remains the recommended lifting technique seems to come down to other factors than just spinal loading such as muscle fatigue or the sensitivity of passive properties of the spine (Bazrgari and Shirazi-Adl, 2007; van der Have et al., 2019). Based on the fatigue-failure-theorem (Gallagher and Heberger, 2013; Gallagher and Schall, 2017) future research should consider the duration of lifting in the risk assessment (van der Have et al., 2019). However, for single repetitions and moderate weights, recommendations should be reevaluated.

In conclusion, this work showed that stoop lifting produced lower total and compressive lumbar loads than squat lifting. Shear loads were generally higher during stoop lifting, except for the L5/S1 segment, where anterior shear loads were higher during squat lifting. While loads consistently increased towards the lower end of the spine, differences in spinal loading between lifting styles were more pronounced in the upper part of the lumbar spine. Considering that freestyle lifting was executed the fastest and stoop lifting the slowest, the differences in spinal loads might have partially been influenced by different lifting speeds. Additionally, the clearly noticeable lumbar spinal flexion occurring during squat lifting suggests that the spine never stays fully neutral during lifting, even when specifically asked to not flex the spine. The findings of this study provide further support to the notion that there is no one-size-fits-all approach. Especially when considering that squat lifting produced higher anterior shear forces in the L5/S1 segment, where the majority of spondylolisthesis and herniated discs occur, guidelines that recommend the squat technique as safe and the stoop technique as dangerous for any kind of lifting scenario should be reevaluated.

DATA AVAILABILITY STATEMENT

The raw data supporting the conclusion of this article will be made available by the authors, without undue reservation.

ETHICS STATEMENT

The local ethics committee (Kantonale Ethikkommission Bern) provided exemption for this study. The patients/participants provided their written informed consent to participate in this study.

AUTHOR CONTRIBUTIONS

MvA contributed to the conception and design of the study, collected, analyzed and interpreted the data/results, and wrote the first draft of the manuscript. ML contributed to the conception and design of the study and collected the data. LC created the musculoskeletal models and performed the simulations. CB and MM contributed to the conception and design of the study and the interpretation of the data. SS contributed to the design of the study, assisted in the collection, analysis and interpretation of the data, and supervised the project. All authors critically revised the manuscript and approved the version to be published.

ACKNOWLEDGMENTS

The authors thank all the volunteers for participating in this study.

SUPPLEMENTARY MATERIAL

The Supplementary Material for this article can be found online at: https://www.frontiersin.org/articles/10.3389/fbioe.2021.769117/full#supplementary-material

REFERENCES

Adler, R. J. T., and Taylor, J. E. (2007). *Random Fields and Geometry*. New York: Springer-Verlag.

Anderson, C. K., and Chaffin, D. B. (1986). A Biomechanical Evaluation of Five Lifting Techniques. *Appl. Ergon.* 17, 2–8. doi:10.1016/0003-6870(86)90186-9

Balagué, F., Mannion, A. F., Pellisé, F., and Cedraschi, C. (2012). Non-specific Low Back Pain. *The Lancet* 379, 482–491. doi:10.1016/s0140-6736(11)60610-7

Bazrgari, B., Shirazi-Adl, A., and Arjmand, N. (2007). Analysis of Squat and Stoop Dynamic Liftings: Muscle Forces and Internal Spinal Loads. *Eur. Spine J.* 16, 687–699. doi:10.1007/s00586-006-0240-7

Bazrgari, B., and Shirazi-Adl, A. (2007). Spinal Stability and Role of Passive Stiffness in Dynamic Squat and Stoop Lifts. *Computer Methods Biomech. Biomed. Eng.* 10, 351–360. doi:10.1080/10255840701436974

Burgess-Limerick, R. (2003). Squat, Stoop, or Something in between? *Int. J. Ind. Ergon.* 31, 143–148. doi:10.1016/s0169-8141(02)00190-7

Caneiro, J. P., O'sullivan, P., Smith, A., Ovrebekk, I. R., Tozer, L., Williams, M., et al. (2019). Physiotherapists Implicitly Evaluate Bending and Lifting with a Round Back as Dangerous. *Musculoskelet. Sci. Pract.* 39, 107–114. doi:10.1016/j.msksp.2018.12.002

Dolan, P., Earley, M., and Adams, M. A. (1994a). Bending and Compressive Stresses Acting on the Lumbar Spine during Lifting Activities. *J. Biomech.* 27, 1237–1248. doi:10.1016/0021-9290(94)90277-1

Dolan, P., Mannion, A. F., and Adams, M. A. (1994b). Passive Tissues Help the Back Muscles to Generate Extensor Moments during Lifting. *J. Biomech.* 27, 1077–1085. doi:10.1016/0021-9290(94)90224-0

Donnally, C. J., Iii, Hanna, A., and Varacallo, M. (2021). Degenerative Disk Disease. in *StatPearls [Internet]. (Treasure Island (FL).* StatPearls Publishing.

Dreischarf, M., Rohlmann, A., Graichen, F., Bergmann, G., and Schmidt, H. (2016). *In Vivo* loads on a Vertebral Body Replacement during Different Lifting Techniques. *J. Biomech.* 49, 890–895. doi:10.1016/j.jbiomech.2015.09.034

Faber, G. S., Kingma, I., Bakker, A. J. M., and van Dieën, J. H. (2009). Low-back Loading in Lifting Two Loads beside the Body Compared to Lifting One Load in Front of the Body. *J. Biomech.* 42, 35–41. doi:10.1016/j.jbiomech.2008.10.013

Frost, D. M., Beach, T. A. C., Callaghan, J. P., and Mcgill, S. M. (2015). The Influence of Load and Speed on Individuals' Movement Behavior. *J. Strength Cond Res.* 29, 2417–2425. doi:10.1519/jsc.0000000000000264

Gagnet, P., Kern, K., Andrews, K., Elgafy, H., and Ebraheim, N. (2018). Spondylolysis and Spondylolisthesis: A Review of the Literature. *J. Orthopaedics* 15, 404–407. doi:10.1016/j.jor.2018.03.008

Gallagher, S., and Heberger, J. R. (2013). Examining the Interaction of Force and Repetition on Musculoskeletal Disorder Risk. *Hum. Factors* 55, 108–124. doi:10.1177/0018720812449648

Gallagher, S., and Marras, W. S. (2012). Tolerance of the Lumbar Spine to Shear: a Review and Recommended Exposure Limits. *Clin. Biomech.* 27, 973–978. doi:10.1016/j.clinbiomech.2012.08.009

Gallagher, S., and Schall Jr., M. C., Jr. (2017). Musculoskeletal Disorders as a Fatigue Failure Process: Evidence, Implications and Research Needs. *Ergonomics* 60, 255–269. doi:10.1080/00140139.2016.1208848

Herzog, W. (1987). Individual Muscle Force Estimations Using a Non-linear Optimal Design. *J. Neurosci. Methods* 21, 167–179. doi:10.1016/0165-0270(87)90114-2

Hof, A. L. (1996). Scaling Gait Data to Body Size. *Gait & Posture* 4, 222–223. doi:10.1016/0966-6362(95)01057-2

Hwang, S., Kim, Y., and Kim, Y. (2009). Lower Extremity Joint Kinetics and Lumbar Curvature during Squat and Stoop Lifting. *BMC Musculoskelet. Disord.* 10, 15. doi:10.1186/1471-2474-10-15

Kemper, A. R., Mcnally, C., and Duma, S. M. (2007). The Influence of Strain Rate on the Compressive Stiffness Properties of Human Lumbar Intervertebral Discs. *Biomed. Sci. Instrum* 43, 176–181.

Khoddam-Khorasani, P., Arjmand, N., and Shirazi-Adl, A. (2020). Effect of Changes in the Lumbar Posture in Lifting on Trunk Muscle and Spinal Loads: A Combined *In Vivo*, Musculoskeletal, and Finite Element Model Study. *J. Biomech.* 104, 109728. doi:10.1016/j.jbiomech.2020.109728

Kingma, I., Bosch, T., Bruins, L., and van Dieën, J. H. (2004). Foot Positioning Instruction, Initial Vertical Load Position and Lifting Technique: Effects on Low Back Loading. *Ergonomics* 47, 1365–1385. doi:10.1080/00140130410001714742

Kingma, I., Faber, G. S., and van Dieën, J. H. (2010). How to Lift a Box that Is Too Large to Fit between the Knees. *Ergonomics* 53, 1228–1238. doi:10.1080/00140139.2010.512983

Kjellberg, K., Lindbeck, L., and Hagberg, M. (1998). Method and Performance: Two Elements of Work Technique. *Ergonomics* 41, 798–816. doi:10.1080/001401398186658

Leskinen, T. P. J., Stålhammar, H. R., Kuorinka, I. A. A., and Troup, J. D. G. (1983). A Dynamic Analysis of Spinal Compression with Different Lifting Techniques. *Ergonomics* 26, 595–604. doi:10.1080/00140138308963378

Marras, W. S., Granata, K. P., Davis, K. G., Allread, W. G., and Jorgensen, M. J. (1999). Effects of Box Features on Spine Loading during Warehouse Order Selecting. *Ergonomics* 42, 980–996. doi:10.1080/001401399185252

Nolan, D., O'sullivan, K., Stephenson, J., O'sullivan, P., and Lucock, M. (2018). What Do Physiotherapists and Manual Handling Advisors Consider the Safest Lifting Posture, and Do Back Beliefs Influence Their Choice? *Musculoskelet. Sci. Pract.* 33, 35–40. doi:10.1016/j.msksp.2017.10.010

Papi, E., Bull, A. M. J., and Mcgregor, A. H. (2020). Alteration of Movement Patterns in Low Back Pain Assessed by Statistical Parametric Mapping. *J. Biomech.* 100, 109597. doi:10.1016/j.jbiomech.2019.109597

Pataky, T. C., Robinson, M. A., and Vanrenterghem, J. (2013). Vector Field Statistical Analysis of Kinematic and Force Trajectories. *J. Biomech.* 46, 2394–2401. doi:10.1016/j.jbiomech.2013.07.031

Pavlova, A. V., Meakin, J. R., Cooper, K., Barr, R. J., and Aspden, R. M. (2018). Variation in Lifting Kinematics Related to Individual Intrinsic Lumbar Curvature: an Investigation in Healthy Adults. *BMJ Open Sport Exerc. Med.* 4, e000374. doi:10.1136/bmjsem-2018-000374

Potvin, J. R., Mcgill, S. M., and Norman, R. W. (1991). Trunk Muscle and Lumbar Ligament Contributions to Dynamic Lifts with Varying Degrees of Trunk Flexion. *Spine* 16, 1099–1107. doi:10.1097/00007632-199109000-00015

Saraceni, N., Kent, P., Ng, L., Campbell, A., Straker, L., and O'sullivan, P. (2020). To Flex or Not to Flex? Is There a Relationship between Lumbar Spine Flexion during Lifting and Low Back Pain? A Systematic Review with Meta-Analysis. *J. Orthop. Sports Phys. Ther.* 50, 121–130. doi:10.2519/jospt.2020.9218

Schaafsma, F. G., Anema, J. R., and Van Der Beek, A. J. (2015). Back Pain: Prevention and Management in the Workplace. *Best Pract. Res. Clin. Rheumatol.* 29, 483–494. doi:10.1016/j.berh.2015.04.028

Schmid, S., Bruhin, B., Ignasiak, D., Romkes, J., Taylor, W. R., Ferguson, S. J., et al. (2017). Spinal Kinematics during Gait in Healthy Individuals across Different Age Groups. *Hum. Movement Sci.* 54, 73–81. doi:10.1016/j.humov.2017.04.001

Schmid, S., Connolly, L., Moschini, G., Meier, M. L., and Senteler, M. (2021). Skin Marker-Based Subject-specific Spinal Alignment Modeling: A Feasibility Study. arXiv:2101.12272.

Straker, L. (2003). Evidence to Support Using Squat, Semi-squat and Stoop Techniques to Lift Low-Lying Objects. *Int. J. Ind. Ergon.* 31, 149–160. doi:10.1016/s0169-8141(02)00191-9

Swiss National Accident Insurance Fund (Suva) (2016). Hebe Richtig - Trage Richtig. Available at: https://www.suva.ch/de-CH/material/Sicherheitsregeln-Tipps/hebe-richtig—trage-richtig-44018d59315931.

The National Institute for Occupational Safety and Health (Niosh) (2007). *Ergonomic Guidelines for Manual Material Handling*. Available at: https://www.cdc.gov/niosh/docs/2007-131.

Troup, J. D. G., Leskinen, T. P. J., Stalhammar, H. R., and Kuorinka, I. A. A. (1983). A Comparison of Intraabdominal Pressure Increases, Hip Torque, and Lumbar Vertebral Compression in Different Lifting Techniques. *Hum. Factors* 25, 517–525. doi:10.1177/001872088302500506

van der Have, A., Van Rossom, S., and Jonkers, I. (2019). Squat Lifting Imposes Higher Peak Joint and Muscle Loading Compared to Stoop Lifting. *Appl. Sci.* 9, 3794. doi:10.3390/app9183794

van Dieën, J. H., Hoozemans, M. J. M., and Toussaint, H. M. (1999). Stoop or Squat: a Review of Biomechanical Studies on Lifting Technique. *Clin. Biomech.* 14, 685–696. doi:10.1016/s0268-0033(99)00031-5

Wang, Z., Wu, L., Sun, J., He, L., Wang, S., and Yang, L. (2012). Squat, Stoop, or Semi-squat: A Comparative experiment on Lifting Technique. *J. Huazhong Univ. Sci. Technol. [Med. Sci.* 32, 630–636. doi:10.1007/s11596-012-1009-3

Zemp, R., List, R., Gülay, T., Elsig, J. P., Naxera, J., Taylor, W. R., et al. (2014). Soft Tissue Artefacts of the Human Back: Comparison of the Sagittal Curvature of the Spine Measured Using Skin Markers and an Open Upright MRI. *PLoS One* 9–e95426. doi:10.1371/journal.pone.0095426

Conflict of Interest: The authors declare that the research was conducted in the absence of any commercial or financial relationships that could be construed as a potential conflict of interest.

frontiers in Bioengineering and Biotechnology

ORIGINAL RESEARCH
published: 15 November 2021
doi: 10.3389/fbioe.2021.767974

Patients With Chronic Low Back Pain Have an Individual Movement Signature: A Comparison of Angular Amplitude, Angular Velocity and Muscle Activity Across Multiple Functional Tasks

Guillaume Christe[1,2]*, *Camille Aussems*[2], *Brigitte M. Jolles*[2,3] and *Julien Favre*[2]

[1]Department of Physiotherapy, HESAV School of Health Sciences, HES-SO University of Applied Sciences and Arts Western Switzerland, Lausanne, Switzerland, [2]Swiss BioMotion Lab, Department of Musculoskeletal Medicine, Lausanne University Hospital and University of Lausanne, Lausanne, Switzerland, [3]Institute of Microengineering, Ecole Polytechnique Fédérale de Lausanne, Lausanne, Switzerland

OPEN ACCESS

Edited by:
Stefan Schmid,
Bern University of Applied Sciences, Switzerland

Reviewed by:
Thomas Matheve,
Universiteit Hasselt, Belgium
André P. G. Castro,
Universidade de Lisboa, Portugal

***Correspondence:**
Guillaume Christe
Guillaume.christe@hesav.ch

Specialty section:
This article was submitted to Biomechanics, a section of the journal Frontiers in Bioengineering and Biotechnology

Received: *31 August 2021*
Accepted: *26 October 2021*
Published: *15 November 2021*

Citation:
Christe G, Aussems C, Jolles BM and Favre J (2021) Patients With Chronic Low Back Pain Have an Individual Movement Signature: A Comparison of Angular Amplitude, Angular Velocity and Muscle Activity Across Multiple Functional Tasks. Front. Bioeng. Biotechnol. 9:767974. doi: 10.3389/fbioe.2021.767974

Despite a large body of evidence demonstrating spinal movement alterations in individuals with chronic low back pain (CLBP), there is still a lack of understanding of the role of spinal movement behavior on LBP symptoms development or recovery. One reason for this may be that spinal movement has been studied during various functional tasks without knowing if the tasks are interchangeable, limiting data consolidation steps. The first objective of this cross-sectional study was to analyze the influence of the functional tasks on the information carried by spinal movement measures. To this end, we first analyzed the relationships in spinal movement between various functional tasks in patients with CLBP using Pearson correlations. Second, we compared the performance of spinal movement measures to differentiate patients with CLBP from asymptomatic controls among tasks. The second objective of the study was to develop task-independent measures of spinal movement and determine the construct validity of the approach. Five functional tasks primarily involving sagittal-plane movement were recorded for 52 patients with CLBP and 20 asymptomatic controls. Twelve measures were used to describe the sagittal-plane angular amplitude and velocity at the lower and upper lumbar spine as well as the activity of the erector spinae. Correlations between tasks were statistically significant in 91 out of 99 cases ($0.31 \leq r \leq 0.96$, all $p < 0.05$). The area under the curve (AUC) to differentiate groups did not differ substantially between tasks in most of the comparisons (82% had a difference in AUC of ≤0.1). The task-independent measures of spinal movement demonstrated equivalent or higher performance to differentiate groups than functional tasks alone. In conclusion, these findings support the existence of an individual spinal movement signature in patients with CLBP, and a limited influence of the tasks on the information carried by the movement measures, at least for the twelve common sagittal-plane measures analysed in this study. Therefore, this work brought critical insight for the interpretation of data in literature reporting differing tasks and for the design of future

studies. The results also supported the construct validity of task-independent measures of spinal movement and encouraged its consideration in the future.

Keywords: low back pain, motion analysis, lumbar, kinematics, electromyography, angle, angular velocity, muscle activity

INTRODUCTION

Alterations in spinal movement have been suggested as one of the key physical factors in the persistence of chronic low back pain (CLBP) (Marras et al., 1995; O'Sullivan, 2005; Dubois et al., 2014), however, the understanding of spinal movement behavior in CLBP remains limited. The abundance of measures used to describe spinal movement, as outlined by two recent systematic reviews (Papi et al., 2018; Moissenet et al., 2021), is undoubtedly one of the reasons limiting a better understanding. Consequently, to advance the field, there is a need to determine if that many measures are needed or if it would be possible to focus on a selection of measures. While characterizing the movement in terms of angular amplitude, angular velocity and muscle activity appears appropriate for a comprehensive description (Laird et al., 2014; Papi et al., 2018; Moissenet et al., 2021), the necessity to test multiple functional tasks remains to be determined.

So far, CLBP spinal movement has been assessed during a range of different functional tasks (Shum et al., 2007; Christe et al., 2016b, 2020; Lima et al., 2018; Matheve et al., 2019). However, these prior works mainly assessed one task at a time, or when multiple tasks were assessed, the influence of the task on spinal movement was not analyzed (Papi et al., 2018; Moissenet et al., 2021). Yet, individual consistency in spinal angular amplitudes across different functional tasks has been demonstrated in pain-free participants (Alqhtani et al., 2015; Seerden et al., 2019), suggesting that it may also be the case for individuals with CLBP and for angular velocity and muscle activity measures. This possibility is particularly supported in the clinical setting, where consistent movement patterns are frequently observed in CLBP patients. If measures from different tasks were to carry similar information (for example, patient X moves with relatively lower flexion than the other individuals independently of the tasks analyzed), this would suggest the existence of "individual spinal movement signatures." Clarifying this point appears essential, as it would help the interpretation of data in literature and the design of new experiments. In fact, on one side, knowing the extend of movement signatures would provide a basis for the comparison of studies testing different tasks and, on the other side, it would provide a rationale for the number and specificity of the tasks to include in future studies.

If individual spinal movement signatures were to exist in CLBP patients, this would question the possibility to develop task–independent measures of spinal movement. Such task–independent measures could produce more robust assessments and reduce the number of variables to deal with in statistical analyses, which would be beneficial for both the design and the interpretation of future studies. If possible, this simplified description of spinal movement could prove particularly useful to detangle the role of spinal movement alterations in CLBP development or recovery and inform rehabilitation principles (Wernli et al., 2020b; Schmid et al., 2021).

Therefore, the first objective of the study was to determine the influence of the functional tasks on the information carried by spinal movement measures. To this end, this study aimed: 1) to analyze the correlations among various functional tasks in patients with CLBP; 2) to compare the performance to differentiate patients with CLBP from asymptomatic controls among functional tasks. Based on prior research, measures corresponding to peaks and ranges of sagittal-plane lumbar angular amplitude and angular velocity, as well as maximal erector spinae activity were analyzed (Shum et al., 2005; Dankaerts et al., 2009; Hidalgo et al., 2012; Christe et al., 2016b, 2020). Following previous work in asymptomatic people and a pilot study in patients with CLBP (Alqhtani et al., 2015; Christe et al., 2016a; Seerden et al., 2019), it was hypothesized that the spinal movement measures would be positively correlated among the functional tasks. It was also hypothesized that there would be no relevant performance difference among functional tasks (Dankaerts et al., 2009; Laird et al., 2014; Christe et al., 2016b, 2020; Moissenet et al., 2021);

The second objective of the study was to determine the construct validity of task–independent measures of spinal movement obtained by grouping measures across multiple tasks. Specifically, we aimed: 3) to compare the performance of task–independent measures to differentiate patients with CLBP from asymptomatic controls to the performance of task-specific measures. It was hypothesized that the performance of task–independent measures would not be inferior compared to the performance of task-specific measures.

MATERIALS AND METHODS

Design

This cross-sectional case-controlled study is reported according to the STROBE (Strengthening the Reporting of Observational Studies in Epidemiology) criteria (von Elm et al., 2007).

Participants and Setting

Recruitment took place in an interdisciplinary rehabilitation program (IRP) at the local university hospital. This IRP is a full time 3-week program that includes patients with difficulties to maintain their leisure and professional activity because of CLBP. Participants to the IRP were invited to take part in the study if they met the inclusion/exclusion criteria. Both males and females could participate if they had a diagnosis of non-specific LBP with

or without leg pain for more than 3 months, a sufficient French level and an age from 18 to 65 years old. Exclusion criteria for the CLBP group in this study were the presence of a diagnosis of specific LBP and/or previous back surgery that limited spinal mobility (i.e., spinal fusion). Asymptomatic controls were a convenience sample recruited via emails and flyers. To be included, they had to have no history of LBP requiring third-party attention during the last 2 years. They were also excluded in the presence of any recent or current episode of LBP. Exclusion criteria for both groups included pregnancy, a body mass index (BMI) above 32 kg/m^2 and other concomitant pain or condition that could compromise the evaluation of lumbar kinematics. The BMI cutoff was selected to limit the influence of body shape on lumbar kinematics and experimental complications, without compromising external validity and patients' recruitment. The research was approved by the local Research Ethics Committee (CER-VD 2018-00188) and all participants signed an informed consent form before enrolment in the study.

Experimental Procedures

Participants were invited to the movement analysis laboratory at the university hospital for a measurement session before the IRP. First, participants completed three reliable and valid questionnaires to document mean pain intensity during the last 24 h, kinesiophobia and catastrophizing using the numeric pain rating scale (24h-NPRS), the Tampa Scale of Kinesiophobia (TSK) and the Pain Catastrophizing Scale (PCS), respectively (Sullivan, 1995; Vlaeyen et al., 1995; Chapman et al., 2011). Then, after having cleaned the skin with alcohol and shaved it, if necessary, two pairs of electrodes were placed bilaterally parallel to the erector spinae fibers 3 cm lateral to the L3 spinous process (Dupeyron et al., 2013; Wong et al., 2016). Participants then performed one submaximal voluntary contraction in crook lying as described by Dankaerts et al. (2004). Reflective markers were then attached to the participants lumbar region and pelvis following a previously described protocol (Seay et al., 2008; Christe et al., 2016b, 2017, 2020). Lumbar markers were placed on the spinous processes of L1, L3 and L5 with four additional markers attached between these markers on each side of the spine, at a distance of 5 cm. Pelvis markers were placed on the posterior superior iliac spines, anterior superior iliac spines and iliac crest tips. Marker trajectories and lumbar muscle activity were measured using an optoelectronic motion capture system with 14 cameras (Vicon, Oxford Metrics, Oxford, United Kingdom) and an electromyography system (Myon, Schwarzenberg, CH) recording synchronously at 120 and 1200 Hz, respectively.

Data collection started with the recording of a reference standing posture, where participants were standing upright and looking forward with arms at 60° of shoulder abduction. Then, five functional tasks were recorded in the same order for every participant to avoid varying remnant effects among participants as some were more exacerbating for participants: standing flexion, sit-to-stand, stepping-up on a 36 cm high step, picking-up a sponge from the floor and lifting a 4.5 kg box from the floor. All functional tasks were first demonstrated in a video with standardized instructions (**Supplementary Appendix SA**). Each functional activity was practiced between one and three times and then recorded three times, except for picking-up that was recorded ten times (for the purpose of another study, Christe et al., 2019). Following the video instruction, and before performing each task, participants rated on a zero to ten scale how much do they think the task to-be-performed is harmful for the back (perceived harm; 0: not harmful at all; 10: extremely harmful). After each task, they also rated their pain during the task with a numeric pain rating scale. At the end of the session, participants completed the French version of the Oswestry Disability Index (ODI) (Fairbank and Pynsent, 2000; Vogler et al., 2008).

Data Processing

Spinal kinematics were calculated based on a three-segment biomechanical model that includes the pelvis and the lower lumbar and upper lumbar spine (Christe et al., 2016b, 2017, 2020). Briefly, markers' trajectories were used to calculate the orientation of anatomical frames embedded in each segment. The joint coordinate system (Grood and Suntay, 1983) was then used to calculate sagittal-plane joint angles at the lower lumbar (LLSa) and the upper lumbar (ULSa) joints. LLSa was defined as the angle between the lower lumbar segment (L3-L5 central and lateral markers) and the pelvis segment, while ULSa was defined as the angle between the upper lumbar segment (L1-L3 central and lateral markers) and the lower lumbar segment. Angles were low-pass filtered using a 15 Hz Butterworth filter. The amplitude of the angles during the reference standing posture were subtracted from the angle curves to limit the inter-individual variations in morphology. Angular velocity curves (LLSv and ULSv) were obtained by numerical differentiation of the angle curves.

Electromyography recordings were band-pass filtered using a Butterworth filter with cutoff frequencies at 20 and 450 Hz. Then, for both muscles, the minimal amplitude of the electromyography signals recorded during the entire session was identified and this minimal amplitude was subtracted from the signals. This operation defined a zero-value (0%) for the electromyography data. Next, for both muscles, the signals were scaled in order to have the amplitude recorded during the submaximal voluntary contraction in crook lying equal 100%. Submaximal contraction was chosen for the normalization because its reliability was shown to be superior to maximal contraction in CLBP patients (Dankaerts et al., 2004).

In order to extract the movement measures from the angular amplitude, angular velocity and muscle activity curves, first, the curves were time-normalized to 0–100% for each repetition of each task. The beginning and the end of the task were determined visually using strict criteria based on markers displacements (Christe et al., 2016b, 2020). Then, following the methodology in prior studies (Christe et al., 2016b, 2017, 2020), the curves were tested using the coefficient of multiple correlation (CMC) (Kadaba et al., 1989) and the curves presenting a characteristic pattern were described by discrete measures. In total, 12 measures were identified. They included the peak flexion angle and sagittal-plane range of motion (ROM) at the LLS ($LLSa_{flexion}$ and $LLSa_{range}$) and at the ULS ($ULSa_{flexion}$ and $ULSa_{range}$); the peak

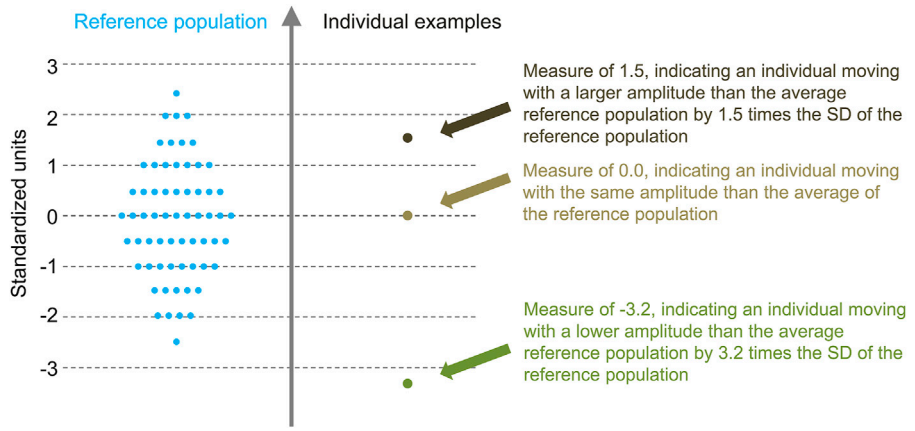

FIGURE 1 | Illustration of the task-independent measures concept. Task-independent measures are expressed according to the mean and SD of the reference population. These dimensionless measures therefore indicate how they situate compared to the reference population.

angular velocity in flexion, the peak angular velocity in extension and the range between velocity peaks at the LLS ($LLSv_{flexion}$, $LLSv_{extension}$ and $LLSv_{range}$) and at the ULS ($ULSv_{flexion}$, $ULSv_{extension}$ and $ULSv_{range}$) and; the peaks of erector spinae muscle activity during the first (EMG_{peak1}) and second (EMG_{peak2}) halves of the tasks. Not all tasks presented the characteristic features necessary to the extraction of the 12 measures. Indeed, $ULSv_{flexion}$, $ULSv_{extension}$, $ULSv_{range}$ and EMG_{peak2} were only present in flexion, picking-up and lifting. The measures were averaged over the repetitions in order to have only one value per participant and task. Finally, for EMG_{peak1} and EMG_{peak2}, the maximal value observed between the left and right erector spinae muscles was kept for analysis.

Task–independent measures were calculated by averaging the measures obtained with the diverse tasks. The averaging was done independently for each participant and measure. To give similar weight to all the tasks, a Z-score transformation was applied to the measures before averaging over the tasks. The transformations were based on the means and standard deviations of the asymptomatic controls. Consequently, as illustrated in **Figure 1**, the task-independent measures were dimensionless: their values indicated how they were situated compared to the reference (asymptomatic) population. All calculations were performed with Matlab (R2019b, MathWorks, Inc, Natick, MA).

Statistical Analysis

The normality of the measures was assessed visually using QQ plots and tested with the Shapiro-Wilk test (Ghasemi and Zahediasl, 2012). Extreme outliers were discarded from the analyses using a standard procedure (Portney and Watkins, 2000).

For the first aim, relationships among functional tasks in patients with CLBP were tested with Pearson correlations. These analyses were performed separately for each of the 12 measures. Correlation coefficients (r) were interpreted as small ($0.1 \leq r < 0.3$), medium ($0.3 \leq r < 0.5$) and large ($r \geq 0.5$) (Cohen, 1988).

For the second aim, we conducted binary logistic regression models with the movement measures as the independent variable and the group as the dependent variable. Regression models were performed separately for each measure of each task. The performance to differentiate patients with CLBP from asymptomatic controls was primarily tested with the area under the curve (AUC) value. These values were categorized as poor (AUC<0.7), acceptable ($0.7 \leq$ AUC <0.8), excellent ($0.8 \leq$ AUC <0.9) or outstanding (AUC≥ 0.9) discriminations (Hosmer et al., 2013). Following these categories, a difference in AUC between tasks above 0.1 was considered indicative of a relevant difference in groups' differentiation performance. For completeness, other usual statistics of logistic regression models were calculated: coefficient of determination (r^2), sensitivity (Sn), specificity (Sp), positive likelihood ratios (LR+) and negative likelihood ratios (LR−). In addition, independent t-tests were conducted to determine if group differences were statistically significant and Cohen's d effect sizes (ES) were computed to quantify the size of the differences between groups (Cohen, 1988). ES were interpreted as very small ($0.01 \leq ES < 0.2$), small ($0.2 \leq ES < 0.5$), moderate ($0.5 \leq ES < 0.8$), large ($0.8 \leq ES < 1.2$), very large ($1.2 \leq ES < 2.0$) and huge ($ES \geq 2.0$) (Cohen, 1988; Sawilowsky, 2009).

For the third aim regarding the construct validity of task–independent measures of spinal movement, binary logistic regression models were conducted for each of the task–independent measure. AUC values were interpreted as detailed above for the tasks' comparison. Independent t-tests and ES were also calculated for task–independent measures. For completeness with the first aim, Pearson correlations were performed between task-independent and task-specific data for each measure. Statistical analyses were performed with SPSS (Version 25, IBM, NY, United States), using a significance level at $\alpha < 0.05$.

Sample Size

To detect a correlation coefficient between functional tasks of $r \geq 0.4$, as reported in prior asymptomatic and pilot studies (Alqhtani

TABLE 1 | Correlations in angular amplitude, angular velocity and muscle activity between different functional tasks. The darkness of the blue represents the strength of the correlation: white: r < 0.3; pale blue: 0.3 ≤ r < 0.5; blue: 0.5 ≤ r < 0.7; dark blue: r ≥ 0.7. Correlations in blue (r ≥ 0.3) all have a p-value <0.05. NA: variables not available as there were no characteristic pattern (see Data Processing). STS: sit-to-stand; LLS: Lower lumbar spine; ULS: Upper lumbar spine. EMG_{peak1}: first peak of maximal paraspinal muscles activity; EMG_{peak2}: second peak of maximal paraspinal muscles activity. Correlations between EMG_{peak2} of flexion, lifting and picking-up and EMG_{peak1} of stepping-up and sit-to-stand are reported in the last line (during stepping-up and sit-to-stand, there is only one peak of paraspinal muscle activity, see Data Processing).

			Flexion Lifting	Flexion Pick	Flexion Step	Flexion STS	Lift Pick	Lift Step	Lift STS	Pick Step	Pick STS	Step STS
Angular amplitude	Peak flexion	$LLSa_{flexion}$	0.77	0.73	0.41	0.72	0.96	0.60	0.80	0.54	0.75	0.68
		$ULSa_{flexion}$	0.76	0.81	0.56	0.69	0.92	0.62	0.71	0.61	0.71	0.77
	Range	$LLSa_{range}$	0.62	0.60	0.24	0.40	0.91	0.37	0.43	0.36	0.49	0.43
		$ULSa_{range}$	0.55	0.72	0.69	0.44	0.79	0.76	0.36	0.95	0.48	0.46
Angular velocity	Peak velocity in flexion	$LLSv_{flexion}$	0.55	0.33	0.06	0.12	0.76	0.21	0.38	0.27	0.58	0.23
		$ULSv_{flexion}$	0.57	0.52	NA	NA	0.52	NA	NA	NA	NA	NA
	Peak velocity in extension	$LLSv_{extension}$	0.38	0.23	0.17	0.31	0.63	0.45	0.60	0.37	0.32	0.38
		$ULSv_{extension}$	0.58	0.48	NA	NA	0.75	NA	NA	NA	NA	NA
	Range	$LLSv_{range}$	0.55	0.35	0.08	0.32	0.76	0.37	0.56	0.33	0.47	0.39
		$ULSv_{range}$	0.64	0.57	NA	NA	0.72	NA	NA	NA	NA	NA
EMG	EMG_{peak1}		0.74	0.64	0.64	0.60	0.74	0.40	0.58	0.33	0.44	0.61
	EMG_{peak2}		0.74	0.65	0.59	0.51	0.71	0.61	0.46	0.55	0.39	NA

et al., 2015; Christe et al., 2016a; Bujang and Baharum, 2016), with a power of 0.8 and α error of 0.05, the minimum sample size in the patients' group was 46. For the logistic regression, the usual recommendations were followed, indicating a minimum of 15 participants per group in the case of models with a single independent variable (Portney and Watkins, 2000). Five asymptomatic participants and six participants with CLBP were added to prevent insufficient power due to potential drop-out or corrupted movement data.

RESULTS

Fifty-two patients with CLBP (sex: 63.5% male; age (mean ± SD): 40.0 ± 10.4 years old; BMI: 25.3 ± 3.3 kg/m^2) and 20 asymptomatic controls (55% male; 38.2 ± 10.9 years old; 22.7 ± 2.8 kg/m^2) were included in the study. The mean 24 h-NPRS, TSK, PCS and ODI scores of the patients were 5.6 ± 2.1, 44.3 ± 7.5, 25.2 ± 11.7 and 35.3 ± 11.2, respectively. Mean pain during movement was 4.6 ± 2.5 during flexion, 4.8 ± 2.7 during lifting, 4.3 ± 2.6 during picking-up, 2.7 ± 2.2 during stepping-up and 2.7 ± 2.5 during sit-to-stand for the patients. Mean perceived harm by the patients for each movement was 4.5 ± 3.5 for flexion, 6.3 ± 3.1 for lifting, 5.4 ± 3.2 for picking-up, 1.9 ± 2.4 for stepping-up and 2.6 ± 3.0 for sit-to-stand. Mean movement measures are reported in **Supplementary Appendix SB** for both groups. Movement data were available for at least 48 CLBP patients and 17 asymptomatic controls.

Correlations between tasks were statistically significant in 91 out of 99 (92%) cases (0.31 ≤ r ≤ 0.96, all $p < 0.05$) and 59 (60%) had a coefficient above 0.5 (**Table 1**; **Figure 2**). For angular amplitude measures, all but one correlation coefficients (39/40) were significant ($p \leq 0.01$). All significant coefficients were above 0.3 and 28 (70%) exceeded 0.5. Correlation coefficients were significant and above 0.3 ($p < 0.05$) in 31/39 (79%) cases for angular velocity measures. The coefficients for angular velocity measures were larger than 0.5 in 16 (41%) cases. All correlations coefficients were significant and above 0.3 ($p < 0.05$) for muscle activity measures and 14/19 were above 0.5 (74%).

The AUC with their 95% confidence interval (CI), as well as the other performance values, of each movement measure in each functional task are presented in **Tables 2–4**. For the angular amplitude measures, five comparisons between tasks out of 40 (13%) reported a difference of AUC above 0.1 (range 0.11–0.15). Performance to differentiate groups during sit-to-stand compared to flexion and lifting was higher for $ULSa_{range}$ (AUC of 0.74 compared to AUC of 0.63 and 0.59, respectively), but was lower for $LLSa_{range}$ (AUC of 0.6 compared to AUC of 0.75 for flexion and AUC of 0.72 for lifting). AUC was also lower during lifting (AUC of 0.66) compared to flexion (AUC of 0.77) for $LLSa_{flexion}$. Regarding angular velocity measures, 7 comparisons out of 42 (17%) reported a difference of AUC above 0.1 (range 0.11–0.14). For $LLSv_{flexion}$, differentiation performance was smaller during sit-to-stand (AUC of 0.76) compared to picking-up, lifting and flexion (0.87 ≤ AUC ≤0.90), and smaller during stepping-up (AUC of

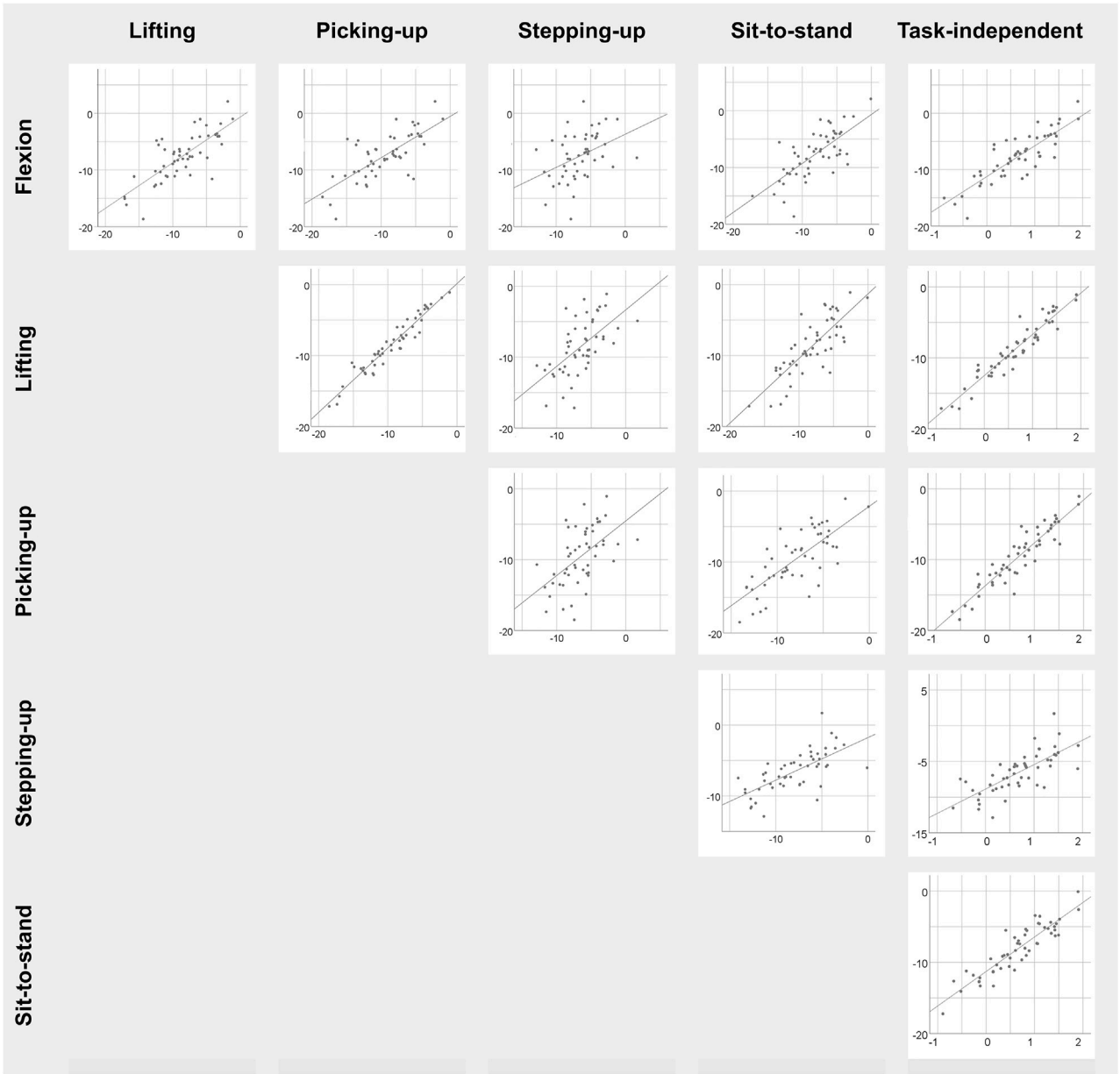

FIGURE 2 | Scatterplots of $LLSa_{flexion}$ among the five specific functional tasks as well as with respect to the task-independent $LLSa_{flexion}$ measure in patients with CLBP. Task-specific measures are in degree and task-independent measures are dimensionless.

0.79) compared to picking-up (AUC of 0.90). AUC during picking-up for $LLSv_{extension}$ (AUC of 0.88) was higher than during stepping-up (AUC of 0.75), and was also higher for $LLSv_{range}$ (AUC of 0.92) compared to stepping-up (AUC of 0.79) and sit-to-stand (AUC of 0.81). Five out of 14 comparisons (36%) for muscle activity measures reported a difference in AUC above 0.1 (range 0.13–0.17). AUC during stepping-up (AUC of 0.51) was lower than during picking-up, lifting and flexion ($0.64 \leq$ AUC ≤ 0.68) for EMG_{peak1}. For EMG_{peak2}, flexion and lifting had higher AUC (AUC of 0.60 and 0.59, respectively) compared to picking-up (AUC of 0.47).

Results from independent t-tests and ES regarding the differences in movement measures between groups are reported in **Figure 3** and **Supplementary Appendix SB**. Patients with CLBP moved with statistically significantly reduced $LLSa_{flexion}$ and $LLSa_{range}$ in all functional tasks compared to asymptomatic controls and all ES were moderate to large. At the ULS, $ULSa_{range}$ during picking-up, stepping-up and sit-to-stand were significantly reduced in patients with CLBP, with moderate to large ES for the three tasks. Angular velocity measures were all significantly reduced in patients with CLBP, and ES were at least large. For muscle activity measures,

TABLE 2 | Logistic regression models for angular amplitude measures. AUC: area under the curve [with its confidence interval (95%CI)]; r^2: coefficient of determination; Sn: sensitivity; Sp: specificity; LR+: positive likelihood ratio; LR−: negative likelihood ratio. Symbols ($^{\circ, \S, \#, *}$) indicate a difference of AUC >0.1 between two tasks or between a specific-task and the task–independent measure.

Variable	Task	AUC	95%CI			r^2	Sn	Sp	LR+	LR-
$LLSa_{flexion}$	Flexion	0.77°	0.64	—	0.9	0.25	92.3	25	1.23	0.31
	Lifting	0.66°	0.5	—	0.81	0.1	100	5.3	1.06	0
	Picking-up	0.69	0.54	—	0.84	0.16	96.1	26.3	1.3	0.15
	Stepping-up	0.67	0.52	—	0.82	0.14	98	26.3	1.33	0.08
	Sit-to-stand	0.7	0.56	—	0.84	0.17	98.1	25	1.31	0.08
	Task–independent	0.71	0.58	—	0.85	0.18	94.2	35	1.45	0.17
$LLSa_{range}$	Flexion	0.75$^{\#}$	0.62	—	0.89	0.26	94.2	40	1.57	0.15
	Lifting	0.72§	0.57	—	0.87	0.22	94.2	26.3	1.28	0.22
	Picking-up	0.68	0.54	—	0.82	0.17	96.1	21.1	1.22	0.18
	Stepping-up	0.65	0.51	—	0.8	0.11	96.1	15.8	1.14	0.25
	Sit-to-stand	0.60$^{\# \S *}$	0.45	—	0.75	0.05	100	10	1.11	0
	Task–independent	0.71*	0.57	—	0.86	0.22	98.1	30	1.4	0.06
$ULSa_{flexion}$	Flexion	0.56	0.42	—	0.7	0.01	100	0	1	-
	Lifting	0.57	0.43	—	0.71	0.02	100	0	1	-
	Picking-up	0.59	0.44	—	0.73	0.03	100	0	1	-
	Stepping-up	0.59	0.45	—	0.74	0.05	100	5	1.05	0
	Sit-to-stand	0.61	0.46	—	0.75	0.05	100	5	1.05	0
	Task–independent	0.59	0.45	—	0.74	0.03	100	0	1	-
$ULSa_{range}$	Flexion	0.63$^{\#}$	0.49	—	0.76	0.06	98.1	0	0.98	-
	Lifting	0.59$^{\S *}$	0.45	—	0.74	0.04	100	0	1	-
	Picking-up	0.69	0.56	—	0.83	1.77	96.2	30	1.37	0.13
	Stepping-up	0.67	0.54	—	0.8	0.12	96.2	20	1.2	0.19
	Sit-to-stand	0.74$^{\# \S}$	0.61	—	0.87	0.22	96.2	30	1.11	0
	Task–independent	0.7*	0.57	—	0.83	0.16	96.2	20	1.2	0.2

EMG_{peak1} during flexion and lifting was significantly higher in patients with CLBP. ES ranged from 0.18 to 0.6 for EMG_{peak1} and from 0.02 to 0.42 for EMG_{peak2}.

Task–independent measures reported AUC between 0.59 and 0.71, between 0.88 and 0.94 and between 0.55 and 0.64 for angular amplitude, angular velocity and muscle activity measures, respectively. Compared to each task, performance to differentiate groups for task–independent measures was superior (AUC difference >0.1) in 7/52 cases (13%) and was not different (AUC difference ≤0.1) in 45/52 cases (87%) (**Tables 2–4**). Correlation coefficients between task-independent and task-specific measures were large for angular amplitudes (range 0.63–0.95, all $p < 0.001$), angular velocities (range 0.74–0.92, all $p < 0.001$) and muscle activities (range 0.70–0.93, all $p < 0.001$) (**Supplementary Appendix SC**). Groups differences were statistically significant for $LLSa_{flexion}$, $LLSa_{range}$, $ULSa_{range}$ and for all angular velocity measures. ES for angular amplitude measures ranged from 0.33 to 0.97, for angular velocity measures from 1.54 to 2.36 and for muscle activity measures from 0.07 to 0.51 (**Figure 3** and **Supplementary Appendix SB**).

DISCUSSION

The correlation and capacity to differentiate patients from controls results indicated a limited influence of the tasks on the information carried by spinal movement measures and highlighted an individual spinal movement signature. This study also showed the construct validity of task–independent measures of spinal movement, and encouraged its consideration in future research. These important findings are discussed in the following sections.

Consistency of Spinal Movement in Different Tasks

Ninety-two percent of the measures were significantly correlated between different functional tasks in patients with CLBP, with correlation coefficients demonstrating at least a medium effect (r ≥ 0.3). The coefficients were even large in 70, 41 and 76% of angular amplitude, angular velocity and muscle activity measures, respectively. Correlation coefficients tended to be larger for peak flexion angle at the lower ($LLSa_{flexion}$) and upper lumbar spine ($ULSa_{flexion}$), which is consistent with what was found in asymptomatic individuals (Alqhtani et al., 2015; Seerden et al., 2019). Interestingly, the present study also demonstrated individual consistency in lumbar angular velocity and in the level of muscle activity, suggesting that the consistency across tasks is not limited to angular amplitudes as previously shown (Alqhtani et al., 2015; Seerden et al., 2019). Correlation coefficients were very large between analogous functional tasks, such as lifting and picking-up, but consistency was also observed between differing tasks, such as flexion and sit-to-stand. While the large standard deviation in most measures of spinal movement in patients with CLBP showed heterogeneity between participants, the correlations between tasks demonstrated consistency within patients.

These findings support an individual spinal movement signature in the sagittal plane in patients with CLBP, suggesting

TABLE 3 | Logistic regression models for angular velocity measures. AUC: area under the curve [with its confidence interval (95%CI)]; r^2: coefficient of determination; Sn: sensitivity; Sp: specificity; LR+: positive likelihood ratio; LR–: negative likelihood ratio. Symbols ($^{\circ, \S, \#, *}$) indicate a difference of AUC >0.1 between two tasks or between a specific-task and the task–independent measure.

Variable	Task	AUC	95%CI			r^2	Sn	Sp	LR+	LR–
$LLSv_{flexion}$	Flexion	0.89°	0.8	—	0.97	0.45	94.2	50	1.88	0.12
	Lifting	0.87$^{\#}$	0.79	—	0.96	0.45	92.3	52.6	1.95	0.15
	Picking-up	0.9§	0.82	—	0.98	0.59	94.1	63.2	2.56	0.09
	Stepping-up	0.79$^{*\ \S}$	0.66	—	0.91	0.3	94.1	42.1	1.63	0.14
	Sit-to-stand	0.76$^{\circ\ \#\ \S\ *}$	0.62	—	0.9	0.29	96.2	40	1.6	0.09
	Task–independent	0.9*	0.82	—	0.99	0.54	96.2	55	2.14	0.07
$LLSv_{extension}$	Flexion	0.85	0.75	—	0.95	0.41	96.2	50	1.92	0.08
	Lifting	0.84	0.74	—	0.94	0.38	94.2	42.1	1.63	0.14
	Picking-up	0.88°	0.79	—	0.97	0.56	94.1	63.2	2.56	0.09
	Stepping-up	0.75$^{\circ\ *}$	0.62	—	0.88	0.2	92	26.3	1.25	0.3
	Sit-to-stand	0.8	0.67	—	0.92	0.37	94.1	52.6	1.99	0.11
	Task–independent	0.88*	0.79	—	0.97	0.52	96.2	55	2.14	0.07
$LLSv_{range}$	Flexion	0.88	0.78	—	0.97	0.48	96.2	55	2.14	0.07
	Lifting	0.89	0.82	—	0.97	0.49	92.3	52.6	1.95	0.15
	Picking-up	0.92°	0.85	—	0.99	0.62	96.1	57.9	2.28	0.07
	Stepping-up	0.79$^{\circ\ *}$	0.66	—	0.92	0.31	92.2	36.8	1.46	0.21
	Sit-to-stand	0.81$^{\circ\ \S}$	0.7	—	0.93	0.39	98.1	50	1.96	0.04
	Task–independent	0.92$^{*\ \S}$	0.85	—	0.99	0.55	96.2	50	1.92	0.08
$ULSv_{flexion}$	Flexion	0.88	0.8	—	0.96	0.51	92.3	55	2.05	0.14
	Lifting	0.93	0.85	—	1	0.67	96.2	78.9	4.56	0.05
	Picking-up	0.85	0.75	—	0.95	0.45	92.3	50	1.85	0.15
	Task–independent	0.94	0.88	—	1	0.69	94.2	65	2.69	0.1
$ULSv_{extension}$	Flexion	0.83	0.73	—	0.92	0.3	92.3	40	1.54	0.19
	Lifting	0.82	0.71	—	0.92	0.27	92.3	17.6	1.12	0.44
	Picking-up	0.83	0.74	—	0.92	0.38	90.4	35	1.39	0.27
	Task–independent	0.88	0.8	—	0.95	0.45	88.5	55	1.97	0.2
$ULSv_{range}$	Flexion	0.87	0.79	—	0.96	0.45	92.3	50	1.85	0.15
	Lifting	0.92	0.85	—	0.99	0.61	92.3	73.7	3.51	0.1
	Picking-up	0.88	0.8	—	0.96	0.51	92.3	65	2.64	0.12
	Task–independent	0.94	0.88	—	0.99	0.66	90.4	70	3.01	0.1

TABLE 4 | Logistic regression models for lumbar muscle activity measures. AUC: area under the curve [with its confidence interval (95%CI)]; r^2: coefficient of determination; Sn: sensitivity; Sp: specificity; LR+: positive likelihood ratio; LR–: negative likelihood ratio. Symbols ($^{\circ, \S, \#, *}$) indicate a difference of AUC >0.1 between two tasks or between a specific-task and the task–independent measure.

Variable	Task	AUC	95%CI			r^2	Sn	Sp	LR+	LR-
EMG_{peak1}	Flexion	0.68°	0.54	—	0.82	0.11	98.1	0	0.98	—
	Lifting	0.68§	0.5	—	0.82	0.1	98	0	0.98	-
	Picking-up	0.64$^{\#}$	0.5	—	0.78	0.09	100	0	1	—
	Stepping-up	0.51$^{\circ\ \S\ \#\ *}$	0.35	—	0.66	0.01	100	0	1	—
	Sit-to-stand	0.6	0.45	—	0.76	0.02	100	0	1	—
	Task–independent	0.64*	0.5	—	0.78	0.08	98.1	0	0.98	—
EMG_{peak2}	Flexion	0.6°	0.44	—	0.75	0.05	98	5	1.03	0.4
	Lifting	0.59§	0.44	—	0.74	0.03	97.9	0	0.98	—
	Picking-up	0.47$^{\circ\ \S}$	0.32	—	0.61	0	100	0	1	—
	Task–independent	0.55	0.41	—	0.7	0	100	0	1	—

that each individual has a consistent spinal movement across tasks. These results questioned the need to analyze multiple tasks involving primarily sagittal-plane movement independently and the need to investigate new primarily sagittal-plane functional tasks in future studies, as those may lead to redundant data, therefore complexifying the procedure without gaining information to improve our understanding of spinal movement in CLBP (Papi et al., 2018; Moissenet et al., 2021). These findings also suggest that spinal movement is probably more influenced by individual factors than by the tasks. However, which individual factors are associated with the spinal movement signature is still unclear. Previous research in patients with LBP reported association between spinal kinematics and pain intensity, psychological characteristics, sex, age and BMI, among others (Mitchell et al., 2008; Arshad et al., 2019; Christe et al., 2021). However, these factors demonstrated only small associations with spinal movement, suggesting that other unknown factors are in play. Consequently, further research is needed to better understand which factors influence the spinal movement signature in patients with CLBP.

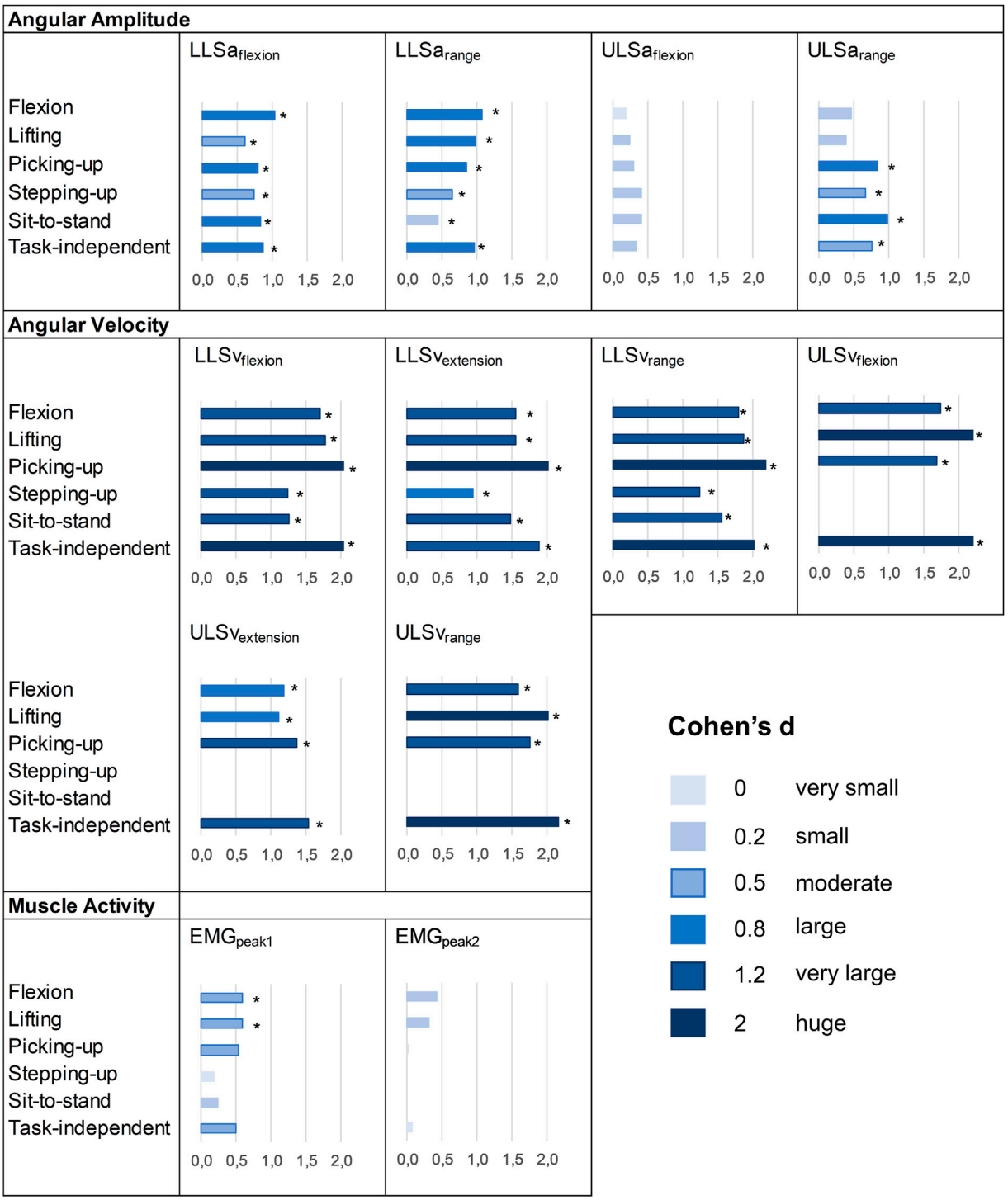

FIGURE 3 | Effect sizes of the differences between patients with CLBP and asymptomatic controls. *: p-value<0.05 at t-tests. No ES means that the variable was not available because there was no characteristic pattern (see Data processing).

Difference in Performance to Differentiate Groups Between Functional Tasks

The functional tasks had little influence on the performance to differentiate patients with CLBP from asymptomatic controls. Less than 20% of the comparisons demonstrated a difference in AUC between tasks larger than 0.1. For angular amplitude measures, performance to differentiate patients from controls was consistent across the tasks in 79% of the comparisons.

Independent t-tests, ES and other outcomes of models' performance also supported these findings. When there was a difference, it was in the ranges of motion and not the peak amplitudes. However, differences were inconsistent among tasks, as sit-to-stand demonstrated higher performance at the $ULSa_{range}$ and poorer performance at the $LLSa_{range}$ compared to flexion and lifting. Regarding angular velocity measures, AUC did not differ substantially in 83% of the comparisons. When it differed, it consistently showed poorer performance during sit-to-stand and stepping-up. Although stepping-up and sit-to-stand also reported mostly very large effect sizes, their capacity to differentiate groups was smaller compared to flexion, lifting and picking-up. Regarding muscle activity measures, the capacity to differentiate groups was poor in all tasks and ES were moderate at most. The performance to differentiate groups was poorer during stepping-up for EMG_{peak1} and during picking-up for EMG_{peak2}.

Globally, these observations indicate that assessing a range of functional tasks in the sagittal-plane may provide similar findings in terms of differentiating patients with CLBP from asymptomatic controls. The differences found between sit-to-stand and stepping-up compared to flexion, lifting and picking-up for angular velocity measures may be explained by the fact that participants with CLBP rated flexion, lifting and picking-up as more painful and more harmful for the back than stepping-up and sit-to-stand. The perceived harm might have led to increased pain-related fear and, together with the higher pain intensity, influenced angular velocity. Yet, these differences did not seem to consistently influence the angular amplitudes, questioning the effect of pain intensity and pain-related fear on lumbar angular amplitude. These findings are in line with a recent meta-analysis that showed a very small association between pain-related fear or pain intensity and spinal angular amplitudes, which was consistent across a wide range of tasks and measures of spinal angular amplitude (Christe et al., 2021). Therefore, although this study showed a redundancy among the tasks, it is possible that some functional tasks may be more sensitive, for example with respect to pain intensity or pain-related fear. In this regard, some authors suggested that selecting a specific task for each individual based on their identified limitations could be helpful when analyzing the relationships between spinal movement and patient-related outcomes (Wernli et al., 2020a). It is currently unknown if selecting one sagittal-plane task based on the individual limitation would be more appropriate to analyze such relationships and future studies should address this gap. If it would be the case, this would support the assessment of one specific primarily sagittal-plane task; the others tasks complexifying the procedure in vain (without brining supplementary information). If not, this might support the use of task–independent measures as discussed below.

Task–Independent Measures of Spinal Movement

In this study, we showed the possibility and potential of averaging spinal movement measures across different functional tasks. Averaging spinal movement measures across multiple tasks was particularly supported by the individual spinal movement signature found in this study. The performance to differentiate groups was higher or did not differ compared to individual tasks in all the measures. Furthermore, angular velocity task–independent measures showed a high performance to differentiate groups, with statistically significant differences between the groups and very large to huge ES. ES were also large for the angular amplitude measures at the lower lumbar spine. Therefore, these results support the construct validity of task–independent measures of spinal movement and its consideration in future research.

Using an "average" measure across different tasks may have some interest in future studies. The method we used is simple as it consisted in averaging the Z-scores of each of the task, which could be easily replicated with any other biomechanical model or measure. These task–independent measures could notably be more robust because they are not reliant on a single task.

Nevertheless, future research is strongly recommended to determine the value of task–independent measures. Based on this study, it is not known if task–independent measures can provide more information than task-specific measures, nor how many movements should be averaged. Furthermore, reliability of averaging spinal movement measures from different functional tasks remains to be tested. While the method of averaging tasks using Z-scores has the advantage of its simplicity, other more advanced methods to group spinal movement measures (i.e., machine learning methods) will also need to be investigated.

Capacity to Differentiate Patients With CLBP From Asymptomatic Controls

While it was not the objective of this study, the capacity of spinal movement measures to differentiate patients with CLBP from asymptomatic controls is worth discussing. First, patients with CLBP moved with reduced sagittal-plane lumbar amplitude and range of motion at the lower lumbar spine, in all functional tasks. ES were moderate to large. However, the low specificity and LR + suggested that small amplitudes are also frequent in asymptomatic controls. Second, angular velocity measures demonstrated very large ES in the majority of the tasks, which were always larger than the ES from angular amplitude or lumbar muscle activity measures. The capacity of angular velocity measures to differentiate patients from controls was even rated as outstanding for flexion, lifting and picking-up. The high sensitivity and very low LR– in all tasks showed that moving with high angular velocity was very rare in our sample of patients with CLBP, suggesting that moving at high angular velocity is very difficult with CLBP. Third, selected peaks of erector spinae activity demonstrated poor performance to differentiate groups. There were only two muscle activity measures that showed a statistically significant difference between the groups, and most ES were small. These findings are in agreement with previous studies analyzing erector spinae activity during dynamic tasks and reporting inconsistent results (Geisser et al., 2005). Yet, when a difference in muscle activity was observed between groups, it corresponded to higher levels of activity in patients with CLBP.

Overall, based on the present findings and previous reports (Shum et al., 2005; Laird et al., 2014; Christe et al., 2016b, 2020; Papi et al., 2018; Moissenet et al., 2021), reduced lumbar amplitude and

angular velocity seems to be key characteristics of patients with CLBP. Furthermore, the consistent reduced sagittal-plane lumbar angular amplitude and velocity across all the functional tasks suggest that these spinal movement alterations generalize across a wide range of daily-life activities. Our results thus support the measurement of lumbar angular amplitude and angular velocity in any functional task in future studies. Nevertheless, there is an urgent need for well-conducted longitudinal studies to detangle if and how spinal kinematic changes are associated with patients' changes in pain and disability (Wernli et al., 2020b; Schmid et al., 2021).

Limitations

This study has some limitations that are important to discuss. First, the asymptomatic population was small, despite a number of participants above the minimum indicated by the sample size calculation (Portney and Watkins, 2000). While the number of participants had certainly little influence on the task comparisons, the performance values from the logistic regression models should be confirmed with larger groups. Second, the findings may not be transferable to all patients with CLBP. Although our results are consistent with current knowledge in the field, patients with CLBP included in this study had high levels of disability, pain-related fear and catastrophizing that are common in patients participating to interdisciplinary rehabilitation programs. These individual factors may have influenced the large differences found between the groups. Third, the tasks were not assessed in random order. Therefore, the higher level of pain found during picking-up and lifting may be related to the fact that these two tasks were collected last (order effect). Fourth, the video recordings used to present the daily-life tasks may have influenced how participants performed the tasks, requesting caution when interpreting the findings in the context of movement behavior. Video recordings were used to give standardized instructions and avoid differences in the ways of completing the tasks. This was particularly important for picking-up and lifting, as these tasks can be performed in different ways (i.e., stoop or squat). While the instructions could have limited inter-individual variability, large variations were observed among individuals, suggesting that participants were not too constrained and could express their individual movement signature. On the other hand, one cannot exclude that more pronounced signatures could have been observed if the tasks would have been less standardized. Finally, this study focused on sagittal-plane lumbar biomechanics during functional tasks primarily involving sagittal-plane movements, because this corresponds to the alterations the most frequently reported in literature and because patients often complain of movement-related pain in primarily sagittal-plane activities. Therefore, it has yet to be determined if other functional tasks with larger solicitations in the frontal and/or transverse–planes, such as gait (Christe et al., 2017; Schmid et al., 2017), would display individual movement signatures in these other planes or even three-dimensionally.

CONCLUSION

This study showed that individuals with CLBP have consistent spinal movement in the sagittal plane across different functional tasks, supporting the existence of an individual biomechanical signature. Furthermore, the capacity to differentiate patients with CLBP from asymptomatic controls did not differ between functional tasks in most of the cases. Therefore, this study highlighted a redundancy among tasks, questioning the most appropriate measures to describe spinal movement behavior in the framework of CLBP. While further research will be necessary in this regard, this study showed the feasibility of task-independent measures, a promising approach towards an effective quantification of spinal movement.

DATA AVAILABILITY STATEMENT

The raw data supporting the conclusion of this article will be made available by the authors, without undue reservation.

ETHICS STATEMENT

The studies involving human participants were reviewed and approved by Research Ethics Committee of VAUD (CER-VD 2018-00188). The patients/participants provided their written informed consent to participate in this study.

AUTHOR CONTRIBUTIONS

GC contributed to the conception of the study, collected the data, analyzed the data, interpreted the results and wrote the initial manuscript. CA processed all the data and edited the manuscript. BJ participated to the conception of the study, edited the manuscript and supervised the project. JF contributed to the conception of the study, interpreted the results, edited the manuscript and supervised the project. All authors approved the final version of the manuscript. Both BJ and JF supervised this research and should be considered as last authors.

FUNDING

This project was partly supported by a grant from the University of Applied Sciences and Arts Western Switzerland//HES-SO, Faculty of Health Science.

ACKNOWLEDGMENTS

We would like to thanks Valentina Pizzolato and Benjamin Coty for their important contribution in markers' tracking and data management.

SUPPLEMENTARY MATERIAL

The Supplementary Material for this article can be found online at: https://www.frontiersin.org/articles/10.3389/fbioe.2021.767974/full#supplementary-material

REFERENCES

Alqhtani, R. S., Jones, M. D., Theobald, P. S., and Williams, J. M. (2015). Correlation of Lumbar-Hip Kinematics Between Trunk Flexion and Other Functional Tasks. *J. Manipulative Physiol. Ther.* 38, 442–447. doi:10.1016/j.jmpt.2015.05.001

Arshad, R., Pan, F., Reitmaier, S., and Schmidt, H. (2019). Effect of Age and Sex on Lumbar Lordosis and the Range of Motion. A Systematic Review and Meta-Analysis. *J. Biomech.* 82, 1–19. doi:10.1016/j.jbiomech.2018.11.022

Bujang, M. A., and Baharum, N. (2016). Sample Size Guideline for Correlation Analysis. *World J. Soc. Sci.* 3, 37. doi:10.22158/wjssr.v3n1p37

Chapman, J. R., Norvell, D. C., Hermsmeyer, J. T., Bransford, R. J., DeVine, J., McGirt, M. J., et al. (2011). Evaluating Common Outcomes for Measuring Treatment Success for Chronic Low Back Pain. *Spine.* 36, S54–S68. doi:10.1097/BRS.0b013e31822ef74d

Christe, G., Crombez, G., Edd, S., Opsommer, E., Jolles, B. M., and Favre, J. (2021). Relationship Between Psychological Factors and Spinal Motor Behaviour in Low Back Pain: a Systematic Review and Meta-Analysis. *Pain.* 162, 672–686. doi:10.1097/j.pain.0000000000002065

Christe, G., Jolles, B. M., and Favre, J. (2019). "Variability of Lumbar Flexion Angle During a Pick up Task in Patients With Chronic Low Back Pain," in *World Conference on Low Back Pain* (Antwerp).

Christe, G., Kade, F., Jolles, B. M., and Favre, J. (2017). Chronic Low Back Pain Patients Walk With Locally Altered Spinal Kinematics. *J. Biomech.* 60, 211–218. doi:10.1016/j.jbiomech.2017.06.042

Christe, G., Redhead, L., Jolles-Haeberli, B., and Favre, J. (2016a). Correlation of Regional Lumbar Kinematics Between Forward Flexion and Functional Activities in Patients With Chronic Low Back Pain. *Man. Ther.* 25, e78. doi:10.1016/j.math.2016.05.127

Christe, G., Redhead, L., Legrand, T., Jolles, B. M., and Favre, J. (2016b). Multi-segment Analysis of Spinal Kinematics During Sit-To-Stand in Patients With Chronic Low Back Pain. *J. Biomech.* 49, 2060–2067. doi:10.1016/j.jbiomech.2016.05.015

Christe, G., Rochat, V., Jolles, B. M., and Favre, J. (2020). Lumbar and Thoracic Kinematics during Step-up: Comparison of Three-Dimensional Angles between Patients With Chronic Low Back Pain and Asymptomatic Individuals. *J. Orthop. Res.* 38, 1248–1256. doi:10.1002/jor.24575

Cohen, J. (1988). *Statistical Power Analysis for the Behavioral Sciences*. Hillsdale, N.J.: L. Erlbaum Associates. Available at: http://www.amazon.com/books/dp/0805802835.

Dankaerts, W., O'Sullivan, P. B., Burnett, A. F., Straker, L. M., and Danneels, L. A. (2004). Reliability of EMG Measurements for Trunk Muscles During Maximal and Sub-Maximal Voluntary Isometric Contractions in Healthy Controls and CLBP Patients. *J. Electromyogr. Kinesiol.* 14, 333–342. doi:10.1016/j.jelekin.2003.07.001

Dankaerts, W., O'Sullivan, P., Burnett, A., Straker, L., Davey, P., and Gupta, R. (2009). Discriminating Healthy Controls and Two Clinical Subgroups of Nonspecific Chronic Low Back Pain Patients Using Trunk Muscle Activation and Lumbosacral Kinematics of Postures and Movements. *Spine.* 34, 1610–1618. doi:10.1097/BRS.0b013e3181aa6175

Dubois, J.-D., Abboud, J., St-Pierre, C., Piché, M., and Descarreaux, M. (2014). Neuromuscular Adaptations Predict Functional Disability Independently of Clinical Pain and Psychological Factors in Patients With Chronic Non-Specific Low Back Pain. *J. Electromyogr. Kinesiol.* 24, 550–557. doi:10.1016/j.jelekin.2014.04.012

Dupeyron, A., Demattei, C., Kouyoumdjian, P., Missenard, O., Micallef, J. P., and Perrey, S. (2013). Neuromuscular Adaptations After a Rehabilitation Program in Patients With Chronic Low Back Pain: Case Series (Uncontrolled Longitudinal Study). *BMC Musculoskelet. Disord.* 14, 277. doi:10.1186/1471-2474-14-277

Fairbank, J. C. T., and Pynsent, P. B. (2000). The Oswestry Disability Index. *Spine.* 25, 2940–2953. doi:10.1097/00007632-200011150-00017

Geisser, M. E., Ranavaya, M., Haig, A. J., Roth, R. S., Zucker, R., Ambroz, C., et al. (2005). A Meta-Analytic Review of Surface Electromyography Among Persons With Low Back Pain and Normal, Healthy Controls. *The J. Pain.* 6, 711–726. doi:10.1016/j.jpain.2005.06.008

Ghasemi, A., and Zahediasl, S. (2012). Normality Tests for Statistical Analysis: A Guide for Non-Statisticians. *Int. J. Endocrinol. Metab.* 10, 486–489. doi:10.5812/ijem.3505

Grood, E. S., and Suntay, W. J. (1983). A Joint Coordinate System for the Clinical Description of Three-Dimensional Motions: Application to the Knee. *J. Biomech. Eng.* 105, 136–144. doi:10.1115/1.3138397

Hidalgo, B., Gilliaux, M., Poncin, W., and Detrembleur, C. (2012). Reliability and Validity of a Kinematic Spine Model During Active Trunk Movement in Healthy Subjects and Patients With Chronic Non-Specific Low Back Pain. *J. Rehabil. Med.* 44, 756–763. doi:10.2340/16501977-1015

Hosmer, D., Lemeshow, S., and Sturdivant, R. (2013). *Applied Logistic Regression*. Third edit. New York, NY: Wiley NJ.

Kadaba, M. P., Ramakrishnan, H. K., Wootten, M. E., Gainey, J., Gorton, G., and Cochran, G. V. B. (1989). Repeatability of Kinematic, Kinetic, and Electromyographic Data in normal Adult Gait. *J. Orthop. Res.* 7, 849–860. doi:10.1002/jor.1100070611

Laird, R. A., Gilbert, J., Kent, P., and Keating, J. L. (2014). Comparing Lumbo-Pelvic Kinematics in People With and Without Back Pain: a Systematic Review and Meta-Analysis. *BMC Musculoskelet. Disord.* 15, 229. doi:10.1186/1471-2474-15-229

Lima, M., Ferreira, A. S., Reis, F. J. J., Paes, V., and Meziat-Filho, N. (2018). Chronic Low Back Pain and Back Muscle Activity During Functional Tasks. *Gait & Posture.* 61, 250–256. doi:10.1016/j.gaitpost.2018.01.021

Marras, W. S., Lavender, S. A., Leurgans, S. E., Fathallah, F. A., Ferguson, S. A., Gary Allread, W., et al. (1995). Biomechanical Risk Factors for Occupationally Related Low Back Disorders. *Ergonomics.* 38, 377–410. doi:10.1080/00140139508925111

Matheve, T., De Baets, L., Bogaerts, K., and Timmermans, A. (2019). Lumbar Range of Motion in Chronic Low Back Pain Is Predicted by Task-Specific, but Not by General Measures of Pain-related Fear. *Eur. J. Pain.* 23, 1171–1184. doi:10.1002/ejp.1384

Mitchell, T., O'Sullivan, P. B., Burnett, A. F., Straker, L., and Smith, A. (2008). Regional Differences in Lumbar Spinal Posture and the Influence of Low Back Pain. *BMC Musculoskelet. Disord.* 9, 152. doi:10.1186/1471-2474-9-152

Moissenet, F., Rose-Dulcina, K., Armand, S., and Genevay, S. (2021). A Systematic Review of Movement and Muscular Activity Biomarkers to Discriminate Non-Specific Chronic Low Back Pain Patients From an Asymptomatic Population. *Sci. Rep.* 11, 1–14. doi:10.1038/s41598-021-84034-x

O'Sullivan, P. (2005). Diagnosis and Classification of Chronic Low Back Pain Disorders: Maladaptive Movement and Motor Control Impairments as Underlying Mechanism. *Man. Ther.* 10, 242–255. doi:10.1016/j.math.2005.07.001

Papi, E., Bull, A. M. J., and McGregor, A. H. (2018). Is There Evidence to Use Kinematic/kinetic Measures Clinically in Low Back Pain Patients? A Systematic Review. *Clin. Biomech.* 55, 53–64. doi:10.1016/j.clinbiomech.2018.04.006

Portney, L. G., and Watkins, M. P. (2000). *Foundations of Clinical Research: Applications to Practice*. Upper Saddle River, NJ: Prentice Hall Health.

Sawilowsky, S. S. (2009). New Effect Size Rules of Thumb. *J. Mod. App. Stat. Meth.* 8, 597–599. doi:10.22237/jmasm/1257035100

Schmid, S., Bangerter, C., Schweinhardt, P., and Meier, M. L. (2021). Identifying Motor Control Strategies and Their Role in Low Back Pain: A Cross-Disciplinary Approach Bridging Neurosciences With Movement Biomechanics. *Front. Pain Res.* 2, 1–8. doi:10.3389/fpain.2021.715219

Schmid, S., Bruhin, B., Ignasiak, D., Romkes, J., Taylor, W. R., Ferguson, S. J., et al. (2017). Spinal Kinematics During Gait in Healthy Individuals Across Different Age Groups. *Hum. Movement Sci.* 54, 73–81. doi:10.1016/j.humov.2017.04.001

Seay, J., Selbie, W. S., and Hamill, J. (2008). In Vivolumbo-Sacral Forces and Moments During Constant Speed Running at Different Stride Lengths. *J. Sports Sci.* 26, 1519–1529. doi:10.1080/02640410802298235

Seerden, S. F. L., Dankaerts, W., Swinnen, T. W., Westhovens, R., de Vlam, K., and Vanwanseele, B. (2019). Multi-Segment Spine and Hip Kinematics in Asymptomatic Individuals During Standardized Return From Forward Bending Versus Functional Box Lifting. *J. Electromyogr. Kinesiol.* 49, 102352. doi:10.1016/j.jelekin.2019.102352

Shum, G. L. K., Crosbie, J., and Lee, R. Y. W. (2005). Symptomatic and Asymptomatic Movement Coordination of the Lumbar Spine and Hip During an Everyday Activity. *Spine.* 30, E697–E702. doi:10.1097/01.brs.0000188255.10759.7a

Shum, G. L. K., Crosbie, J., and Lee, R. Y. W. (2007). Movement Coordination of the Lumbar Spine and Hip During a Picking up Activity in Low Back Pain Subjects. *Eur. Spine J.* 16, 749–758. doi:10.1007/s00586-006-0122-z

Sullivan, M. J. L., Bishop, S. R., and Pivik, J. (1995). The Pain Catastrophizing Scale: Development and Validation. *Psychol. Assess.* 7, 524–532. doi:10.1037/1040-3590.7.4.524

Vlaeyen, J. W. S., Kole-Snijders, A. M. J., Boeren, R. G. B., and van Eek, H. (1995). Fear of Movement/(re)injury in Chronic Low Back Pain and its Relation to Behavioral Performance. *Pain.* 62, 363–372. doi:10.1016/0304-3959(94)00279-N

Vogler, D., Paillex, R., Norberg, M., de Goumoëns, P., and Cabri, J. (2008). Validation Transculturelle de l'Oswestry Disability Index en Français. *Ann. de Réadaptation de Médecine Physique.* 51, 379–385. doi:10.1016/j.annrmp.2008.03.006

von Elm, E., Altman, D. G., Egger, M., Pocock, S. J., Gøtzsche, P. C., and Vandenbroucke, J. P. (2007). The Strengthening the Reporting of Observational Studies in Epidemiology (STROBE) Statement: Guidelines for Reporting Observational Studies. *The Lancet.* 370, 1453–1457. doi:10.1016/S0140-6736(07)61602-X

Wernli, K., O'Sullivan, P., Smith, A., Campbell, A., and Kent, P. (2020a). Movement, Posture and Low Back Pain. How Do They Relate? A Replicated Single-Case Design in 12 People With Persistent, Disabling Low Back Pain. *Eur. J. Pain.* 24, 1831–1849. doi:10.1002/ejp.1631

Wernli, K., Tan, J.-S., O'Sullivan, P., Smith, A., Campbell, A., and Kent, P. (2020b). Does Movement Change When Low Back Pain Changes? A Systematic Review. *J. Orthop. Sports Phys. Ther.* 50, 664–670. doi:10.2519/jospt.2020.9635

Wong, A. Y. L., Parent, E. C., Prasad, N., Huang, C., Chan, K. M., and Kawchuk, G. N. (2016). Does Experimental Low Back Pain Change Posteroanterior Lumbar Spinal Stiffness and Trunk Muscle Activity? A Randomized Crossover Study. *Clin. Biomech.* 34, 45–52. doi:10.1016/j.clinbiomech.2016.03.006

Conflict of Interest: The authors declare that the research was conducted in the absence of any commercial or financial relationships that could be construed as a potential conflict of interest.

frontiers in Bioengineering and Biotechnology

ORIGINAL RESEARCH
published: 18 November 2021
doi: 10.3389/fbioe.2021.751155

Walking Biomechanics and Spine Loading in Patients With Symptomatic Lumbar Spinal Stenosis

Seyed Javad Mousavi[1,2], *Andrew C. Lynch*[1], *Brett T. Allaire*[1], *Andrew P. White*[1,2] *and Dennis E. Anderson*[1,2]*

[1]*Department of Orthopaedic Surgery, Beth Israel Deaconess Medical Center, Boston, MA, United States,* [2]*Department of Orthopaedic Surgery, Harvard Medical School, Boston, MA, United States*

Symptomatic lumbar spinal stenosis is a leading cause of pain and mobility limitation in older adults. It is clinically believed that patients with lumbar spinal stenosis adopt a flexed trunk posture or bend forward and alter their gait pattern to improve tolerance for walking. However, a biomechanical assessment of spine posture and motion during walking is broadly lacking in these patients. The purpose of this study was to evaluate lumbar spine and pelvic sagittal angles and lumbar spine compressive loads in standing and walking and to determine the effect of pain and neurogenic claudication symptoms in patients with symptomatic lumbar spinal stenosis. Seven participants with symptomatic lumbar spinal stenosis, aged 44–82, underwent a 3D opto-electronic motion analysis during standing and walking trials in asymptomatic and symptomatic states. Passive reflective marker clusters (four markers each) were attached to participants at T1, L1, and S2 levels of the spine, with additional reflective markers at other spinal levels, as well as the head, pelvis, and extremities. Whole-body motion data was collected during standing and walking trials in asymptomatic and symptomatic states. The results showed that the spine was slightly flexed during walking, but this was not affected by symptoms. Pelvic tilt was not different when symptoms were present, but suggests a possible effect of more forward tilt in both standing ($p = 0.052$) and walking ($p = 0.075$). Lumbar spine loading during symptomatic walking was increased by an average of 7% over asymptomatic walking ($p = 0.001$). Our results did not show increased spine flexion (adopting a trunk-flexed posture) and only indicate a trend for a small forward shift of the pelvis during both symptomatic walking and standing. This suggests that provocation of symptoms in these patients does not markedly affect their normal gait kinematics. The finding of increased spine loading with provocation of symptoms supports our hypothesis that spine loading plays a role in limiting walking function in patients with lumbar spinal stenosis, but additional work is needed to understand the biomechanical cause of this increase.

Keywords: lumbar spinal stenosis, trunk posture, spine motion, compressive loading, optoelectronic motion capture, gait

OPEN ACCESS

Edited by:
Marwan El-Rich, Khalifa University, United Arab Emirates

Reviewed by:
Navid Arjmand, Sharif University of Technology, Iran
Judith Meakin, University of Exeter, United Kingdom

***Correspondence:**
Dennis E. Anderson
danders7@bidmc.harvard.edu

Specialty section:
This article was submitted to Biomechanics, a section of the journal Frontiers in Bioengineering and Biotechnology

Received: *31 July 2021*
Accepted: *06 October 2021*
Published: *18 November 2021*

Citation:
Mousavi SJ, Lynch AC, Allaire BT, White AP and Anderson DE (2021) Walking Biomechanics and Spine Loading in Patients With Symptomatic Lumbar Spinal Stenosis. Front. Bioeng. Biotechnol. 9:751155. doi: 10.3389/fbioe.2021.751155

INTRODUCTION

Lumbar spinal stenosis (LSS) is a common degenerative spinal condition with the prevalence of 19%–47% in adults over age 60, depending on the criteria used. Lumbar spinal stenosis is symptomatic in 10%–14% of the adult population, and its prevalence and associated health and economic consequences are expected to increase with the aging of the population (Katz and Harris, 2008; Kalichman et al., 2009; Ishimoto et al., 2012). The most common symptom attributed to LSS is neurogenic claudication characterized by pain and discomfort radiating from the spine to the legs along with sensory loss, fatigue, weakness, and balance problems (Katz and Harris, 2008; Suri et al., 2010). Limited tolerance for standing and walking is characteristic of symptomatic LSS and is the leading cause of disability and restricted mobility, and it is also the most frequent indication for spinal surgery, in patients over 65 years old (Deyo et al., 2010; Hijikata et al., 2020). LSS symptoms are often initiated or provoked by walking or prolonged standing, particularly when the lumbar spine is in extended (lordotic or upright) postures, and gradually aggravated to the point that the patient stops walking. Trunk flexion or bending forward can partially relieve the symptoms by reducing the magnitude of lumbar lordosis, increasing spinal canal diameter, and decompressing the nerves (Katz and Harris, 2008). Therefore, it is clinically believed that patients with LSS adopt a flexed (hunched) trunk posture or bend forward and alter their gait pattern to improve tolerance for walking (Katz and Harris, 2008). While these clinical observations are the basis for some of the therapeutic exercises and clinical recommendations to increase walking capacity in patients with LSS, they have not yet been scientifically tested and quantified.

A biomechanical assessment of spine posture and motion during walking is broadly lacking in patients with LSS, and the available results are not consistent (Toosizadeh et al., 2015; Wang et al., 2021). To the authors' knowledge and a recently published systematic review (Wang et al., 2021), only three studies investigated spine kinematics (postural angles) in patients with LSS during walking, and two of them reported kinetic variables including hip and knee flexion moments and paravertebral muscle activities (Kuwahara et al., 2016; Goto et al., 2017; Igawa et al., 2018). The study of Goto et al. (2017) is the only one that measured the spine flexion angle of five men and one woman with LSS during the beginning of treadmill walking and when leg symptoms appeared. Thoracic and pelvic angles (reflecting the absolute movement in space) were increased after walking, but the spine angle reflecting the relative movement between the thorax and pelvis did not significantly change when symptoms appeared.

The purpose of this study was to evaluate trunk posture, particularly lumbar spine and pelvis angles, and lumbar spine compressive loads in standing and walking and to determine the effect of pain and neurogenic claudication symptoms, in patients with symptomatic lumbar spinal stenosis. Optoelectronic motion analysis along with detailed musculoskeletal modeling have been recently implemented in healthy and patient populations to measure spine posture and motion and estimate spine loading during walking and activities of daily living (Schmid et al., 2016; Mousavi et al., 2018; Burkhart et al., 2020). Here, we utilize this methodology to characterize lumbar spine posture, pelvic tilt, and spine loading in patients with LSS during standing and walking and to determine whether these parameters change following provocation of neurogenic claudication symptoms.

We hypothesized that patients would display an increased trunk flexion posture and spine loading during walking and in the presence of claudication symptoms.

METHODS

Subjects

Seven participants aged 44–82, with symptomatic LSS confirmed by imaging and clinical examination, who were scheduled for spine decompression surgery (laminectomy with or without fusion) for lumbar spinal stenosis were recruited. Characteristics of the participants (four women and three men) are presented in **Table 1**. These were the mean ± SD of age: 64.4 ± 13.8 years, height: 164 ± 9.5 cm, body mass: 79 ± 29.8 kg, and BMI: 29.2 ± 3.8 kg/m^2. Participants were excluded if they had conditions (unrelated to LSS) that altered walking or spine function, such as history of traumatic spinal injury or surgery, vascular insufficiency, Parkinson's disease, stroke, or cognitive impairment. The study was approved by the Institutional Review Board of Beth Israel Deaconess Medical Center, and all patients provided written informed consent prior to participation.

Experimental Procedure

All patients underwent a 3D opto-electronic motion analysis during standing and walking trials between 2 and 10 days

TABLE 1 | Characteristics of the participants.

Participants	Age	Sex	Height (cm)	Weight (kg)	BMI (kg/m^2)	Surgery level	Pain at rest[a]	Pain after walking[a]	Walking capacity time (min)
1	50	F	166.3	73.3	26.5	L3–S1	3	6	30
2	82	F	158.9	79.9	31.7	L2–L5	8	10	2.4
3	73	M	170.6	100.5	34.5	L3–L5	3	6	15
4	44	M	172.7	72.5	24.3	L5–S1	2	4	17
5	66	F	149.8	71.1	31.7	L3–L5	5	7	3.8
6	75	F	155.8	62	25.5	L4–L5	1	2	1.7
7	61	M	175.2	93.4	30.4	L5–S1	3	8	1.7

[a]*Based on the Brief Pain Inventory (BPI) at rest and after walking capacity test. Zero (0) denotes no pain and 10 denotes the worst pain.*

TABLE 2 | Testing procedure and outcome measurements.

Asymptomatic state		Symptomatic state
Trunk posture	**Walking capacity test to provoke symptoms**	Trunk posture
Spine and hip motion		Spine and hip motion
Spine loading		Spine loading

before surgery. Passive reflective marker clusters (four markers each) were attached to participants at T1, L1, and S2 levels of the spine, with additional reflective markers at other thoracic and lumbar spinal levels, as well as the head, manubrium of the sternum, posterior superior iliac spines, shoulders, upper and lower arms and legs, and feet. The marker position was recorded by a motion analysis system (Vicon Motion Systems, Centennial, CO).

Tasks

Whole-body motion data was collected in asymptomatic and symptomatic states. Asymptomatic state refers to the state or time that participants did not experience any neurogenic claudication symptoms. Almost all of the participants experienced a range of back and/or leg pain during the relaxed sitting position, but they were able to distinguish this pain from the neurogenic claudication symptoms that are usually provoked during walking and forced them to stop or limit their walking. To produce the symptomatic state, participants performed a standard walking capacity test, walking over ground or on a motorized treadmill at a self-selected pace until reporting the onset of neurogenic claudication symptoms, up to a maximum of 30 min (Rainville et al., 2012). Time to onset of symptoms and distance walked were recorded. Participants reported their pain severity both before and after provocation based on the 10 Brief Pain Inventory. The following tasks were conducted in a consecutive order (**Table 2**): 1) static upright standing posture (asymptomatic), 2) walking at a self-selected pace without neurogenic claudication symptoms present (asymptomatic) (three trials), 3) walking after onset of neurogenic claudication symptoms (symptomatic) (three trials), and 4) static upright standing posture (symptomatic).

Data Processing and Musculoskeletal Modeling

A whole-body musculoskeletal model was created for each participant, incorporated with our established model of the thoracolumbar spine, and adjusted according to patient age, sex, height, weight, motion analysis measurements, and standing spine radiographs (Bruno et al., 2015; Bruno et al., 2017; Burkhart et al., 2020) (**Figure 1**). Base model was first adjusted according to anthropometrics and marker data in a neutral posture using the OpenSim scale tool (Delp et al., 2007). Lumbar spine curvature was assessed from the subject's pre-treatment standing radiograph (available from the online medical records); thoracic curvature (Cobb angle) was estimated based on our recently proposed regression equation using the participant's thoracic angle calculated from spine markers, age, and BMI, and intervertebral angles in the model were adjusted accordingly producing a subject-specific model (Hashemirad et al., 2013; Grindle et al., 2020). Measured marker data for standing and walking trials were applied to the subject-specific model to estimate movements of the spine and other body joints. Similar to prior studies, we applied kinematic constraints to limit spinal degrees of freedom

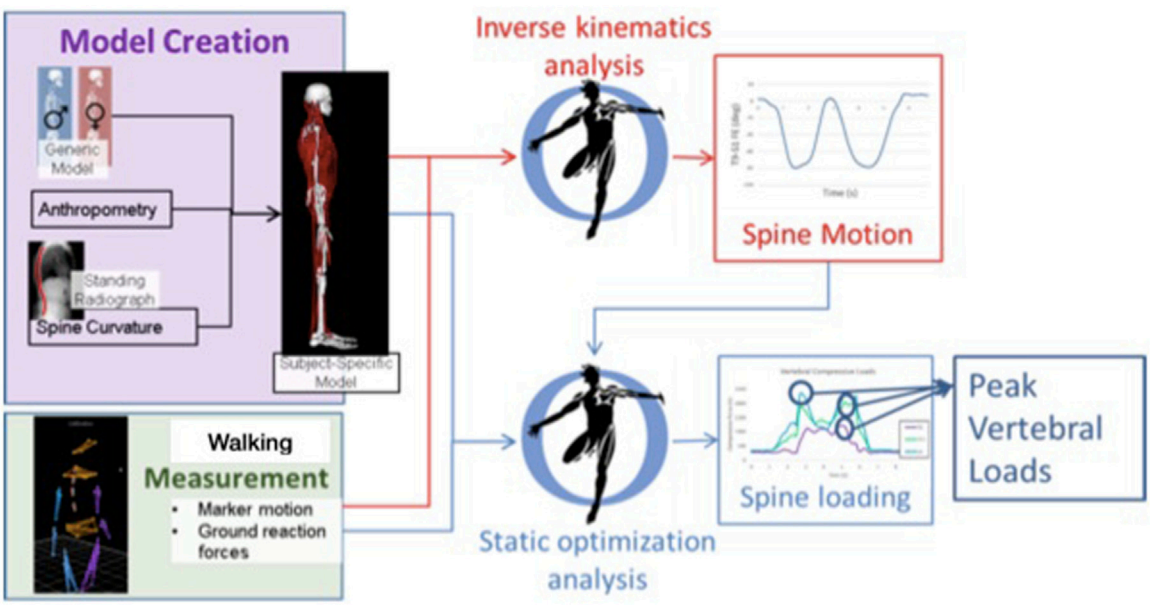

FIGURE 1 | Basic workflow for creating subject-specific musculoskeletal model to determine spine motion and loading. Walking trials were measured, and outcomes of body motion and loading were evaluated for a single gait cycle in each trial. Spine loading was evaluated during standing and walking trials.

TABLE 3 | Mean (SD) of average postural measurements (forward pelvic tilt, spinal flexion, and pelvic tilt + spinal flexion) relative to asymptomatic neutral standing, in asymptomatic walking, symptomatic walking, and symptomatic neutral standing.

	Asymptomatic walking	Symptomatic walking	Symptomatic neutral standing
Pelvic tilt (°)	0.7 (4.5)	1.2 (4.3)[c]	1.1 (1.2)[b]
Spine flexion (°)	3.4 (3.4)[a]	3.4 (2.6)[a]	−1.4 (2.9)
Pelvic tilt + spine flexion (°)	4.1 (2.6)[a]	4.6 (3.2)[a]	−0.3 (2.6)

[a]*Different than 0 (*p *< 0.05).*
[b]*Different than 0 (*p *= 0.052).*
[c]*Different than asymptomatic walking (*p *= 0.075).*

when evaluating spinal motion (Actis et al., 2018; Ignasiak et al., 2018; Beaucage-Gauvreau et al., 2019; Alemi et al., 2021). We allowed six spinal degrees of freedom in our models, two each in flexion-extension, lateral bending, and axial rotation, which produces realistic, repeatable spine motions from motion analysis data with relatively low marker error (Alemi et al., 2021). With this, the flexion-extension motion of the spine has two independent coordinates applied to sections T1–T9 and T9–S1, respectively, and the reported spine flexion outcome in this study is the flexion of the T9–S1 segment of the spine (Alemi et al., 2021). An inverse kinematics analysis was performed to evaluate body positions during standing and walking, including lumbar flexion/extension angles and pelvic anterior/posterior tilt. Kinematics were applied in a static optimization analysis to solve for muscle and joint loads, and thereby lumbar spine compressive loading, during standing and walking trials. The magnitude of peak compressive load within each subject was evaluated as the average of the peak load at all lumbar vertebral levels. The outcomes of pelvic tilt, spine flexion, pelvic tilt plus spine flexion, and lumbar compressive load were then averaged across one gait cycle. Postural outcomes were referenced to the asymptomatic neutral standing trial. Secondary outcomes of peak angle and ROM of the hips, pelvis, and spine during walking were also evaluated.

Statistical Analysis

Mixed-effects regression analysis was used to examine the effects of walking and symptoms on the outcome measures, with participant as a random effect. Lumbar load was analyzed similarly for the effects of walking and symptoms.

RESULTS

Participants walked for an average of 10.0 min (range 1.7–30.0 min) to provoke symptoms and reported an average increase in pain by 2.6 points (range 1–5), from 3.57 to 6.14 ($p < 0.05$) (**Table 1**). Mean (SD) of the lumbar spine flexion, forward pelvic tilt (pelvic flexion), and spine flexion + pelvic tilt angles were 3.4° (3.4°), 0.7° (4.5°), and 4.1° (2.6°), respectively, in asymptomatic walking and 3.4° (2.6°), 1.2° (4.3°), and 4.6° (3.2°), respectively, in symptomatic walking (**Table 3**). Example kinematics data from a single participant during a single gait cycle in three independent trials is presented in **Figure 2**. The spine was slightly flexed during walking, but this was not affected by symptoms. Pelvic tilt was not different when symptoms were present, but suggests a possible effect of more forward tilt in both standing (average change 1.1°, $p = 0.052$) and walking (average change 0.5°, $p = 0.075$). Provocation of symptoms did not affect the peak angle or ROM of the hips, pelvis, or spine during walking (**Table 3**). Lumbar loading averaged 564 (217) N in asymptomatic standing and was increased by an average of 26% during asymptomatic walking. Loading in symptomatic standing was not larger than asymptomatic standing, while loading during symptomatic walking (769 ± 269) was increased by an average of 7% over asymptomatic walking (704 ± 221) ($p = 0.001$). **Figure 3** shows peak compressive loading of each lumbar level in standing and walking.

DISCUSSION

Our results did not show increased spine flexion (adopting a trunk-flexed posture) and only indicate a trend for a small forward shift of the pelvis during both symptomatic walking and standing. This suggests that provocation of symptoms in patients with symptomatic LSS does not markedly affect their normal gait kinematics and does not support our overall hypothesis. Our results are in line with Goto et al. (2017) who reported increased thoracic and pelvic sagittal plane angles, but no change in spine flexion angle, immediately after the symptoms appeared. While bending forward during clinical examination can relieve pain and symptoms in patients with LSS, our results are not in line with the clinical observations that patients with LSS bend forward or adopt a stooped posture during walking to improve tolerance for walking, by relieving pressure on the nerves (Katz and Harris, 2008). We also noticed that forward pelvic tilt (pelvic flexion) when symptoms are present was associated with age in standing position (**Figure 4**), but spine flexion and loading was not. This suggests that the effects of LSS symptoms may not be uniform, but dependent on patient characteristics. A recent motion analysis study on patients with LSS showed that the patients adopt two different strategies during walking; some of them used a trunk-flexed posture to increase step length and hip extension angle, while others walked with upright trunk posture to decrease step length and hip extension angle (Igawa et al., 2018). Both of these patterns were attributed to patients' efforts to decrease the activation of psoas major muscles and therefore decrease the degree of lumbar lordosis during walking, but the study did not compare kinematics with and without symptoms (Igawa et al., 2018). A

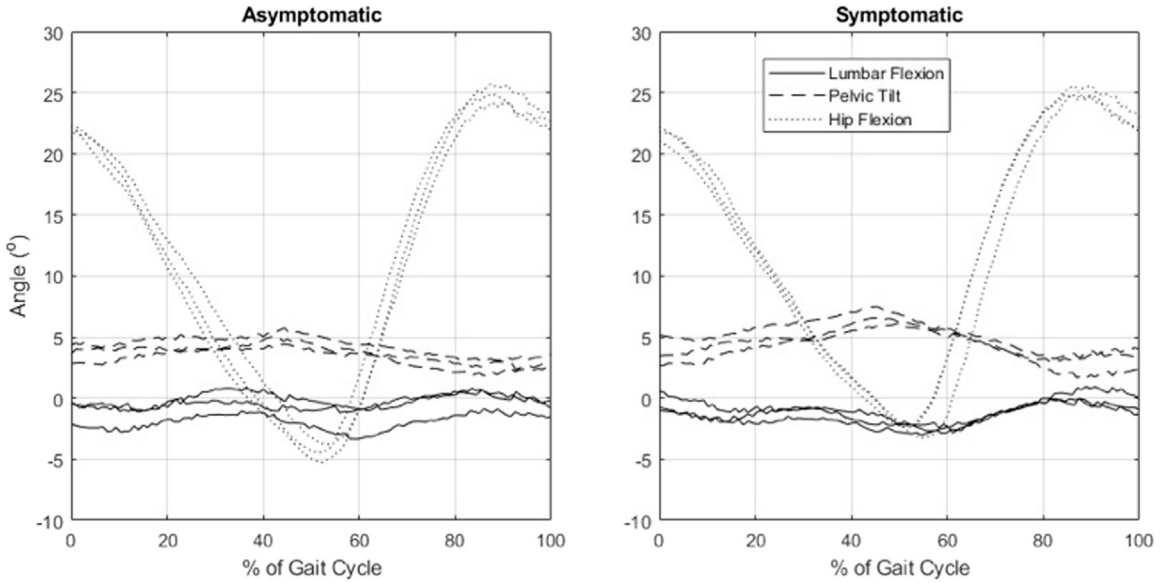

FIGURE 2 | Example data from a participant with symptomatic lumbar spinal stenosis showing sagittal plane pelvic, spinal, and hip kinematics during a single gait cycle in three independent trials, as evaluated by optical motion capture and inverse kinematics analysis.

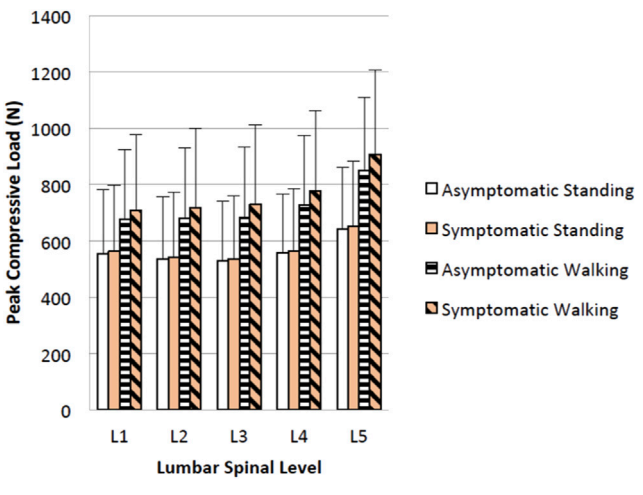

FIGURE 3 | Mean (SD) of peak lumbar loads for asymptomatic and symptomatic standing and walking.

recent standing radiographic study also showed that patients with LSS with mild to moderate spinopelvic deformity [defined as 10° or more difference between pelvic incidence (PI) and lumbar lordosis (LL) angles, also called PI-LL mismatch] chose a trunk-flexed strategy, but patients with moderate to severe deformity adopted a more upright posture (Buckland et al., 2016). Finally, while adopting a trunk-flexed posture strategy might be temporarily effective in reducing symptoms in some patients, walking with this position is posturally unstable and energy inefficient, as it demands compensatory motions and higher muscular activity to maintain dynamic balance (Saha et al., 2007; Saha et al., 2008). This may soon lead to general or local muscular fatigue, forcing patients to stop or limit their walking.

Our results suggest an increase in lumbar spinal compressive loading when the neurogenic claudication symptoms were provoked. Loads on the spine cannot be measured directly, although musculoskeletal modeling can be used to estimate spinal loading given appropriate measurements of body motion. This is the first study to estimate the magnitude of lumbar spine loading during walking in asymptomatic and symptomatic states in patients with LSS. The increased lumbar compressive loading may be partially explained by the observed changes in the overall trunk kinematics in symptomatic state, though these changes were not statistically significant. However, other possible changes in spine and lower extremity kinematics and kinetics could also lead to increased loading, such as increased non-sagittal motions, increased dynamic variability of trunk motion (or sway), or increased ground reaction forces. Future analyses are needed to explore these possibilities to identify the mechanisms by which spine loading is increased in these patients.

While compelling research supports the link between higher spine loading and increased risk of spinal tissue injury and back pain (van Dieën et al., 2009), it is also plausible that increased spine loading may aggravate symptoms and decrease walking capacity in patients with LSS by reducing the size of the spinal canal and dural sac cross-section and diameter or increasing epidural pressure. This assumption can be supported by imaging studies that reported a reduction of the dural sac cross-sectional area in weight-bearing standing position compared to supine position, which was associated with increased severity of symptoms and decreased walking capacity in patients with LSS (Kanno et al., 2012; Lau et al., 2017). In addition, loading and unloading the spine through a weight vest or vertical traction

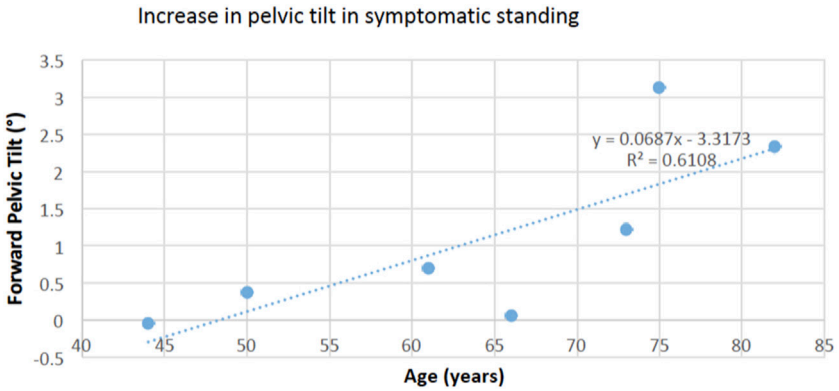

FIGURE 4 | The increase in forward pelvic tilt in symptomatic standing was positively associated with age (p = 0.038), suggesting a larger effect in older adults.

harness in LSS patients while walking on a treadmill resulted in shorter and longer time for appearance of symptoms and total walking time, respectively (Oğuz et al., 2007). Our results show that spine loading increases by an average of 48 N with symptoms, while Oğuz et al. (2007) reported that wearing a weighted vest of 10 kg, or approximately 98 N, reduced total walking time in LSS patients by about 25%. Thus, the increased loading seen here with symptoms is of a magnitude that is likely to significantly impact walking performance in this population.

Physical therapy plays a central role in treatment of LSS symptoms with generally low effectiveness, though the evidence is limited and not consistent (Ammendolia et al., 2013; Schneider et al., 2019). In addition, the current therapeutic exercises do not specifically target underlying biomechanical and neuromuscular factors behind symptom provocation or mobility limitation. Decompression surgery with or without fusion can directly address the underlying pathology of nerve compression, and once the pressure on the nerves is released, tolerance for walking reliably improves (Katz and Harris, 2008; Weinstein et al., 2010; Fritsch et al., 2017). However, approximately one third of the patients are not satisfied with the postoperative outcomes, mainly in terms of residual pain and poor function (Weinstein et al., 2010; Rainville et al., 2012; Fritsch et al., 2017). Therefore, future biomechanical studies are required to assess how gait and posture change with surgical or rehabilitative treatments and whether these changes can contribute to the post-treatment improvement in patient outcomes and walking capacity (Toosizadeh et al., 2015; Goto et al., 2017; Wang et al., 2021).

We acknowledge the small sample size as a limitation of this study that may limit generalizability of the findings. However, the repeated-measure nature of the analyses reduces the impact of the small sample size, and the evaluation of walking biomechanics before and after provocation of symptoms is a novel aspect and strength of this study. While evaluation of spine loading is another strength of this study, the use of musculoskeletal models has a number of associated limitations. Spine loading estimates are not very sensitive to cost function in a standard optimization approach (Arjmand and Shirazi-Adl, 2006), as used here, but a limitation of standard optimization is that it does not accurately predict antagonistic muscle activations, which occur in a variety of trunk loading conditions (Granata and Marras, 1995; Granata et al., 2005) and could play an important role in patients with LSS. Electromyography-assisted or double-linear optimization approaches could be used in future studies to address this limitation and improve predictions of spine loading during walking (Li and Chow, 2020). Overall, additional studies are needed to alleviate these shortcomings and to determine the effects of rehabilitation and surgical treatments on spine loading and postural outcomes.

CONCLUSION

In patients with LSS, spinal flexion was not increased after provocation of symptoms, which does not support the hypothesis and commonly held assumption that patients adopt flexed spine postures to increase spinal canal diameter and decompress the nerves, thereby relieving or delaying symptoms. A biomechanical analysis showed that spine loading increased in the symptomatic state, supporting the idea that spine loading, symptoms, and walking limitations are all interconnected. Additional studies of walking and spine biomechanics in this population are needed to better understand this issue (Suda et al., 2002; Comer et al., 2010).

DATA AVAILABILITY STATEMENT

The original contributions presented in the study are included in the article/supplementary material, and further inquiries can be directed to the corresponding author.

ETHICS STATEMENT

The studies involving human participants were reviewed and approved by the Institutional Review Board of Beth Israel Deaconess Medical Center. The patients/participants provided their written informed consent to participate in this study.

AUTHOR CONTRIBUTIONS

SM, AW, and DA substantially contributed to the conception and design of the study. SM, AL, AW, and DA contributed to the collection of human subjects' data. SM, AL, BA, and DA contributed to data processing, creation of subject-specific models, model inverse kinematics analyses, and static optimization analysis. SM and DA performed statistical analyses. SM wrote the first draft of the article. All authors contributed to the article and approved the submitted version.

FUNDING

This work was funded by grants from the NRSA Institutional Research Training Grants (T32AR55885) and the Department of Orthopaedic Surgery at Beth Israel Deaconess Medical Center, with support from Harvard Catalyst | The Harvard Clinical and Translational Science Center (National Center for Advancing Translational Sciences, National Institutes of Health Award UL1 TR002541) and financial contributions from Harvard University and its affiliated academic healthcare centers. The study sponsors had no role in the study design, data collection, analysis, article preparation, or the decision to submit the article for publication.

ACKNOWLEDGMENTS

The authors would like to acknowledge Daniel Grindle, Mehdi Alemi, and Umesh Metkar for contributions to data collection and Katelyn Burkhart and Jacob Banks for data analysis.

REFERENCES

Actis, J. A., Honegger, J. D., Gates, D. H., Petrella, A. J., Nolasco, L. A., and Silverman, A. K. (2018). Validation of Lumbar Spine Loading from a Musculoskeletal Model Including the Lower Limbs and Lumbar Spine. *J. Biomech.* 68, 107–114. doi:10.1016/j.jbiomech.2017.12.001

Alemi, M. M., Burkhart, K. A., Lynch, A. C., Allaire, B. T., Mousavi, S. J., Zhang, C., et al. (2021). The Influence of Kinematic Constraints on Model Performance during Inverse Kinematics Analysis of the Thoracolumbar Spine. *Front. Bioeng. Biotechnol.* 9, 688041. doi:10.3389/fbioe.2021.688041

Ammendolia, C., Stuber, K. J., Rok, E., Rampersaud, R., Kennedy, C. A., Pennick, V., et al. (2013). Nonoperative Treatment for Lumbar Spinal Stenosis with Neurogenic Claudication. *Cochrane Database Syst. Rev.* 8, CD010712. doi:10.1002/14651858.CD010712

Arjmand, N., and Shirazi-Adl, A. (2006). Sensitivity of Kinematics-Based Model Predictions to Optimization Criteria in Static Lifting Tasks. *Med. Eng. Phys.* 28, 504–514. doi:10.1016/j.medengphy.2005.10.001

Beaucage-Gauvreau, E., Robertson, W. S. P., Brandon, S. C. E., Fraser, R., Freeman, B. J. C., Graham, R. B., et al. (2019). Validation of an OpenSim Full-Body Model with Detailed Lumbar Spine for Estimating Lower Lumbar Spine Loads during Symmetric and Asymmetric Lifting Tasks. *Comput. Methods Biomech. Biomed. Eng.* 22, 451–464. doi:10.1080/10255842.2018.1564819

Bruno, A. G., Bouxsein, M. L., and Anderson, D. E. (2015). Development and Validation of a Musculoskeletal Model of the Fully Articulated Thoracolumbar Spine and Rib Cage. *J. Biomech. Eng.* 137, 081003. doi:10.1115/1.4030408

Bruno, A. G., Burkhart, K., Allaire, B., Anderson, D. E., and Bouxsein, M. L. (2017). Spinal Loading Patterns from Biomechanical Modeling Explain the High Incidence of Vertebral Fractures in the Thoracolumbar Region. *J. Bone Miner Res.* 32, 1282–1290. doi:10.1002/jbmr.3113

Buckland, A. J., Vira, S., Oren, J. H., Lafage, R., Harris, B. Y., Spiegel, M. A., et al. (2016). When Is Compensation for Lumbar Spinal Stenosis a Clinical Sagittal Plane Deformity. *Spine J.* 16, 971–981. doi:10.1016/j.spinee.2016.03.047

Burkhart, K., Grindle, D., Bouxsein, M. L., and Anderson, D. E. (2020). Between-session Reliability of Subject-specific Musculoskeletal Models of the Spine Derived from Optoelectronic Motion Capture Data. *J. Biomech.* 112, 110044. doi:10.1016/j.jbiomech.2020.110044

Comer, C. M., White, D., Conaghan, P. G., Bird, H. A., and Redmond, A. C. (2010). Effects of Walking with a Shopping Trolley on Spinal Posture and Loading in Subjects with Neurogenic Claudication. *Arch. Phys. Med. Rehabil.* 91, 1602–1607. doi:10.1016/j.apmr.2010.07.006

Delp, S. L., Anderson, F. C., Arnold, A. S., Loan, P., Habib, A., John, C. T., et al. (2007). OpenSim: Open-Source Software to Create and Analyze Dynamic Simulations of Movement. *IEEE Trans. Biomed. Eng.* 54, 1940–1950. doi:10.1109/TBME.2007.901024

Deyo, R. A., Mirza, S. K., Martin, B. I., Kreuter, W., Goodman, D. C., and Jarvik, J. G. (2010). Trends, Major Medical Complications, and Charges Associated with Surgery for Lumbar Spinal Stenosis in Older Adults. *JAMA* 303, 1259–1265. doi:10.1001/jama.2010.338

Fritsch, C. G., Ferreira, M. L., Maher, C. G., Herbert, R. D., Pinto, R. Z., Koes, B., et al. (2017). The Clinical Course of Pain and Disability Following Surgery for Spinal Stenosis: a Systematic Review and Meta-Analysis of Cohort Studies. *Eur. Spine J.* 26, 324–335. doi:10.1007/s00586-016-4668-0

Goto, T., Sakai, T., Enishi, T., Sato, N., Komatsu, K., Sairyo, K., et al. (2017). Changes of Posture and Muscle Activities in the Trunk and Legs during Walking in Patients with Lumbar Spinal Stenosis after Decompression Surgery. A Preliminary Report. *Gait & Posture* 51, 149–152. doi:10.1016/j.gaitpost.2016.10.006

Granata, K. P., and Marras, W. S. (1995). The Influence of Trunk Muscle Coactivity on Dynamic Spinal Loads. *Spine* 20, 913–919. doi:10.1097/00007632-199504150-00006

Granata, K. P., Rogers, E., and Moorhouse, K. (2005). Effects of Static Flexion-Relaxation on Paraspinal Reflex Behavior. *Clin. Biomech.* 20, 16–24. doi:10.1016/j.clinbiomech.2004.09.001

Grindle, D. M., Mousavi, S. J., Allaire, B. T., White, A. P., and Anderson, D. E. (2020). Validity of Flexicurve and Motion Capture for Measurements of Thoracic Kyphosis vs Standing Radiographic Measurements. *JOR Spine* 3, e1120. doi:10.1002/jsp2.1120

Hashemirad, F., Hatef, B., Jaberzadeh, S., and Ale Agha, N. (2013). Validity and Reliability of Skin Markers for Measurement of Intersegmental Mobility at L2-3 and L3-4 during Lateral Bending in Healthy Individuals: a Fluoroscopy Study. *J. Bodywork Mov. Therapies* 17, 46–52. doi:10.1016/j.jbmt.2012.04.010

Hijikata, Y., Kamitani, T., Otani, K., Konno, S., Fukuhara, S., and Yamamoto, Y. (2020). Association of Lumbar Spinal Stenosis with Severe Disability and Mortality Among Community-Dwelling Older Adults. *Spine (Phila Pa)*, 46, E784–E790. doi:10.1097/BRS.0000000000003912

Igawa, T., Katsuhira, J., Hosaka, A., Uchikoshi, K., Ishihara, S., Matsudaira, K., et al. (2018). Kinetic and Kinematic Variables Affecting Trunk Flexion during Level Walking in Patients with Lumbar Spinal Stenosis. *PLoS One* 13, e0197228. doi:10.1371/journal.pone.0197228

Ignasiak, D., Rüeger, A., Sperr, R., and Ferguson, S. J. (2018). Thoracolumbar Spine Loading Associated with Kinematics of the Young and the Elderly during Activities of Daily Living. *J. Biomech.* 70, 175–184. doi:10.1016/j.jbiomech.2017.11.033

Ishimoto, Y., Yoshimura, N., Muraki, S., Yamada, H., Nagata, K., Hashizume, H., et al. (2012). Prevalence of Symptomatic Lumbar Spinal Stenosis and its Association with Physical Performance in a Population-Based Cohort in Japan: the Wakayama Spine Study. *Osteoarthritis and cartilage* 20, 1103–1108. doi:10.1016/j.joca.2012.06.018

Kalichman, L., Cole, R., Kim, D. H., Li, L., Suri, P., Guermazi, A., et al. (2009). Spinal Stenosis Prevalence and Association with Symptoms: the Framingham Study. *Spine J.* 9, 545–550. doi:10.1016/j.spinee.2009.03.005

Kanno, H., Ozawa, H., Koizumi, Y., Morozumi, N., Aizawa, T., Kusakabe, T., et al. (2012). Dynamic Change of Dural Sac Cross-Sectional Area in Axial Loaded

Magnetic Resonance Imaging Correlates with the Severity of Clinical Symptoms in Patients with Lumbar Spinal Canal Stenosis. *Spine* 37, 207–213. doi:10.1097/BRS.0b013e3182134e73

Katz, J. N., and Harris, M. B. (2008). Lumbar Spinal Stenosis. *N. Engl. J. Med.* 358, 818–825. doi:10.1056/NEJMcp0708097

Kuwahara, W., Deie, M., Fujita, N., Tanaka, N., Nakanishi, K., Sunagawa, T., et al. (2016). Characteristics of Thoracic and Lumbar Movements during Gait in Lumbar Spinal Stenosis Patients before and after Decompression Surgery. *Clin. Biomech.* 40, 45–51. doi:10.1016/j.clinbiomech.2016.10.016

Lau, Y. Y. O., Lee, R. K. L., Griffith, J. F., Chan, C. L. Y., Law, S. W., and Kwok, K. O. (2017). Changes in Dural Sac Caliber with Standing MRI Improve Correlation with Symptoms of Lumbar Spinal Stenosis. *Eur. Spine J.* 26, 2666–2675. doi:10.1007/s00586-017-5211-7

Li, S. S. W., and Chow, D. H. K. (2020). Comparison of Predictions between an EMG-Assisted Approach and Two Optimization-Driven Approaches for Lumbar Spine Loading during Walking with Backpack Loads. *Hum. Factors* 62, 565–577. doi:10.1177/0018720819851299

Mousavi, S. J., Tromp, R., Swann, M. C., White, A. P., and Anderson, D. E. (2018). Between-session Reliability of Opto-Electronic Motion Capture in Measuring Sagittal Posture and 3-D Ranges of Motion of the Thoracolumbar Spine. *J. Biomech.* 79, 248–252. doi:10.1016/j.jbiomech.2018.08.033

Oğuz, H., Levendoğlu, F., Öğün, T. C., and Tantuğ, A. (2007). Loading Is More Effective Than Posture in Lumbar Spinal Stenosis: a Study with a Treadmill Equipment. *Eur. Spine J.* 16, 913–918. doi:10.1007/s00586-007-0317-y

Rainville, J., Childs, L. A., Peña, E. B., Suri, P., Limke, J. C., Jouve, C., et al. (2012). Quantification of Walking Ability in Subjects with Neurogenic Claudication from Lumbar Spinal Stenosis-A Comparative Study. *Spine J.* 12, 101–109. doi:10.1016/j.spinee.2011.12.006

Saha, D., Gard, S., Fatone, S., and Ondra, S. (2007). The Effect of Trunk-Flexed Postures on Balance and Metabolic Energy Expenditure during Standing. *Spine* 32, 1605–1611. doi:10.1097/BRS.0b013e318074d515

Saha, D., Gard, S., and Fatone, S. (2008). The Effect of Trunk Flexion on Able-Bodied Gait. *Gait & Posture* 27, 653–660. doi:10.1016/j.gaitpost.2007.08.009

Schmid, S., Studer, D., Hasler, C.-C., Romkes, J., Taylor, W. R., Lorenzetti, S., et al. (2016). Quantifying Spinal Gait Kinematics Using an Enhanced Optical Motion Capture Approach in Adolescent Idiopathic Scoliosis. *Gait & Posture* 44, 231–237. doi:10.1016/j.gaitpost.2015.12.036

Schneider, M. J., Ammendolia, C., Murphy, D. R., Glick, R. M., Hile, E., Tudorascu, D. L., et al. (2019). Comparative Clinical Effectiveness of Nonsurgical Treatment Methods in Patients with Lumbar Spinal Stenosis. *JAMA Netw. Open* 2, e186828. doi:10.1001/jamanetworkopen.2018.6828

Suda, Y., Saitou, M., Shibasaki, K., Yamazaki, N., Chiba, K., and Toyama, Y. (2002). Gait Analysis of Patients with Neurogenic Intermittent Claudication. *Spine* 27, 2509–2513. doi:10.1097/00007632-200211150-00016

Suri, P., Rainville, J., Kalichman, L., and Katz, J. N. (2010). Does This Older Adult with Lower Extremity Pain Have the Clinical Syndrome of Lumbar Spinal Stenosis. *JAMA* 304, 2628–2636. doi:10.1001/jama.2010.1833

Toosizadeh, N., Yen, T. C., Howe, C., Dohm, M., Mohler, J., Najafi, B., et al. (2015). Gait Behaviors as an Objective Surgical Outcome in Low Back Disorders: A Systematic Review. *Clin. Biomech.* 30, 528–536. doi:10.1016/j.clinbiomech.2015.04.005

van Dieën, J. H., and van der Beek, A. J. (2009). "Work-related Low Back Pain: Biomechanical Factors and Primary Prevention," in *Ergonomics for Rehabilitation Professionals*. Editor S. Kumar (Boca Raton, FL: Taylor & Francis/CRC Press), 359–395. doi:10.1201/9780849382697-19

Wang, J., Ullah, S., Solano, M. A., Overley, S. C., Bumpass, D. B., and Mannen, E. M. (2021). Changes in Kinematics, Kinetics, and Muscle Activity in Patients with Lumbar Spinal Stenosis during Gait: Systematic Review. *Spine J.* S1529-9430 (21), 00724–00725. doi:10.1016/j.spinee.2021.06.003

Weinstein, J. N., Tosteson, T. D., Lurie, J. D., Tosteson, A., Blood, E., Herkowitz, H., et al. (2010). Surgical versus Nonoperative Treatment for Lumbar Spinal Stenosis Four-Year Results of the Spine Patient Outcomes Research Trial. *Spine* 35, 1329–1338. doi:10.1097/BRS.0b013e3181e0f04d

Conflict of Interest: The authors declare that the research was conducted in the absence of any commercial or financial relationships that could be construed as a potential conflict of interest.

frontiers in Bioengineering and Biotechnology

BRIEF RESEARCH REPORT
published: 11 January 2022
doi: 10.3389/fbioe.2021.750246

Patient-Specific Variations in Local Strain Patterns on the Surface of a Trussed Titanium Interbody Cage

Arjan C. Y. Loenen[1,2], *Jérôme Noailly*[3], *Keita Ito*[2], *Paul C. Willems*[1], *Jacobus J. Arts*[1,2] *and Bert van Rietbergen*[1,2]*

[1]*Laboratory for Experimental Orthopaedics, Department of Orthopaedic Surgery, CAPHRI, Maastricht University Medical Center, Maastricht, Netherlands,* [2]*Orthopaedic Biomechanics, Department of Biomedical Engineering, Eindhoven University of Technology, Eindhoven, Netherlands,* [3]*Department of Information and Communication Technologies, BCN MedTech, Universitat Pompeu Fabra, Barcelona, Spain*

OPEN ACCESS

Edited by:
Dennis E. Anderson, Harvard Medical School, United States

Reviewed by:
Pascal Buenzli, Queensland University of Technology, Australia
Enrico Dall'Ara, The University of Sheffield, United Kingdom

***Correspondence:**
Bert van Rietbergen
b.v.rietbergen@tue.nl

Specialty section:
This article was submitted to Biomechanics, a section of the journal Frontiers in Bioengineering and Biotechnology

Received: *30 July 2021*
Accepted: *21 December 2021*
Published: *11 January 2022*

Citation:
Loenen ACY, Noailly J, Ito K, Willems PC, Arts JJ and van Rietbergen B (2022) Patient-Specific Variations in Local Strain Patterns on the Surface of a Trussed Titanium Interbody Cage. Front. Bioeng. Biotechnol. 9:750246. doi: 10.3389/fbioe.2021.750246

Introduction: 3D printed trussed titanium interbody cages may deliver bone stimulating mechanobiological strains to cells attached at their surface. The exact size and distribution of these strains may depend on patient-specific factors, but the influence of these factors remains unknown. Therefore, this study aimed to determine patient-specific variations in local strain patterns on the surface of a trussed titanium interbody fusion cage.

Materials and Methods: Four patients eligible for spinal fusion surgery with the same cage size were selected from a larger database. For these cases, patient-specific finite element models of the lumbar spine including the same trussed titanium cage were made. Functional dynamics of the non-operated lumbar spinal segments, as well as local cage strains and caudal endplate stresses at the operated segment, were evaluated under physiological extension/flexion movement of the lumbar spine.

Results: All patient-specific models revealed physiologically realistic functional dynamics of the operated spine. In all patients, approximately 30% of the total cage surface experienced strain values relevant for preserving bone homeostasis and stimulating bone formation. Mean caudal endplate contact pressures varied up to 10 MPa. Both surface strains and endplate contact pressures varied more between loading conditions than between patients.

Conclusions: This study demonstrates the applicability of patient-specific finite element models to quantify the impact of patient-specific factors such as bone density, degenerative state of the spine, and spinal curvature on interbody cage loading. In the future, the same framework might be further developed in order to establish a pipeline for interbody cage design optimizations.

Keywords: low back pain, interbody fusion, finite element analysis, patient-specific, trussed titanium cage, bone mechanobiology, strain

INTRODUCTION

Lumbar interbody fusion (LIF) is a well-accepted treatment for low back pain symptoms that emerge from segmental mechanical instability (Fritzell et al., 2001; Bhalla et al., 2017). During LIF surgery, the intervertebral disc (IVD) of the affected segment is replaced by an interbody fusion cage. Interbody cages provide immediate mechanical support and serve as scaffold to facilitate bone growth in the intervertebral space and fuse the two adjacent vertebrae (Bagby, 1988). Although cages are usually enriched with bone graft (substitute) to foster bone formation (Duarte et al., 2017), both material and design of the inserted cage dominate the mechanical interplay and define the initial interface between host tissue and cage. Current interbody fusion cages still render suboptimal fusion rates following LIF treatment (Meng et al., 2021). For this reason, novel interbody cages are still being developed and introduced into the clinic.

One specific technique utilized to manufacture a new generation of interbody cages is metal additive manufacturing (Arts et al., 2020), commonly known as 3D printing. It builds an object layer-by-layer by selectively adding material where needed, thus enabling production of tailored porous implant designs that are biomechanically optimized (Tan et al., 2017; Pobloth et al., 2018). Examples of such novel 3D printed metal interbody cages are trussed titanium interbody fusion cages (Hunt et al., 2021). Trussed cages encompass a network of linear beam elements (struts) that join at several intersections within the design. These highly porous cages provide an open architecture to accommodate bone ingrowth and may deliver bone stimulating mechanobiological strains to the cells attached to the strut surfaces.

Previous *ex vivo* research quantified the strain in all the struts of a trussed cage under moderate (1,000 N) and strenuous (2,000 N) axial compressive loads, by using high resolution micro computed tomography (CT) imaging (Caffrey et al., 2016). Assuming that strain amplitudes over 200 με (microstrain, 10^{-6} strain) are relevant to both preserve bone homeostasis and stimulate bone formation (Duncan and Turner, 1995), it was concluded that physiological loading of the cages induced strut strains consistent with those reported to maintain bone balance. Accordingly, it was demonstrated that cage design (e.g. diameter of struts) could be adjusted in order to tailor the strains induced by physiological mechanical loads (Caffrey et al., 2018).

Although the aforementioned *ex vivo* investigations provide valuable insights into the size and distribution of strut strains under physiological loading conditions and allow to explore design modifications, the experimental set-up entailed several limitations. Firstly, loading protocols were limited to static axial compression to allow for microCT image analysis. Secondly, strain magnitudes were quantified per strut, based on the change in total strut length, disregarding local strains within the struts that potentially arise from bending behavior. Thirdly, the actual *in vivo* strain regimes may depend on many additional factors, including cage placement and patient-specific factors such as weight, bone density, degenerative state of the spine, and spinal curvature (Polikeit et al., 2003a; Abbushi et al., 2009; Naserkhaki et al., 2016; Galbusera et al., 2021). The influence of patient-specific variations on local strain regimes thus remains unknown.

Therefore, this study aimed to determine patient-specific variations in local strain patterns on the surface of a trussed titanium interbody fusion cage. Finite element (FE) modeling enables simulation of several physiological loading conditions and quantification of local strain values within spinal (sub) structures as well as within the cages (Goel et al., 2006; Gustafson et al., 2017). Additionally, the effect of patient-specific factors can be examined by studying the variation between different patient-specific models. Patient-specific FE models of four patients eligible for spinal fusion surgery were modified to simulate a posterior lumbar interbody fusion (PLIF) treatment with trussed titanium cages. Functional dynamics of the non-operated lumbar spinal segments, and the local cage strains and endplate stresses at the operated segment, were evaluated under physiological extension/flexion movement of the lumbar spine.

MATERIALS AND METHODS

Patient-Specific FE Models of the Intact Lumbar Spine

Four patients were selected from a database of patients eligible for a spinal fusion operation as available from the earlier EU-funded MySpine project (EU FP7-ICT 269909). These patients were selected because they had similar vertebral sizes, such that the same cage design and size could be used in all patients, thereby excluding variation in the results due to differences in cage size. For all four patients, patient-specific FE models of the lumbar spine were available. The FE models were composed of the lumbar vertebrae (L1-L5), the IVDs (L1-2 to L5-S1), and the major ligaments per spinal motion segment. Detailed descriptions of patient data, model generation, and underlying material models can be found elsewhere (Malandrino et al., 2015; Rijsbergen et al., 2018) and are only described briefly here. Based on segmentations of vertebral structures via CT data and segmentations of IVD structures via magnetic resonance imaging (MRI) data, a generic FE model was morphed to patient-specific spinal geometries (Castro-Mateos et al., 2014; Castro-Mateos et al., 2015; Castro-Mateos et al., 2016).

Patient-specific trabecular bone densities were integrated in the models by defining transversely isotropic linear elastic material properties for each element, based on the mean CT gray value calculated within the representative volume of each element (Blanchard et al., 2016). Bony posterior elements, facets, and bony endplates were modeled as isotropic linear elastic materials, whereas the sacrum and cortical bone were modeled as orthotropic linear elastic materials. Surface articulation in the facet joints was assumed to be frictionless and resolved with a penalty normal stiffness of 200 N/mm (Schmidt et al., 2009). Cartilage endplates were modeled as isotropic poro-elastic materials, whereas the nucleus pulposus (NP) and annulus fibrosis (AF) were both modelled as poro-hyperelastic materials (Malandrino et al., 2014). The role of cross-ply

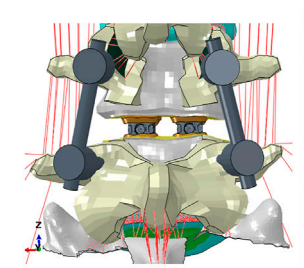

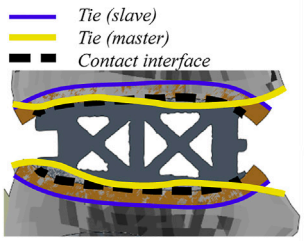

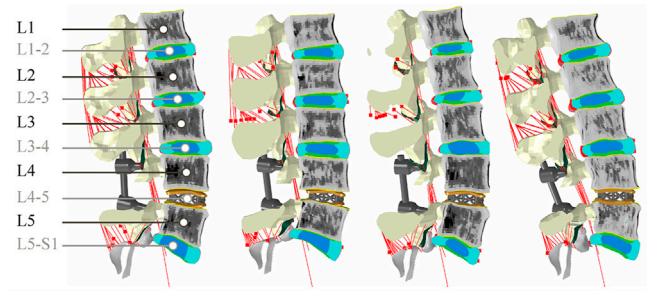

	Patient 1	Patient 2	Patient 3	Patient 4
Gender	Female	Male	Female	Female
Age [year]	41	39	55	34
Weight [kg]	60	70	74	70
Length [cm]	168	172	167	164
Lordosis [°]	40	37	36	29
Pfirrmann grade				
L1-2	II	II	III	II
L2-3	II	II	III	II
L3-4	II	II	III	II
L5-S1	IV	IV	III	II

FIGURE 1 | Top left: posterior view of segment L4-5 following PLIF surgery. A complete laminectomy was performed and two interbody cages were inserted. Bottom left: graphical overview of the interaction properties prescribed for cage vertebra interaction. The outer surface of the contact layer (purple) is rigidly tied to the associated bony endplate surface (yellow). Hard normal contact and a coefficient of friction of 0.20 were used to describe the contact between the cage and the inner surface of the contact layer (dashed black line). Right: a midsagittal cut of each of the four operated patient-specific models with corresponding demographic data. The different colors in the models represent different material properties.

collagen fibers present in the AF was implemented by adding an additional anisotropic term to the strain energy density function (Malandrino et al., 2013). Darcy's law was used to determine the fluid pore pressure. The total stress in the poro-(hyper)elastic elements was defined as the sum of the fluid pore pressure and the porous solid stress as derived from the strain energy density function. An additional swelling pressure-related term was introduced for the NP to model proteoglycan-induced swelling of the IVD. Strain-dependent permeability was implemented and updated during the simulations for each poro-(hyper) elastic material model (Malandrino et al., 2015). Exact material parameters of the IVD substructures depended on the degenerative state of the IVD, which was previously determined by an experienced radiologist using the MRI data and the Pfirrmann grading system (Pfirrmann et al., 2001). The included ligaments were described as hypoelastic unidirectional materials of which the parameters differed per ligament type and disc level (Noailly et al., 2012). Pfirrmann grade-dependent material parameters for IVD substructures were optimized based on *ex vivo* creep tests of monosegments, and independent validation was achieved for the full L1-S1 patient-specific model thanks to *ex vivo* kinematic measurements (Malandrino et al., 2015). **Supplemental material 1** provides a summary of the materials used within the FE models.

Patient-Specific FE Models of the Operated Lumbar Spine

Each of the four patient-specific FE models was modified to represent a situation directly after L4-5 PLIF surgery. A complete laminectomy was simulated which resulted in the removal of the elements of the spinous process and of all connecting ligaments at L4. In addition, the facet joints between L4 and L5, and the L4-5 IVD were virtually resected by eliminating the corresponding elements (**Figure 1**, top left).

In order to build the cage model to be implanted in each patient-specific model, a prototype trussed titanium PLIF cage was scanned at a 37 μm isotropic resolution in a microCT 100 system (SCANCO Medical AG, Brüttisellen, Switzerland) to retrieve the as-manufactured geometry of the cage. Scan data was imported into image processing software for design and modeling (Mimics Innovation Suite, Materialise, Leuven, Belgium). Following segmentation of the cage, a FE mesh was generated that consisted of 97,186 quadratic tetrahedral elements with a target triangle edge length of 0.30 mm to describe submillimeter details. **Supplementary material 2** shows the geometry of the cage and how the meshing procedure affected the level of detail in surface features that was retained in the eventual cage models.

In order to accommodate interactive placement of the cages into the intervertebral disc space, without the need for laborious remeshing of the adjacent vertebrae, contact layers were introduced. Contact layers conforming to the top and bottom curvature of the cage were designed by using a computer aided design software (NX 12, Siemens PLM software, Plano TX, United States). These layers were 2.0 mm thick. They were imported in ABAQUS/Standard (Simulia, Inc., Providence, RI, United States) version 2018 and meshed, leading to approximately 25,000 linear brick elements per contact layer with a target triangle edge length of 0.33 mm. These layers, representing the cage endplate interface, were modeled as an isotropic linear elastic material with a Young's modulus of

1,000 MPa and a Poisson's ratio of 0.30 (Polikeit et al., 2003b). Although this stiffness value is believed to resemble the cage endplate interface appropriately, the exact stiffness depends on endplate preparation technique and might vary from the stiffness of cancellous up to cortical bone (100–10,000 MPa). To investigate the effect of these variations, a side study was performed (see **Supplementary material 3**).

To match the shape of the contact layers with the exterior struts of the cage, a deformable contact simulation was performed. Interaction between the inner surface of the contact layer and the interbody cage was modelled as hard normal contact with a coefficient of friction of 0.20 (Vadapalli et al., 2006). Then, the contact layers were moved 0.30 mm towards the cage and were allowed to deform, as the contact with the cage, modelled as a rigid body, was detected. The resulting deformed mesh of the contact layers was saved in its stress-free state, and the meshes of two interbody cages (one left and one right) and the corresponding contact layers were manually positioned within each patient-specific lumbar FE model to simulate an L4-5 interbody fusion. The outer surfaces of the contact layers were then rigidly tied to the bony endplate surface of the associated vertebra (**Figure 1**, bottom left). Because cage positioning is a manual procedure both in our models and in the clinic, the exact cage position can vary. To investigate the effect of these variations, a side study was performed (see **Supplementary material 3**).

Interbody cages were modelled as isotropic linear elastic titanium (Ti-6Al-4V, Young's modulus of 116 GPa, Poisson's ratio of 0.32). Finally, titanium (Ti-6Al-4V) pedicle screw and rod instrumentations were implemented in the models, based on anatomical landmarks of the spine. Pedicle screws (32 mm shaft length, 5 mm diameter) were fixed in the vertebrae and spinal rods (5 mm diameter) were fixed in the screw heads by embedding constraints. **Figure 1** shows segment L4-5 following PLIF surgery and visualizes the imposed interaction properties between cage, contact layer, and vertebrae. In addition, the four operated models are visualized in this figure.

Boundary and Loading Conditions

The caudal end of each lumbar spine model was completely constrained in all modeling steps. In the first step (8 h), the cranial end remained unconstrained allowing pre-swelling of the poro-(hyper)elastic IVD elements. In the second step (5 s), a patient-specific compressive load was applied to the spine by means of the follower load technique (Renner et al., 2007). Two node connector elements were placed bilaterally through the vertebral centers in the sagittal plane in order to apply a compressive load that is oriented tangent to the spinal curvature. Patient-specific magnitudes of the follower load (range 368–454 N) were based on previous literature (Han et al., 2013). In the third step (5 s), an extension or flexion movement was simulated. A total deflection of 20° was imposed at the cranial end of L1 while constraining all off-axis rotations. Simultaneously, the patient-specific follower load was set to increase during extension (range 748–888 N) and flexion (range 976 to 1,148 N). The patient-specific magnitudes of the follower load per loading condition were derived from the data of Han et al. by interpolating the literature values of the resultant force at spinal level L1 to the patient-specific weight and length characteristics of the patients included in this study.

Output Analysis

ABAQUS/Standard (Simulia, Inc., Providence, RI, United States) version 2018 was used to solve extension and flexion simulations for each of the four patient-specific models. Load-deflection curves were determined for the complete lumbar spine and per non-operated functional spinal unit (FSU) as described before (Loenen et al., 2021). In addition, the intradiscal pressure (IDP) was quantified in the NP of the IVDs. It was defined as the superposition of the average pore pressure and the average axial component of the solid matrix stress. The absolute maximum principal strain values in the spinal cages were visualized and the percentage of surface nodes that exceeded an absolute strain value of 200 με was quantified for each loading condition. Additionally, the normal contact pressures at the caudal cage-contact layer interface were visualized and the mean caudal contact pressure was quantified for each loading condition.

RESULTS

Figure 1 provides an overview of the demographic data of the four patients included in this study (one male and three female). As patients were selected to fit the same cage size, the population comprised a relatively narrow weight and length range (60–74 kg and 164–172 cm). Lumbar lordotic angles ranged from 29 to 40° while degenerative state of the non-operated discs varied from Pfirrmann grade II to IV. Different gray value intensities and distributions in the trabecular bone regions indicate the differences in bone density between vertebrae and patients.

Figure 2 displays the total lumbar spine motion, the angular motion per FSU, and the IDP per IVD during extension/flexion movement. The four S1-L1 patient-specific models showed comparable asymmetrical extension/flexion flexibility profiles but differed in terms of reaction moment magnitudes at 20°, in both extension (range −9.9 to −7.7 Nm) and flexion (range 17.3–25.8 Nm). These patient-specific differences were also reflected in the angular motion per FSU, especially in flexion at L5-S1. L5-S1 was also the disc with most patient-to-patient variability in terms of degenerative state (**Figure 1**). The IDP over all discs in neutral position, under follower load compression, ranged from 0.4 to 0.8 MPa. In general, it increased more in flexion (range 1.3–2.7 MPa) than in extension (range 0.6–1.1 MPa). Again, patient-specific variations were most pronounced in flexion at the L5-S1 level. The Pfirrmann grade III L3-4 IVD model (patient 3) led to clearly lower IDP values than the grade II L3-4 IVD models of the other patients, during the flexion movement.

Since the two inserted PLIF cages (left, right) demonstrated similar deformations within one patient for each of the loading conditions, **Figure 3** illustrates only the calculation outcomes in the right cage of patient 1. In neutral position, only small strain values (<200 με) were calculated in the cage. In extension, strains

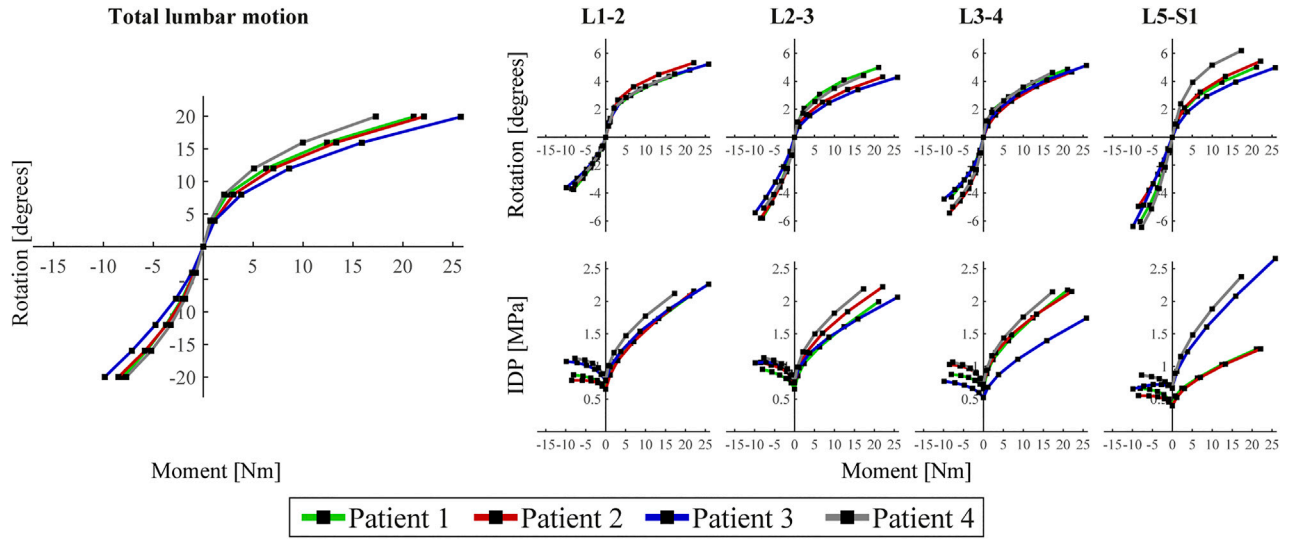

FIGURE 2 | Left: Load-deflection curve of the total lumbar spine for the four patient-specific models. Rotation represents rotation of the cranial endplate of L1 in the sagittal plane and moment is the reaction moment required to obtain these rotation values. Right: angular motion per functional spinal unit (FSU) and intradiscal pressure (IDP) per intervertebral disc (IVD) of the unoperated levels of each of the four patients. For all (sub)figures, negative and positive moments/rotations describe extension and flexion, respectively.

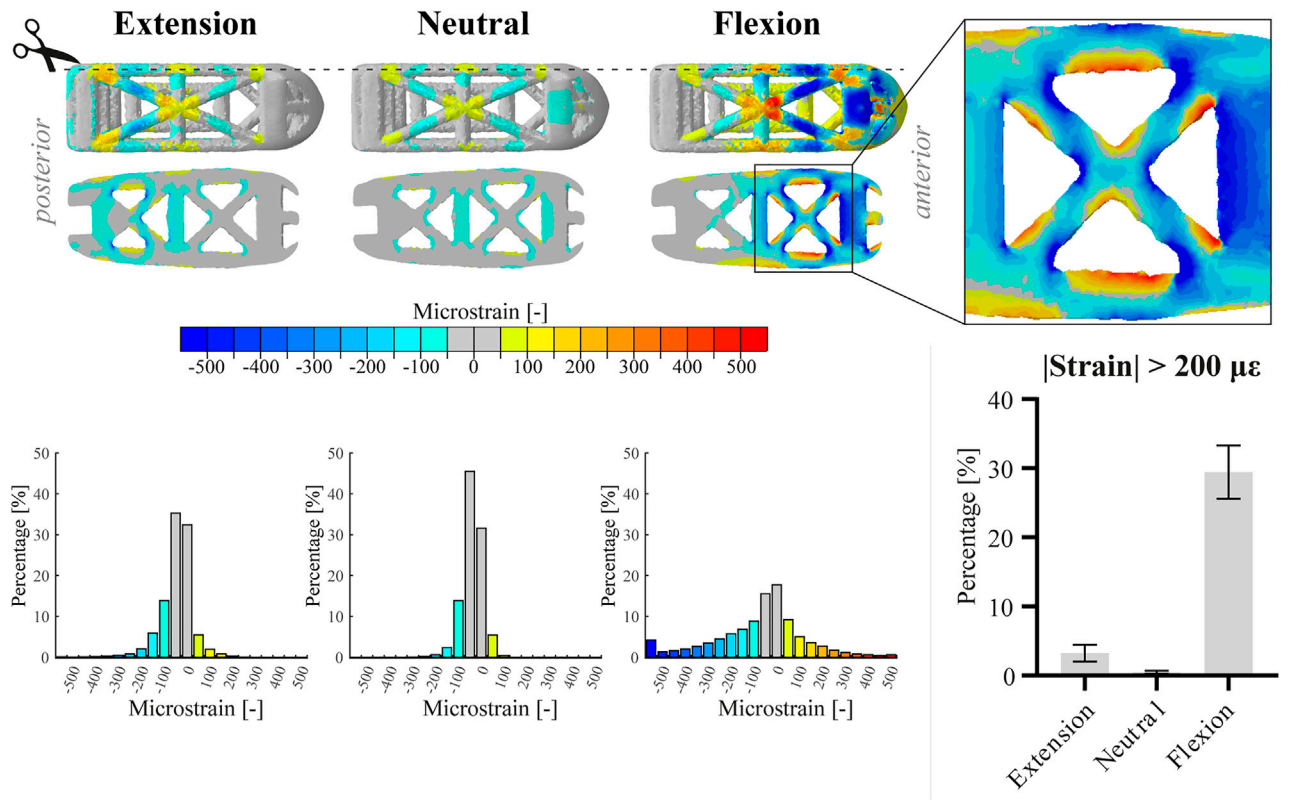

FIGURE 3 | Top part of the figure shows the absolute maximum principal strain values (top view and sagittal cut, respectively) on the right cage of patient 1 in extension, neutral, and flexion position. Additionally, an enlarged view of the anterior part of the cage in flexion is displayed. The three histograms correspond to the images above and represent the relative amount of surface nodes [%] for different strain ranges. For the bar chart, data of both cages within one patient were amalgamated. The bar chart displays the relative amount of surface nodes [%] exceeding an absolute strain value of 200 με for the different loading conditions. Bars represent the mean and 95% confidence interval of the patient population (n = 4).

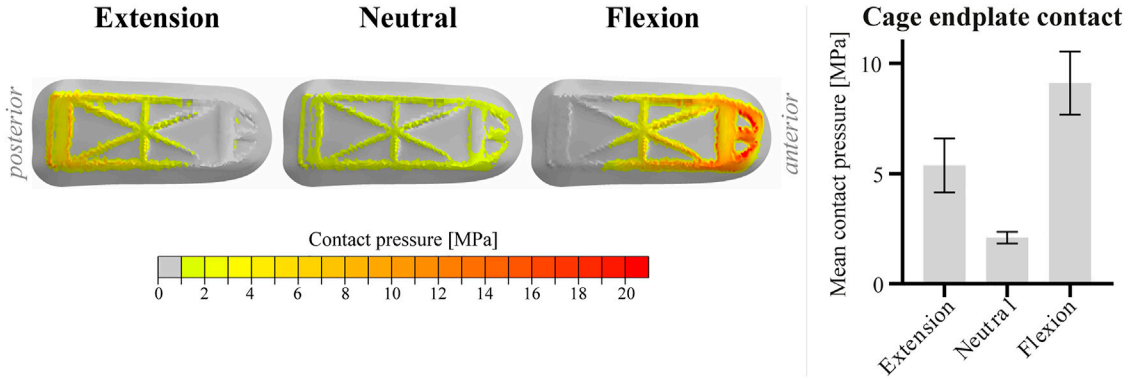

FIGURE 4 | Visualization of the contact pressure of the right cage of patient 1 on the caudal contact layer in extension, neutral and flexion position. For the bar chart, data of the two caudal contact layers within one patient were amalgamated. The bar chart displays the mean caudal contact pressure for the different loading conditions. Bars represent the mean and 95% confidence interval of the patient population (n = 4).

shifted to the posterior side of the cage and values increased up to approximately 300 με. In flexion, strains shifted to the anterior side of the cage and locally, values exceeded 500 με. For all loading conditions, both compressive (negative) and tensile (positive) strains were present at the struts. In the enlarged inset, struts show compressive strain on the one side and tensile strain on the other side, indicating inwards bending of the struts during flexion. The bar chart demonstrates that the relative amount of surface exceeding 200 με varied more between loading conditions than between patients, whereas the coefficient of variation in flexion was 8.3%. The peak von Mises stresses within the PLIF cages ranged from 248 to 304 MPa over the different patients, which is far below the yield stress of 3D printed titanium.

Since the two caudal contact layers (left, right) within one patient showed similar behavior for each of the loading conditions, **Figure 4** shows only the graphical output at the right caudal contact layer of patient 1. Comparable to the strain distribution in the cages, the caudal contact pressure shifts posteriorly and anteriorly in extension and flexion, respectively. Highest caudal contact pressures were observed anteriorly in the flexion configuration. Like the relative amount of surface exceeding 200 με, the mean caudal contact pressure varied more between loading conditions than between patients (see bar chart). The coefficient of variation of the mean caudal contact pressure in flexion was 9.9% between patients.

DISCUSSION

The main purpose of this study was to determine patient-specific variations in local strain patterns on the surface of trussed titanium interbody fusion cages. These variations were analyzed in a specific subgroup allowing for implementation of one specific PLIF cage size for all included patients. The results demonstrate that within this specific subgroup patient-specific factors such as weight, bone density, degenerative state of the spine, and spinal curvature did affect local strain regimes; however, loading conditions in this group had a much more prominent impact on both size and distribution of the strains. The same trend was observed for the mean contact pressure of the cages at the caudal vertebral endplates. It should however be emphasized that the patient dataset in current research did not include any patients with comorbidities like previous lumbar surgery, heavy smoking, drug use or other conditions affecting bone or disc metabolism, osteoporosis, obesity, or scoliosis. Therefore, this patient cohort does not reflect the broad patient population undergoing spinal fusion surgery. Inclusion of patients with these comorbidities could provide additional insight as to what patient-specific constraints need to be taken into consideration and how to optimize implant design to address these conditions.

Although the lumbar spine models used in this research were validated in earlier studies, further validation would be warranted, particularly because the earlier studies did not include the instrumentation modeled in this research. A logical next step would be to validate the predicted strains within the cages using *ex vivo* spine testing of operated spines such that the FE results can be verified against the *ex vivo* observations. Subsequently, a patient study in which strain results, obtained from patient-specific models, are correlated with the postoperative progression of bone growth would provide further clinical evidence.

The operated patient-specific lumbar spine models in this study are somewhat stiff in flexion and somewhat compliant in extension (Panjabi et al., 1994; Dreischarf et al., 2014). This behavior might be caused by the surgical modifications to the intact models, as spinal fusion surgery generally increases the stiffness of the spine more in flexion than in extension movement (Molz et al., 2003). Since the rotational contribution of FSU L4-5 is known to be proportionally larger in flexion compared to extension (Pearcy et al., 1984), this effect might have been enhanced as all patients were scheduled for L4-5 interbody fusion. Additionally, the implementation of the follower load might have had a minor effect on angular motion per FSU (Rohlmann et al., 2001). The differences observed between

patients on total lumbar motion level mainly emerged from FSU L5-S1, whose degenerative state varied most substantially between patients (range II to IV on the Pfirrmann grading system). Because the reduced disc height of a degenerated disc presumably increases the stiffness of the FSU (Muriuki et al., 2016), different load-deflection curves between segments could be expected. Mean IDP values in neutral position were consistent with *in vivo* data and increased, in accordance with previous literature, more substantially in flexion than in extension (Wilke et al., 2001). As IDP is known to increase more significantly in flexion in the fused spine compared to the native spine (Weinhoffer et al., 1995), IDP values were found to be in the high-end regime. The differences in IDP observed for disc L3-4 and L5-S1 in flexion correspond with loss of water in the more degenerated discs, inducing lower IDP values (Sato et al., 1999). Overall, all patient-specific models revealed physiologically realistic functional dynamics of the operated spine.

The percentage of the cage that experienced strains consistent with those reported to maintain bone balance under physiological loading in the current study were slightly less than those found in the aforementioned study that investigated a different trussed titanium cage under moderate (1,000 N) axial compression (Caffrey et al., 2016), i.e., up to 50% of the free struts was loaded beyond 200 με in the *ex vivo* study versus up to 30% of the total surface in current *in silico* approach. These differences, however, might be explained by the fact that in the *ex vivo* study a larger cage was used, which has a relatively smaller screw insertion block. In the prototype PLIF cage of the current study the screw insertion block carries a relatively large part of the load, thereby reducing the load on the struts. Therefore, it can be expected that for a similar cage design the actual strain values would compare well to those reported in the earlier study.

In current research, a value of 200 με was adopted in order to quantify the percentage of surface that experienced a strain value relevant for preserving bone homeostasis and stimulating bone formation. It has however been described before that the exact strain threshold for maintaining bone mass is a nonlinear function of the daily loading cycle number (Rubin et al., 2001). Stimuli with magnitudes of 200 με are estimated to require approximately 35,000 loading cycles per day (once every 2–3 s) to maintain bone mass, whereas for mechanical stimuli with a frequency in the order of 10^6 to 10^7 per day (10–100 cycles per second) even strain values lower than 10 με are suggested to be capable of stimulating bone formation (Qin et al., 1998). Patient-specific spinal motion profiles may therefore be required to interpret the strain values more appropriately. Moreover, it is worthwhile to emphasize that these reference strain values originate from bone remodeling research and it is unknown to what extent these values can be directly translated towards a former intervertebral disc, i.e., a cartilaginous environment. Once interbody fusion has progressed between the vertebrae, these values would be directly applicable. This would, however, require extension of the FE models to include the formation of bone within the cages and was outside the scope of this research.

Although the FE models were intended to predict strain values at the surface of trussed cages on submillimeter scale, they do not provide a full characterization of the mechanical stimuli the attached cells might perceive in an *in vivo* situation. This is because the exact micro-to nanoscale surface features at the struts, the way cells could be attached to the struts (bridged versus non-bridged), and other mechanical stimuli like fluid flow and hydrostatic pressure in the cages were not involved in current FE models (Kapur et al., 2003; Zhao et al., 2015; Hasegawa et al., 2020). Also, the trussed titanium cage model did not take surface micro-to nanostructure and strut composition in consideration. This simplified cage model therefore provides only a limited representation of the cage properties regarding its *in vivo* mechanobiological response. In order to accurately represent this response, multi-scale modelling will be required including microstructural features that include cell-strut interaction and fluid flow within the cage.

Since the posterior side of the PLIF cage is shielded more by the pedicle screw and rod instrumentation than the anterior side, higher strains could be found in the anterior part of the cage under extension/flexion movement. Assuming the higher strains will indeed accelerate bone formation at the anterior side of the cage, this would be favorable from a biomechanical point of view as PLIF segments that are partially fused anteriorly are found to be more stable than those partially fused posteriorly (Bono et al., 2007).

Current research used a subset of patient-specific FE models to predict the impact of patient-specific factors on cage level. The same framework could also serve as a platform to evaluate several design modifications of the interbody cages iteratively. Design modifications might be considered in order to target higher surface strains or to distribute the strains more homogenously across the whole cage. However, the ultimate strength of the proposed design modifications should also be continuously monitored as interbody cages should also withstand high peak forces in the lumbar spine (Ledet et al., 2018). Additionally, modified designs could change the amount of direct cage to endplate contact thus affecting the stresses on the endplate and the risk for cage subsidence (Steffen et al., 2000). Cage design optimization algorithms would therefore require a cost function that assesses a combination of several output metrics. In the future, development of such algorithms may facilitate interbody cage design optimizations.

It should be noted that the current study analyzed the behavior of one specific trussed titanium cage geometry used for LIF treatment with a posterior approach (PLIF cage) and that results might be different for other cage geometries. In fact, the choice for another surgical approach, like anterior lumbar interbody fusion (ALIF), would affect the output on the cage level by multiple means. ALIF surgery requires only one large cage as the anterior approach provides full access to the ventral side of the operated spinal segment (Mobbs et al., 2015). Since each single cage contains a screw anchoring point to enable cage insertion during surgery, one trussed ALIF cage contains relatively more struts than two trussed PLIF cages. Additionally, one ALIF cage generally comprehends a larger footprint on the vertebral endplate than two PLIF cages do. Moreover, ALIF surgery can be performed as stand-alone procedure, which generally means there is some additional fixation that can be instrumented

anteriorly directly after cage placement (e.g., an anterior fixating plate), but there is no pedicle screw and rod instrumentation or other supplemental posterior fixation involved (Manzur et al., 2019). The different types of additional fixation in PLIF and ALIF surgery obviously result in different loading patterns on the interbody fusion construct (Choi et al., 2013).

In conclusion, this study demonstrates the applicability of patient-specific FE models to quantify the impact of patient-specific factors as weight, bone density, degenerative state of the spine, and spinal curvature on interbody cage loading. As the resulting surface strains were very similar for the different patient-specific models in the selected patient group, it can be concluded that the trussed design is rather robust from a mechanobiological perspective. In the future, the same framework might be further developed in order to establish a pipeline for interbody cage design optimizations.

DATA AVAILABILITY STATEMENT

The datasets presented in this article are not readily available because the data is kept at the different institutes according to project regulations and the institutions involved follow national regulations with regard to data. Requests to access the datasets should be directed to BvR, b.v.Rietbergen@tue.nl.

ETHICS STATEMENT

The studies involving human participants were reviewed and approved by the Scientific Research Ethics Committee of the Medical Research Council (751/PI/2010) of the National Center for Spinal Disorders, Budapest, Hungary. The patients/participants provided their written informed consent to participate in this study.

AUTHOR CONTRIBUTIONS

AL, JA, and BvR contributed to the conception and design of the study. JN provided access to the original database of the computer models and assisted on technical matters. KI, PW, JA, and BvR supervised the project and contributed to the interpretation and presentation of the results. AL wrote the first draft of the manuscript. All authors contributed to the article and approved the submitted version.

FUNDING

The research for this paper was financially supported by the Prosperos project, funded by the Interreg VA Flanders—the Netherlands program, CCI grant no. 2014TC16RFCB046.

SUPPLEMENTARY MATERIAL

The Supplementary Material for this article can be found online at: https://www.frontiersin.org/articles/10.3389/fbioe.2021.750246/full#supplementary-material

REFERENCES

Abbushi, A., Čabraja, M., Thomale, U.-W., Woiciechowsky, C., and Kroppenstedt, S. N. (2009). The Influence of Cage Positioning and Cage Type on Cage Migration and Fusion Rates in Patients with Monosegmental Posterior Lumbar Interbody Fusion and Posterior Fixation. *Eur. Spine J.* 18 (11), 1621–1628. doi:10.1007/s00586-009-1036-3

Arts, M., Torensma, B., and Wolfs, J. (2020). Porous Titanium Cervical Interbody Fusion Device in the Treatment of Degenerative Cervical Radiculopathy; 1-year Results of a Prospective Controlled Trial. *Spine J.* 20 (7), 1065–1072. doi:10.1016/j.spinee.2020.03.008

Bagby, G. W. (1988). Arthrodesis by the Distraction-Compression Method Using a Stainless Steel Implant. *Orthopedics* 11 (6), 931–934. doi:10.3928/0147-7447-19880601-13

Bhalla, A., Schoenfeld, A. J., George, J., Moghimi, M., and Bono, C. M. (2017). The Influence of Subgroup Diagnosis on Radiographic and Clinical Outcomes after Lumbar Fusion for Degenerative Disc Disorders Revisited: A Systematic Review of the Literature. *Spine J.* 17 (1), 143–149. doi:10.1016/j.spinee.2016.09.021

Blanchard, R., Morin, C., Malandrino, A., Vella, A., Sant, Z., and Hellmich, C. (2016). Patient-Specific Fracture Risk Assessment of Vertebrae: A Multiscale Approach Coupling X-ray Physics and Continuum Micromechanics. *Int. J. Numer. Meth. Biomed. Engng.* 32 (9), e02760. doi:10.1002/cnm.2760

Bono, C. M., Khandha, A., Vadapalli, S., Holekamp, S., Goel, V. K., and Garfin, S. R. (2007). Residual Sagittal Motion after Lumbar Fusion. *Spine* 32 (4), 417–422. doi:10.1097/01.brs.0000255201.74795.20

Caffrey, J. P., Alonso, E., Masuda, K., Hunt, J. P., Carmody, C. N., Ganey, T. M., et al. (2018). Strains in Trussed Spine Interbody Fusion Implants Are Modulated by Load and Design. *J. Mech. Behav. Biomed. Mater.* 80, 203–208. doi:10.1016/j.jmbbm.2018.02.004

Caffrey, J. P., Cory, E., Wong, V. W., Masuda, K., Chen, A. C., Hunt, J. P., et al. (2016). *Ex Vivo* Loading of Trussed Implants for Spine Fusion Induces Heterogeneous Strains Consistent with Homeostatic Bone Mechanobiology. *J. Biomech.* 49 (16), 4090–4097. doi:10.1016/j.jbiomech.2016.10.051

Castro-Mateos, I., Pozo, J. M., Eltes, P. E., Rio, L. D., Lazary, A., and Frangi, A. F. (2014). 3D Segmentation of Annulus Fibrosus and Nucleus Pulposus from T2-Weighted Magnetic Resonance Images. *Phys. Med. Biol.* 59 (24), 7847–7864. doi:10.1088/0031-9155/59/24/7847

Castro-Mateos, I., Pozo, J. M., Lazary, A., and Frangi, A. (2015). "3D Vertebra Segmentation by Feature Selection Active Shape Model," in *Recent Advances in Computational Methods and Clinical Applications for Spine Imaging*. Editors J. Yao, B. Glocker, T. Klinder, and S. Li (Cham: Springer International Publishing), 241–245. doi:10.1007/978-3-319-14148-0_22

Castro-Mateos, I., Pozo, J. M., Lazary, A., and Frangi, A. F. (2016). "Automatic Construction of Patient-Specific Finite-Element Mesh of the Spine from IVDs and Vertebra Segmentations," in Proceedings Volume 9788, Medical Imaging 2016: Biomedical Applications in Molecular, Structural, and Functional Imaging, San Diego, CA, March 29, 2016, 97881U. doi:10.1117/12.2217343

Choi, K.-C., Ryu, K.-S., Lee, S.-H., Kim, Y. H., Lee, S. J., and Park, C.-K. (2013). Biomechanical Comparison of Anterior Lumbar Interbody Fusion: Stand-Alone Interbody Cage versus Interbody Cage with Pedicle Screw Fixation -

a Finite Element Analysis. *BMC Musculoskelet. Disord.* 14 (1), 220. doi:10.1186/1471-2474-14-220

Dreischarf, M., Zander, T., Shirazi-Adl, A., Puttlitz, C. M., Adam, C. J., Chen, C. S., et al. (2014). Comparison of Eight Published Static Finite Element Models of the Intact Lumbar Spine: Predictive Power of Models Improves when Combined Together. *J. Biomech.* 47 (8), 1757–1766. doi:10.1016/j.jbiomech.2014.04.002

Duarte, R. M., Varanda, P., Reis, R. L., Duarte, A. R. C., and Correia-Pinto, J. (2017). Biomaterials and Bioactive Agents in Spinal Fusion. *Tissue Eng. B: Rev.* 23 (6), 540–551. doi:10.1089/ten.TEB.2017.0072

Duncan, R. L., and Turner, C. H. (1995). Mechanotransduction and the Functional Response of Bone to Mechanical Strain. *Calcif Tissue Int.* 57 (5), 344–358. doi:10.1007/BF00302070

Fritzell, P., Hägg, O., Wessberg, P., and Nordwall, A. (2001). 2001 Volvo Award Winner in Clinical Studies: Lumbar Fusion Versus Nonsurgical Treatment for Chronic Low Back Pain. *Spine* 26 (23), 2521–2532. doi:10.1097/00007632-200112010-00002

Galbusera, F., Niemeyer, F., Tao, Y., Cina, A., Sconfienza, L. M., Kienle, A., et al. (2021). ISSLS Prize in Bioengineering Science 2021: *In Vivo* Sagittal Motion of the Lumbar Spine in Low Back Pain Patients-A Radiological Big Data Study. *Eur. Spine J.* 30, 1108–1116. doi:10.1007/s00586-021-06729-z

Goel, V. K., Panjabi, M. M., Patwardhan, A. G., Dooris, A. P., and Serhan, H. (2006). Test Protocols for Evaluation of Spinal Implants. *J. Bone Jt. Surg Am* 88 (Suppl. 2), 103–109. doi:10.2106/jbjs.e.01363

Gustafson, H. M., Cripton, P. A., Ferguson, S. J., and Helgason, B. (2017). Comparison of Specimen-Specific Vertebral Body Finite Element Models with Experimental Digital Image Correlation Measurements. *J. Mech. Behav. Biomed. Mater.* 65, 801–807. doi:10.1016/j.jmbbm.2016.10.002

Han, K.-S., Rohlmann, A., Zander, T., and Taylor, W. R. (2013). Lumbar Spinal Loads Vary with Body Height and Weight. *Med. Eng. Phys.* 35 (7), 969–977. doi:10.1016/j.medengphy.2012.09.009

Hasegawa, M., Saruta, J., Hirota, M., Taniyama, T., Sugita, Y., Kubo, K., et al. (2020). A Newly Created Meso-, Micro-, and Nano-Scale Rough Titanium Surface Promotes Bone-Implant Integration. *Int. J. Mol. Sci.* 21 (3), 783. doi:10.3390/ijms21030783

Hunt, J. P., Begley, M. R., and Block, J. E. (2021). Truss Implant Technology for Interbody Fusion in Spinal Degenerative Disorders: Profile of Advanced Structural Design, Mechanobiologic and Performance Characteristics. *Expert Rev. Med. Devices* 18, 707–715. doi:10.1080/17434440.2021.1947244

Kapur, S., Baylink, D. J., and William Lau, K.-H. (2003). Fluid Flow Shear Stress Stimulates Human Osteoblast Proliferation and Differentiation through Multiple Interacting and Competing Signal Transduction Pathways. *Bone* 32 (3), 241–251. doi:10.1016/s8756-3282(02)00979-1

Ledet, E. H., Liddle, B., Kradinova, K., and Harper, S. (2018). Smart Implants in Orthopedic Surgery, Improving Patient Outcomes: A Review. *Innov. Entrep Health* 5, 41–51. doi:10.2147/ieh.S133518

Loenen, A. C. Y., Noriega, D. C., Ruiz Wills, C., Noailly, J., Nunley, P. D., Kirchner, R., et al. (2021). Misaligned Spinal Rods Can Induce High Internal Forces Consistent with Those Observed to Cause Screw Pullout and Disc Degeneration. *Spine J.* 21 (3), 528–537. doi:10.1016/j.spinee.2020.09.010

Malandrino, A., Lacroix, D., Hellmich, C., Ito, K., Ferguson, S. J., and Noailly, J. (2014). The Role of Endplate Poromechanical Properties on the Nutrient Availability in the Intervertebral Disc. *Osteoarthritis and Cartilage* 22 (7), 1053–1060. doi:10.1016/j.joca.2014.05.005

Malandrino, A., Noailly, J., and Lacroix, D. (2013). Regional Annulus Fibre Orientations Used as a Tool for the Calibration of Lumbar Intervertebral Disc Finite Element Models. *Comput. Methods Biomech. Biomed. Eng.* 16 (9), 923–928. doi:10.1080/10255842.2011.644539

Malandrino, A., Pozo, J. M., Castro-Mateos, I., Frangi, A. F., van Rijsbergen, M. M., Ito, K., et al. (2015). On the Relative Relevance of Subject-Specific Geometries and Degeneration-Specific Mechanical Properties for the Study of Cell Death in Human Intervertebral Disk Models. *Front. Bioeng. Biotechnol.* 3, 5. doi:10.3389/fbioe.2015.00005

Manzur, M., Virk, S. S., Jivanelli, B., Vaishnav, A. S., McAnany, S. J., Albert, T. J., et al. (2019). The Rate of Fusion for Stand-Alone Anterior Lumbar Interbody Fusion: A Systematic Review. *Spine J.* 19 (7), 1294–1301. doi:10.1016/j.spinee.2019.03.001

Meng, B., Bunch, J., Burton, D., and Wang, J. (2021). Lumbar Interbody Fusion: Recent Advances in Surgical Techniques and Bone Healing Strategies. *Eur. Spine J.* 30 (1), 22–33. doi:10.1007/s00586-020-06596-0

Mobbs, R. J., Phan, K., Malham, G., Seex, K., and Rao, P. J. (2015). Lumbar Interbody Fusion: Techniques, Indications and Comparison of Interbody Fusion Options Including PLIF, TLIF, MI-TLIF, OLIF/ATP, LLIF and ALIF. *J. Spine Surg.* 1 (1), 2–18. doi:10.3978/j.issn.2414-469X.2015.10.05

Molz, F. J., Partin, J. I., and Kirkpatrick, J. S. (2003). The Acute Effects of Posterior Fusion Instrumentation on Kinematics and Intradiscal Pressure of the Human Lumbar Spine. *J. Spinal Disord. Tech.* 16 (2), 171–179. doi:10.1097/00024720-200304000-00009

Muriuki, M. G., Havey, R. M., Voronov, L. I., Carandang, G., Zindrick, M. R., Lorenz, M. A., et al. (2016). Effects of Motion Segment Level, Pfirrmann Intervertebral Disc Degeneration Grade and Gender on Lumbar Spine Kinematics. *J. Orthop. Res.* 34 (8), 1389–1398. doi:10.1002/jor.23232

Naserkhaki, S., Jaremko, J. L., and El-Rich, M. (2016). Effects of Inter-Individual Lumbar Spine Geometry Variation on Load-Sharing: Geometrically Personalized Finite Element Study. *J. Biomech.* 49 (13), 2909–2917. doi:10.1016/j.jbiomech.2016.06.032

Noailly, J., Ambrosio, L., Elizabeth Tanner, K., Planell, J. A., and Lacroix, D. (2012). In Silico evaluation of a New Composite Disc Substitute with a L3-L5 Lumbar Spine Finite Element Model. *Eur. Spine J.* 21 (Suppl. 5), 675–687. doi:10.1007/s00586-011-1716-7

Panjabi, M. M., Oxland, T. R., Yamamoto, I., and Crisco, J. J. (1994). Mechanical Behavior of the Human Lumbar and Lumbosacral Spine as Shown by Three-Dimensional Load-Displacement Curves. *J. Bone Jt. Surg.* 76 (3), 413–424. doi:10.2106/00004623-199403000-00012

Pearcy, M., Portek, I., and Shepherd, J. (1984). Three-Dimensional X-ray Analysis of Normal Movement in the Lumbar Spine. *Spine* 9 (3), 294–297. doi:10.1097/00007632-198404000-00013

Pfirrmann, C. W. A., Metzdorf, A., Zanetti, M., Hodler, J., and Boos, N. (2001). Magnetic Resonance Classification of Lumbar Intervertebral Disc Degeneration. *Spine* 26 (17), 1873–1878. doi:10.1097/00007632-200109010-00011

Pobloth, A.-M., Checa, S., Razi, H., Petersen, A., Weaver, J. C., Schmidt-Bleek, K., et al. (2018). Mechanobiologically Optimized 3D Titanium-Mesh Scaffolds Enhance Bone Regeneration in Critical Segmental Defects in Sheep. *Sci. Transl. Med.* 10 (423), eaam8828. doi:10.1126/scitranslmed.aam8828

Polikeit, A., Ferguson, S. J., Nolte, L. P., and Orr, T. E. (2003a). Factors Influencing Stresses in the Lumbar Spine after the Insertion of Intervertebral Cages: Finite Element Analysis. *Eur. Spine J.* 12 (4), 413–420. doi:10.1007/s00586-002-0505-8

Polikeit, A., Ferguson, S. J., Nolte, L. P., and Orr, T. E. (2003b). The Importance of the Endplate for Interbody Cages in the Lumbar Spine. *Eur. Spine J.* 12 (6), 556–561. doi:10.1007/s00586-003-0556-5

Qin, Y.-X., Rubin, C. T., and McLeod, K. J. (1998). Nonlinear Dependence of Loading Intensity and Cycle Number in the Maintenance of Bone Mass and Morphology. *J. Orthop. Res.* 16 (4), 482–489. doi:10.1002/jor.1100160414

Renner, S. M., Natarajan, R. N., Patwardhan, A. G., Havey, R. M., Voronov, L. I., Guo, B. Y., et al. (2007). Novel Model to Analyze the Effect of a Large Compressive Follower Pre-Load on Range of Motions in a Lumbar Spine. *J. Biomech.* 40 (6), 1326–1332. doi:10.1016/j.jbiomech.2006.05.019

Rijsbergen, M. v., van Rietbergen, B., Barthelemy, V., Eltes, P., Lazáry, Á., Lacroix, D., et al. (2018). Comparison of Patient-Specific Computational Models vs. Clinical Follow-Up, for Adjacent Segment Disc Degeneration and Bone Remodelling after Spinal Fusion. *PLoS One* 13 (8), e0200899. doi:10.1371/journal.pone.0200899

Rohlmann, A., Neller, S., Claes, L., Bergmann, G., and Wilke, H.-J. (2001). Influence of a Follower Load on Intradiscal Pressure and Intersegmental Rotation of the Lumbar Spine. *Spine* 26 (24), E557–E561. doi:10.1097/00007632-200112150-00014

Rubin, C. T., Sommerfeldt, D. W., Judex, S., and Qin, Y.-X. (2001). Inhibition of Osteopenia by Low Magnitude, High-Frequency Mechanical Stimuli. *Drug Discov. Today* 6 (16), 848–858. doi:10.1016/s1359-6446(01)01872-4

Sato, K., Kikuchi, S., and Yonezawa, T. (1999). *In Vivo* Intradiscal Pressure Measurement in Healthy Individuals and in Patients with Ongoing Back Problems. *Spine (Phila Pa 1976)* 24 (23), 2468–2474. doi:10.1097/00007632-199912010-00008

Schmidt, H., Midderhoff, S., Adkins, K., and Wilke, H.-J. (2009). The Effect of Different Design Concepts in Lumbar Total Disc Arthroplasty on the Range of Motion, Facet Joint Forces and Instantaneous center of Rotation of a L4-5 Segment. *Eur. Spine J.* 18 (11), 1695–1705. doi:10.1007/s00586-009-1146-y

Steffen, T., Tsantrizos, A., and Aebi, M. (2000). Effect of Implant Design and Endplate Preparation on the Compressive Strength of Interbody Fusion Constructs. *Spine* 25 (9), 1077–1084. doi:10.1097/00007632-200005010-00007

Tan, X. P., Tan, Y. J., Chow, C. S. L., Tor, S. B., and Yeong, W. Y. (2017). Metallic Powder-Bed Based 3D Printing of Cellular Scaffolds for Orthopaedic Implants: A State-Of-The-Art Review on Manufacturing, Topological Design, Mechanical Properties and Biocompatibility. *Mater. Sci. Eng. C* 76, 1328–1343. doi:10.1016/j.msec.2017.02.094

Vadapalli, S., Sairyo, K., Goel, V. K., Robon, M., Biyani, A., Khandha, A., et al. (2006). Biomechanical Rationale for Using Polyetheretherketone (PEEK) Spacers for Lumbar Interbody Fusion-A Finite Element Study. *Spine* 31 (26), E992–E998. doi:10.1097/01.brs.0000250177.84168.ba

Weinhoffer, S. L., Guyer, R. D., Herbert, M., and Griffith, S. L. (1995). Intradiscal Pressure Measurements above an Instrumented Fusion. *Spine* 20 (5), 526–531. doi:10.1097/00007632-199503010-00004

Wilke, H.-J., Neef, P., Hinz, B., Seidel, H., and Claes, L. (2001). Intradiscal Pressure Together with Anthropometric Data - a Data Set for the Validation of Models. *Clin. Biomech.* 16, S111–S126. doi:10.1016/S0268-0033(00)00103-0

Zhao, F., Vaughan, T. J., and McNamara, L. M. (2015). Multiscale Fluid-Structure Interaction Modelling to Determine the Mechanical Stimulation of Bone Cells in a Tissue Engineered Scaffold. *Biomech. Model. Mechanobiol* 14 (2), 231–243. doi:10.1007/s10237-014-0599-z

Conflict of Interest: AL reports investigator salary from 4WEB EU funded in parts by the Prosperos project, Interreg VA Flanders – In Netherlands program, CCI grant no. 2014TC16RFCB046.

The remaining authors declare that the research was conducted in the absence of any commercial or financial relationships that could be construed as a potential conflict of interest.

frontiers in Bioengineering and Biotechnology

ORIGINAL RESEARCH
published: 13 January 2022
doi: 10.3389/fbioe.2021.751193

Alteration of the Sitting and Standing Movement in Adult Spinal Deformity

*Eddy Saad[1], Karl Semaan[1], Georges Kawkabani[1], Abir Massaad[1], Renee Maria Salibv[1], Mario Mekhael[1], Marc Fakhoury[1], Krystel Abi Karam[1], Elena Jaber[1], Ismat Ghanem[1], Virginie Lafage[2], Wafa Skalli[3], Rami Rachkidi[1] and Ayman Assi[1,3]**

[1]Faculty of Medicine, University of Saint-Joseph, Beirut, Lebanon, [2]Orthopaedics Surgery, Lenox Hill Hospital, New York, NY, United States, [3]Institut de Biomécanique Humaine Georges Charpak, Arts et Métiers, Paris, France

Adults with spinal deformity (ASD) are known to have spinal malalignment affecting their quality of life and daily life activities. While walking kinematics were shown to be altered in ASD, other functional activities are yet to be evaluated such as sitting and standing, which are essential for patients' autonomy and quality of life perception. In this cross-sectional study, 93 ASD subjects (50 ± 20 years; 71 F) age and sex matched to 31 controls (45 ± 15 years; 18 F) underwent biplanar radiographic imaging with subsequent calculation of standing radiographic spinopelvic parameters. All subjects filled HRQOL questionnaires such as SF36 and ODI. ASD were further divided into 34 ASD-sag (with PT > 25° and/or SVA >5 cm and/or PI-LL >10°), 32 ASD-hyperTK (with only TK >60°), and 27 ASD-front (with only frontal malalignment: Cobb >20°). All subjects underwent 3D motion analysis during the sit-to-stand and stand-to-sit movements. The range of motion (ROM) and mean values of pelvis, lower limbs, thorax, head, and spinal segments were calculated on the kinematic waveforms. Kinematics were compared between groups and correlations to radiographic and HRQOL scores were computed. During sit-to-stand and stand-to-sit movements, ASD-sag had decreased pelvic anteversion (12.2 vs 15.2°), hip flexion (53.0 vs 62.2°), sagittal mobility in knees (87.1 vs 93.9°), and lumbar mobility (L1L3-L3L5: –9.1 vs –6.8°, all $p < 0.05$) compared with controls. ASD-hyperTK showed increased dynamic lordosis (L1L3–L3L5: –9.1 vs –6.8°), segmental thoracic kyphosis (T2T10–T10L1: 32.0 vs 17.2°, C7T2–T2T10: 30.4 vs 17.7°), and thoracolumbar extension (T10L1–L1L3: –12.4 vs –5.5°, all $p < 0.05$) compared with controls. They also had increased mobility at the thoracolumbar and upper-thoracic spine. Both ASD-sag and ASD-hyperTK maintained a flexed trunk, an extended head along with an increased trunk and head sagittal ROM. Kinematic alterations were correlated to radiographic parameters and HRQOL scores. Even after controlling for demographic factors, dynamic trunk flexion was determined by TK and PI-LL mismatch (adj. $R^2 = 0.44$). Lumbar sagittal ROM was determined by PI-LL mismatch (adj. $R^2 = 0.13$). In conclusion, the type of spinal deformity in ASD seems to determine the strategy used for sitting and standing. Future studies should evaluate whether surgical correction of the deformity could restore sitting and standing kinematics and ultimately improve quality of life.

Keywords: adult spinal deformity (ASD), kinematics, sitting, standing, radiograph assessment, movement analysis, quality of life

OPEN ACCESS

Edited by:
Lennart Scheys, KU Leuven, Belgium

Reviewed by:
Sagrario Pérez- De La Cruz, University of Almeria, Spain
Pieter Severijns, KU Leuven, Belgium

****Correspondence:***
Ayman Assi
ayman.assi@usj.edu.lb

Specialty section:
This article was submitted to Biomechanics, a section of the journal Frontiers in Bioengineering and Biotechnology

Received: *31 July 2021*
Accepted: *03 December 2021*
Published: *13 January 2022*

Citation:
Saad E, Semaan K, Kawkabani G, Massaad A, Salibv RM, Mekhael M, Fakhoury M, Karam KA, Jaber E, Ghanem I, Lafage V, Skalli W, Rachkidi R and Assi A (2022) Alteration of the Sitting and Standing Movement in Adult Spinal Deformity. Front. Bioeng. Biotechnol. 9:751193. doi: 10.3389/fbioe.2021.751193

1 INTRODUCTION

With the aging of the population, degenerative diseases have been increasing in prevalence (Safaee et al., 2020) and placing a significant burden on the healthcare system (Pellisé et al., 2015).

Adult spinal deformity (ASD) encompasses a multitude of pathological entities mainly resulting from a primary degenerative process, but also from trauma or progression of a pathology of the spine such as adolescent idiopathic scoliosis or Scheuermann's hyperkyphosis (Aebi, 2005). These seemingly heterogeneous diseases all demonstrate postural malalignment defined by the presence of at least one of the following radiographic criteria: pelvic tilt (PT) > 25°, sagittal vertical axis (SVA) > 50 mm, coronal Cobb angle > 20°, thoracic kyphosis (TK) > 60°, and pelvic incidence–lumbar lordosis (PI-LL) mismatch > 10°, according to the International Spine Study Group (Schwab et al., 2012; Bakhsheshian et al., 2017; Kim et al., 2017).

Adults with spinal deformity are known to present with spinal malalignment and recruit compensation mechanisms at the hips and knees to maintain balance (Le Huec et al., 2019). These radiographic alterations and compensation strategies have been shown to affect the patients' health-related quality of life (HRQOL) and limit their daily life activities (Christopher Kieser and Wyatt, 2019). In fact, it is estimated that ASD have some of the most impaired HRQOL scores among all chronic diseases (Pellisé et al., 2015).

Motion analysis is increasingly being used to assess functionality in ASD subjects. Kawkabani et al. have shown that ASD subjects walked slower with an increased double support phase, and maintained a flexed attitude in their thorax, hips, and knees while walking (Kawkabani et al., 2021). Severijns et al. also described a similar finding in ASD subjects with a decompensated sagittal deformity (Severijns et al., 2021). Although walking is an essential activity in daily life, limitations in other activities are usually observed when collecting HRQOL outcomes. Thus, kinematics of daily life activities, other than walking, should be assessed in ASD to better address the quality-of-life concerns in these patients.

Sitting and standing represent important life activities that are commonly used during the day. To be fully functional, an individual must hold the sitting position for a long time while being able to transition from the sitting to the standing position and vice versa. In fact, an alteration of this activity in the elderly was a predictor of dependence, institutionalization, and even mortality (Hirvensalo et al., 2000; Yamada and Demura, 2009). Furthermore, sitting and standing constitute complex tasks requiring fine musculoskeletal coordination and thus are expected to be affected in patients with spinal deformity (Sadeghi et al., 2013).

Few studies have previously explored alterations of the sit-to-stand movement in ASD. In particular, Bailey et al. used a 3D depth-camera to describe motion kinematics and kinetics from 15 ASD patients, both pre- and postoperatively, compared with 10 controls. They showed that ASD patients had increased peak sagittal vertical axis (SVA) during sit-to-stand as well as increased lumbar and lower limb torques, which could be corrected by surgical interventions (Bailey et al., 2019). However, the segmental motion of the spine was not analyzed and further subdivision of the ASD population according to the type of spinal deformity was not possible due to the small sample size.

Therefore, the aim of our study was to evaluate pelvis, lower limb, trunk, spinal segment, and head kinematics in ASD subjects with different types of spinal deformity, during the sit-to-stand and stand-to-sit movements as well as their relationships with their HRQOL scores and radiographic parameters.

2 MATERIALS AND METHODS

2.1 Study Design

This is a cross-sectional IRB-approved study (CEHDF1259) evaluating kinematic alterations in different subgroups of ASD subjects compared with controls. All participants signed an informed consent prior to the trials.

2.2 Participants

ASD subjects were referred to our laboratory by their physicians for pain and/or disability. Inclusion criteria included the presence of at least one of the following radiographic alterations: pelvic tilt (PT) >25°, sagittal vertical axis (SVA) >50 mm, pelvic incidence–lumbar lordosis mismatch (PI-LL) >10°, thoracic kyphosis (TK) >60°, and/or coronal Cobb angle >20° (Schwab et al., 2012; Kim et al., 2017), as well as being older than 20 years and reporting pain or discomfort. Subjects presenting with other motion altering disorders (neurological, rheumatic, infectious, tumoral, or other diseases) or a history of spine or lower limb surgery were excluded from our study.

Asymptomatic control subjects were recruited following a call that was made within our institution. Inclusion criteria included being at least 20 years old. Exclusion criteria included the presence of longstanding pain or disability, musculoskeletal (adolescent idiopathic scoliosis, Scheuermann's disease . . .) or neurological (spinal stenosis, sciatica . . .) disorders, acute injury, prior history of spine or lower limb surgery, and the presence of one of the radiographic criteria that characterize ASD.

Mild degenerative modifications were not considered as exclusion criteria if they did not cause clinical manifestations (pain and/or disability) since some degree of degenerative changes is inevitable with age.

2.3 Data Acquisition

2.3.1 Demographics

Age (year), sex (F/M), height (cm), weight (kg), and BMI (kg/m^2) were collected for each subject.

2.3.2 Radiographic Parameters

All subjects underwent low dose EOS full-body biplanar X-rays in the free-standing position (Chaibi et al., 2012) (EOS Imaging, Paris, France) (**Figure 1A**). Three-dimensional reconstructions of the subjects' spine, pelvis, and lower limbs were performed using Stereos (v1.8.99.20R) (**Figure 1B**). The following spino-pelvic were extracted from the 3D reconstructions: pelvic incidence PI (°), radiographic pelvic tilt PT (°), L1S1 lumbar lordosis LL (°),

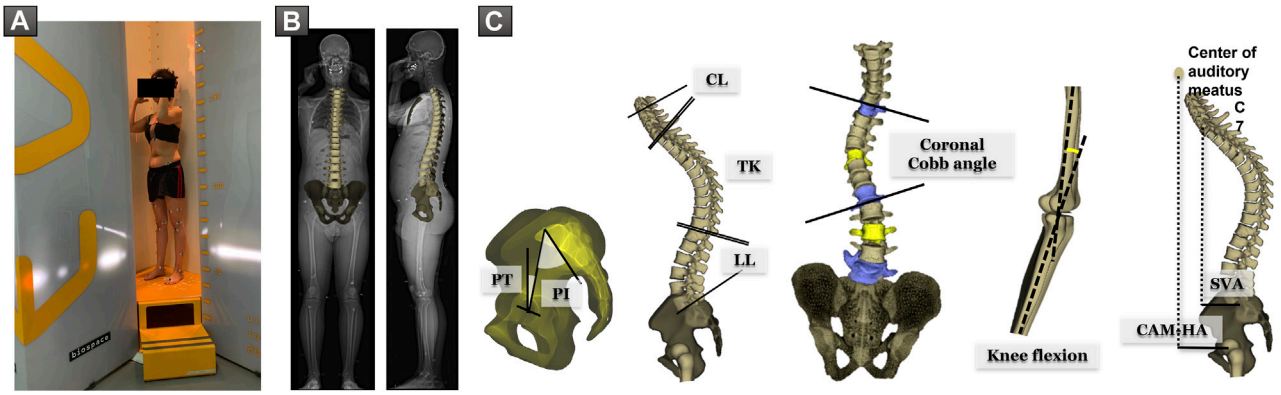

FIGURE 1 | (A) Subject in the free-standing position during acquisition of EOS biplanar X-rays. **(B)** 3D reconstruction of the spine and pelvis. **(C)** Spino-pelvic and postural parameters: pelvic incidence PI (°), pelvic tilt PT (°), L1S1 lumbar lordosis LL (°), T1T12 thoracic kyphosis TK (°), C2C7 cervical lordosis CL (°), knee flexion (°), coronal Cobb angle (°), sagittal vertical axis SVA (mm), and distance from center of auditory meatus plumb line to hip-axis CAM-HA (mm).

PI–LL mismatch (°), T1T12 thoracic kyphosis TK (°), coronal Cobb angle (°), and knee flexion (°). C2C7 cervical lordosis CL (°), sagittal vertical axis SVA (mm), and distance from center of auditory meatus plumb line to hip-axis CAM-HA (mm) were extracted from standing radiographs (**Figure 1C**).

Based on their radiographic alterations, ASD subjects were subdivided into three groups:

ASD-sag: presenting with a sagittal malalignment: SVA > 50 mm and/or PT > 25° and/or PI-LL > 10°, irrespective of the presence of a coronal Cobb angle deformity or a thoracic hyperkyphosis;
ASD-hyperTK: presenting with only a thoracic hyperkyphosis TK > 60°;
ASD-front: presenting with only a Coronal Cobb angle > 20°.

2.3.3 HRQOL Questionnaires

All subjects filled the following HRQOL questionnaires:

SF-36 with both its physical (PCS) and mental (MCS) components, on a scale of 0–100, decreasing with severity, and normalized to the local population;
Oswestry Disability Index (ODI) measures disability on a scale of 0–100, increasing with severity;
Beck's Depression Inventory (BDI) evaluates depression, on a scale of 0–63, increasing with severity;
Visual Analog Scale (VAS) measures pain intensity on a scale of 0–10, increasing with severity.

2.3.4 Motion Analysis

Motion capture was performed using the Vicon opto-electronic system (Vicon Motion Systems, Oxford, UK). The acquisition was completed using eight infrared cameras (Vero 2.2, 200 Hz) and two front and side video cameras. A calibration was carried out before each acquisition. Forty-one markers were used, four of which were placed on a band positioned on the patient's head. Lower limb markers were placed according to the Davis protocol (Davis et al., 1991) on the following structures: anterosuperior and posterosuperior iliac spines, distal third of the femur, lateral knee condyles, distal third of the tibia, lateral malleoli, calcaneum, and base of second metatarsal. Trunk and spine markers were positioned according to the Leardini protocol (Leardini et al., 2011) on the following bony landmarks: both acromions, suprasternal notch, xiphoid process, and spinous processes of C7, T2, T10, L1, L3, and L5 vertebrae (**Figure 2A**).

Subjects were asked to sit on a backless stool, with their feet flat on the ground. The height of the seat was adjusted so that hips and knees were both at 90°. Subjects were then instructed to stand up without support, while looking straight ahead. In case they were not able to stand on their own, they were allowed to lean on their thighs. Subjects had to remain upright for 5 s before sitting down again in their seat, while keeping the gaze straight ahead and without leaning. Subjects were excluded when markers, especially those of the pelvis, were not visible during motion tracking (**Figure 2B**).

The position of each marker was verified on the standing biplanar radiographs and, if necessary, the 3D coordinates of the marker in its correct anatomical position were measured on standing radiographs in the corresponding body segment's frame of reference and used to reconstruct the marker on ProCalc (Vicon, Oxford, UK) to correspond to the anatomical landmark. The position of the markers was instantly detected in the room's frame of reference and enabled the reconstruction of the various body segments: the head, trunk, pelvis, and the segments of the lower limbs, using Nexus and ProCalc (Vicon). The motion of each segment relative to the other allowed the extraction of kinematic curves for each joint in the three planes of space. The motions of the head, trunk, and pelvis were also calculated in the room's frame of reference. This correction was applied only on markers within a rigid body segment (i.e., pelvis, head ...) and not on isolated markers such as those of the spine since it is not possible to predict their accurate position relative to other markers during motion.

Segmental analysis of the spine was also performed using the following segments: L3L5, L1L3, T10L1, T2T10, and C7T2 (**Figure 2C**). The angles between adjacent segments were

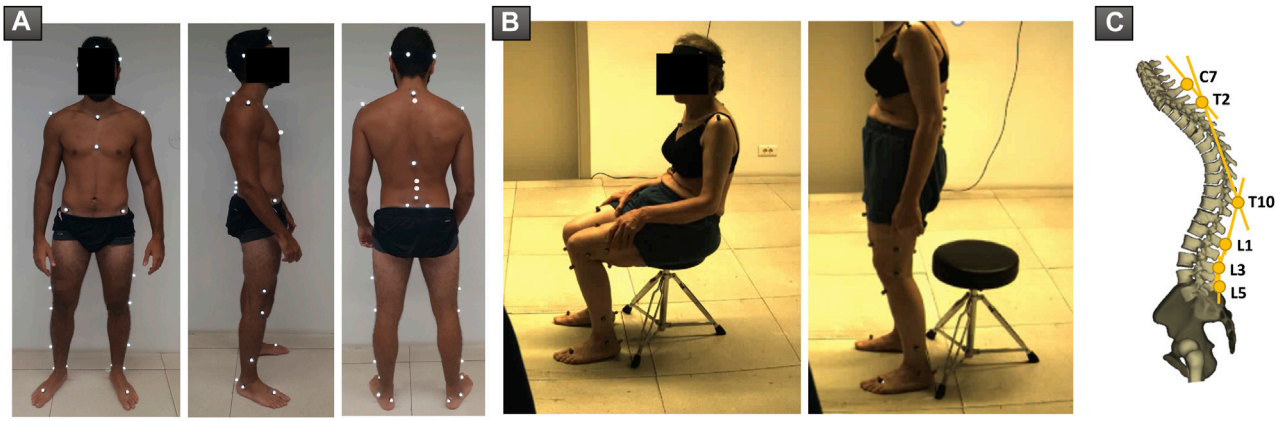

FIGURE 2 | (A) Positioning of markers used during acquisition of sit-to-stand and stand-to-sit movements. **(B)** Patient during acquisition, in the sitting and standing positions, respectively. **(C)** Representation of spine segments as described by Leardini et al.

extracted in the sagittal plane. For example, for the angle between L1L3 and L3L5 representing lumbar lordosis, increasing values denote a loss of lumbar lordosis, while decreasing values signal an increased lumbar lordosis. In addition, the angle between the pelvis and the L3L5 segment was calculated.

A cycle for either the sit-to-stand or stand-to-sit movement was delimited starting the first frame before the beginning of the movement defined as the initial horizontal displacement of a head or trunk marker, until the next frame after the stop of the movement defined as the final frame where no further movement was detected along the trajectories of all markers. Oscillations, occurring before and after the sit-to-stand and stand-to-sit movements and defined by a reversal in motion direction of the markers, were excluded from the cycle. Cycles were then normalized between 0 and 100%.

Several trials were recorded for each subject. Consistency between trials was verified on the kinematic waveforms in Polygon (Vicon). One repeatable trial was selected for each subject and exported in Excel.

The kinematic curves of the various parameters allowed the extraction of the maximum, minimum, and mean values as well as the range of motion (ROM) corresponding to the difference between the two extremes, both during the sitting–standing and the standing–sitting transitions. Kinematic parameters were computed in Matlab (Mathworks, Natick, USA; R2016a).

2.4 Statistical Analysis

The distribution of all variables was assessed for normality using Shapiro–Wilk test. Since most parameters did not follow a normal distribution, nonparametric tests were used for statistical analysis.

Demographic parameters were compared between ASD and controls using Mann–Whitney test. Sex was compared using χ^2 test.

HRQOL scores, and standing radiographic and kinematic parameters (mean, maximum, minimum, and range of motion ROM) during sit-to-stand and stand-to-sit movements were compared between ASD groups and controls using Kruskal–Wallis test followed by Conover–Iman pairwise comparisons.

The relationships between kinematic alterations and both radiographic parameters and HRQOL scores were investigated using Pearson's correlation.

Determinants of kinematic alterations were explored using a multivariate analysis (stepwise multiple linear regression) with demographic and standing radiographic parameters as independent variables. Adjusted R^2, standardized β coefficients, and p-values were reported for each model.

Statistical analyses were performed using XLSTAT (version 2019; Addinsoft, Paris, France). The level of significance was set at 0.05 and adjusted by a Bonferroni correction when necessary.

3 RESULTS

3.1 Demographics

In total, 93 ASD [50 ± 20 years old (20–85); 71 F and 22 M] and 31 controls [45 ± 15 years old (21–76); 18 F and 13 M] were included in our study. There were no significant differences in age or sex distribution between the two groups ($p = 0.10$ and $p = 0.06$ resp.). There was no statistically significant difference in weight nor BMI between both groups (weight: ASD: 71 ± 15 kg vs controls: 69 ± 13 kg, $p = 0.63$; BMI: ASD: 27 ± 5 kg/m^2 vs controls: 25 ± 3 kg/m^2, $p = 0.21$). ASD were on average 5 cm shorter than controls (ASD: 162 ± 10 cm vs controls: 167 ± 8 cm, $p = 0.01$).

ASD subjects were further divided into 34 ASD-sag, 32 ASD-hyperTK, and 27 ASD-front.

3.2 Standing Radiographic Parameters

All groups had similar PI values (ASD: 52 ± 11° vs controls: 52 ± 10°, $p = 0.19$). As expected, ASD-sag had an increased SVA (58.4 ± 52.5 mm vs controls: −2.2 ± 22.1 mm, $p < 0.001$), CAM-HA (27.5 ± 68.7 mm vs controls: −17.1 ± 29.4 mm, $p = 0.005$), and PT (27.8 ± 10.8° vs controls: 10.5 ± 6.2°, $p < 0.001$) when compared with the other groups. They also presented with a

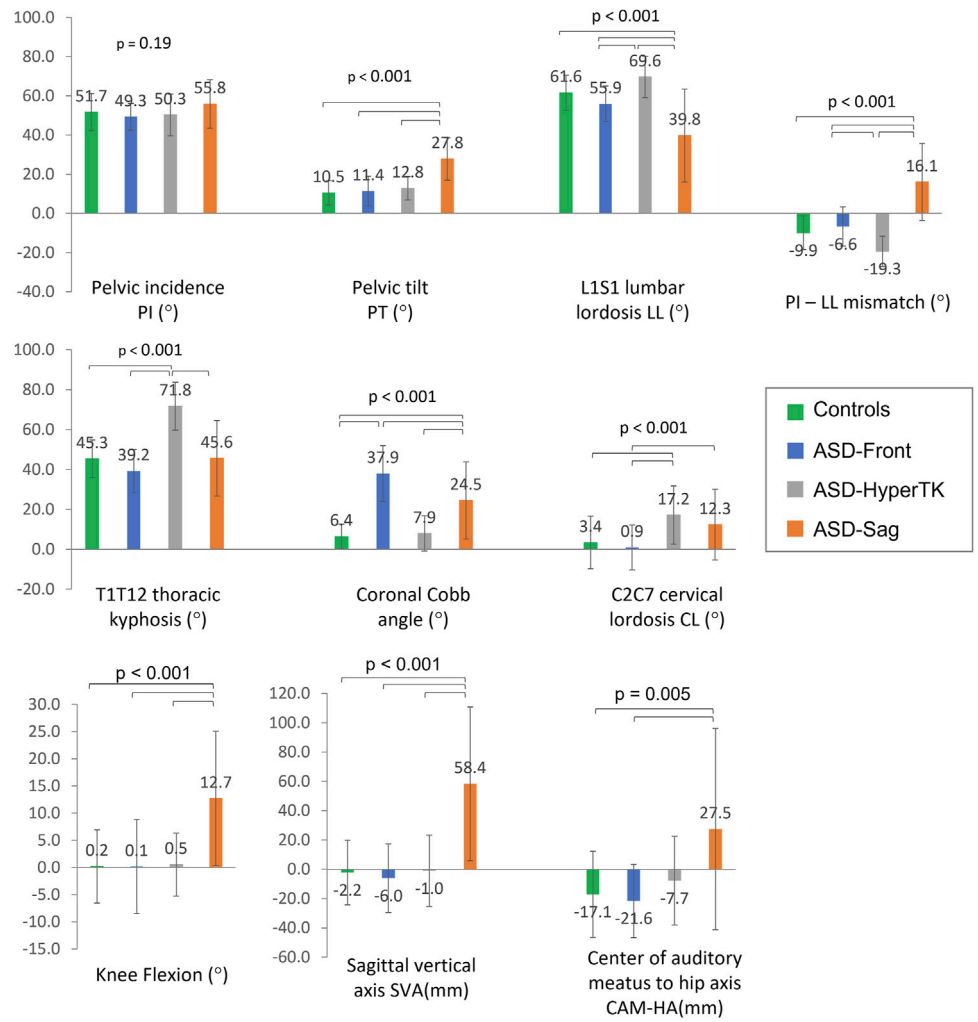

FIGURE 3 | Comparison of spino-pelvic and postural parameters between subgroups: controls, ASD-front, ASD-hyperTK, and ASD-sag.

decreased LL and an increased PI-LL mismatch (39.8 ± 23.7° and 16.1 ± 19.6° resp., *vs.* controls: 61.6 ± 9.0° and −9.9 ± 8.6° resp., both $p < 0.001$), as well as an increased knee flexion (12.7 ± 12.4° vs controls: 0.2 ± 6.8°, $p < 0.001$) when compared with other groups. ASD-hyperTK showed an increased TK (71.8 ± 12° vs controls: 45.3 ± 9.4°, $p < 0.001$), LL (69.6 ± 10.5° vs controls: 39.8 ± 23.7°, $p < 0.001$), and CL (17.2 ± 14.6° vs controls: 3.4 ± 13.2°, $p < 0.001$) compared with other groups. ASD-front presented with an increased coronal Cobb angle compared with other groups (37.9 ± 14.0° vs controls: 6.4 ± 6.2°, $p < 0.001$) (**Figure 3**).

3.3 HRQOL Scores

All ASD subjects showed altered HRQOL scores, with ASD-sag being the most affected, followed by ASD-hyperTK and then ASD-front. ASD-sag had a significantly decreased PCS (ASD-sag: 36.2 ± 8.1 vs controls: 50.1 ± 7.7, $p < 0.001$) and MCS (ASD-sag: 48.8 ± 10.1 vs controls: 55.0 ± 6.3, $p = 0.005$). They showed moderate levels of pain (VAS: 6.7 ± 2.6 vs 1.3 ± 0.7, $p < 0.001$), significantly increased disability (ODI: 38.0 ± 16.9 vs 3.2 ± 5.0, $p < 0.001$), and higher depression levels (BDI: 11.3 ± 10.0 vs 2.2 ± 3.8, $p < 0.001$) (**Table 1**).

3.4 Sitting/Standing Kinematics

Spine, pelvis, and lower limb kinematics were almost similar during both sit-to-stand (**Table 2**) and stand-to-sit transitions (**Supplementary Table 1**).

During sitting and standing movements, when compared with controls, ASD-sag presented with a decreased mean pelvic anteversion (dynamic pelvic tilt: 12.2 vs 15.2°, $p = 0.006$), mean hip flexion (53.0 vs 62.2°, $p = 0.006$), and knee and ankle sagittal ROM (87.1 vs 93.9°, $p = 0.01$ and 17.9 vs 22.8°, $p < 0.001$ resp.). At the spinal segmental level, ASD-sag presented with a decreased lumbar sagittal ROM when compared with the other subgroups (L1L3–L3L5: 9.1 vs 16.5° in controls, $p < 0.001$).

ASD-hyperTK showed similar lower limb kinematics compared with controls. However, at the spinal level, they had an increased dynamic lumbar lordosis (mean L1L3–L3L5: −9.1 vs −6.8° in controls, $p = 0.04$), increased extension at the

TABLE 1 | Comparison of health-related quality of life (HRQOL) scores between subgroups: controls, ASD-front, ASD-hyperTK, and ASD-sag.

	Mean ± SD				*P*-value	Controls *vs* ASD-front	Controls *vs* ASD-hyperTK	Controls *vs* ASD-sag	ASD-front vs ASD-hyperTK	ASD-front *vs* ASD-sag	ASD-hyperTK vs ASD-sag
	Controls	ASD-front	ASD-hyperTK	ASD-sag							
Short Form-36 (SF-36)											
Physical Component Summary (PCS)	50.1 ± 7.7	44.8 ± 9.6	40.5 ± 7.2	36.2 ± 8.1	<**0.001**		*	*		*	
Mental Component Summary (MCS)	55.0 ± 6.3	48.4 ± 6.7	51.7 ± 9.2	48.8 ± 10.1	**0.005**	*		*			
Visual Analog Scale (VAS)	1.3 ± 0.7	4.2 ± 2.6	6.1 ± 2.7	6.7 ± 2.6	<**0.001**	*	*	*	*	*	
Oswestry Disability Index (ODI)	3.2 ± 5.0	20.9 ± 20.2	27.2 ± 16.3	38.0 ± 16.9	<**0.001**	*	*	*		*	*
Beck's Depression Inventory (BDI)	2.2 ± 3.8	8.7 ± 6.3	10.5 ± 7.5	11.3 ± 10.0	<**0.001**	*	*	*			

**Bold value, significant* p-*value.*

thoracolumbar junction (mean T10L1–L1L3: −12.4 vs −5.5°, $p < 0.001$), and more flexed thoracic segments (mean T2T10–T10L1: 32.0 vs 17.2°, mean C7T2–T2T10: 30.4 vs 17.7°, both $p < 0.001$) when compared with controls. They also showed increased sagittal ROM both at the thoracolumbar junction (ROM T10L1–L1L3: 16.3 *vs.* 9.8°, $p = 0.004$) and the upper thoracic level (ROMC7T2–T2T10: 18.1 vs 11.0°, $p = 0.04$).

Both ASD-sag and ASD-hyperTK maintained a flexed trunk during sit-to-stand and stand-to-sit movements (mean trunk flexion/extension: 28.6 and 25.1° resp., vs 15.9° in controls, $p < 0.001$) along with an extended head (mean head flexion/extension: −13.8 and −5.3° resp., vs 8.9° in controls, $p < 0.001$). Both groups also had increased trunk and head sagittal ROM (44.2 and 43.5° vs 34.6°; 40.9 and 36.9° vs 16.9° resp., both $p < 0.001$).

ASD-front had sitting and standing kinematics that were comparable with controls.

Waveforms of major kinematic differences between ASD subgroups and controls are displayed in **Figure 4**.

3.5 Univariate Analysis

Altered sitting and standing kinematics were significantly correlated with standing radiographic parameters and HRQOL scores. In particular, lumbar ROM and hip flexion were negatively correlated to SVA ($r = -0.26$ and $r = -0.25$ resp., $p = 0.004$ and $p = 0.005$ resp.), PT ($r = -0.29$ and $r = -0.37$ resp., $p = 0.001$ and $p < 0.001$ resp.), and PI-LL mismatch ($r = -0.31$ and $r = -0.32$ resp., both $p < 0.001$). Mean trunk flexion as well as trunk and head sagittal ROM were positively correlated to TK ($r = 0.45$, $r = 0.28$, and $r = 0.28$ resp., all $p = 0.001$) and PT ($r = 0.38$, $r = 0.21$, and $r = 0.21$ resp., $p < 0.001$, $p = 0.002$, and $p = 0.002$ resp.).

Furthermore, mean thorax flexion as well as trunk and head sagittal ROM were negatively correlated to PCS ($r = -0.44$, $r = -0.27$, and $r = -0.26$ resp., $p < 0.001$, $p = 0.002$, and $p = 0.004$ resp.) but positively correlated to VAS ($r = 0.44$, $r = 0.27$, and $r = 0.30$ resp., $p < 0.001$, $p = 0.003$, and $p = 0.001$ resp.), ODI ($r = 0.46$, $r = 0.30$, and $r = 0.34$ resp., all $p < 0.001$), and BDI ($r = 0.31$, $r = 0.33$, and 0.32 resp., all $p < 0.001$) (**Figure 5**).

3.6 Determinants of Kinematic Alterations

The multivariate analysis showed that even after controlling for demographic factors, kinematic alterations could be determined by spino-pelvic parameters:

Dynamic trunk flexion was determined by TK and PI-LL mismatch (adj. $R^2 = 0.44$; $\beta = 0.55$ and $\beta = 0.35$ resp., $p < 0.001$). Dynamic L1L3–L3L5 lumbar lordosis was determined by PI-LL mismatch and knee flexion (adj. $R^2 = 0.29$; $\beta = 0.47$ and $\beta = 0.19$ resp., $p < 0.001$). Dynamic T2T10–T10L1 thoracic kyphosis was determined by TK and PT (adj. $R^2 = 0.62$; $\beta = 0.44$ and $\beta = 0.15$ resp., $p < 0.001$).

Lumbar sagittal ROM was determined by PI-LL mismatch (adj. $R^2 = 0.13$; $\beta = -0.23$, $p < 0.001$). Head sagittal ROM was determined by TK and PT (adj. $R^2 = 0.17$; $\beta = 0.28$ and $\beta = 0.21$ resp., $p < 0.001$).

4 DISCUSSION

Patients with adult spinal deformity (ASD) are known to have quality of life (HRQOL) alterations and functional limitations (Pellisé et al., 2015; Christopher Kieser and Wyatt, 2019). While gait adaptations in ASD have been previously described in the literature (Kawkabani et al., 2021), alterations in other daily life activities, such as sitting and standing, have been poorly characterized. Furthermore, ASD represent a complex and heterogeneous entity differing in radiographic alterations, HRQOL scores, and even outcome after surgical intervention (Bess et al., 2016; Bakhsheshian et al., 2017; Yang et al., 2019). It is therefore crucial to subdivide the ASD population depending on the type of spinal deformity to better understand their motion alterations and provide appropriate treatment. This study recruited 93 ASD subjects with different types of spinal

TABLE 2 | Comparison of sit-to-stand kinematics between the four subgroups: controls, ASD-front, ASD-hyperTK, and ASD-sag.

		Mean ± SD				*P*-value	Controls vs ASD-front	Control vs ASD-hyperTK	Control *vs.* ASD-sag	ASD-front vs hyperTK	ASD -front vs ASD-sag	ASD-hyperTK vs ASD-sag
		Controls	ASD-front	ASD-hyperTK	ASD-sag							
Pelvis												
	Mean pelvic tilt (°)	15.2 ± 7.5	17.8 ± 5.6	14.1 ± 8.7	12.2 ± 9.8	**0.006**					*	
	ROM pelvic tilt (°)	37.2 ± 6.2	35.1 ± 6.0	36.1 ± 6.8	37.1 ± 7.0	0.60						
	Mean pelvic obliquity (°)	–0.1 ± 1.5	0.4 ± 1.7	0.7 ± 2.3	0.2 ± 2.5	0.26						
	ROM pelvic obliquity (°)	4.3 ± 1.9	3.7 ± 1.1	4.5 ± 2.5	5.7 ± 5.2	0.68						
	Mean pelvic rotation (°)	–0.5 ± 2.8	–0.3 ± 3.2	1.2 ± 3.3	–0.4 ± 3.8	0.10						
	ROM pelvic rotation (°)	4.9 ± 2.5	4.7 ± 1.8	5.2 ± 2.4	6.2 ± 3.1	0.20						
Hip												
	Mean hip flexion/extension (°)	57.8 ± 11.5	62.2 ± 7.7	59.2 ± 10.7	53 ± 11.2	**0.01**					*	
	ROM hip flexion/extension (°)	86.7 ± 10.6	86.6 ± 6.2	85.4 ± 14.8	81.5 ± 15.1	0.19						
Knee												
	Mean knee flexion/extension (°)	58.3 ± 10.3	61.6 ± 6.4	60.8 ± 9.9	58.8 ± 10.4	0.65						
	ROM knee flexion/extension (°)	93.9 ± 9.6	94.4 ± 7.9	89.1 ± 16.4	87.1 ± 9.3	**0.01**			*		*	
Ankle												
	Mean dorsiflexion/plantar flexion (°)	17.8 ± 8.2	17.7 ± 11.6	17.1 ± 5.6	15.7 ± 10.8	0.5						
	ROM dorsiflexion/plantar flexion (°)	22.8 ± 7.8	23.8 ± 6.7	19.9 ± 5.8	17.9 ± 5.6	**0.001**			*		*	
Head												
	Mean head flexion/extension (°)	10.5 ± 12.3	3.9 ± 14.6	2.4 ± 8.6	–3.4 ± 14.6	**0.001**		*	*			
	ROM head flexion/extension (°)	16.2 ± 7.6	19.6 ± 16.8	24.8 ± 14.6	25.6 ± 12	**0.003**			*		*	
Trunk												
	Mean trunk flexion/extension (°)	13.8 ± 6.1	12.7 ± 7.4	22.2 ± 8.0	23.9 ± 6.1	<**0.001**		*	*	*	*	
	ROM trunk flexion/extension (°)	35.4 ± 7.8	35.4 ± 9.9	41.2 ± 9.8	39.7 ± 10.6	**0.03**						
Spine segments												
	Mean flexion/extension pelvis—L3L5 (°)	19.6 ± 8.4	25.0 ± 8	24 ± 9.1	17.5 ± 10	**0.01**					*	*
	ROM flexion/extension pelvis—L3L5 (°)	41.1 ± 7.2	40 ± 7.6	41.9 ± 6.7	42 ± 8.1	0.58						
	Mean flexion/extension L1L3–L3L5 (°)	–6.8 ± 5.9	–5.7 ± 6.3	–9.1 ± 6.3	–3 ± 9.7	**0.04**						*
	ROM flexion/extension L1L3–L3L5 (°)	16.5 ± 10	14.0 ± 5.4	13.9 ± 9.2	9.1 ± 6.3	<**0.001**			*		*	*
	Mean flexion/extension T10L1–L1L3 (°)	–5.5 ± 6.4	–6.9 ± 7.1	–12 ± 9.9	–1.9 ± 11.3	<**0.001**		*				*
	ROM flexion/extension T10L1–L1L3 (°)	11.5 ± 9.3	8.3 ± 6.2	12.2 ± 5.9	9.3 ± 6.3	0.09						
	Mean flexion/extension T2T10–T10L1 (°)	17.2 ± 6.1	9.5 ± 7.4	32 ± 10.3	21.8 ± 10.9	<**0.001**	*	*		*	*	*
	ROM flexion/extension T2T10–T10L1 (°)	6.5 ± 3.1	5.9 ± 4.1	7.4 ± 4.2	9 ± 12.9	0.73						
	Mean flexion/extension C7T2–T2T10 (°)	17.7 ± 6.5	21.6 ± 8.6	30.4 ± 9.6	25.2 ± 8	<**0.001**		*	*	*		
	ROM flexion/extension C7T2–T2T10 (°)	11 ± 6.5	12.5 ± 5.7	18.1 ± 11.9	14.2 ± 11.2	**0.04**		*				

ROM, range of motion.

**Bold value, significant* p*-value.*

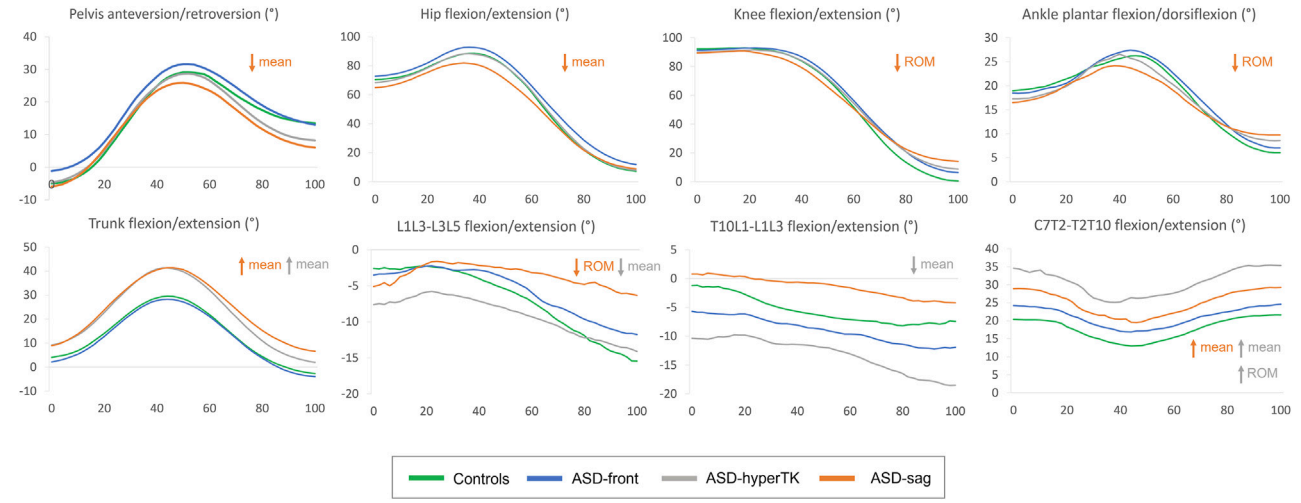

FIGURE 4 | Average kinematic waveforms for each subgroup during the sit-to-stand movement cycle (normalized between 0 and 100%). ROM, range of motion. Statistically significant differences during sit-to-stand only have been represented.

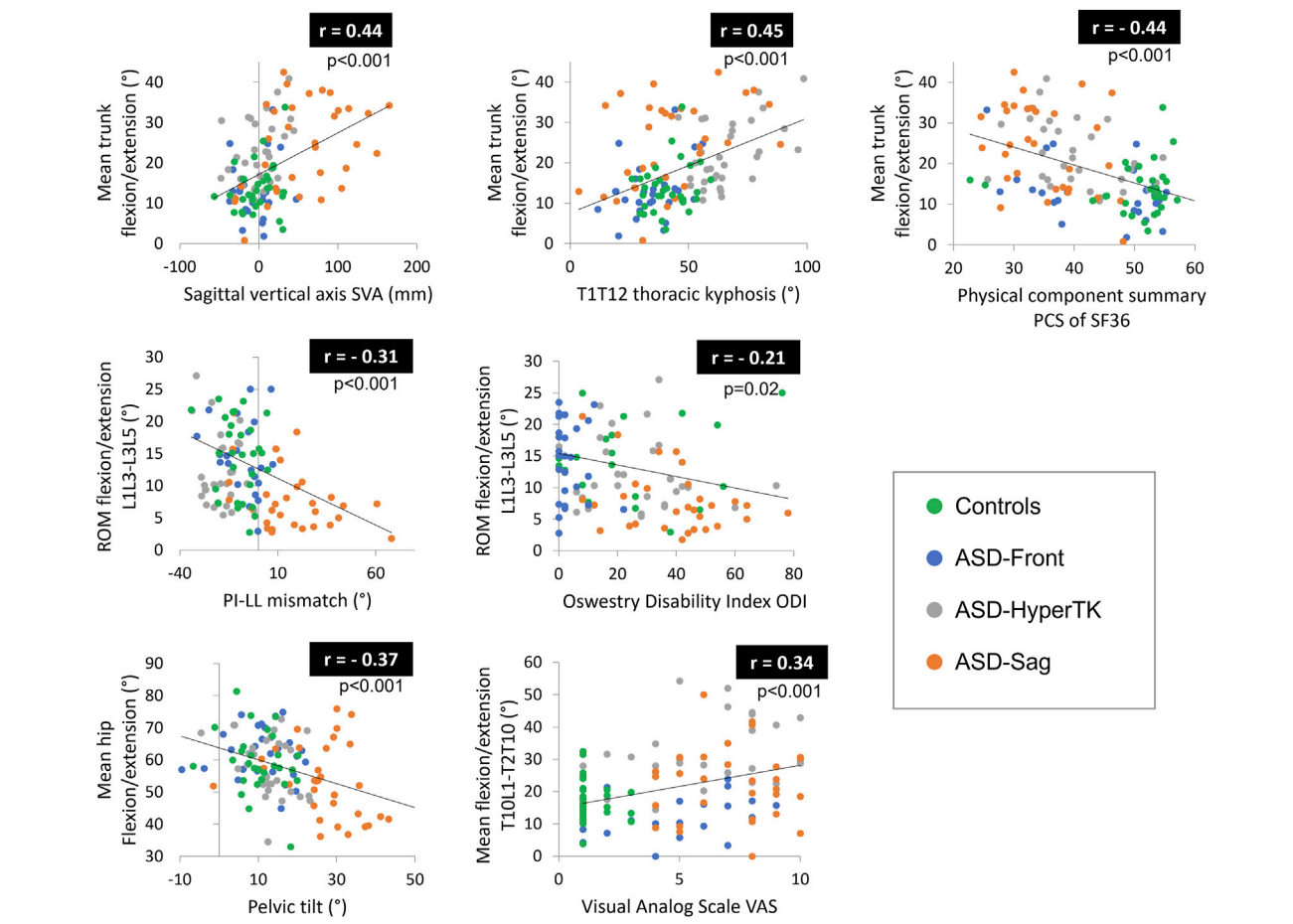

FIGURE 5 | Correlations between altered kinematic parameters and both radiographic parameters and health-related quality of life (HRQOL) scores. ROM, range of motion.

deformity and 31 controls to describe kinematic alterations in each ASD subgroup, divided according to their spinal deformity, during sit-to-stand and stand-to-sit movements, and further investigate the relationships between these kinematic changes and radiographic parameters as well as HRQOL scores.

The ASD population included in this study was found to have standing radiographic alterations comparable with those described in previous studies (Le Huec et al., 2019). ASD-sag had a loss of lumbar lordosis with a forward shift of the trunk. This resulted in increased pelvic retroversion and knee flexion to maintain their center of gravity above their feet. ASD-hyperTK presented with a thoracic hyperkyphosis that was compensated by an increase in lumbar lordosis and cervical lordosis without the need for other compensating mechanisms in the pelvis or lower limbs. ASD-front presented only with a coronal Cobb angle that did not affect their sagittal balance. Furthermore, ASD patients had significant pain (higher VAS) and HRQOL score alterations both on the physical (lower PCS and greater ODI) and mental components (lower MCS and higher BDI), as reported in previous studies (Pellisé et al., 2015; Diebo et al., 2018b, 2018a). These alterations were more pronounced in ASD-sag and to a lesser degree in ASD-hyperTK and ASD-front.

During sit-to-stand, the control group showed kinematics similar to those described in previous studies (Schenkman et al., 1990; Roebroeck et al., 1994; Tully et al., 2005). Initial forward propulsion of the trunk was mainly achieved by hip flexion. This acquired flexion momentum allowed them to achieve lift-off, while starting to extend their knees. At the same time, controls started to gradually increase ankle dorsiflexion, further projecting their trunk anteriorly. Afterwards, subjects simultaneously extended their lumbar spines, hips, knees, and ankles to reach the erect standing position. The thoracic spine underwent an initial compensatory extension followed by flexion during the transition to the erect phase. Horizontal gaze was maintained by an initial extension of the head and neck followed by flexion. Stand-to-sit kinematics showed mostly the same sequence of events, in reverse.

During sit-to-stand and stand-to-sit movements, ASD-sag showed altered pelvis and lower limb parameters. They had a more retroverted pelvis during motion, a previously described compensation mechanism in the standing position that allowed them to maintain their center of gravity over their base of support (Le Huec et al., 2019). They also presented with a limited hip flexion capacity and decreased mobility in their knees and ankles.

Since hip flexion is measured as the motion of the femur relative to the pelvis, pelvic retroversion in ASD-sag, which is the case here, could result in an apparent decrease of hip flexion. However, if the decreased mean hip flexion was solely due to pelvic retroversion, one would expect hip flexion to be also decreased during the final stage of motion when the subject assumes the standing position where pelvic retroversion is prominent as shown in **Figure 4** in this group. On further examination of the corresponding kinematic curve (**Figure 4**), peak hip flexion seems to be the most affected in ASD-sag. This corroborates results by Bailey et al. who had previously demonstrated that ASD patients had a decreased peak of hip flexion during sit-to-stand, along with an increased energy expenditure at this level (Bailey et al., 2019). Limitation in hip flexion could serve to prevent additional forward bending of the trunk in the sitting position and during the transition from sitting to standing, since ASD-sag already present with an increased trunk flexion during motion.

The decreased lower limb mobility during sitting and standing has also been described during walking, especially at the level of the knees. As mentioned earlier, in the static standing position, knee flexion acts as a compensation mechanism that repositions the center of gravity above the feet. The same mechanism is also maintained during walking, therefore limiting knee extension and leading to decreased knee ROM during gait and eventually decreased step length (Kawkabani et al., 2021; Severijns et al., 2021). However, in the static sitting position, the height of the seat was adjusted so that all individuals had the same initial knee flexion of 90°. Therefore, the decrease in knee ROM seen during sit-to-stand in ASD-sag only reflects the lack of knee extension in the standing position, as shown in the final stage of the knee kinematic curve (**Figure 4**).

At the level of the ankles, ASD-sag presented with limited peak dorsiflexion, which could act to prevent excessive forward bending of the trunk when transitioning from the sitting to the standing position, similar to the limitation in peak hip flexion. Furthermore, they had increased dorsiflexion in the final stage of the motion, while assuming the static standing position. Increased ankle dorsiflexion has previously been described as a compensation mechanism associated with knee flexion in ASD (Ferrero et al., 2016). Both decreased peak dorsiflexion and increased dorsiflexion in the final standing stage seem to explain the decreased ankle ROM seen in ASD-sag.

At the segmental level of the spine, ASD-sag also showed a decrease in lumbar (L1L3–L3L5) mobility during sit-to-stand and stand-to-sit. This is in agreement with other studies that showed a lesser variation of radiographic lumbar lordosis between the standing and sitting positions in ASD (Buckland et al., 2020). ASD-sag showed a fixed and decreased lumbar lordosis during the whole sit-to-stand in contrast to the other groups who were able to restore normal lumbar lordosis during standing (**Figure 4**). Indeed, loss of lumbar lordosis is regarded as the *primum movens* of the degenerative sagittal deformity seen in ASD (Le Huec et al., 2019).

ASD-hyperTK did not present significant differences in pelvic or lower limb kinematics compared with controls. This further highlights the fact that in ASD-hyperTK, no alteration or compensatory mechanism is seen at the level of the pelvis and lower limbs since thoracic hyperkyphosis is compensated by lumbar and cervical hyperlordosis when analyzing standing radiographic posture. However, these more pronounced spinal curvatures were reflected in spine segmental kinematics as increased dynamic lumbar (L1L3–L3L5) lordosis, increased extension at the thoracolumbar junction (T10L1–L1L3) as well as a more flexed thoracic segments (C7T2–T2T10 and T2T10–T10L1) when compared with controls. These increased curvatures required an increased mobility of the spine during motion. This was apparent at the thoracolumbar junction (T10L1–L1L3) as well as the upper thoracic spine

(C7T2–T2T10). This finding confirms other observations showing that in the thoracic spine, the highest segmental ROM in the sagittal plane occurred at the upper-thoracic and thoracolumbar levels (Morita et al., 2014).

Overall, both ASD-sag and ASD-hyperTK maintained a flexed trunk during sit-to-stand and stand-to-sit. This forward inclination of the trunk is a characteristic feature of ASD in the standing position and has been shown to persist during gait in ASD individuals (Kawkabani et al., 2021). Furthermore, this was also described in other studies where peak dynamic SVA during sit-to-stand was shown to be increased in ASD (Bailey et al., 2019). This forward increase could also serve to increase stability by facilitating the transition of their center of gravity from the seat's wide base to the narrower base of their feet (Hughes et al., 1994). In fact, sit-to-stand transition requires acquiring initial momentum through combined hip and lumbar flexion, which is then transferred to the trunk allowing the propulsion of the subject from the seat. This requires high levels of neuromuscular control, which might be altered in individuals with spinal deformity and compensating mechanisms (Arima et al., 2018; Laratta et al., 2019). An alternative strategy described as a "stabilization" strategy involves moving the center of gravity above the base of the feet first and then extending the lower limbs and trunk to assume the standing position (Hughes et al., 1994). The forward increase of the trunk can move the center of gravity easily to the narrow base of the feet without needing to go through an unstable phase of momentum transfer. As shown previously, different strategies were adopted as compensatory mechanisms for the forward bending of the trunk. ASD-sag who presented with a more rigid spine recruited compensatory mechanisms in their lower limbs with a reduced peak hip flexion and reduced ankle dorsiflexion. ASD-hyperTK compensated by increasing the mobility of their upper thoracic and thoracolumbar spines. Both strategies prevented excessive trunk flexion and loss of balance.

To maintain a horizontal gaze, ASD-sag and ASD-hyperTK needed to further extend their head during motion, as described in previous studies where radiographic cervical lordosis was shown to increase parallel to the increase in SVA (Diebo et al., 2016). The findings of this study showed that these modifications were associated with a compensatory increase in mobility of the trunk and head in both ASD-sag and ASD-hyperTK.

ASD-front had similar kinematics compared with controls. This reflects the fact than an isolated scoliosis does not affect sagittal balance and therefore motion during sit-to-stand and stand-to-sit, which mostly occur in the sagittal plane (Gilleard et al., 1999).

The kinematic modifications observed in the ASD subgroups were correlated to the radiographic alterations. In particular, an increase in radiographic PT, SVA, and PI-LL, the main altered parameters in ASD-sag, was correlated to a decreased lumbar mobility and decreased hip flexion. Mean trunk flexion as well as trunk and head sagittal ROM were positively correlated to TK, the main driver of the deformity in ASD-hyperTK, and PT, the main compensating mechanism in ASD-sag. Furthermore, kinematic alterations were also correlated to the HRQOL score alterations in ASD.

Our study had several limitations. First, even though sex distribution did not significantly differ between ASD subjects and controls, sex ratios were not identical (ASD: 71F/22M vs controls: 18F/13M). Furthermore, both groups covered a wide range of age groups. Demographics such as age and sex are known to affect mobility in asymptomatic subjects (Zhou et al., 2020a; 2020b). However, even after controlling for demographics as confounding variables, kinematics were still different between groups. Second, some subjects with severe deformities were not able to stand up without assistance. They were therefore allowed to lean on their thighs during sit-to-stand transition. While this strategy might affect sit-to-stand kinematics, excluding these subjects would have resulted in a selection bias where only milder deformities are included, potentially masking the differences between subgroups. Furthermore, the "hands on knees" strategy was allowed since ground reaction forces and average events times were shown to be similar to rising from the seat with arms free or with crossed arms (Etnyre and Thomas, 2007). Finally, errors inherent to the marker model and tracking system could affect the validity of our data, especially in the spinal segment. For instance, fixed segments were used to describe spine kinematics, instead of a subject-specific model. However, this model has already been studied in the literature and was shown to have good intra-subject repeatability (Leardini et al., 2011). Furthermore, the values of kinematic parameters for the control group in this study were similar to those initially described by Leardini et al.

Nevertheless, this study described patterns of movement alterations that are specific to each subgroup of ASD deformity and that might have clinical implications. ASD with a sagittal malalignment had decreased lumbar mobility during sit-to-stand. Surgical fixation of the spine might lead to more altered spine kinematics, requiring further compensating mechanisms in the adjacent spinal segments, pelvis, and lower limbs. In ASD with an isolated thoracic hyperkyphosis, increased mobility of the thoracic spine at both its upper and lower ends could serve as a compensation mechanism during sit-to-stand. Surgical correction of the deformity could also increase the rigidity of these segments, therefore limiting the compensatory ability of the spine and recruiting additional compensation mechanisms in the pelvis and lower limbs. It is still not clear if surgery is able to restore normal kinematics in ASD. Bailey et al. have shown that peak trunk flexion was reduced and peak hip flexion was increased postoperatively, along with a decrease in lumbar and hip torques. However, energy expenditure at the level of the knees was increased and spine kinematics were not studied (Bailey et al., 2019). In other studies, alterations in limb kinematics and spatio-temporal parameters during gait were not corrected postoperatively (Severijns et al., 2021). This highlights the need for future studies that would be able to assess the effect of surgery on daily life activities and that could determine which subset of ASD patients might benefit the most from surgical interventions.

In conclusion, both ASD with sagittal malalignment and those with an isolated hyperkyphosis had a flexed trunk attitude,

compensated by an extended head and an increased mobility of their trunk and heads during the sit-to-stand and stand-to-sit movements. ASD-sag had limited lumbar and lower limb mobility similar to the alterations seen during walking. ASD-hyperTK had a flexed attitude at the thoracic spinal segments compensated by an increased extension in the lumbar and thoracolumbar segments, along with an increased mobility at the upper-thoracic and thoracolumbar junction. These kinematic alterations were correlated to radiographic spino-pelvic malalignment and HRQOL deteriorations. Future studies should address whether spinal corrective surgery or physical reeducation are able to improve sitting and standing kinematics in ASD patients and therefore their quality of life.

DATA AVAILABILITY STATEMENT

The raw data supporting the conclusions of this article will be made available by the authors, without undue reservation.

ETHICS STATEMENT

The studies involving human participants were reviewed and approved by CE Hotel Dieu de France, Universite Saint-Joseph de Beyrouth (CEHDF1259). The patients/participants provided their written informed consent to participate in this study.

AUTHOR CONTRIBUTIONS

Data collection: ES, KS, GK, RS, MM, EJ, KA, MF, AM. Statistics: AA, ES, AM, KS. Data interpretation: ES, AM, AA, RR, WS, VL, IG. Article writing: ES, KS, AA. Assistance in figures, tables, and layout: KS, GK, RS, MM, EJ, KA, MF, AM. Study design: AA, RR, WS, VL.

FUNDING

This research was funded by the University of Saint-Joseph (grant FM361), EUROSPINE (TFR 2020#22), CEDRE project (46556SG) and CNRS-L.

SUPPLEMENTARY MATERIAL

The Supplementary Material for this article can be found online at: https://www.frontiersin.org/articles/10.3389/fbioe.2021.751193/full#supplementary-material

REFERENCES

Aebi, M. (2005). The Adult Scoliosis. *Eur. Spine J.* 14, 925–948. doi:10.1007/s00586-005-1053-9

Arima, H., Glassman, S. D., JR, Dimar, J. R., Matsuyama, Y., and Carreon, L. Y. (2018). Neurologic Comorbidities Predict Proximal Junctional Failure in Adult Spinal Deformity. *Spine Deformity* 6, 576–586. doi:10.1016/J.JSPD.2018.01.008

Bailey, J. F., Matthew, R. P., Seko, S., Curran, P., Chu, L., Berven, S. H., et al. (2019). Issls Prize in Bioengineering Science 2019: Biomechanical Changes in Dynamic Sagittal Balance and Lower Limb Compensatory Strategies Following Realignment Surgery in Adult Spinal Deformity Patients. *Eur. Spine J.* 28, 905–913. doi:10.1007/s00586-019-05925-2

Bakhsheshian, J., Scheer, J. K., Gum, J. L., Horner, L., Hostin, R., Lafage, V., et al. (2017). Comparison of Structural Disease Burden to Health-Related Quality of Life Scores in 264 Adult Spinal Deformity Patients with 2-Year Follow-Up. *Clin. Spine Surg.* 30, E124–E131. doi:10.1097/BSD.0000000000000470

Bess, S., Line, B., Fu, K.-M., McCarthy, I., Lafage, V., Schwab, F., et al. (2016). The Health Impact of Symptomatic Adult Spinal Deformity. *Spine (Phila. Pa. 1976).* 41, 224–233. doi:10.1097/BRS.0000000000001202

Buckland, A. J., Abotsi, E. J., Vasquez-Montes, D., Ayres, E. W., Varlotta, C. G., and Vigdorchik, J. M. (2020). Lumbar Spine Degeneration and Flatback Deformity Alter Sitting-Standing Spinopelvic Mechanics-Implications for Total Hip Arthroplasty. *The J. Arthroplasty* 35, 1036–1041. doi:10.1016/j.arth.2019.11.020

Chaibi, Y., Cresson, T., Aubert, B., Hausselle, J., Neyret, P., Hauger, O., et al. (2012). Fast 3D Reconstruction of the Lower Limb Using a Parametric Model and Statistical Inferences and Clinical Measurements Calculation from Biplanar X-Rays. *Comp. Methods Biomech. Biomed. Eng.* 15, 457–466. doi:10.1080/10255842.2010.540758

Christopher Kieser, D., and Wyatt, M. (2021). "The Functional Effects of Adult Spinal Deformity and the Effectiveness of Surgery," in *Spinal Deformities in Adolescents, Adults and Older Adults* (IntechOpen). doi:10.5772/intechopen.90054

Davis, R. B., Õunpuu, S., Tyburski, D., and Gage, J. R. (1991). A Gait Analysis Data Collection and Reduction Technique. *Hum. Mov. Sci.* 10, 575–587. doi:10.1016/0167-9457(91)90046-Z

Diebo, B. G., Challier, V., Henry, J. K., Oren, J. H., Spiegel, M. A., Vira, S., et al. (2016). Predicting Cervical Alignment Required to Maintain Horizontal Gaze Based on Global Spinal Alignment. *Spine (Phila. Pa. 1976)* 41, 1795–1800. doi:10.1097/BRS.0000000000001698

Diebo, B. G., Cherkalin, D., Jalai, C. M., Shah, N. V., Poorman, G. W., Beyer, G. A., et al. (2018a). Comparing Psychological burden of Orthopaedic Diseases against Medical Conditions: Investigation on Hospital Course of Hip, Knee, and Spine Surgery Patients. *J. Orthopaedics* 15, 297–301. doi:10.1016/j.jor.2018.02.010

Diebo, B. G., Segreto, F. A., Segreto, F. A., Jalai, C. M., Vasquez-Montes, D., Bortz, C. A., et al. (2018b). Baseline Mental Status Predicts Happy Patients after Operative or Non-operative Treatment of Adult Spinal Deformity. *J. Spine Surg.* 4, 687–695. doi:10.21037/jss.2018.09.11

Etnyre, B., and Thomas, D. Q. (2007). Event Standardization of Sit-To-Stand Movements. *Phys. Ther.* 87, 1651–1666. doi:10.2522/PTJ.20060378

Ferrero, E., Liabaud, B., Challier, V., Lafage, R., Diebo, B. G., Vira, S., et al. (2016). Role of Pelvic Translation and Lower-Extremity Compensation to Maintain Gravity Line Position in Spinal Deformity. *Spi* 24, 436–446. doi:10.3171/2015.5.SPINE14989

Gilleard, W., Crosbie, J., and Smith, R. (1999). Coronal and Transverse Plane Kinematics and Kinetics of Sit-To-Stand. *Knee* 4, 9–11.

Hirvensalo, M., Rantanen, T., and Heikkinen, E. (2000). Mobility Difficulties and Physical Activity as Predictors of Mortality and Loss of independence in the Community-Living Older Population. *J. Am. Geriatr. Soc.* 48, 493–498. doi:10.1111/j.1532-5415.2000.tb04994.x

Hughes, M. A., Weiner, D. K., Schenkman, M. L., Long, R. M., and Studenski, S. A. (1994). Chair Rise Strategies in the Elderly. *Clin. Biomech.* 9, 187–192. doi:10.1016/0268-0033(94)90020-5

Kawkabani, G., Saliby, R. M., Mekhael, M., Rachkidi, R., Massaad, A., Ghanem, I., et al. (2021). Gait Kinematic Alterations in Subjects with Adult Spinal Deformity and Their Radiological Determinants. *Gait Posture* 88, 203–209. doi:10.1016/j.gaitpost.2021.06.003

Kim, H. J., Iyer, S., Zebala, L. P., Kelly, M. P., Sciubba, D., Protopsaltis, T. S., et al. (2017). Perioperative Neurologic Complications in Adult Spinal Deformity Surgery. *Spine (Phila. Pa. 1976)* 42, 420–427. doi:10.1097/BRS.0000000000001774

Laratta, J. L., Glassman, S. D., Atanda, A. A., Dimar, J. R., Gum, J. L., Crawford, C. H., III, et al. (2019). The Berg Balance Scale for Assessing Dynamic Stability and Balance in the Adult Spinal Deformity (ASD) Population. *J. Spine Surg.* 5, 451–456. doi:10.21037/JSS.2019.09.15

Le Huec, J. C., Thompson, W., Mohsinaly, Y., Barrey, C., and Faundez, A. (2019). Sagittal Balance of the Spine. *Eur. Spine J.* 28, 1889–1905. doi:10.1007/s00586-019-06083-1

Leardini, A., Biagi, F., Merlo, A., Belvedere, C., and Benedetti, M. G. (2011). Multi-segment Trunk Kinematics during Locomotion and Elementary Exercises. *Clin. Biomech.* 26, 562–571. doi:10.1016/J.CLINBIOMECH.2011.01.015

Morita, D., Yukawa, Y., Nakashima, H., Ito, K., Yoshida, G., Machino, M., et al. (2014). Range of Motion of Thoracic Spine in Sagittal Plane. *Eur. Spine J.* 23, 673–678. doi:10.1007/S00586-013-3088-7

Pellisé, F., Vila-Casademunt, A., Vila-Casademunt, A., Ferrer, M., Domingo-Sàbat, M., Bagó, J., et al. (2015). Impact on Health Related Quality of Life of Adult Spinal Deformity (ASD) Compared with Other Chronic Conditions. *Eur. Spine J.* 24, 3–11. doi:10.1007/s00586-014-3542-1

Roebroeck, M. E., Doorenbosch, C. A. M., Harlaar, J., Jacobs, R., and Lankhorst, G. J. (1994). Biomechanics and Muscular Activity during Sit-To-Stand Transfer. *Clin. Biomech.* 9, 235–244. doi:10.1016/0268-0033(94)90004-3

Sadeghi, M., Emadi Andani, M., Bahrami, F., and Parnianpour, M. (2013). Trajectory of Human Movement during Sit to Stand: a New Modeling Approach Based on Movement Decomposition and Multi-phase Cost Function. *Exp. Brain Res.* 229, 221–234. doi:10.1007/S00221-013-3606-1

Safaee, M. M., Ames, C. P., and Smith, J. S. (2020). Epidemiology and Socioeconomic Trends in Adult Spinal Deformity Care. *Neurosurgery* 87, 25–32. doi:10.1093/NEUROS/NYZ454

Schenkman, M., Berger, R. A., Riley, P. O., Mann, R. W., and Hodge, W. A. (1990). Whole-Body Movements during Rising to Standing from Sitting. *Phys. Ther.* 70, 638–648. doi:10.1093/ptj/70.10.638

Schwab, F., Ungar, B., Blondel, B., Buchowski, J., Coe, J., Deinlein, D., et al. (2012). Scoliosis Research Society-Schwab Adult Spinal Deformity Classification. *Spine (Phila. Pa. 1976)* 37, 1077–1082. doi:10.1097/BRS.0b013e31823e15e2

Severijns, P., Moke, L., Overbergh, T., Beaucage-Gauvreau, E., Ackermans, T., Desloovere, K., et al. (2021). Dynamic Sagittal Alignment and Compensation Strategies in Adult Spinal Deformity during Walking. *Spine J.* 21, 1059–1071. doi:10.1016/j.spinee.2021.02.017

Tully, E. A., Fotoohabadi, M. R., and Galea, M. P. (2005). Sagittal Spine and Lower Limb Movement during Sit-To-Stand in Healthy Young Subjects. *Gait Posture* 22, 338–345. doi:10.1016/j.gaitpost.2004.11.007

Yamada, T., and Demura, S.-i. (2009). Relationships between Ground Reaction Force Parameters during a Sit-To-Stand Movement and Physical Activity and Falling Risk of the Elderly and a Comparison of the Movement Characteristics between the Young and the Elderly. *Arch. Gerontol. Geriatr.* 48, 73–77. doi:10.1016/j.archger.2007.10.006

Yang, J., Lafage, V., Lafage, R., Smith, J., Klineberg, E. O., Shaffrey, C. I., et al. (2019). Determinants of Patient Satisfaction 2 Years after Spinal Deformity Surgery A Latent Class Analysis. *Spine*.44, E45–E52. doi:10.1097/BRS.0000000000002753

Zhou, S., Li, W., Wang, W., Zou, D., Sun, Z., Xu, F., et al. (2020a). Sagittal Spinal and Pelvic Alignment in Middle-Aged and Older Men and Women in the Natural and Erect Sitting Positions: A Prospective Study in a Chinese Population. *Med. Sci. Monit.* 26, 1–9. doi:10.12659/MSM.919441

Zhou, S., Sun, Z., Li, W., Wang, W., Su, T., Du, C., et al. (2020b). The Standing and Sitting Sagittal Spinopelvic Alignment of Chinese Young and Elderly Population: Does Age Influence the Differences between the Two Positions? *Eur. Spine J.* 29, 405–412. doi:10.1007/s00586-019-06185-w

Conflict of Interest: The authors declare that the research was conducted in the absence of any commercial or financial relationships that could be construed as a potential conflict of interest.

Advantages of publishing in Frontiers

OPEN ACCESS
Articles are free to read for greatest visibility and readership

FAST PUBLICATION
Around 90 days from submission to decision

HIGH QUALITY PEER-REVIEW
Rigorous, collaborative, and constructive peer-review

TRANSPARENT PEER-REVIEW
Editors and reviewers acknowledged by name on published articles

Frontiers
Avenue du Tribunal-Fédéral 34
1005 Lausanne | Switzerland

Visit us: www.frontiersin.org
Contact us: frontiersin.org/about/contact

REPRODUCIBILITY OF RESEARCH
Support open data and methods to enhance research reproducibility

DIGITAL PUBLISHING
Articles designed for optimal readership across devices

FOLLOW US
@frontiersin

IMPACT METRICS
Advanced article metrics track visibility across digital media

EXTENSIVE PROMOTION
Marketing and promotion of impactful research

LOOP RESEARCH NETWORK
Our network increases your article's readership